Human Mononuclear Phagocyte Kinetics in Health and Inflammation

A thesis submitted for the degree of Doctor of Philosophy, University College London.

Amit Ashok Patel

Submitted: November 2019

Declaration

'*I, Amit Ashok Patel confirm that the work presented in this thesis is my own unless otherwise stated. Where information has been derived from other sources, I confirm that this has been indicated in the thesis*'

November 2019

Abstract

The mononuclear phagocyte system comprises three types of cells: monocytes, macrophages and dendritic cells (DC). The kinetics underlying their generation, differentiation and disappearance are critical to understanding how these cells maintain tissue homeostasis as well as orchestrating the immune response. Currently, the circulating kinetics of these cells remain unknown in humans.

The kinetic profiles of circulating monocyte subsets (classical, intermediate and non-classical) and DC subsets (pDC, pre-DC, cDC1 and cDC2) were examined in humans for the first time using stable isotope labelling in the form of deuterated glucose. Monocyte subsets appeared sequentially in the circulation which was demonstrated to be due to a developmental relationship between these cells. Pre-DC and cDC appeared prior to monocytes whereas pDC were observed later.

After establishing the turnover of circulating mononuclear phagocytes under steady physiological conditions, the kinetics were then examined following experimental human endotoxemia. A temporary loss of circulating mononuclear phagocytes was observed at early time points, classical monocytes were the first to re-appear within the circulation due to an early emergency release from the bone marrow.

Finally, in a human model of local inflammation, the infiltrating kinetics of monocyte and DC subsets were examined in the skin. Particularly, pre-DC were observed at higher concentrations compared to the blood which also expressed co-stimulatory molecules (CD80 and CD86), suggestive of an effector cell phenotype. The infiltration of novel cDC2 subsets was also observed.

In summary, this thesis illustrates the kinetic and developmental profiles of human mononuclear phagocytes under steady-state and experimental inflammation.

Impact Statement

From an academic point of view, the work in this thesis takes advantage of cutting-edge science to explore the fundamental biology of human immune cells *in vivo*. Given the broad diversity of immune cells, a fundamental starting place for any scientist entering the field is understanding the basic biology of these cells i.e. the development, turnover and the inter-relationship of these cells. Although a simple question, answering this in the human setting can be challenging. The work in this thesis explores this foundational biology of human mononuclear phagocytes.

Knowledge of the turnover and relationship of immune cells under inflammatory conditions may also open therapeutic avenues. These data might help explain the unsuccessful results seen in clinical trials targeting mononuclear phagocytes in chronic diseases. Knowledge concerning which subsets of mononuclear phagocyte drive the aetiology of disease will similarly help identify therapeutic approaches to target these cells. Knowing how often these cells are replenished from the bone marrow and their role in inflammation permits for the timely administration of drugs to target these cells and boost them when they are beneficial or reduce them when detrimental.

Part of the work presented in this thesis has already been disseminated through publications and presentations at conferences. The impact of this to the scientific community can be appreciated where published work from this thesis has reached almost 200 citations over two years. A further final manuscript is currently in preparation.

Publications

Foote, J.R., **Patel, A.A.,** Yona, S., Segal, A.W., 2019. Variations in the phagosomal environment of human neutrophils and mononuclear phagocyte subsets. Front. Immunol. 10, 188.

Gill, U.S., Pallett, L.J., Thomas, N., Burton, A.R., **Patel, A.A.,** Yona, S., Kennedy, P.T.F., Maini, M.K., 2019. Fine needle aspirates comprehensively sample intrahepatic immunity. Gut 68, 1493–1503.

Janela, B., **Patel, A.A.,** Lau, M.C., Goh, C.C., Msallam, R., Kong, W.T., Fehlings, M., Hubert, S., Lum, J., Simoni, Y., Malleret, B., Zolezzi, F., Chen, J., Poidinger, M., Satpathy, A.T., Briseno, C., Wohn, C., Malissen, B., Murphy, K.M., Maini, A.A., Vanhoutte, L., Guilliams, M., Vial, E., Hennequin, L., Newell, E., Ng, L.G., Musette, P., Yona, S., Hacini-Rachinel, F., Ginhoux, F., 2019. A Subset of Type I Conventional Dendritic Cells Controls Cutaneous Bacterial Infections through VEGFα-Mediated Recruitment of Neutrophils. Immunity 50, 1069-1083.e8.

Maini, A., Foote, J.R., Hayhoe, R., **Patel, A.A.,** O'Brien, A., Avraham-Davidi, I., Yona, S., 2018. Monocyte and Neutrophil Isolation, Migration, and Phagocytosis Assays. Curr. Protoc. Immunol. 122, e53.

Patel, A.A., Yona, S., 2018. Phagocyte Development. In: ELS. John Wiley & Sons, Ltd, Chichester, UK, pp. 1–13.

Patel, A.A., Yona, S., 2019. Inherited and Environmental Factors Influence Human Monocyte Heterogeneity. Front. Immunol. 10, 2581.

Patel, A.A., Zhang, Y., Fullerton, J.N., Boelen, L., Rongvaux, A., Maini, A.A., Bigley, V., Flavell, R.A., Gilroy, D.W., Asquith, B., Macallan, D., Yona, S., 2017. The fate and lifespan of human monocyte subsets in steady-state and systemic inflammation. J. Exp. Med. 214, 1913–1923.

Acknowledgements

Although a thesis is demonstrative of one's work, the work here would not have been brought to reality without the support of others.

First, I would like to express my deepest appreciation for the guidance, perseverance and wisdom provided by my supervisor and friend, Dr. Simon Yona. You've provided me with encouragement and now the opportunity to hopefully become a successful scientist. Secondly, I am very thankful to Prof. Derek Gilroy. The work presented in this thesis builds on the established blister model in your lab and would not have been possible without your guidance and support (and numerous rounds on a Friday evening). I would like to thank all staff within the Division of Medicine and Infection and Immunity who have given me advice along this journey.

As science is a collaborative project, the studies in this thesis are the sum of numerous experts within the field. I'd like to thank the following as their advice and encouragement was essential in producing this thesis. Prof. Derek Macallan and Dr. Yan Zhang for their expertise regarding human *in vivo* labelling. Dr. Becca Asquith and Dr. Lies Boelen who carried out the mathematical modelling. Prof. Richard Flavell FRS and Dr. Anthony Rongvaux for providing the humanised MISTRG mice. Dr Venetia Bigley for the human bone marrow analysis. Dr. Florent Ginhoux and Dr. Charles-Antoine Dutertre for their advice on identifying novel DC subsets and single-cell RNA sequencing. The clinicians of the Gilroy group (Dr. James Fullerton, Dr. Alexander Maini and Dr. James Glanville) who aided with the clinical aspects in this thesis. Jamie Evans for his endless knowledge on flow cytometry and the infinite hours of cell sorting. Finally, Prof. Mala Maini, Dr. Laura Pallett, Prof. Anthony Segal, Dr. Juliet Foote, Dr. Baptiste Janela for the enjoyable collaborative projects that arose during this PhD.

I can't forget the past and present of G19. You've all helped me get to where I am and are probably the liveliest of the groups in the Rayne building, there's no such thing as a dull day around you (probably as most of them end up at the bar)! A special thanks to Parinaaz, James, Karen and Liv not only for your scientific input but also for memorable times (and daily memes) which I will particularly miss. I'm also extending this to Rikah. I could list all the memories, but I fear it'd be longer than my actual references! You somehow turned those unbearable days upside down and I don't think I can thank you enough. The same goes for my friends, those times you helped keep me grounded and focused won't be forgotten.

Last but not least, my parents, who have made it possible for me to come this far and supporting me these extra few years of being a student. Thank-you.

Table of Contents

Materials and Methods

Discussion

Table of Figures

Table of Tables

Abbreviations and Acronyms

ACK	Ammonium-Chloride-Potassium
AF	Alexa Fluor
AIC	Akaike information criterion
AIDS	Acquired immune deficiency syndrome
ANOVA	Analysis of variance
APC	Allophycocyanin
BTLA	B- and T-lymphocyte attenuator
BV	Brilliant Violet
CD	Custer of differentiation
cDC	Classical Dendritic Cell
cDC1	Classical Dendritic Cell type 1
cDC2	Classical Dendritic Cell type 2
CLEC9a	C-type lectin domain family 9 member A
CLP	Common Lymphoid Progenitor
CMP	Common Myeloid Progenitor
CSF1	Colony stimulating factor 1
Cy7	Cyanine 7
DAPI	4’,6-diamidino-2-phenylindole
DC	Dendritic Cell
DLL-1	Delta-like ligand 1
DNA	Deoxyribonucleic acid
DNGR-1	Dendritic cell NK-lectin group receptor 1
EDTA	Ethylenediamine tetraacetic acid
EMP	Erythro-myeloid progenitors
FACS	Fluorescence Activated Cell Sorting
FCS	Fetal calf serum
FITC	Fluorescein Isothiocyanate
FLT3	fms like tyrosine kinase 3
FMO	Fluorescence Minus One
FSC	Forward Scatter
GC/MS	Gas chromatography–mass spectrometry
GMP	Granulocyte-macrophage progenitor
HIV	Human Immunodeficiency Virus

HLA	Human Leukocyte Antigen
HSC	Hematopoietic stem cells
HSCT	Hematopoietic stem cell transplantation
IFN	Interferon
IL	Interleukin
IRF	Interferon-regulatory factor
LFA-1	Lymphocyte function-associated antigen 1
LPS	Lipopolysaccharide
M-CSF	Macrophage colony-stimulating factor
MDP	Monocyte/dendritic cell precursor
MHC	Major histocompatibility complex
MPS	Mononuclear phagocyte system
NK	Natural Killer
PBMC	Peripheral blood mononuclear cells
PBS	Phosphate-buffered saline
PCR	Polymerase chain reaction
pDC	Plasmacytoid dendritic cell
PE	Phycoerythrin
PerCP/cy5.5	Peridinin-chlorophyll-protein Complex Cy5.5
PSGL1	P-selectin glycoprotein ligand-1
RNA	Ribonucleic acid
RPM	Revolutions per minute
RPMI	Roswell Park Memorial Institute
SD	Standard deviation
SLAN	6-Sulfo LacNAc
SLE	Systemic lupus erythematosus
SSC	Side scatter
Th	T helper cell
TLR	Toll-like receptor
TNFα	Tumour necrosis factor alpha
Treg	T regulatory cell
UV	Ultraviolet

Chapter 1

Introduction

1.1 The Immune Response

> '*If ever there was a romantic chapter in pathology, it has surely been that of the story of phagocytosis'* – Sir Joseph Lister (1896)

Inflammation has been recognised since the time of the ancient Egyptians where records of pus formations were described as 'the demon of disease'. Aulus Cornelius Celsus characterised inflammation at the macroscopic level as a combination of heat (*calor*), pain (*dolor*), redness (*rubor*) and swelling (*tumor*). Loss of function was later recognised as the 5th cardinal sign of inflammation by Rudolph Virchow. Although these manifestations appear unpleasant, John Hunter recognised inflammation as a teleologically 'salutary reaction'. The inflammatory reaction concerns the vascular, neurological, humoral and cellular responses, which all occur in a timely fashion.

The majority of cellular responses during an inflammatory reaction arise from cells of the immune system. Broadly speaking, the immune system can be divided into innate and adaptive immunity. Innate immunity is viewed as a rapid non-specific response and does not possess immunological memory, although evidence regarding trained immunity may challenge this (Arts *et al.,* 2018; Mitroulis *et al.,* 2018; Quintin *et al.,* 2012). On the other hand, adaptive immunity is slower in response but is advantageous to the host as immune memory allows a heightened and rapid response when re-encountering pathogens. These two arms of the immune system work in tandem to restore balance within the host following injury or infection.

The actions of innate and adaptive immunity are owed to the function of white blood cells or leukocytes. Polymorphonuclear leukocytes (PMNs) are named due to their multi-lobed nucleus and comprise of predominantly neutrophils with the remainder including eosinophils, basophils and resident mast cells. These cells are also collectively referred to as granulocytes, owed to the

high density of cytoplasmic granules. Mononuclear leukocytes include lymphocytes, monocytes, macrophages and dendritic cells (DC). Peripheral blood also contains erythrocytes and platelets which can be clearly distinguished from leukocytes by the absence of a nucleus.

This thesis focuses on a group of cells, termed mononuclear phagocytes which include monocytes, macrophages and DC.

1.2 A Brief History of Mononuclear Phagocytes

The origin of mononuclear phagocytes dates back to seminal studies in 1880. Aniline and cytological stains identified cells with a kidney bean-shaped nuclei which Paul Ehrlich termed 'übergangsformen' (transitional/bridging cell), today known as monocytes (Guilliams *et al.,* 2018; Naegeli, 1908) (**Figure 1.1**). In 1882, Elie Metchnikoff first described cells 'eating to defend' during his eminent experiment in Messina, demonstrating starfish larvae engulfing a pierced rose thorn (Metchnikoff, 1893; Vikhanski, 2016). This pivotal observation laid the foundations for 'phagocytosis', a term coined by Carl Claus and Metchnikoff himself (Gordon, 2008).

These phagocytic cells are distributed throughout the body in several organs and attempts were made to classify these cells into a system. Metchnikoff called these cells 'macrophages' (meaning big eaters) to distinguish them from 'microphages' (now known as polymorphonuclear leukocytes) (Metchnikov, 1892) and led him to the term 'macrophage system'.

In 1924, Aschoff expanded this definition to include several other cell types and designated the term 'reticuloendothelial system'. This classification included cells thought to be capable of phagocytosis and share a common lineage (Aschoff, 1924). Later this concept was criticised, as Maximow showed that cells of the reticuloendothelial system are distinct from one another in terms of both morphology and function (Maximow, 1927). In addition, upon reviewing the methodology implemented by Aschoff, Ralph van Furth states the dyes were not restricted to phagocytosis and pinocytosis may have resulted in labelling of certain cells with minor

phagocytic function (van Furth *et al.,* 1972). As a result, a better classification of these cells was required.

Figure 1.1 **Historical description of monocytes**

Various stains identified 1. Lymphocyten: lymphocyte, 2. Grosse mononukleäre Zellen: Great mononuclear cell, 3. Übergangsformen: transitional cell (monocyte), 4. Neutrophile: neutrophil, 5. Eosinophile: eosinophile, 6. Basophile (Mast) Leukocyten: basophil or mast cell (From Naegeli, 1908)

Attention soon turned to the origin of these macrophages, and one of the earliest *in vivo* studies established blood monocyte differentiation into macrophage-like cells upon extravasation into tissues (Ebert and Florey, 1939). This had been suggested from prior studies *in vitro*, where monocytes and macrophages exhibited a similar morphology when cultured and were regarded as 'variations of a single cell type' (Carrel and Ebeling, 1926). Later experiments confirmed a likely bone marrow origin of macrophages in 1963 (Balner, 1963). Using mouse bone marrow chimeras and antibodies against donor bone marrow cells, host peritoneal macrophages were demonstrated to be of donor origin. Collectively, these studies led to the belief that these highly phagocytic mononuclear phagocytes are developmentally related. It was proposed mononuclear phagocytes originated from the bone marrow, travel to the tissues via the bloodstream where they become tissue macrophages. In 1969, Zanvil Alexander Cohn, Ralph van Furth and James Gerald Hirsch used this evidence to define the 'mononuclear phagocyte system' (MPS) (van Furth *et al.,* 1972, 1970).

In 1970, Emil R. Unanue introduced the idea of macrophages presenting antigen to lymphocytes (Unanue and Cerottini, 1970). Later, Ralph Steinman identified a novel cell type with a stellate morphology amongst adherent mononuclear phagocytes which he called dendritic cells (Steinman and Cohn, 1973). A series of papers describing and characterising these cells were published in the Journal of Experimental Medicine from 1973-1975. These cells were the unique potent activators of naïve T cells in comparison to other antigen presenting cells (Steinman and Witmer, 1978) and were regarded as 'accessory' cells that linked innate and adaptive immunity (Nussenzweig and Steinman, 1980; Steinman *et al.,* 1983). van Furth soon recognised these cells as a member of the MPS resulting in the current definition of mononuclear phagocytes to date.

1.3 Macrophages

Following the Conference on Mononuclear Phagocytes in Leiden in 1969, Ralph van Furth and colleagues proposed that '*free*' or '*fixed*' macrophages are '*probably of monocytic origin*' which '*originate from precursor cells in the bone marrow, transported via the peripheral blood as monocytes*' (van Furth *et al.,* 1972). Studies have now challenged this current textbook definition and prompted the need to redefine the MPS.

1.3.1 Macrophage nomenclature

As the name suggests, tissue resident macrophages reside throughout the body in various organs. Macrophage nomenclature is primarily based on anatomical location or after the scientist who discovered the macrophage population e.g. microglia in the brain, Kuppfer cells in the liver, osteoclasts in the bone and Langerhans cells in the skin. Macrophages from specific tissues exhibit unique a gene expression profile dictated by their microenvironment (Lavin *et al.,* 2014). As a result, genes specific for various macrophage populations have been identified, *sall1* expression is specific to microglia (Buttgereit *et al.,* 2016) while *spi-c* expression identifies splenic macrophages (Kohyama *et al.,* 2009) and *clec4f* finds Kuppfer cells (Scott *et al.,* 2016).

1.3.2 Embryonic origin of macrophages

It is a widely held view that monocytes are circulating precursors to tissue resident macrophages and DC. At the same time van Furth proposed the majority of macrophages are repopulated from monocytes (van Furth *et al.,* 1972), studies observed macrophage development in the yolk sac prior to bone marrow haematopoiesis (Cline and Moore, 1972; Takahashi, 1989). Cline and Moore suggested these yolk sac macrophages develop via monocytes, however, with the introduction of electron microscopy, yolk sac macrophages were observed to appear one day prior to monocytes (Takahashi, 1989). This was one of the earliest studies to report macrophage development independent of monocytes.

Haematopoiesis occurs in successive waves within the developing embryo, initially occurring in the extra-embryonic yolk sac before transferring to the fetal liver until birth where haematopoiesis is ultimately transferred to the bone marrow and spleen. Primitive haematopoiesis begins in the yolk sac, where erythromyeloid progenitors (EMP) give rise to erythrocytes, macrophages and mast cells (Palis *et al.,* 1999). Recent studies have reported a pre-macrophage precursor downstream of the EMP, which arises in the yolk sac before colonising embryonic tissues around embryonic day 9.5 (E9.5) at the same time as organogenesis (Mass *et al.,* 2016). Pre-macrophages are subjected to tissue-specific signals, which sculpt a specific tissue-resident macrophage phenotype (Lavin *et al.,* 2014).

The development of hematopoietic stem cell (HSC) lineages within the fetal liver marks the onset of definitive haematopoiesis. The distinction of yolk sac derived macrophages and fetal liver derived macrophages can be distinguished by the transcription factor, Myb, which is indispensable for HSC development (Schulz *et al.,* 2012). In *Myb*$^{-/-}$ mice, macrophages of yolk sac origin were still present in the skin, spleen, pancreas, kidney and lung, whereas HSC-derived cells were absent (Schulz *et al.,* 2012), demonstrating the distinction between yolk sac derived macrophages and HSC derived cells.

Genetic fate-mapping techniques have also supported the observation that the majority of tissue-resident macrophages are embryonically derived (Epelman *et al.,* 2014; Ginhoux *et al.,* 2010; Hashimoto *et al.,* 2013; Schulz *et al.,* 2012; Yona *et al.,* 2013). Ginhoux and colleagues established that microglia are exclusively yolk sac derived and are subsequently maintained during adulthood through longevity and self-renewal (Ginhoux *et al.,* 2010) (**Figure 1.2**). This study took advantage of the runt-related transcription factor 1 (Runx1) where its expression is restricted to the yolk sac during E6.5 and E8 before the development of definitive haematopoiesis, therefore allowing the origin of yolk sac derived macrophages to be fate mapped. Interestingly, the origin of the Langerhans cells (the macrophages of the epidermal layer of skin) was also examined using *Runx1*^{CreER} mouse model and shown to have a dual origin

from both yolk sac and fetal liver (Hoeffel *et al.,* 2012). These embryonic macrophages can persist throughout life with very little or no monocyte input depending on the tissue compartment (Hashimoto *et al.,* 2013; Liu *et al.,* 2019; Yona *et al.,* 2013).

Examples from the human setting have also demonstrated the longevity of macrophages. Patients deficient in monocytes and other bone marrow-derived cells retain normal Langerhans cells and other tissue macrophage populations, suggesting that the development of these populations is independent of bone marrow-derived monocytes (Bigley *et al.,* 2011). Interestingly, donor alveolar macrophages have been observed three and a half years later in patients with lung transplants (Nayak *et al.,* 2016). Similar observations have been noted for Langerhans cells. Following human hand allograft, Langerhans cells remained of donor origin when examined ten years following transplantation (Kanitakis *et al.,* 2011).

These studies challenge the current view of the MPS as macrophages can arise and are independently maintained of monocytes, at least under steady-state. However, there are exceptions to this rule. Some embryonic macrophages are not maintained and are replaced by bone marrow derived monocytes where they rely on a continuous influx of these cells for replenishment (Bain *et al.,* 2014; Epelman *et al.,* 2014; Liu *et al.,* 2019; Mossadegh-Keller *et al.,* 2017; Tamoutounour *et al.,* 2013; Zigmond *et al.,* 2012) (**Figure 1.2**). It is unclear why some embryonic macrophages persist in some tissues and are replaced in others. One hypothesis may be that low grade inflammation at the tissue is responsible for monocyte recruitment, as germ-free mice exhibit reduced numbers of monocyte derived macrophages (Bain *et al.,* 2014). Alternatively, tissue specific microenvironments could affect the competitive nature of monocytes vs macrophages, as fetal liver monocytes outcompete yolk sac derived macrophages and adult bone marrow monocytes when populating the alveolar macrophage compartment (van de Laar *et al.,* 2016). This has led to the introduction of the macrophage niche theory, where monocytes can compete with self-renewing macrophages to fill a vacant position (Guilliams and Scott, 2017). Alternatively, these embryonic macrophages may only be necessary during

embryonic development after which they are replaced by monocytes which are more suitably adapted for adulthood (Machiels *et al.,* 2017). Finally, it is possible that as organs grow and develop, more available niches are available which are readily filled by monocytes.

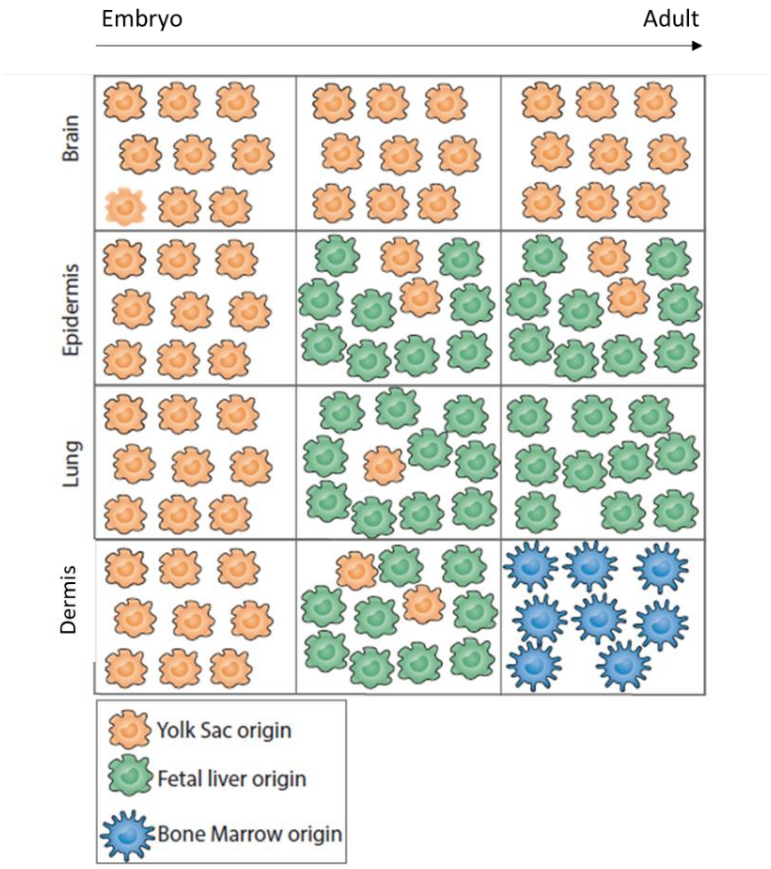

Figure 1.2 **Macrophage Ontogeny**

Tissue macrophage compartments can be composed of three major sources. Tissue resident macrophages are initially laid down by yolk sac progenitors. In some tissues (i.e. microglia of the brain), these macrophages persist. Following the onset of definitive haematopoiesis, fetal liver monocytes can compete and replace macrophages of yolk sac origin as observed for Langerhans of the skin and lung alveolar macrophages. Finally, embryonic macrophages can be replaced by adult bone marrow monocytes as observed for dermal $CD14^{+}$ cells (From Patel and Yona, 2018).

1.3.3 Macrophage function

1.3.3.1 Homeostatic functions

Given the distinction between the precursor-product relationship between macrophages and monocytes, attention soon focused on the function of embryonic macrophages. Aside from their role in immune defence, macrophages play a key role in tissue homeostasis and organogenesis (Mass *et al.,* 2016). Microglia are vital in synaptic pruning during development, as their absence results in neurological disorders (Paolicelli *et al.,* 2011). The role of macrophage colony-stimulating factor (M-CSF) or colony-stimulating factor 1 (CSF1) in macrophage maintenance is appreciated in *Csf1*$^{-/-}$ and *Csfr1*$^{-/-}$ mice, otherwise known as osteopetrotic mice. As the name suggests, these mice lack osteoclasts resulting in skeletal deformities ultimately leading to osteopetrosis (Dai *et al.,* 2002; Ryan *et al.,* 2001). Splenic red pulp macrophages are necessary for phagocytosis of senescent red blood cells (Kohyama *et al.,* 2009), similarly, alveolar macrophages play an important role in clearing surfactant, the build-up of which leads to pulmonary alveolar proteinosis (van de Laar *et al.,* 2016). Perhaps a common function of all macrophages taken for granted is the continual clearance of apoptotic cells (Roberts *et al.,* 2017). Collectively these studies demonstrate the developmental and homeostatic functions of macrophages under steady physiological conditions.

As macrophage ontogeny has gained a considerable amount of attention over the last few years, it is equally as important to know whether ontogeny dictates function. In the case of alveolar macrophages, yolk sac derived macrophages, fetal liver and bone marrow derived macrophages exhibited similar gene expression profiles and could clear surfactant to prevent alveolar proteinosis (van de Laar *et al.,* 2016). On the other hand, it is possible embryonic macrophages cannot perform similar functions to monocyte-derived macrophages as others have found that monocyte derived alveolar macrophages could prevent allergy-induced asthma unlike those of embryonic origin (Machiels *et al.,* 2017). It is possible that ontogeny alone does not dictate function, and the distinction in function may be appreciated during inflammation.

Macrophages are recognised as highly plastic cells. Consequently, it has been examined whether macrophages from one tissue can be re-programmed when placed into a different tissue site. The transfer of peritoneal macrophages into the lung resulted in a change of the gene expression profile closely resembling that of lung macrophages (Lavin *et al.,* 2014). However, others have demonstrated that transferring peritoneal macrophages, Kupffer cells or colon macrophages into the lung did not clear surfactant as efficiently as bona fide alveolar macrophages (van de Laar *et al.,* 2016), suggesting irreversible programming of tissue resident macrophage function.

1.3.3.2 Inflammatory functions

In addition to performing homeostatic functions, resident macrophages are located at tissue sites to detect infection and injury and contribute to the initiation of the immune response. The role of macrophages as sentinel cells can be appreciated following their depletion in a model of acute peritonitis which resulted in a blunted infiltration of polymorphonuclear cells (Cailhier *et al.,* 2005). Interestingly, it has recently been shown following smaller microlesions that macrophages 'cloak' these areas to prevent excess neutrophil-driven tissue damage leading to inflammation (Uderhardt *et al.,* 2019).

Surprisingly, following the initiation of the immune response, a reduction in macrophages occurs, a phenomenon known as the 'macrophage disappearance reaction' first described in 1963 (Barth *et al.,* 1995; Nelson, 1963). During zymosan-induced peritonitis, a reduced recovery of resident macrophages was reported (Davies *et al.,* 2013; Zhang *et al.,* 2019). This observation has been extended to other tissues, where fewer numbers of alveolar macrophages are found following influenza challenge (Lauder *et al.,* 2011). The reason for the macrophage disappearance has recently been explored by Zhang and colleagues, where macrophages form clots and adhere to tissues resulting in reduced recovery of these cells (Zhang *et al.,* 2019). Coagulation factors have been implicated as the use of anticoagulants and the knockout of coagulation factors do not result in macrophage disappearance. The fate of these macrophage clots remains unclear. During the resolution phase of inflammation, recovery of resident

macrophage numbers may occur by proliferation (Davies *et al.,* 2011) or by repopulation of monocyte-derived cells as discussed below (Section 1.4.4). An exception to the macrophage disappearance paradigm can be observed in T helper cell (Th) type 2 immune response, where tissue resident macrophages proliferate in an interleukin (IL)-4 dependent manner to overcome helminth infections without the need of monocyte input (Jenkins *et al.,* 2011).

Controversially, macrophages have been categorised depending on their activation state, as either classically (M1) or alternatively (M2) activated, initially proposed by Charles Mills (Mills *et al.,* 2000). Put simply, M1 macrophages have been referred to as 'fight and kill' whereas M2 macrophages 'fix and heal' (Mills, 2012). Since, Mantovani and colleagues have described further macrophages states (M2a, M2b, M2c) to account for the spectrum of activation observed from various stimuli (Mantovani *et al.,* 2004). It is unlikely macrophages behave in this binary manner and are instead a heterogeneous group of cells that exist in various states *in vivo*. It has been demonstrated that genes associated with M2 macrophages induced by IL-4 or IL-13 *in vitro*, were not identified in the *in vivo* setting and vice versa (Hassanzadeh Ghassabeh *et al.,* 2006). Most importantly, the M1/M2 nomenclature system was initially proposed for bona fide macrophages isolated from murine tissue, however, for feasibility in humans, this has been extended to *in vitro* cultures of monocyte-derived cells. As described below (Section 1.4.4), functional differences exist between bona-fide macrophages and monocyte-derived cells during inflammation, therefore such nomenclature system proposed for macrophages has resulted in confusion within the field.

1.4 Determining myeloid fate

In contrast to macrophages, monocytes and DC are continuously produced from bone marrow precursors. Definitive haematopoiesis is marked by the generation of HSC within the fetal liver up until birth where it is then transferred to the bone marrow. In a simplistic model, HSC give rise to progeny that progressively become more and more restricted towards a single lineage whilst losing their ability for self-renewal. The immediate successor to HSC are multipotential progenitors which at this stage develop down a myeloid or lymphoid route, via common myeloid progenitors (CMP) or common lymphoid progenitors (CLP), respectively (Akashi *et al.,* 2000; Kondo *et al.,* 1997). CLP give rise to lymphoid blood cells including T, B and natural killer (NK) cells but lack the ability to mature into myeloerythoid cells, whereas CMP give rise to megakaryocyte-erythroid progenitors or granulocyte and macrophage progenitors (GMP) (Iwasaki and Akashi, 2007).

1.5 Monocytes

1.5.1 Monocyte subsets

The term 'monocyte' was introduced as early as 1910 by Artur Pappenheim (Pappenheim and Ferrata, 1910). Following the initial recognition of monocytes by microscopy, with the advent of polychromatic flow cytometry, human monocytes were demonstrated to express high levels of the lipopolysaccharide (LPS) co-receptor, CD14 (Griffin *et al.,* 1981). It was later identified in 1989, that $CD14^+$ monocytes, could be further subdivided by differential expression of CD16 (Fcγ receptor III) (Passlick *et al.,* 1989). This enabled the classification of three principal human monocyte subsets: $CD14^+$ $CD16^-$ monocytes, also referred to as ''classical'' monocytes, $CD14^+$ $CD16^+$ ("intermediate") and $CD14^{lo}$ $CD16^+$ (''non-classical'') monocytes. Monocyte heterogeneity also exists in other species, including, mice, rats, pigs and cows (Ziegler-Heitbrock, 2014).

In mice, CX_3CR1 expression in *Cx3cr1*^{gfp} mice led to the identification of CX_3CR1^{lo} $Ly6C^{hi}$ classical and CX_3CR1^{hi} $Ly6C^{lo}$ non-classical monocytes (Geissmann *et al.,* 2003). Since, additional markers

have been shown to be differentially expressed between human and mouse monocyte subsets (Cros *et al.,* 2010; Damasceno *et al.,* 2016; Ingersoll *et al.,* 2010).

While it is accepted that three human monocytes subsets exist, further subsets have been described. Human non-classical monocytes can be divided further by 6-sulfo LacNAc (SLAN) expression, which is a carbohydrate modification of P selectin glycoprotein ligand 1 (PSGL-1) (Cros *et al.,* 2010; Schäkel *et al.,* 2002, 1999, 1998). With advances in technology, the introduction of single cell RNA-sequencing has allowed for the unbiased identification of further heterogeneity within the intermediate population (Villani *et al.,* 2017). Mass cytometry analysis of human monocytes has also resulted in the identification of eight monocyte subsets (Hamers *et al.,* 2019). It now remains to be shown whether functional differences exist between these proposed subsets. In mice, heterogeneity has also been observed amongst classical monocytes (Menezes *et al.,* 2016; Yáñez *et al.,* 2017), where two developmental routes have been proposed which result in neutrophil-like and dendritic cell-like classical monocytes which are differentially generated depending on the microbial stimuli (Yáñez *et al.,* 2017). However, phenotypic markers are lacking to distinguish the two populations within the pool of Ly6C^{hi} classical monocytes. Similarly, a population of YM1^{+} Ly6C^{hi} monocytes with immunoregulatory phenotype are greatly expanded in the bone marrow, blood and spleen of mice following intravenous challenge with LPS, which are not detected under steady-state conditions (Ikeda *et al.,* 2018). Furthermore, during fibrosis, a novel Ly6C^{lo} monocyte subset is present only under inflammatory conditions (Satoh *et al.,* 2017). These segregated nucleus-containing atypical Ly6C^{lo} (SatM) monocytes do not arise from the conventional monocyte/DC progenitor (MDP) differentiation route and do not arise from Ly6C^{hi} progenitors. Collectively these studies suggest haematopoiesis under inflammatory conditions may deviate from the conventional pathway of monocyte development and warrants the need for further studies to investigate monocyte heterogeneity.

1.5.2 Ontogeny and Development

The MDP gives rise to monocytes and DC but lacks neutrophil potential in mice (Bajaña *et al.,* 2012) and humans (Lee *et al.,* 2015). The MDP is the predecessor to the common DC precursor (CDP) and the common monocyte progenitor (cMoP) (**Figure 1.3**). cMoP are restricted to the development of monocytes in mice (Hettinger *et al.,* 2013) and humans (Kawamura *et al.,* 2017). Commitment to monocyte development at the cMoP stage is dependent on the transcription factor, interferon-regulatory factor (IRF)8 (Sichien *et al.,* 2016). This is consistent with the observation in patients bearing mutations in IRF8 who are also deficient of circulating monocytes (Hambleton *et al.,* 2011). IRF8 is thought to regulate the *Klf4* gene, indicated by the absence of *Klf4* mRNA in Irf8-deficient mice and that *Klf4*$^{-/-}$ fetal liver cells gave rise to very few classical monocytes (Alder *et al.,* 2008), a phenotype reminiscent of Irf8-deficient mice. Upon the introduction of *Klf4* mRNA into these mice, monocyte differentiation was partially rescued (Kurotaki *et al.,* 2013).

After the generation of bone marrow monocytes, these cells will eventually egress into the circulation. Recently, a transitional pre-monocyte population was described within the bone marrow defined by CXCR4 expression. CCR2^{lo} CXCR4^{hi} Ly6C^{hi} classical monocytes arise from cMoP where CXCR4 prevents egression into the bone marrow (Chong *et al.,* 2016; Jung *et al.,* 2015). These cells mature into CCR2^{hi} CXCR4^{lo} Ly6C^{hi} monocytes before they are released into the circulation in a CCR2-dependent manner (Serbina and Pamer, 2006).

Given the heterogeneity of monocyte subsets, their relationship to one another has been thoroughly investigated in mice. It is widely acknowledged Ly6C^{hi} classical monocytes are precursor cells to Ly6C^{lo} non-classical monocytes (Hettinger *et al.,* 2013; Liu *et al.,* 2019; Mildner *et al.,* 2017; Varol *et al.,* 2007; Yona *et al.,* 2013). Adoptive transfer experiments confirmed the developmental relationship between these cells (Mildner *et al.,* 2017; Varol *et al.,* 2007). The generation of Ly6C^{lo} non-classical monocytes is thought to occur both in the bone marrow and blood from classical monocytes (Yona *et al.,* 2013). In humans, the relationship between

monocyte subsets has not been investigated, though it is hypothesised a similar relationship exists: a question this thesis aims to address.

Studies have also investigated the signals which trigger this development. The maturation of classical monocytes into non-classical monocytes is partially facilitated via delta-like ligand 1 (DLL-1) ligation with Notch2 (Gamrekelashvili *et al.,* 2016). The expression of DLL-1 is enriched on endothelial cells found within vascular niches in the bone marrow and spleen (Gamrekelashvili *et al.,* 2016), where classical monocytes in contact with these vessels are required for maturation into non-classical monocytes (Bianchini *et al.,* 2019). Studies have also identified transcription factors that are important in completing this conversion. Mildner and colleagues observed that C/EBPβ expression gradually increases during the conversion from Ly6C^{hi} classical monocytes to Ly6C^{lo} non-classical monocytes and also following the adoptive transfer of classical Ly6C^{hi} monocytes (Mildner *et al.,* 2017). Mice lacking this transcription factor are characterised by an absence of non-classical monocytes. *Nr4a1* (*Nur77*) is one of the genes regulated by C/EBPβ (Mildner *et al.,* 2017), which is an essential survival factor of non-classical monocytes (Hanna *et al.,* 2011). Nr4a1-deficient mice exhibit high rates of apoptosis of bone marrow non-classical monocytes and are therefore characterised by a strong reduction of this monocyte subset in the circulation (Hanna *et al.,* 2011). While these experiments implicate a role for the C/EBPβ-NR4A1 axis in non-classical monocyte development and survival, other studies have suggested additional pathways of Nr4a1 regulation. Klf2 has been demonstrated to regulate *Nr4a1* expression via the enhancer 2 domain, which is specific for non-classical monocyte development (Thomas *et al.,* 2016). Therefore, it appears that multiple non-redundant mechanisms are required for the progression of monocyte development and maintenance. In humans, expression of NR4A1 and KLF2 have been detected in non-classical monocytes (Thomas *et al.,* 2016), therefore, similar mechanisms of monocyte regulation may be conserved across species.

1.5.3 Homeostatic function of Monocytes

Not all embryonic macrophages persist throughout adulthood, therefore these compartments rely on a constant replenishment. This role has been ascribed to classical monocytes (Bain *et al.,* 2014; Epelman *et al.,* 2014; Kim *et al.,* 2016; Liu *et al.,* 2019; Mossadegh-Keller *et al.,* 2017; Tamoutounour *et al.,* 2013). Furthermore, others have also described the ability of classical monocytes to enter tissues where they can survey the tissues and recirculate to lymph nodes whilst maintaining their blood phenotype (Jakubzick *et al.,* 2013). On the other hand, non-classical monocytes reside within the circulation where they crawl along the endothelium in a lymphocyte function-associated antigen 1 (LFA-1) dependent manner surveying for damage (Auffray *et al.,* 2007; Carlin *et al.,* 2013), hence earning the name 'patrolling' monocytes.

1.5.4 Inflammatory function of Monocytes

As early as 1939, monocytes were observed to extravasate in response to tissue injury, where they mature into monocyte-derived cells (Ebert and Florey, 1939). Ly6C^{hi} classical monocytes are typically referred to as 'inflammatory' monocytes, as they preferentially home to inflamed tissues and mature into monocyte-derived cells (Geissmann *et al.,* 2003).

CCR2-deficient mice lack circulating Ly6C^{hi} classical monocytes and exhibit a reduction in Ly6C^{lo} non-classical monocytes, therefore can be used examine the relevance of monocytes at sites of inflammation (Nahrendorf *et al.,* 2007; Serbina and Pamer, 2006; Tsou *et al.,* 2007). In the absence of CCR2^{+} monocytes, an increased burden of bacterial infection has been observed and these mice are unable to clear the infection (Kurihara *et al.,* 1997; Serbina *et al.,* 2003). While CCR2 is required for the bone marrow egression of monocytes, the question arises whether a similar mechanism occurs for blood to tissue infiltration. Studies suggest that the early infiltration of monocytes is CCR2-dependent whereas later stages are CCR2-independent (Serbina and Pamer, 2006; Swirski *et al.,* 2009; Tsou *et al.,* 2007; Zigmond *et al.,* 2012).

It was initially proposed that monocytes infiltrate in a biphasic manner, initially by Ly6C^{hi} monocytes and later by Ly6C^{lo} monocytes into the myocardium after myocardial infarction (Nahrendorf *et al.,* 2007). Later studies demonstrated the Ly6C^{lo} phenotype was in fact due to in situ conversion from Ly6C^{hi} monocyte-derived cells (Hilgendorf *et al.,* 2014). Similar observations have been made *in vivo* during sterile hepatic injury (Dal-Secco *et al.,* 2015). Once classical monocytes enter tissues they initially take on a proinflammatory phenotype and later mature into an anti-inflammatory phenotype (Arnold *et al.,* 2007; Hilgendorf *et al.,* 2014; Nahrendorf *et al.,* 2007; Zigmond *et al.,* 2012). In a model of skeletal injury, Arnold and colleagues have demonstrated pro-inflammatory monocytes derived cells express high levels of tumour necrosis factor alpha (TNFα) and IL-1β mRNA transcripts and later mature into cells that stimulate myogenesis and fibre growth to restore muscle structure (Arnold *et al.,* 2007).

As classical monocyte-derived cells downregulate Ly6C and upregulate CX_3CR1 (Dal-Secco *et al.,* 2015; Zigmond *et al.,* 2012), they are difficult to distinguish from non-classical monocytes and their progeny. However, the use of Nr4a1-deficient mice (Hanna *et al.,* 2011), has allowed studies to examine the contribution of non-classical monocytes in inflammation. It has since been shown, Ly6C^{lo} non-classical monocytes limit the accumulation of amyloid beta in Alzheimer's disease (Michaud *et al.,* 2013). Additionally, in the absence of non-classical monocytes, increase tumour metastasis to the lung was observed (Hanna *et al.,* 2015), under normal conditions these cells would recruit and activate NK cells. Pro-inflammatory functions have also been attributed to non-classical monocytes where they drive the development of rheumatoid arthritis (Misharin *et al.,* 2014). Specifically, following depletion of monocytes, transfer of non-classical monocytes led to an increase in ankle thickening and increased clinical score in these mice compared to classical monocytes. Of note, Nr4a1 is also expressed in macrophages (Hilgendorf *et al.,* 2014), therefore Thomas and colleagues have generated mice with E2-domain deficiency of *Nr4a1*, allowing for the specific ablation of non-classical

monocytes while preserving the inhibitory effects of Nr4a1 on macrophage function (Thomas *et al.,* 2016).

Regarding the fate of monocyte-derived cells following inflammation, a number of studies have demonstrated engraftment into the long-lived macrophage pool. In models of peritonitis, it has been demonstrated monocyte derived cells persist in tissues up to 8 weeks, where their phenotype gradually changes into that of resident macrophages (Newson *et al.,* 2014; Yona *et al.,* 2013). Similar observations have been extended to the liver (Blériot *et al.,* 2015) and lung (Machiels *et al.,* 2017; Misharin *et al.,* 2017). Expectedly, exceptions have been observed where following infection with influenza or LPS, recruited monocyte derived cells are cleared in a Fas-dependent manner (Janssen *et al.,* 2011). In addition, in mouse models of experimental allergic encephalomyelitis, monocyte-derived cells do not contribute to the resident microglia pool (Ajami *et al.,* 2011). The macrophage niche theory proposes that a niche is filled by the competition between an embryonic macrophage or monocyte derived cell (Guilliams and Scott, 2017), and the tissue specific microenvironment may dictate this result accounting for these discrepancies between tissues.

In the above scenarios where monocyte derived cells persist, one can question whether monocyte-derived cells exhibit the same function as their embryonically derived counterparts. 10 months following the engraftment of monocyte derived cells into the lung, these cells were very similar to alveolar macrophages and only exhibited a difference of 330 differentially expressed genes (Misharin *et al.,* 2017). In a separate study, replacement of alveolar macrophages with monocyte-derived cells in response to herpesvirus resulted in protection against house dust mite induced asthma (Machiels *et al.,* 2017). Whereas, mice exposed to only house dust mite developed allergic asthma. These studies demonstrate, in addition to ontogeny, the context in which monocytes are recruited and the type of stimuli may also shape the function of these cells.

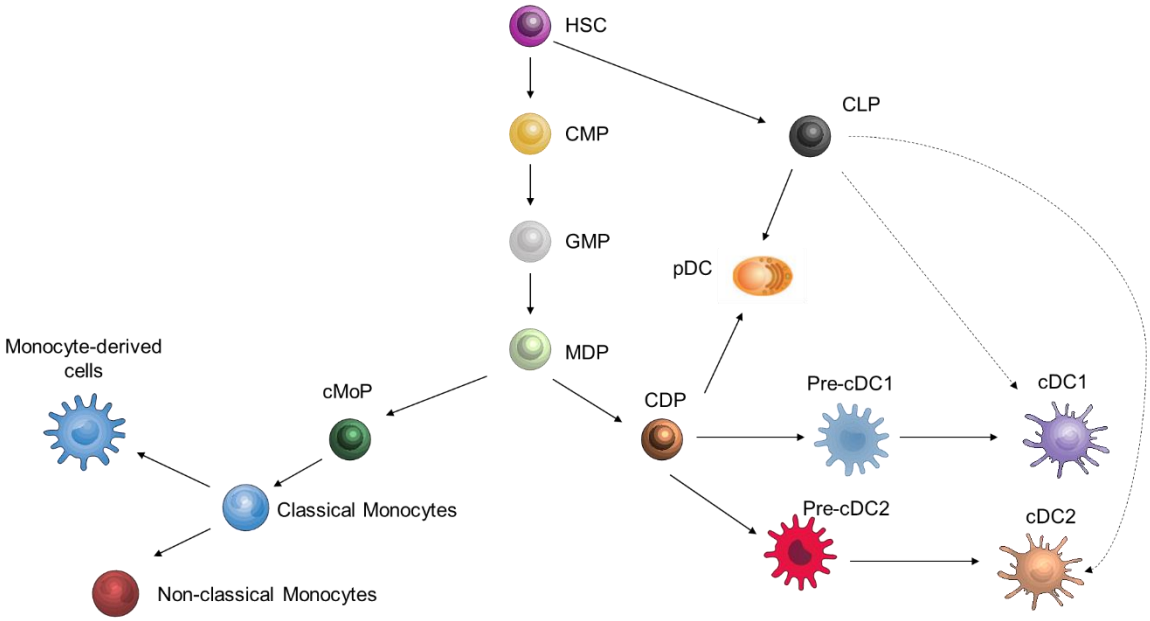

Figure 1.3 **Steady-state monocyte and dendritic cell development**

Monocyte and dendritic cells diverge at the monocyte/dendritic cell precursor (MDP) stage. The common monocyte progenitor (cMoP) give rise exclusively to monocytes and their derivatives. The common dendritic cell progenitor (CDP) produces cDC1, cDC2 and pDC, however these cells are thought to also have lymphoid contribution. Hematopoietic stem cell (HSC), common myeloid progenitor (CMP), common lymphoid progenitor (CLP), granulocytes/macrophage progenitor (GMP).

1.6 Dendritic Cells

Following their discovery in the early 1970s, dendritic cells (DC) are now recognised for their ability to prime naïve T cells and are regarded as the bridging cell between innate and adaptive immunity. DC express high levels of major histocompatibility complex (MHC) I and II molecules, a key molecule needed to initiate T cell responses (Nussenzweig *et al.,* 1980; Steinman *et al.,* 1979). Studies from Nussenzweig and Steinmann demonstrated that activation of T cells with DC was far more potent than any other antigen presenting cell or lymphoid cells (Nussenzweig *et al.,* 1980). Consequently, this raises the question of why DC are more primed to activating T cells. DC possess lower amounts of lysosomal proteases in comparison to macrophages (Delamarre *et al.,* 2005) which may be reflected in the partial hydrolysis of proteins (Chain *et al.,* 1986), needed for efficient MHC presentation. In addition, differences in the pH of phagocytic vacuole between DC and monocyte-derived cells might consequently influence enzyme activity involved in antigen presentation (Foote *et al.,* 2019).

1.6.1 Murine DC subsets

Following the identification of DC, splenic and thymic DC were demonstrated to be a heterogeneous population composed of multiple subsets that can be distinguished by CD4 and CD8 expression (Ardavin and Shortman, 1992; Vremec *et al.,* 1992). To date, two major branches of DC have been described; classical DC (cDC) and plasmacytoid DC (pDC). In mice, cDC are composed of two subsets characterised by their expression of CD8α and CD103 or CD11b expression depending on their location in lymphoid or nonlymphoid tissues (**Table 1.1**). Within the literature lymphoid DC are regarded as resident DC, whereas non-lymphoid DC are also known as migratory DC. To avoid confusion, DC subsets are divided into three major subsets pDC, cDC1 or cDC2 (**Table 1.1**). Of note, cDC2 heterogeneity has been noted, where Notch2-dependent (Lewis *et al.,* 2011; Satpathy *et al.,* 2013) and Klf4-dependent (Tussiwand *et al.,* 2015) subsets have been described.

	Human	Mouse	
		Lymphoid tissue	Nonlymphoid tissue
cDC1	CD141$^+$ CLEC9a$^+$	CD8$^+$	CD103$^+$
cDC2	CD1c$^+$	CD11b$^+$	CD11b$^+$

Table 1.1 **Classical dendritic cell subsets**

Classical dendritic cell (cDC) are divided into cDC1 and cDC2 in humans and mice and can be identified by the expression of surface markers listed.

1.6.2 Human DC subsets

Circulating human DC were first identified in 1982 (Van Voorhis *et al.,* 1982). Three major human DC subsets have been described: cDC1, cDC2 and pDC, which have been approved by the Nomenclature Committee of the International Union of Immunological Societies (Guilliams *et al.,* 2016; Ziegler-Heitbrock *et al.,* 2010) (**Figure 1.3 and Table 1.1**). Homology is conserved from mice to humans. Studies have aligned human blood and tissue CD141$^+$ DC with that of lymphoid CD8α$^+$ and non-lymphoid CD103$^+$ DC in mice (Bachem *et al.,* 2010; Haniffa *et al.,* 2012). Similarly, human CD1c$^+$ DC lies in close alignment with murine CD11b$^+$ DC (Haniffa *et al.,* 2012; Schlitzer *et al.,* 2013). Whereas cDC were first discovered in the mouse spleen (Steinman and Cohn, 1973), pDC were first described in humans as interferon (IFN) producing cells (Feldman and Fitzgerald-Bocarsly, 1990; Perussia *et al.,* 1985; Siegal *et al.,* 1999) and later identified in mice (Asselin-Paturel *et al.,* 2001).

Further heterogeneity exists within the human cDC2 and pDC compartment (Dutertre *et al.,* 2019; See *et al.,* 2017; Villani *et al.,* 2017). Recently, cDC2 have been shown to consist of four novel subsets (Dutertre *et al.,* 2019), and the pDC population is composed of a bona fide pDC and a newly described pre-DC population capable of maturing into both cDC1 and cDC2 (See *et al.,* 2017; Villani *et al.,* 2017). The distinction between pre-DC and pDC can be appreciated in patients with Pitt-Hopkins syndrome who suffer from haploinsufficiency of *TCF4* which encodes

the gene, E2-2, specific for pDC development (Cisse *et al.,* 2008; Ghosh *et al.,* 2010). These patients have a significant reduction in circulating pDC yet pre-DC remain unaffected (See *et al.,* 2017), highlighting the distinct lineage of the two subsets. Given the recent identification of these cells, little is known regarding their fate and function.

1.6.3 Ontogeny and Development

DC development relies on fms-like tyrosine kinase 3 (Flt3) expression on HSC and DC precursors, as Flt3-deficient mice exhibit a reduction of pDC and cDC in secondary lymphoid organs while other myeloid cells are unaffected (Waskow *et al.,* 2008). Whether DC are derived from lymphoid or myeloid progenitors remains unclear. Both lymphoid and myeloid precursors can give rise to DC as demonstrated by adoptive transfer of CMP and CLP (Manz *et al.,* 2001; Traver *et al.,* 2000). However, studies have demonstrated that CMP produced the majority of cDC subsets, as they are more abundant than CLP (Manz *et al.,* 2001). Similarly, fate-mapping studies examining the origins of T cells, simultaneously demonstrated that approximately 10% of cDC were of lymphoid origin (Schlenner *et al.,* 2010). In contrast, human CLP have been described to efficiently produce cDC1 in comparison to CMP, though no functional or gene differences were observed between the sources of cDC1 (Helft *et al.,* 2017). It is possible that DC developmental cannot be categorised into the conventional myeloid or lymphoid pathway.

A major breakthrough in understanding DC development stemmed from the discovery of the MDP that gives rise exclusively to monocytes and DC (Bajaña *et al.,* 2012). However, it was the discovery of the CDP downstream of the MDP that gives rise exclusively to pDC and cDC but not monocytes (Lee *et al.,* 2015; Liu *et al.,* 2009; Onai *et al.,* 2007) that established DC to have their own lineage. Intermediates between the CDP and cDC have been identified as the cDC precursor (pre-cDC) which enter the circulation and develop into cDC upon entering the peripheral tissues (Donnenberg *et al.,* 2001; Ginhoux *et al.,* 2009; Liu *et al.,* 2009; Naik *et al.,* 2007, 2006; O'Keeffe *et al.,* 2003). The commitment to a cDC1 or cDC2 has been proposed to occur within the bone marrow at the pre-DC stage, where pre-cDC1 and pre-cDC2 progenitors have been identified

(Cabeza-Cabrerizo *et al.,* 2019; Grajales-Reyes *et al.,* 2015; Naik *et al.,* 2007, 2006; Schlitzer *et al.,* 2015; Sichien *et al.,* 2016). In humans, both pre-cDC and cDC coexist within the circulation (See *et al.,* 2017; Villani *et al.,* 2017), the contribution of both these populations to tissue cDC remains to be fully resolved. On the other hand, pDC are found as mature cells within the bone marrow (Onai *et al.,* 2013; Rodrigues *et al.,* 2018).

1.6.3.1 pDC vs cDC commitment

The discovery of the CDP and DC precursors demonstrated these cells were restricted to pDC and cDC lineages (Liu *et al.,* 2009; Naik *et al.,* 2007; Onai *et al.,* 2007). Consequently, emphasis on myeloid origin was assumed for pDC and cDC which were believed to diverge at this stage.

pDC highly express the transcription factor E2-2 in comparison to lymphocytes, monocytes and cDC (Cisse *et al.,* 2008). Mice harbouring a mutation in the *E2-2* gene show a significant reduction in pDC, whereas other cells remain unaffected supporting a role for E2-2 in pDC maintenance. E2-2 itself is regulated by various transcription factors including Id2 found in cDC, which prevents E2-2 binding to enhancer sequences (Cisse *et al.,* 2008), thereby favouring the cDC developmental path. Further upstream, the transcription factor Zeb2 represses Id2, consequently allowing E2-2 to promote pDC development (Scott *et al.,* 2016). Taken together, these studies highlight the roles of Zeb2, E2-2 and Id2 in pDC and cDC development.

These studies may represent one branch of the pDC lineage. Akin to cDC, lymphoid origin of pDC has been described by several studies (Dress *et al.,* 2019; Onai *et al.,* 2013; Rodrigues *et al.,* 2018), where over 80% of pDC have been observed to be lymphoid derived (Schlenner *et al.,* 2010). Amongst the bone marrow $Flt3^+$ population, an IL-$7R\alpha^+$ population has been described as the major source of pDC in comparison to myeloid CDP route (Dress *et al.,* 2019; Onai *et al.,* 2013; Rodrigues *et al.,* 2018). Similarly, DNGR-1 fate mapping demonstrated successful labelling along the CDP-cDC axis but labelled pDC to a lesser extent (Schraml *et al.,* 2013).

Evidence for the dual origin of pDC can be appreciated where lymphoid derived pDC express recombination-activation genes and therefore demonstrate D_H-J_H recombination, whereas CDP-derived pDC lack this enzyme and consequently no gene rearrangement was observed (Onai *et al.,* 2013; Pelayo *et al.,* 2005). Collectively, these studies demonstrated that pDC are predominantly lymphoid derived yet are still considered as DC for the time being.

1.6.3.2 cDC1 development

In mice, the development of cDC1 is regulated by numerous transcription factors including Id2, Irf8, Batf3 and Nfil3 (Aliberti *et al.,* 2003; Ginhoux *et al.,* 2009; Hacker *et al.,* 2003; Kashiwada *et al.,* 2011; Sichien *et al.,* 2016). The transition from MDP to CDP is Irf8 dependent (Sichien *et al.,* 2016), therefore essential for DC subsets. However, after this stage Irf8 is dispensable for pDC and cDC2 development but is necessary for cDC1 development (Sichien *et al.,* 2016), consequently cDC1 are referred to as $Irf8^+$ DC. In line with these observations in mice, human mutations in IRF8 (K108E), results in an autosomal recessive immunodeficiency characterised by a loss of circulating monocytes, pDC and cDC (Hambleton *et al.,* 2011), suggesting IRF8 also acts at early stages to specify DC and monocyte development. An elegant study performed by Jackson *et al.,* purified cDC1 subsets and their precursors and identified the sequential requirement of Irf8 followed by Id2 then Batf3 (Jackson *et al.,* 2011). Id2-deficient and Batf3-deficient mice exhibit a similar phenotype to Irf8-deficient mice with the absence of $CD103^+$ cDC and reduced numbers of CD8+ cDC in the spleen under steady-state (Hildner *et al.,* 2008; Kusunoki *et al.,* 2003).

1.6.3.3 cDC2 development

$CD11b^+$ DC are the predominant DC subset in lymphoid organs. This subset of DC has been previously referred to as $Irf4^+$ DC as Irf4 is required for their development (Suzuki *et al.,* 2004); however, further subdivisions such as Notch2- and Klf4-dependent cDC2 populations have been described (Lewis *et al.,* 2011; Satpathy *et al.,* 2013; Tussiwand *et al.,* 2015). In humans, an IRF8

mutation (T80A) results in a selective loss of cDC2 (Hambleton *et al.,* 2011). Therefore, whilst in mice, Irf8 is specific to cDC1 development this may not be the case in the human setting.

1.6.4 DC Function

DC function can be appreciated from CD11c-diphtheria toxin receptor mice (Jung *et al.,* 2002). In these mice, diphtheria toxin receptor is expressed under the promoter for CD11c, resulting in the depletion of $CD11c^+$ cells which include DC upon diphtheria toxin administration. As a result, these mice lack cytotoxic T cell responses in response to *Listeria monocytogenes* (Jung *et al.,* 2002), highlighting the importance of DC in bridging the innate and adaptive immune response. However, CD11c expression is not restricted to DC and can be found on monocyte-derived cells, tissue resident macrophages and a population of NK cells. New models have since been generated to probe the function of individual DC subsets.

1.6.4.1 cDC1 function

In mice, cDC1 are viewed as the key DC subset capable of cross presentation, a process where exogenous antigen can be presented to $CD8^+$ T cells via MHC I molecules (den Haan *et al.,* 2000; Haniffa *et al.,* 2012; Pooley *et al.,* 2001). Batf3-deficient mice are characterised by a loss cDC1, as a result, these mice lack $CD8^+$ T cell response to viral infections and tumours (Hildner *et al.,* 2008), highlighting the importance of cross presentation associated with this subset. Of note, human cDC2 have been observed to cross present antigen to cytotoxic $CD8^+$ T cells (Yu *et al.,* 2013), therefore this function may not be unique to cDC1, at least in humans.

cDC1 exhibit specialised functions owed to an array of receptors expressed by this subset. Toll-like receptor (TLR) 3 is expressed by cDC1 in both mice (Davey *et al.,* 2010) and humans (Hémont *et al.,* 2013) and recognises double stranded ribonucleic acid (RNA), key for priming antiviral cytotoxic T cell responses (Davey *et al.,* 2010). C-type lectin domain family 9 member A (CLEC9a) is also highly specific to cDC1 and facilitates the cross presentation of antigens from necrotic cells to $CD8^+$ T cells (Sancho *et al.,* 2009). Finally, following $CD8^+$ T cell recognition, XCL1 is

secreted from T cells and interacts with XCR1 on cDC1 to stabilise DC-T cell interactions eliciting the production of IFN-γ and cytotoxic T cell responses (Dorner *et al.,* 2009).

1.6.4.2 cDC2 function

Whilst murine models exist to study the specific functions of cDC1, models with a specific deletion of cDC2 are lacking. In addition, given cDC2 are a heterogeneous population, models are needed targeting these individual subsets. $Klf4^+$ cDC2 are found within several lymphoid and peripheral tissues. They are implicated in directing Th2 immunity as mice lacking this subset of DC exhibit lower rates of survival with *Schistosoma mansoni* infection (Tussiwand *et al.,* 2015). On the other hand, $Notch2^+$ cDC2 have been acknowledged in Th17 immunity (Lewis *et al.,* 2011) and a source of IL-23 which is required for survival in mice infected with *Citrobacter rodentium* (Satpathy *et al.,* 2013). In comparison to cDC1, cDC2 appear to better at mounting $CD4^+$ T cell responses (Pooley *et al.,* 2001), likely due to increased expression of proteins relating to MHC II presentation (Dudziak *et al.,* 2007). Furthermore, where human cDC1 express a limited number of TLR ligands (TLR1, 3, 6 and 10), cDC2 express a broader range of TLR ligands (TLR 1, 2, 4, 5, 6, 8 and 10) (Hémont *et al.,* 2013), and may play a more significant role in sensing pathogens.

1.6.4.3 pDC function

In 1957, IFNs were first recognised as mediators which could restrict viral infection (Isaacs and Lindenmann, 1957). Studies investigated the identity of these natural IFN producing cells, which in 1999 were shown to be overlap with pDC (Siegal *et al.,* 1999). pDC are consequently recognised as potent producers of type 1 IFN in response to viral infections, which is likely owed to their high expression of TLR7 and TLR9 (Hémont *et al.,* 2013).

E2-2 deficient mice are devoid of pDC, therefore, it came as no surprise that IFNα was undetected following stimulation with CpG in these mice (Cisse *et al.,* 2008). These observations are reflected in patients with Pitt–Hopkins syndrome who are haploinsufficient for the gene

E2-2 and present with few circulating pDC that are also unable to elicit a response to CpG (Cisse *et al.,* 2008).

As pDC have been described to arise from multiple lineages (Onai *et al.,* 2013; Rodrigues *et al.,* 2018), the question arises whether functional differences have been attributed. Both lymphoid and myeloid derived pDC were capable of producing IFN-α production in response to CpG-A, however myeloid derived pDC were more capable of inducing T cell proliferation and IFN-γ production from T cells (Pelayo *et al.,* 2005; Rodrigues *et al.,* 2018). Similarly human pDC have been reported to induce proliferation of naïve $CD4^+$ T cells (Matsui *et al.,* 2009), however this likely due to contaminating pre-cDC rather than two functionally distinct lineages of human pDC (See *et al.,* 2017; Villani *et al.,* 2017).

1.6.4.4 Central and peripheral tolerance

In addition to the activation of T cells, DC also play a key immunoregulatory role to prevent hyperactivation of the immune system.

Thymic resident cDC1, migratory cDC2 and pDC all play a key role in the elimination of autoreactive T cells. The role of DC in central tolerance can be appreciated in CD11c-Cre mice lacking DC, which exhibit an increased frequency of $CD4^+$ thymocytes and autoimmune features which could be reversed following reconstitution with wild-type bone marrow. (Ohnmacht *et al.,* 2009). The efficiency of DC in removing self-reactive T cells can be observed from studies where DC expressing MHC II I-E molecules resulted in the negative selection of $CD4^+$ T cells that were reactive against I-E (Brocker, 1999). The deletion of thymocytes constitutes one mechanism of DC induced tolerance. Thymic cDC1 and cDC2 can also induce T regulatory (Treg) cells (Coquet *et al.,* 2013; Proietto *et al.,* 2008), although via differing mechanisms. Resident cDC1 can induce Treg cells via CD70 expression and their ability to do so was hindered in CD70-deficient mice, however, cDC2 were unaffected (Coquet *et al.,* 2013), suggesting an alternate mechanism for this subset. Additionally, thymic pDC can prime positively selected $CD4^+$ $CD8^+$

thymocytes into Treg cells (Martín-Gayo *et al.,* 2010), although to a lesser extent compared to cDC (Coquet *et al.,* 2013; Proietto *et al.,* 2008).

In the case that central tolerance is not a completely effective mechanism, peripheral tolerance serves an additional layer of protection against self-reactivity occurring in the periphery. Successful DC presentation to T cells requires the presence of co-stimulatory molecules. DC presentation of antigen alone to T cells led to a dramatic reduction in T cells and the remaining T cells became unresponsive to further antigen challenge (Hawiger *et al.,* 2001). However, in the presence of CD40 activation, prolonged T cell activation was observed, demonstrating in the absence of additional co-stimulatory molecules, T cell deletion and anergy is induced. In addition, splenic and lung tissue cDC1 can phagocytose apoptotic cells and cross present antigen to $CD8^+$ T cells, resulting in the deletion of these cells (Desch *et al.,* 2011; Liu *et al.,* 2002; Qiu *et al.,* 2009). In the absence of cDC1, cross presentation to $CD8^+$ T cells was consequently affected and these mice failed to induce tolerance against antigens presented by apoptotic cells (Qiu *et al.,* 2009). Peripheral tolerance can also take place in the form of Treg cell induction. Jones and colleagues demonstrated that DC expressing BTLA govern Treg cell conversion, moreover this mechanism was restricted to cDC1 (Jones *et al.,* 2016). Nevertheless, cDC2 can induce the developmental of Treg cells via retinoic acid, which is owed to their increased expression of a retinal dehydrogenase (Coombes *et al.,* 2007; Guilliams *et al.,* 2010). The production of retinoic acid is key to the development of $Foxp3^+$ Treg cells, as DC which do not normally induce Foxp3 expression, are capable to do so in the presence of retinoic acid (Coombes *et al.,* 2007).

1.7 Turnover and kinetics of mononuclear phagocytes

Studies continue to refine the mononuclear phagocyte heterogeneity and elucidate their function under steady physiological conditions and during inflammation. Alongside function, understanding the homeostatic kinetic profiles and turnover which govern the generation, maturation and disappearance of these cells are key to the fundamental biology of these cells. To preserve this state of wellbeing, the body must adapt to environmental changes including infection and injury. To understand the adaptation of the immune response, the cellular kinetics of the inflammatory response is of great importance.

1.7.1 Macrophages

Investigations into the kinetics of monocytes and macrophages started at early as 1968 by van Furth and Cohn (van Furth and Cohn, 1968). Using stable isotope-labelled thymidine, it was shown that peritoneal macrophages exhibit very low labelling rates in comparison to highly labelled blood monocytes. Unaware at the time, these data supported the maintenance of macrophage populations independent of monocytes. van Furth later recognised that several studies demonstrated a low percentage of local macrophage proliferation. He proposed that the turnover of macrophages relies on the influx monocytes, local proliferation and the death of macrophages (van Furth, 1989).

Since our understanding that most macrophages are embryonically derived, studies have examined whether these embryonic macrophages are replaced with time and if so at what rate. Recently, an elegant study by Liu and colleagues identified a fate-mapping model where almost 100% labelling was observed in monocytes (Liu *et al.,* 2019). As a result, the contribution of monocytes to tissue resident macrophages could be examined. Lung alveolar macrophages, splenic macrophages, peritoneal macrophages and dermal macrophages had a steady contribution from monocytes over time (**Figure 1.4)**, however, the rates were not calculated. In tissues such as the brain, epidermis and liver, very little to no contribution was observed in the

microglia, Langerhans cells and Kuppfer cells. Interestingly, patients that have undergone lung transplantation retain donor alveolar macrophages up to three and a half years post transplantation (Nayak *et al.,* 2016). Langerhans cells also remained of donor origin when examined ten years following human hand allograft (Kanitakis *et al.,* 2011). An interesting study by Réu and colleagues took advantage of atmospheric ^{14}C and demonstrated that human microglia have a life-span of approximately 4.2 years and renew at a rate of 28% per year (Réu *et al.,* 2017).

Collectively, these studies support the idea of minimal monocyte contribution to some tissue macrophage compartments and some, where there is a higher rate replacement by monocytes over time.

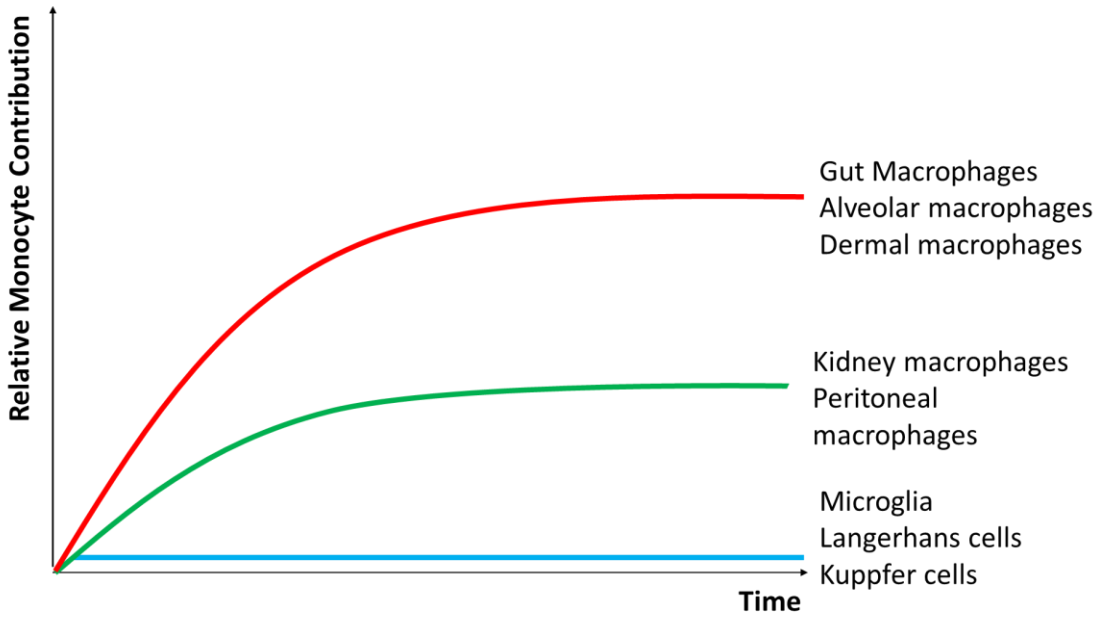

Figure 1.4 **Macrophage Kinetics**

Embryonic tissue macrophages are replaced by bone marrow-derived monocytes throughout life in some tissues such as the gut, peritoneum and dermis. However, the rates of replacement are tissue-specific.

1.7.2 Monocytes

Initially, studies investigating the turnover of monocytes in mice, suggested a circulating half-life of 22 hours, resulting in an average circulating lifespan of 32 hours (van Furth and Cohn, 1968). In addition, labelling kinetics of bone marrow monocyte precursors allowed for the approximation of 1 hour as the minimum time required for cells to enter circulation from the last mitotic division in mice. It was proposed that 40% of the monocyte pool are replaced each day. van Furth also performed studies examining monocyte turnover under inflammatory conditions (Van Furth *et al.,* 1973). Following intraperitoneal challenge with fetal calf serum, labelled monocytes were seen earlier in the circulation in comparison to control mice and at much higher numbers. It was proposed, the maturation period between the promonocyte to monocyte stage was shorter during inflammation to allow for the increased monocyte production.

More recently, Yona and colleagues have previously demonstrated the turnover of monocyte subsets using BrdU (Yona *et al.,* 2013). BrdU was initially observed in classical monocytes and later in non-classical monocytes. The half-life of these cells was estimated at 20 hours and 2.2 days, respectively.

In human patients undergoing hematopoietic stem cell transplantation (HSCT), preconditioning resulted in monocytopenia followed by repopulation of $CD14^+$ monocytes and 2 days later by $CD16^+$ monocytes (McGovern *et al.,* 2014). Studies have looked at the turnover of human monocytes as a total population, where the half-life of $CD14^+$ monocytes has been proposed to be 2.2 days (Mohri *et al.,* 2001) or a lifespan of 4.25 days in a separate study (Whitelaw, 1972). Whitelaw also calculated that monocytes leave the bone marrow after a maturation period of 16-26 hours. However, the turnover of individual subsets remains to be elucidated.

1.7.3 Dendritic cells

The turnover of tissue DC subsets has been widely investigated in mice. Initial studies suggested 10% of splenic DC turnover each day (Steinman *et al.,* 1974), however, this was later corrected to a much shorter turnover time of 1.1 hours (unpublished data discussed in van Furth, 1989). Later studies using BrdU, demonstrated splenic DC subsets were rapidly labelled, which was thought to be attributed to the rapid replenishment from circulating DC precursors (Kamath *et al.,* 2002). However, splenic DC are also proliferative therefore the labelling is likely to represent a combination of *in situ* proliferation and blood derivation (Liu *et al.,* 2007). Parabiosis experiments have examined the decay of parabiont-derived DC in the lymphoid and non-lymphoid organs and were demonstrated to be cleared within 10-14 days (half-life 5-7 days) (Liu *et al.,* 2007). Taking into consideration, DC replenishment from blood precursors, DC division and DC death, this study also calculated that lymphoid organ cDC are replenished at a rate of 4,300 cells per hour. Of note, pDC have a much slower turnover in comparison to cDC (O'Keeffe *et al.,* 2002), which is reflected in their lower rates of production in the bone marrow (Pelayo *et al.,* 2005).

Following HSCT, human dermal DC were replaced by donor origin within 40 days (Haniffa *et al.,* 2009), and in separate study, approximately 94% were donor derived within 18-56 days post HSCT (Auffermann-Gretzinger *et al.,* 2006).

As circulating DC are present at low levels in mice, their kinetics have not been examined. Nevertheless, studies performed in macaques have demonstrated DC kinetics are distinct from that of monocytes (Sugimoto *et al.,* 2015). Specifically, cDC2 were observed prior to monocytes whereas pDC appeared at much later time points. However, studies have not yet extended these observations to the human setting.

1.8 Ontogeny based approach of the mononuclear phagocyte system

As discussed above, mononuclear phagocytes exhibit broad functions. Nevertheless, cells are categorised as either monocyte, macrophage or DC based primarily on functional attributes. Such classification has become confusing due to overlapping roles between different cells of the MPS. A cell with a potent ability to stimulate naïve T cells may be defined as a DC, whereas the same cell may also have a high phagocytic ability and may be regarded as a macrophage. For example, in the dermis, the term 'CD14$^+$ DC' has been widely used to describe a population of cells capable of priming T cells (Haniffa *et al.,* 2012; Klechevsky *et al.,* 2008; Nestle *et al.,* 1993). A more recent study has shown these cells to be more transcriptionally related to macrophages yet are derived from monocytes (McGovern *et al.,* 2014). Similarly, SLAN$^+$ cells have been described as potent activators of naïve T cells (Schäkel *et al.,* 1999, 1998), therefore allowing these cells to be called SLAN$^+$ DC. However, in regards to the expression of surface membrane markers, these cells are akin to monocytes (Cros *et al.,* 2010). Consequently, it was recently proposed whether classification primarily by ontogeny may provide a more robust definition of these cells (**Figure 1.5**). Where the origin of the mononuclear phagocyte is known, the cell can be identified as either a macrophage, monocyte-derived cell or a DC.

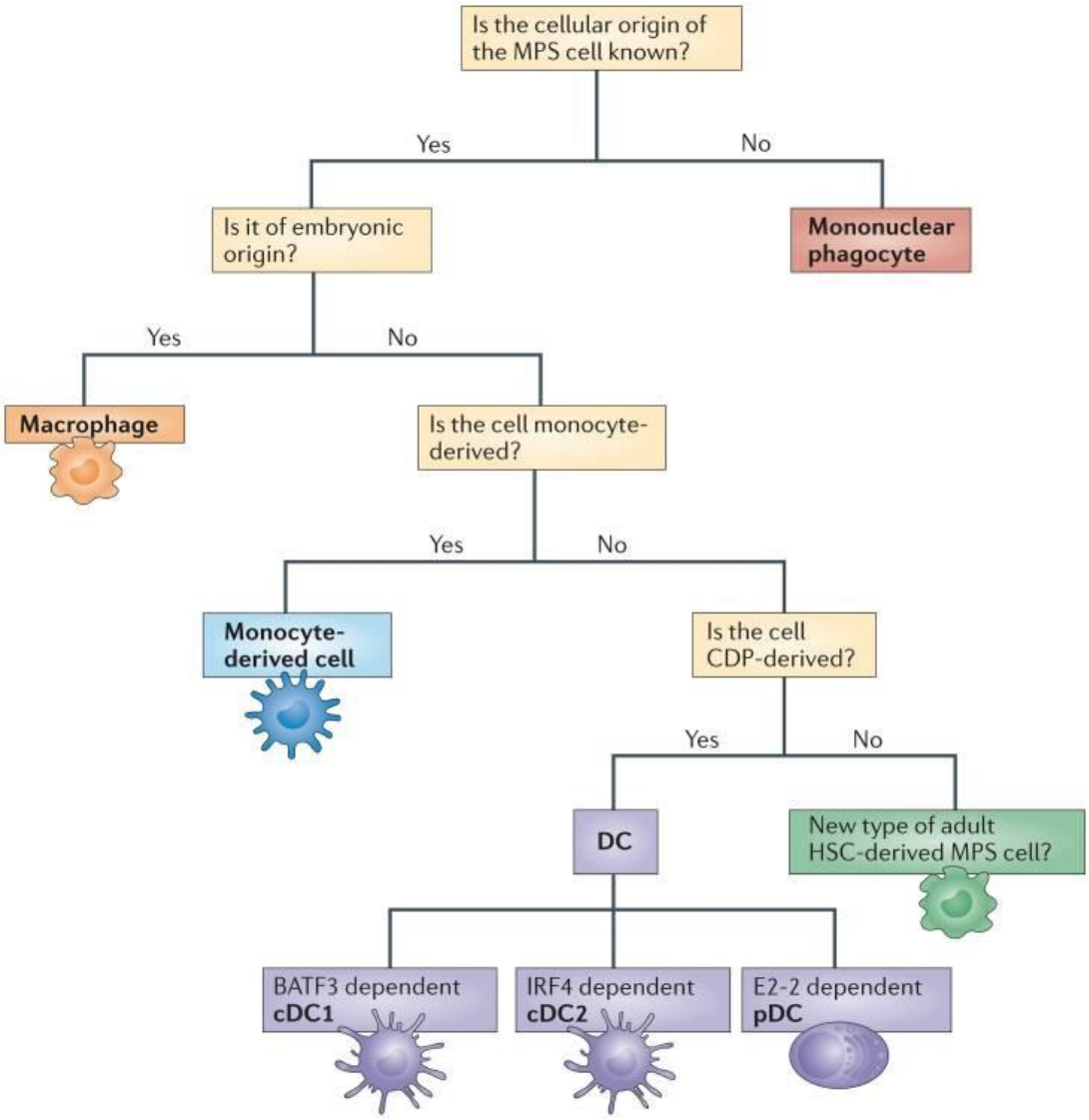

Figure 1.5 **An ontogeny based approach to classify mononuclear phagocytes**

Classification of mononuclear phagocytes by function can lead to a confusing nomenclature for cells of the mononuclear phagocyte system (MPS). It was proposed, cells be defined initially by origin. Mononuclear phagocytes of embryonic origin are regarded as bona fide macrophages, those that arise from monocytes should be termed monocyte-derived cells. Finally, cell derived from a common dendritic cell precursor (CDP) should be classed as a dendritic cell (DC), which can be further subdivided into cDC1, cDC2 or pDC depending on transcription factors expressed. (Image from Guilliams *et al.,* 2014).

1.9 Hypothesis and Aims

The MPS has gained a considerable amount of attention, particularly regarding the origin and development of cells. Whilst studies in rodents and non-human primates have explored the kinetic turnover of circulating mononuclear phagocytes, in humans, the kinetic profiles underlying the generation, maturation and disappearance of these cells remains unknown.

1.9.1 General Hypothesis

Blood mononuclear phagocytes circulate in a homoeostatic dynamic equilibrium where each subset has a defined kinetic profile that is consequently impacted during inflammation.

1.9.2 Aims

- Generate a comprehensive gating strategy to identify monocyte and DC subsets
- Examine the *in vivo* kinetics of circulating human monocyte and DC subsets using stable isotope labelling
- Demonstrate how experimental systemic inflammation impacts on the profile of monocyte and DC subsets
- Examine the infiltration of monocyte and DC subsets in response to local inflammation

Chapter 2

Materials and Methods

2.1 Blood Collection

2.1.1 Subjects

The studies performed in this thesis were performed in human volunteers (unless specified otherwise). I am grateful to all volunteers who consented to take part in these studies.

2.1.1.1 Ethical approval

All volunteers gave written informed consent and all studies were conducted according to the principles of the declaration of Helsinki after approval by the relevant institutional review boards. For deuterium and steady-state experiments, NRES Committee West London [10/H0803/102] and University College London Research Ethics Committee [8081/001] and [8081/002]. For the endotoxemia study, University College London Research Ethics Committee [5060/001]. Intradermal injection of ultraviolet (UV)-killed *Escherichia coli* (*E. coli*) was also approved by the University College London Research Ethics Committee [10527/001] and [1309/005]. Newcastle and North Tyneside Research Ethics Committee approved the bone marrow biopsy (REC 14/NE/113) and hip (REC 14/NE/1212) procedures.

2.1.1.2 Inclusion and exclusion criteria

All subjects in this study were healthy, young (18-50 years), non-smoking consented individuals. Volunteers taking medication were excluded from the study. Those enrolled were asked to refrain from alcohol consumption 48 hours prior to the onset of the study.

Prior to deuterium administration, intravenous endotoxin challenge and intradermal challenge with UV-killed *E. coli*, volunteers were screened to ensure eligibility for the study.

2.1.2 PBMC Isolation

All consented volunteers were bled from the median cubital vein using a 20 gauge butterfly needle and aseptic non-touch technique. Blood was collected in sodium heparin treated vacutainers (Greiner Bio-One Biosciences, Kremsmünster, Austria), inverted several times and diluted with an equal amount of Dulbecco's Phosphate-Buffered Saline (PBS) (Corning,

Flintshire, UK). Diluted blood was carefully layered over 15 ml of density gradient media (Ficoll-Paque Plus™, GE Healthcare, Little Chalfont, Buckinghamshire, UK) to avoid mixing in a 50 ml centrifuge tube (Corning, Flintshire, UK). The sample was centrifuged at 1000 x *g* for 20 minutes at 20°C with no brake and low acceleration in an Eppendorf centrifuge 5810 (Eppendorf, Stevenage, UK). The cloudy interphase layer/peripheral blood mononuclear cells (PBMC) was transferred to a clean centrifuge tube using a sterile Pasteur pipette. An equivalent volume of PBS was added to the mononuclear cells. The centrifuge tube was gently inverted, centrifuged at 300 x *g* for 10 minutes at 4°C (with brake and acceleration on) and the supernatant was discarded. The cell pellet was then resuspended in the appropriate media for downstream application.

2.1.3 Whole Blood Erythrocyte Lysis

Blood was collected in K2-Ethylenediamine tetraacetic acid (EDTA) treated vacutainers (BD Biosciences, Wokingham, UK). Blood was mixed with ammonium-chloride-potassium (ACK) lysing buffer (NH_4Cl 8,024 mg/L, $KHCO_3$ 1,001 mg/L, $EDTA.Na_2{\cdot}2H_2O$ 3.722 mg/L) (Lonza, Berkshire, UK) in a 1:9 ratio and allowed to stand until transparent (approximately 5 minutes) at room temperature (20°C) before centrifuged at 300 x *g* for 5 minutes at 20°C. The supernatant was discarded and the cell pellet was washed with 5 ml PBS and centrifuged at 300 x *g* for 5 minutes at 4°C and then resuspended in the appropriate media for downstream application.

2.1.4 Plasma collection

Blood was collected in sodium heparin treated vacutainers and centrifuged at 2500 x *g*, 10 minutes at room temperature with brake and acceleration on. Plasma was aliquoted in protein LoBind eppendorfs (Eppendorf, Stevenage, UK) and stored at -80°C.

2.1.5 Serum collection

Blood was collected in serum-separating tubes (BD Biosciences, Wokingham, UK) and allowed to clot for 30 minutes at room temperature. Tubes were centrifuged at 2000 x *g*, 10 minutes at

20°C. Serum was aliquoted into protein LoBind eppendorfs and placed in a heat block for 45 minutes at 56°C to heat inactivate proteins.

2.1.6 Finger prick samples

Volunteer's fingertips were disinfected with 70% isopropyl alcohol wipes (Universal, Middlesex, UK). After puncturing the fingertip with a blood lancet, the first drop of blood was wiped with a clean tissue. Blood was gently squeezed onto a clean filter paper and allowed to air dry. Samples were stored at 4°C.

2.2 Flow Cytometry

Flow cytometry is a widely used method for quantitative analysis of cell protein expression (intracellular and surface), function and cell profiling. This technique enables cells to be distinguished according to their size, granularity and protein expression. Protein expression is detected by measuring the fluorescence intensity emitted from fluorochromes attached to antibodies to detect proteins of interest. As cells enter the flow cytometer, they are accelerated past various lasers emitting different wavelengths of light. Fluorochromes are excited by these lasers and in turn, emit light at wavelengths which are detected. These resulting signals are measured and relayed as mean fluorescence intensity (MFI).

2.2.1 Cell surface staining

Freshly isolated PBMC were isolated from blood (Section 2.1.2). Up to $1x10^7$ cells/100µl FACS Buffer (PBS, 2mM EDTA, 5% fetal calf serum (FCS)) were stained. A list of the antibodies used in this thesis can be found in **Table 2.1**. Cells were stained for 30 minutes at 4°C in the dark. Prior to the addition of antibodies, Human TruStain FcX (Biolegend, London, UK) was added to prevent non-specific binding at Fc receptors for 15 minutes. If two or more Brilliant dyes were used together, Brilliant Stain buffer (BD Biosciences) was also added to the antibody cocktail to prevent cross-reactivity of Brilliant fluorescent polymer dyes. For blister samples, UV excited cell viability dye (Invitrogen, Paisley, UK) was used at 1:1000 to gate out dead cells. Following

staining, cells were washed and resuspended in FACS buffer ready for flow cytometry analysis or washed in PBS if intracellular staining was also to be performed.

2.2.2 Intracellular staining

Following membrane surface staining (Section 2.2.1), up to 3-5 x10^6 cells were washed in PBS and resuspend in 200µl/well of Fixation Buffer (4% Paraformaldehyde) (Biolegend, London, UK) in a 96-well conical bottom polypropylene plate (Thermo Fisher, Paisley, UK). Cells were fully resuspended and incubated in the dark at 4°C for 30 minutes. Following manufacturer's instructions, cells were washed with permeabilisation buffer (0.5% Saponin) (Biolegend, London, UK) and centrifuged at 300 x *g* for 5 minutes at 4°C with brake and acceleration on. The cell pellet was resuspended in 100 µl permeabilisation buffer with the working intracellular antibody concentration (**Table 2.1**). Cells were stained for 30 minutes in the dark at 4°, then washed with 200 µl permeabilisation buffer, centrifuged at 300 x *g* at 4°C for 5 minutes and finally resuspended in FACS buffer ready for flow cytometry analysis.

To perform intranuclear staining, the same protocol was followed, except using a Foxp3/transcription factor staining buffer kit (Invitrogen, Paisley, UK).

2.2.3 Fluorescence Activated Cell Sorting (FACS)

2.2.3.1 Cell preparation

PBMC were isolated as described in Section 2.1.2. To minimise sorting time, pre-enrichment for $CD3^-$ cells was performed by removing $CD3^+$ cells. Prior to membrane staining, up to 10^7 PBMC/80µl FACS buffer was stained with 20 µl of CD3 MicroBeads (Miltenyi Biotech, Surrey, UK). Cells were incubated for 15 minutes in the refrigerator (4°C), washed with FACS buffer and centrifuged at 300 x *g* for 5 minutes at 4°C with brake and acceleration. Up to 10^8 cells were resuspended in 500 µl FACS buffer and scaled up accordingly for higher cell numbers. LS separation columns (Miltenyi Biotech, Surrey, UK) were attached to a QuadroMACS separator (Miltenyi Biotech, Surrey, UK) and washed with 3 ml of FACS buffer. The cell suspension was loaded into the column and the unlabelled $CD3^-$ cell fraction was collected into a 15 ml centrifuge tube. The column was washed a further three times with 3 ml of FACS buffer. The $CD3^-$ PBMC fraction was counted (Section 2.3.1) and centrifuged at 300 x *g* for 5 minutes at 4°C, with brake and acceleration, before surface staining was performed (Section 2.2.1).

2.2.3.2 Cell sorting

Cells of interest were bulk sorted into round-bottom polypropylene tubes (Fisher Scientific, Loughborough, UK) containing 100% FCS (Gibco, Paisley, UK). Sorted cell counts were obtained and purity was also analysed when feasible. Cells were centrifuged at 300 x g for 5 minutes at 4°C, with brake and acceleration and resuspended in the appropriate media for downstream application.

For single cell RNA sequencing, cells were sorted into 96-well polymerase chain reaction (PCR) plates (Bio-Rad, Hertfordshire, UK) containing 2 µl of 1mg/ml UltraPure bovine serum albumin (Thermo Fisher, Paisley, UK) and 1 µl of 10mM deoxyribonucleotide triphosphate (New England Biolabs, Hitchin, UK). Plates were sealed with a PCR plate sealing film (Bio-Rad, Hertfordshire, UK) and stored at -80°C.

All cell sorting was performed by Mr. Jamie Evans or Dr. Simon Yona. Single cell RNA sequencing analysis was performed in collaboration with Dr. Florent Ginhoux and Dr. Charles-Antoine Dutertre at A*STAR, Singapore Immunology Network.

2.2.4 Isotype controls and FMOs

Non-specific binding of antibodies can occur via the Fc region of antibodies. When measuring surface membrane marker or intracellular protein expression, isotype controls were implemented to control for non-specific binding. Isotype controls were matched to the antibody for host species, immunoglobulin class, light chain and fluorochrome. The same quantity of isotype was added to the cell sample as was with the primary antibody. Fluorescence Minus One (FMO) controls were used to demonstrate background fluorescence in a particular channel of interest to ensure the positive population was properly identified. For example, **Figure 2.1** demonstrates how an FMO identifies the background fluorescence in the BV605 channel. Non-specific binding can be observed by the shift in fluorescence between the isotype control and the FMO control. These controls allow the true staining of the CD34 primary antibody to be appreciated.

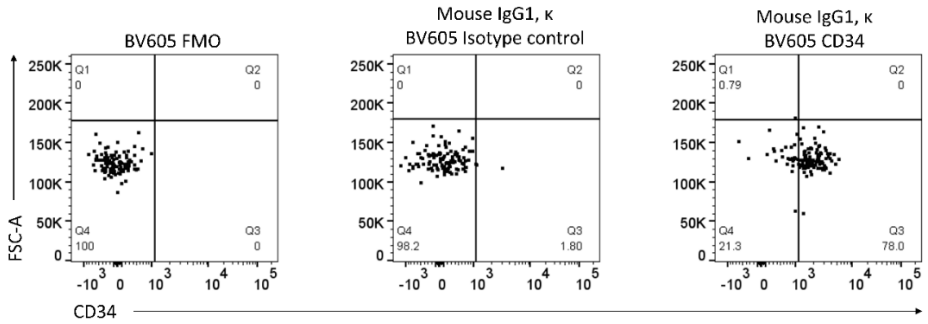

Figure 2.1 **Isotype controls and FMOs**

Pre-DC were identified within the PBMC fraction by flow cytometry. CD34 expression was analysed (right) in conjunction with the corresponding isotype control (middle) and FMO (left).

2.2.5 Compensation controls

Single colour compensation controls are necessary for multi-colour flow cytometry to account for spectral overlap between fluorochromes. UltraComp eBeads compensation beads (Invitrogen, Paisley, UK) contain positive beads that bind antibodies and negative beads that serve as a baseline fluorescence. One drop (50 µl) of compensation beads was stained with each fluorochrome. Beads were incubated for 30 minutes at 4°C in the dark, then washed with FACS buffer at 1000 x *g* for 3 minutes at 4°C before resuspended in 500 µl of FACS buffer.

2.2.6 Sample recording and analysis

Cell samples were analysed using LSR Fortessa X-20 (BD Biosciences) or FACS Aria II (BD Biosciences). FlowJo software (Tree Star Inc.) and Cytobank (Cytobank, Inc.) were used to analyse flow cytometry data.

2.2.7 Antibody Table

Marker	Target	Fluorochrome	Clone	Company	Dilution
AXL	Human	APC	#108724	R&D	1:20
CCR2	Human	PE-Cy7	K036C2	Biolegend	1:50
CD100	Human	Biotin	REA316	Miltenyi Biotec	1:10
CD11b	Human	PerCP/Cy5.5	ICRF44	Biolegend	1:50
CD11c	Human	BV421	B-ly6	BD	1:50
CD11c	Human	BV785	B-ly6	BD	1:50
CD11c	Human	PE-Cy7	B-ly6	BD	1:50
CD11c	Human	V450	B-ly6	BD	1:50
CD123	Human	BUV395	7G3	BD	1:100
CD123	Human	PerCP/Cy5.5	7G3	BD	1:100
CD14	Human	BUV805	M5E2	BD	1:100
CD14	Human	APC-Cy7	M5E2	Biolegend	1:50
CD14	Human	FITC	M5E2	Biolegend	1:50
CD14	Human	PE	M5E2	Biolegend	1:50
CD141	Human	BV711	1A4	BD	1:50
CD141	Human	PE-Dazzle	M80	Biolegend	1:50
CD141	Human	PE-Cy7	M80	Biolegend	1:50
CD141	Human	PerCP/Cy5.5	M80	Biolegend	1:50
CD16	Human	AF700	3G8	Biolegend	1:50
CD16	Human	APC	3G8	Biolegend	1:50
CD16	Human	APC-Cy7	3G8	Biolegend	1:50
CD16	Human	BV711	3G8	Biolegend	1:50
CD16	Human	PE-Cy7	3G8	Biolegend	1:50
CD16	Human	FITC	3G8	Biolegend	1:50
CD163	Human	BV785	GHI/61	Biolegend	1:50
CD19	Human	PE-Dazzle	HIB19	Biolegend	1:50
CD19	Human	FITC	HIB19	Biolegend	1:50
CD1c	Human	APC-Cy7	L161	Biolegend	1:50
CD1c	Human	BV421	L161	Biolegend	1:50
CD1c	Human	BV510	L161	Biolegend	1:50
CD1c	Human	BV605	L161	Biolegend	1:50
CD1c	Human	PE	L161	Biolegend	1:50
CD1c	Human	PE-Cy7	L161	Biolegend	1:50
CD2	Human	PE-Cy7	RPA-2.10	Biolegend	1:50
CD20	Human	PE-Dazzle	2H7	Biolegend	1:50
CD20	Human	FITC	2H7	Biolegend	1:50
CD203c	Human	PE	FR3-16A11	Miltenyi Biotec	1:50
CD3	Human	FITC	HIT3a	Biolegend	1:50
CD3	Human	PE-Dazzle	HIT3a	Biolegend	1:50

CD303	Human	BV711	201A	Biolegend	1:50
CD33	Human	BV605	P67.6	Biolegend	1:50
CD33	Human	BV711	P67.6	Biolegend	1:50
CD34	Human	BV605	581	Biolegend	1:50
CD34	Human	BV785	581	Biolegend	1:50
CD36	Human	APC-Cy7	5-271	Biolegend	1:50
CD39	Human	PE-Cy7	A1	Biolegend	1:50
CD45	Human	AF700	2D1	Biolegend	1:50
CD45	Mouse	AF700	30F11	Biolegend	1:50
CD45RA	Human	BV711	HI100	Biolegend	1:50
CD5	Human	BV605	L17F12	Biolegend	1:50
CD5	Human	PE	UCHT2	Biolegend	1:100
CD56	Human	PE-Dazzle	QA17A16	Biolegend	1:50
CD56	Human	FITC	QA17A16	Biolegend	1:50
CD62L	Human	PerCP/Cy5.5	DREG-56	Biolegend	1:50
CD64	Human	BV605	10.1	Biolegend	1:50
CD66b	Human	AF700	G10F5	Biolegend	1:50
CD66b	Human	PE-Dazzle	G10F5	Biolegend	1:50
CD66b	Human	FITC	G10F5	Biolegend	1:50
CD80	Human	BV605	L307.4	BD	1:50
CD86	Human	AF700	2331 (FUN-1)	BD	1:50
CD88	Human	FITC	S5/1	Biolegend	1:50
CD89	Human	FITC	A59	Biolegend	1:50
CLEC9a	Human	BV421	3A4	BD	1:50
CLEC9a	Human	PE	8F9	Biolegend	1:50
CLEC9a	Human	APC	8F9	Miltenyi Biotec	1:50
CX_3CR1	Human	PE	2A9-1	Biolegend	1:50
CX_3CR1	Human	PerCP/Cy5.5	2A9-1	Biolegend	1:50
FcεR1α	Human	PE-Dazzle	AER-37	Biolegend	1:50
HLA-DR	Human	V500	G46-6	BD	1:50
HLA-DR	Human	BV510	L243	Biolegend	1:40
IRF4	Human	PerCP/Cy5.5	IRF4.3E3	Biolegend	1:100
IRF8	Human	PE	REA516	Miltenyi Biotec	1:100
Ki67	Human	PE-Cy7	20Raj1	eBioscience	1:100
Siglec6	Human	FITC	REA852	Miltenyi Biotec	1:100
Siglec6	Human	PE	REA852	Miltenyi Biotec	1:50
SLAN	Human	APC	DD-1	Miltenyi Biotec	1:20
Streptavidin	Human	BUV737	-	BD	1:20

Table 2.1 **List of antibodies used for flow cytometry**

These dilutions were used when staining 1ml of ACK lysed blood (or approximately 3-5 x10^6 cells) (Section 2.1.3). Of note, staining was performed in FACS buffer in a final staining volume of 100 µl. When staining larger numbers of cells for FACS, the recommended amount of antibody was used according to the manufacturer's instructions.

2.2.8 Clone Comparisons

Several antibody clones exist for detecting a particular antigen. Due to the limitations of fluorochrome conjugates available, more than one antibody clone was sometimes used. To assess clone quality, ACK lysed blood was stained with each clone for comparison and analysed by flow cytometry.

2.2.8.1 CD11c

CD11c expression was primarily used to identify classical dendritic cells. The clone, B-ly6, resulted in a better resolution of the CD11c$^+$ population than the 3.9 clone (**Figure 2.2**). The B-ly6 clone was used in this thesis.

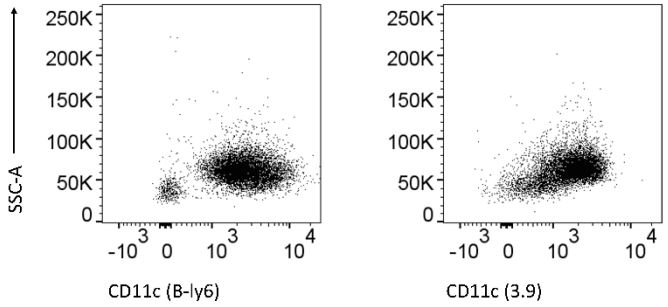

Figure 2.2 **CD11c clone comparison**

Expression profile of CD11c clones (B-ly6 and 3.9) on Lin$^-$ HLA-DR$^+$ cells.

2.2.8.2 CD141 and CLEC9a

CD141 was predominantly used to identify CD141$^+$ CLEC9a$^+$ DC. Both CD141 clones (1A4 and M80) identified similar percentages of cells that were also CLEC9a$^+$ (**Figure 2.3**) and were used in this thesis.

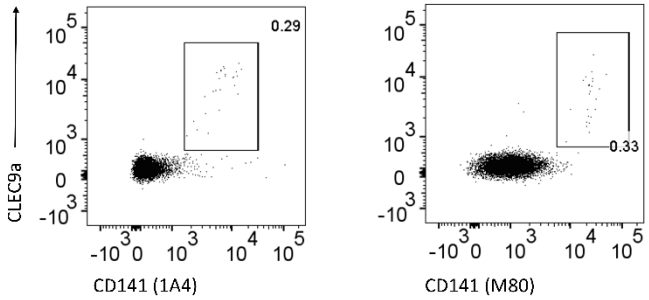

Figure 2.3 **CD141 clone comparison**

Expression profiles of CD141 clones (1A4 and M80) on Lin$^-$ HLA-DR$^+$ cells. The percentage of CD141$^+$ CLEC9a$^+$ DC was assessed with each CD141 clone.

In addition, two clones of CLEC9a (8F9 and 3A4) were compared (**Figure 2.4**) and identified a similar percentage of CD141$^+$ CLEC9a$^+$ DC.

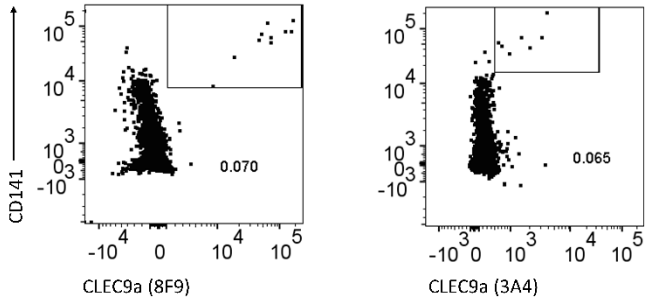

Figure 2.4 **CLEC9a clone comparison**

Expression profiles of CLEC9a clones (8F9 and 3A4) on Lin$^-$ HLA-DR$^+$ cells. The percentage of CD141$^+$ CLEC9a$^+$ DC was assessed with each clone.

2.2.8.3 CD5

CD5 clones (L17F12 and UCHT2) stained a similar percentage of cells (**Figure 2.5**) and were used interchangeably throughout this thesis.

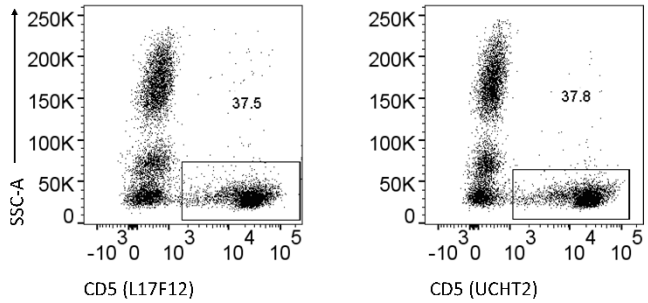

Figure 2.5 **CD5 clone comparison**

Expression profiles of CD5 clones (L17F12 and UCHT2) on all white blood cells. The percentage of $CD5^+$ cells was assessed with each clone.

2.2.8.4 HLA-DR

Human Leukocyte Antigen (HLA)-DR clones (L243 and G46-6) stained a similar percentage of $Lineage^-$ cells, although the G46-6 clone provided better resolution (**Figure 2.6**) and was the preferred choice.

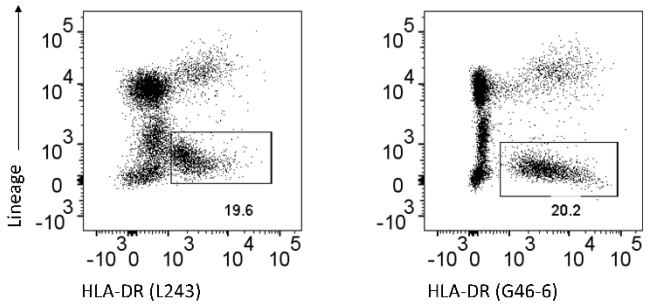

Figure 2.6 **HLA-DR clone comparison**

Expression profiles of HLA-DR clones (L243 and G46-6) are shown on PBMCs. The percentage of Lin^- $HLA\text{-}DR^+$ cells were assessed with each clone.

2.2.8.5 Siglec6

Siglec6 clones (767329 and REA852) were stained separately in conjunction with AXL, to identify Siglec6^{+} AXL^{+} DC. The 767329 clones did not clearly identify these cells whereas this cell population was clear with the REA852 clone (**Figure 2.7**) The latter clone was used throughout this thesis.

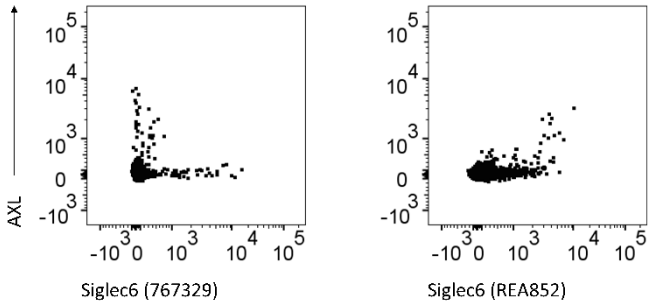

Figure 2.7 **Siglec6 clone comparison**

Expression profiles of AXL and Siglec6 clones (767329 and REA852) are shown on Lin^{-} HLA-DR^{+}.

2.3 Cell Counts

2.3.1 Automated Cell Counter

Approximate cell counts to numerate cells for staining were performed using a Countess automated cell counter (#C10277) (Invitrogen, Paisley, UK). 10 µl of cell solution was resuspended with 10 µl of trypan blue (0.4%) (Invitrogen, Paisley, UK). 10 µl of this mix was added to Countess cell counting slides (Invitrogen, Paisley, UK) to be counted. Values were reported as a concentration and then scaled to the original volume the cell sample to calculate total cell count.

2.3.2 Counting Beads

Flow cytometry CountBright cell counting beads (Invitrogen, Paisley, UK) were used to calculate the absolute numbers of cells in blood and blister samples. Beads were used at room temperature, vortexed for 30 seconds and 25 µl was immediately added to a stained sample in 300 µl prior to flow cytometry analysis. After running the sample on the flow cytometer, the beads could be identified as high side scatter (SSC) and low forward scatter (FSC), and further identified as they fluoresce in all channels due their broad excitation wavelength range (**Figure 2.8**).

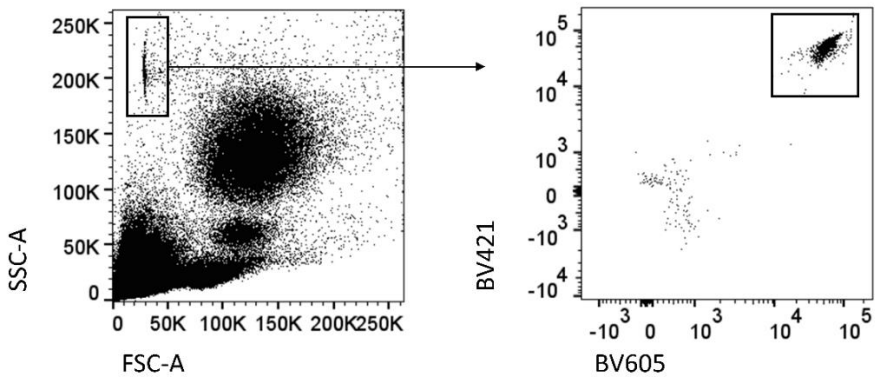

Figure 2.8 **Counting bead gating strategy**

Flow cytometry CountBright counting beads were added to cell samples. Beads were identified as high SSC and low FSC and count be further identified by their high fluorescence in other channels.

With the recorded bead event, total cell event and the total number of beads added in 25 µl, the number of cells in the sample could be calculated using the following equation:

$$\frac{number\ of\ cell\ events}{number\ of\ bead\ events} \times number\ of\ beads\ added\ = total\ number\ of\ cells$$

2.3.3 Clinical Blood Report

EDTA treated blood samples were sent to The Doctor's Laboratory (London, UK), where full clinical blood counts were obtained. Major cell populations were identified using size and granularity measurements.

2.4 Human bone marrow biopsy

Human bone marrow biopsy samples were obtained from hematopoietic stem cell donors or femoral heads following total hip replacement. Samples were processed and analysed by flow cytometry in collaboration with Dr. Venetia Bigley at Newcastle University.

2.5 Cell Cycle Profiling

Cells express Ki67 in all stages of the cell cycle (G_1, S phase, G_2 and mitosis) except G_0 (Gerdes *et al.,* 1984). The deoxyribonucleic acid (DNA) content of cells in G_0 and G_1 can be regarded as 'n', cells in S phase in the process of replicating their DNA and by the G_2 phase have double the DNA content (2n). 4',6-diamidino-2-phenylindole (DAPI) binds to DNA and can be used to quantify DNA content. Cells with double DNA content (i.e. divided cells) can be identified as they will have double the fluorescence (Pozarowski and Darzynkiewicz, 2004). Using DAPI in conjunction with Ki67, different stages of the cell cycles were analysed.

2.5.1 Sample preparation

Surface staining was performed on PBMC as in Section 2.2.1. Cells were fixed and permeabilised with FoxP3/transcription factor staining buffer set (Section 2.2.2). Cells were intracellularly stained with Ki67 (1:100) and 0.5 ug/ml DAPI with 200 µg/ml RNase A and 500U/ml RNase T1 (Thermo Fisher, Paisley, UK) for 30 minutes, in the dark at room temperature. RNAse treatment was necessary as DAPI can also bind to RNA. Cells were washed with permeabilisation buffer, centrifuged at 300 x *g* at 4°C for 5 minutes with brake and acceleration and finally resuspended in FACS buffer ready for flow cytometry analysis.

2.5.2 Analysis

To examine the cell cycle status of cells by flow cytometry, cells of interest were first identified. As an example, PBMC were examined for Ki67 and DAPI expression (**Figure 2.9**). Ki67^{-} DAPI^{lo} were regarded as cells in G_0, Ki67^{+} DAPI^{lo} as G_1 and Ki67^{+} DAPI$^{int/hi}$ were identified as S phase, G_2 and mitotic cells. Of note, Ki67^{-} DAPI^{hi} cells were thought to be contaminating doublets.

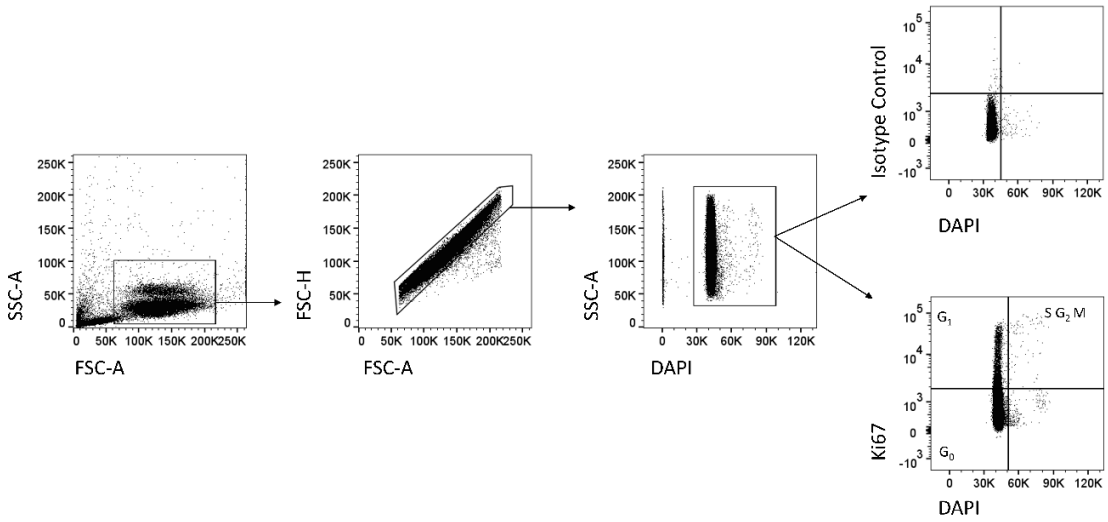

Figure 2.9 **Cell Cycle Analysis**

PBMC were analysed for Ki67 and DAPI expression. Ki67^{+} cells were defined using an isotype control. Cells were divided into Ki67^{-} DAPI^{low}, Ki67^{+} DAPI^{low} and Ki67^{+} DAPI$^{int/hi}$ cells, corresponding to G_0, G_1 and S phase, G_2 or M phase, respectively.

Image cytometry operates in a similar fashion to flow cytometry. In addition to measuring protein expression, the localisation of the protein can be visualised in/on the cell itself. As cell images are recorded, this technique was implemented to visualise the different stages of the cell cycle by gating on the populations defined by Ki67 and DAPI (**Figure 2.10**). Ki67^{-} DAPI^{lo} cells were single cells representative of G_0 cells. Cells in G_1 were similar to those in G_0 except they can be observed to express Ki67. Ki67^{+} DAPI^{hi} cells represent cells in S phase, G_2 and mitosis. Often a single cell with double nuclei could be observed and sometimes two cells could be observed. Finally, Ki67^{-} DAPI^{hi} cells were also imaged. All cells in this gate consisted of two adjacent cells. It

was unclear whether these cells represent doublets or cells which have just left telophase, as decreased Ki67 expression has been observed towards the end of mitosis (Braun *et al.,* 1988). Imaging cytometry was performed on ImageStreamX Mk2 (Amnis) and analysed using IDEAS v6.2 (Amnis).

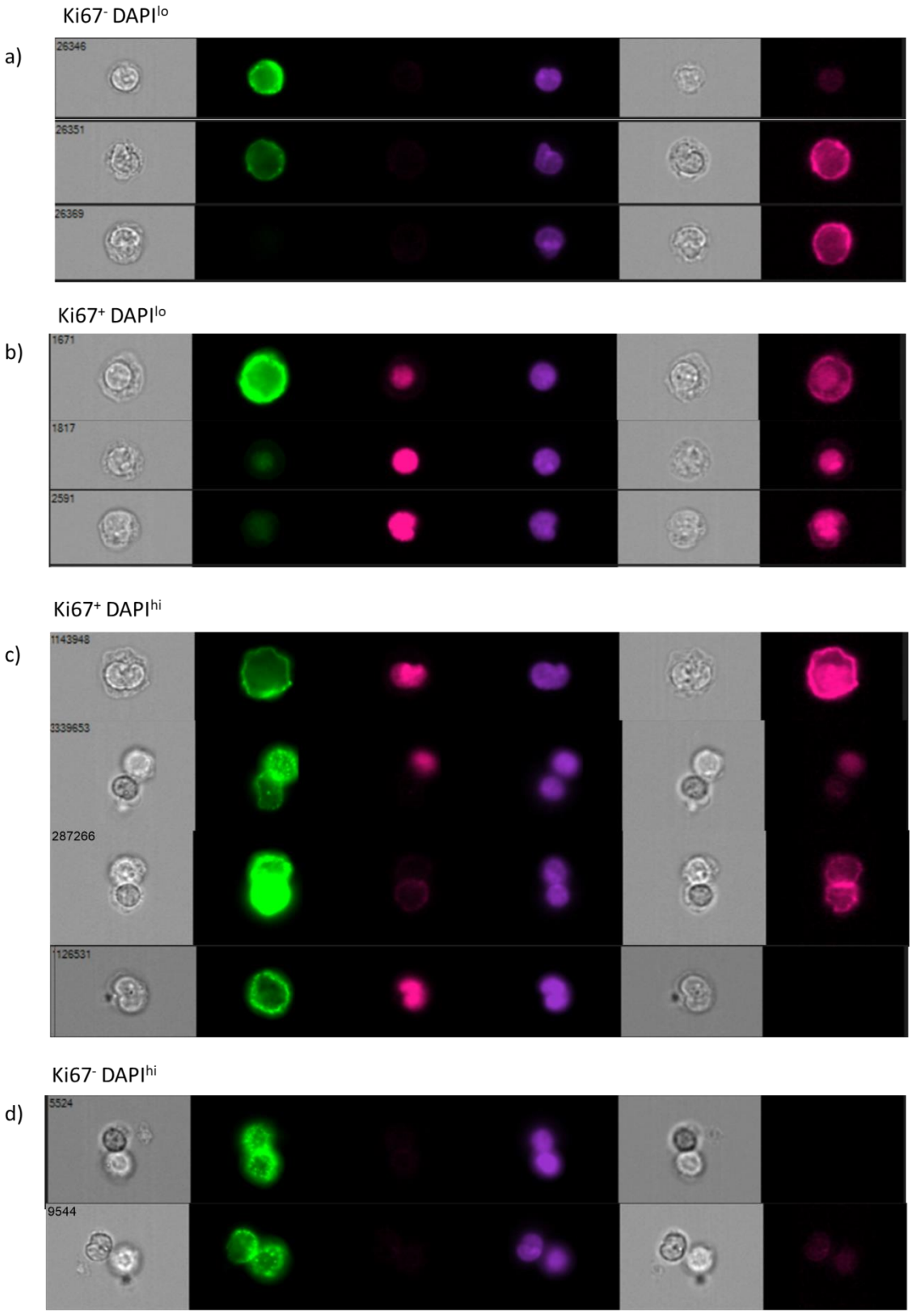

Figure 2.10 **Cell Cycle Imaging**

PBMC were stained with lineage (CD3, CD19, CD20, CD56, CD66b) (green), HLA-DR (pink; last column), Ki67 (pink; 3rd column) and DAPI (purple). Cells were identified as either a) $Ki67^{-}$ $DAPI^{lo}$, b) $Ki67^{+}$ $DAPI^{lo}$, c) $Ki67^{+}$ $DAPI^{hi}$ or d) $Ki67^{-}$ $DAPI^{hi}$. Representative of n=2 individual experiments.

2.6 *In vitro* monocyte culture

PBMC were stained (Section 2.2.1) and classical monocytes were isolated by FACS (Section 2.2.3). 96-well Nunc UpCell flat-bottom plates (Thermo Fisher, Paisley, UK) were coated with or without 1 µg Delta-like ligand 1 (DLL-1) (AdipoGen Life Sciences, Switzerland) in 100 µl PBS overnight at 4°C as previously described (Murata *et al.,* 2010). Wells were washed with PBS and 1 x10^5 classical monocytes was seeded in 200 µl/well Roswell Park Memorial Institute (RPMI) 1640 (Thermo Fisher, Paisley, UK) supplemented with 10% autologous serum, macrophage colony-stimulating factor (M-CSF) (10ng/ml) (Invitrogen, Paisley, UK), thrombopoietin (20ng/ml) (Invitrogen, Paisley, UK), stem-cell factor (10ng/ml) (Invitrogen, Paisley, UK), insulin-like growth factor 2 (20ng/ml) (Invitrogen, Paisley, UK) and fibroblast growth factor-1 (10 ng/ml) (Invitrogen, Paisley, UK) and Heparin (25U/ml). Cells were harvested with cold PBS containing 10mM EDTA and 4mg/ml lidocaine (Sigma Aldrich, Dorset, UK). Cells were washed with PBS and resuspended in FACS buffer, before stained and analysed by flow cytometry.

2.7 Cytospins

Cells were resuspended at 5 x10^5/ml in PBS (+10% FCS). 200 µl was added to a cuvette attached to a slide and a filter card which was bound with a metal holder. Cells were spun at 800 revolutions per minute (RPM) for 8 minutes using a Shandon Cytospin 2, slides were carefully detached from the cuvette and filter card and air dried for 30 minutes. Slides were dipped five times in fixation solution (Thermo Fisher), dried for another 30 minutes, dipped 8 times in Eosin solution (Thermo Fisher) and 4 times in Methylene Blue solution (Thermo Fisher), then washed in tap water. Once dried, DPX was applied to the slides and covered with a coverslip. Cells were analysed using a Nanazoom Digital Pathology (NDP) (Hamamatsu) and images were analysed using NDP.view2 software (Hamamatsu).

2.8 Human in *vivo* deuterium labelling

In vivo deuterium labelling was performed in collaboration with Prof. Derek Macallan and Dr. Yan Zhang at St. George's, University of London. Consented healthy male volunteers were orally administered 20 g of deuterated glucose (6,6-D2) (Cambridge Isotope Laboratories Inc., Massachusetts, United States) dissolved in 100 ml of bottled still water (Highland Spring) over a 3 hour period (**Table 2.2**). In addition, finger prick blood samples (Section 2.1.6) were taken at several time points.

Time	Time elapsed from 1st dose (mins)	Dose (ml)	Finger prick blood sample
09:00	0	40	Yes
09:30	30	10	Yes
10:00	60	10	Yes
10:30	90	10	
11:00	120	10	Yes
11:30	150	10	
12:00	180	10	Yes
12:30	210		Yes
13:00	240		Yes
15:00	360		Yes
17:00	480		Yes
09:00	24 hours		Yes

Table 2.2 **Deuterated glucose dosing schedule**

Dosing regimen for oral administration 20g of deuterated glucose resuspended in 100 ml of drinking water. Following an initial 40 ml priming dose, 10 ml was administered every 30 minutes thereafter.

Volunteers were asked to fast on the day as an increased turnover of glucose is observed during the postprandial state, resulting in increased enrichment of deuterated glucose when administered. To measure plasma enrichment of deuterated glucose, finger prick blood samples were analysed by gas chromatography-mass spectroscopy (GC/MS). 80 ml venous blood was drawn a selected time points, and cells of interested were sorted by FACS (**Figure 2.11**). Cell pellets were stored in protein LoBind eppendorfs at -80°C until ready for analysis by GC/MS. Deuterium enrichment was measured by Dr. Yan Zhang at St. George's Hospital.

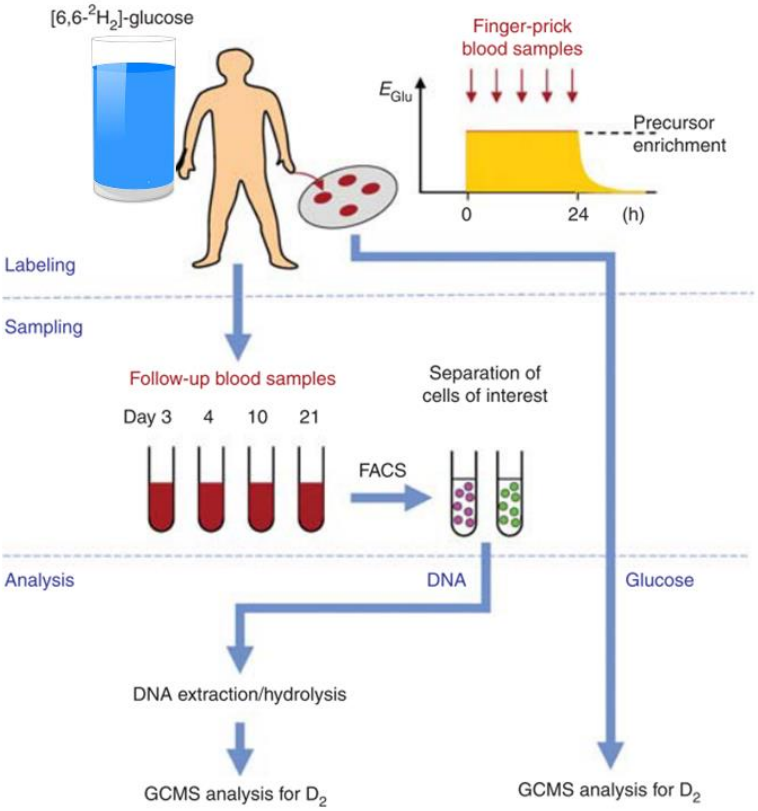

Figure 2.11 **Schematic illustration of deuterium labelling**

An overview of deuterium labelling divided into labelling, sampling and analysis stages. Volunteers were administered deuterated glucose during which plasma enrichment was measured. Venous blood samples were taken over a period of 30 days, where cells of interest were isolated by FACS. Cells were analysed for deuterium enrichment by gas chromatography/mass spectroscopy (Image modified from Macallan *et al.,*).

2.9 Mathematical Modelling

Mathematical models were applied to deuterium labelling kinetic data to estimate unknown parameters such as the delay, rates and lifespan of these cells. Mathematical modelling was performed in collaboration with Dr. Becca Asquith and Dr. Lies Boelen at Imperial College London. R packages modFit and dede were used to fit the model to the observed values of deuterium enrichment. The algorithm minimizes the sum of squared residuals between the modelled curves and observed values. The sum of squared residuals were corrected for a small

sample size using an Akaike information criterion, which also allowed for comparisons between models.

2.9.1 Human Monocyte Model

Based on the kinetic profiles of human monocyte subsets and bone marrow composition, a likely biological scenario was proposed. This scenario provided the basis for the model (**Figure 2.12**). In addition to proposing this model, Tak *et al.,* proposed intermediate monocytes convert to non-classical monocytes outside the circulation (Tak *et al.,* 2017a). This model was tested by incorporating a delay parameter (Δ_3).

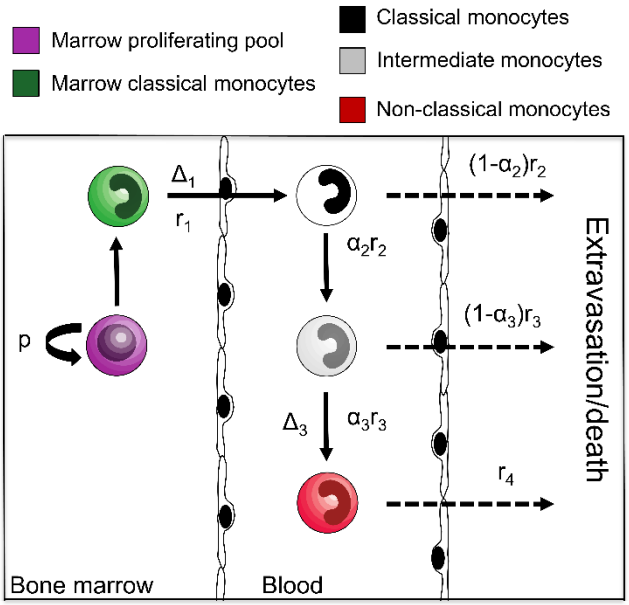

Figure 2.12 **Human Monocyte Mathematical Model**

Based on a likely biological scenario, a mathematical model was implemented to estimate the proliferation rates, lifespan, delay periods regarding human monocyte subsets. Bone marrow progenitors proliferate (p) and give rise to classical monocytes in the bone marrow which reside in this compartment (Δ_1) before released into the circulation at a rate of r_1. A proportion of circulating classical monocytes (α_2) will mature into intermediate monocytes at a rate of r_2. It was assumed classical monocytes that don't mature into intermediate monocytes ($1-\alpha_2$) leave the circulation also at a rate of r_2. Similarly, a fraction of intermediate monocytes mature into non-classical monocytes (α_3) at a rate of r_3 and a the remaining ($1-\alpha_3$) will leave at the same rate (r_3). In addition, a delay parameter (Δ_3) between intermediate and non-classical monocyte differentiation was tested.

N was denoted as the number of bone marrow classical monocytes, B_1 as blood classical monocytes, B_2 as the number of blood intermediate monocytes and B_3 as the number of blood non-classical monocytes. It was assumed that all compartments are in steady-state. The size of the blood compartments were taken from flow cytometry data.

The dynamics of these four compartments could be described by the following equations:

$$\frac{dN}{dt} = pN - r_1 N$$

$$\frac{dB_1}{dt} = r_1 N(t - \Delta_3) - r_2 B_1$$

$$\frac{dB_2}{dt} = \alpha_2 r_2 B_1 - r_3 B_2$$

$$\frac{dB_3}{dt} = \alpha_3 r_3 B_2(t - \Delta_3) - r_4 B_3$$

It is assumed that all the compartments are in steady state. The relative sizes of B_1, B_2, and B_3 were taken from flow cytometry data for each individual. From these equations, the dynamics of the fraction of labelled cells in each compartment can be derived: F_N for the bone marrow and F_x for blood compartments B_x:

$$\frac{dF_N}{dt} = pU(t)b - r_1 F_N$$

$$\frac{dF_1}{dt} = r_1 \frac{N}{B_1} F_N(t - \Delta_1) - r_2 F_1$$

$$\frac{dF_2}{dt} = \alpha_2 r_2 \frac{B_1}{B_2} F_1 - r_3 F_2$$

$$\frac{dF_3}{dt} = \alpha_3 r_3 \frac{B_2}{B_3} F_2(t - \Delta_3) - r_4 F_3$$

U(t) is the precursor enrichment (plasma glucose) at time t, described empirically as a plateau function with exponential decay.

2.10 Human Endotoxin Model

2.10.1 Endotoxin Challenge

2ng/kg Clinical Centre Reference Endotoxin (CCRE, *E. coli* O:113 EC-6, NIH, Bethesda, United States) was administered intravenously (I.V.) to consented healthy male volunteers by Dr. James Fullerton, as previously described (Fullerton *et al.,* 2016). Participants were asked to refrain consuming food from midnight prior to I.V. endotoxin administration and coffee and alcohol 48 hours before. After administering I.V. endotoxin, blood samples were taken at baseline, 2, 4, 6, 8, 24, 48, 72 and 96 hours and 7 days post challenge and analysed by flow cytometry in addition to The Doctor's Laboratory for full blood counts (Section 2.3.3).

2.10.2 Endotoxin Challenge with Deuterium labelling

In order to assess the origin of monocytes during endotoxin challenge, subjects received deuterated glucose 20 hours prior to endotoxin administration (**Figure 2.13**). Monocyte subsets were sorted by FACS at baseline, 8, 24, 48, 72 hours and 7 days post challenge and labelling kinetics were analysed as described (Section 2.8).

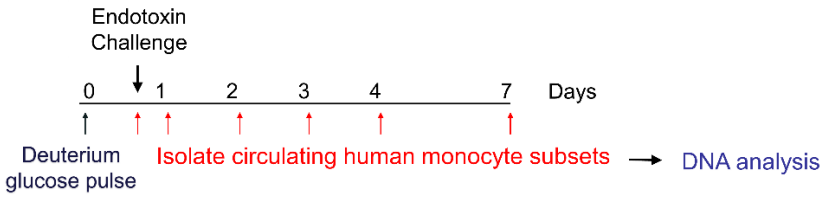

Figure 2.13 **Endotoxin Protocol Outline**

Volunteers were administered 20g of deuterated glucose 20 hours prior to endotoxin challenge. Monocyte subsets were isolated by FACS at 8, 24, 48, 72 hours and 7 days post endotoxin challenge and analysed for deuterium labelled DNA by GC/MS.

2.11 UV-killed *E. coli* human blister model

2.11.1 Administration of UV-killed *E. coli* and sample collection

Escherichia coli (E. coli) (Strain: NCTC 10418, Public Health England, UK) were grown and killed by UV light, as previously described (Motwani *et al.,* 2016). Bacterial counts were determined by optical density and resuspended to a count of 1.5 x 10^8/ml in sterile saline where non-viability was confirmed by UCLH Microbiology department. Following screening and consent of healthy male volunteers, 1.5 x 10^7 UV-killed *E. coli* in 100 µl saline was intradermally injected using a 30 gauge needle into each forearm approximately 7 cm from the cubital fossa by clinicians (Dr. Alexander Maini and Dr. James Glanville). A 10 mm diameter suction blister was induced at either 6, 24, 48 or 96 hours post-challenge over the challenged site by a negative pressure instrument (NP-4, Electronic diversities Ltd., Maryland, United States). After placing the suction chamber over the site, negative pressure was gradually applied from 2 to 10 inches of Mercury (Hg) (**Table 2.3**). If a blister formed before maximum pressure, the pressure was maintained at that level until the blister was fully formed.

Pressure (Hg)	Time (minutes)
2	1
3	1
4	1
5	5
6	5
7	10
8	10
9	Until blister forms

Table 2.3 **Blister formation**

A suction chamber was placed over the injected site and negative pressure was gradually applied from 2 to 9 Hg periodically.

Once a blister was formed, the pressure was gradually reduced by 1 Hg every minute and aspirated immediately using a 23 gauge needle. All exudate was collected using a pipette into a 96-well plate containing 50 µl of 3% sodium citrate in PBS. The blistered site was then sterilised with antiseptic spray and covered with an adhesive surgical dressing.

2.11.2 Sample preparation

After collecting the blister sample, 96-well plates were centrifuged at 1000 x *g*, for 5 minutes at 4°C. Blister fluid was aliquoted into protein LoBind eppendorfs and stored at -80°C. Eppendorfs were weighed with and without blister fluid to estimate the volume of blister fluid and 0.05 g was further subtracted to account for the 50 µl of sodium citrate. The blister cell pellet was resuspended in FACS buffer, stained and prepared as described in Section 2.2.1. Cells were analysed by flow cytometry or single cell sorted by FACS into 96-well plates (Section 2.2.3).

2.11.3 Laser Doppler Imaging

Non-invasive blood flow measurements were also taken at the challenged site. To measure blood flow at the site of inflammation, Laser Doppler imaging was implemented. Red and infrared wavelengths of light are emitted at the site, the laser light is then scattered by red blood cells, where the scatter is proportional to both the concentration and speed of red blood cells. A flux image was generated and indicates areas of high and low blood flow. Measurements were made using a moorLDI2 Laser Doppler imager (Moor Instruments Ltd, Axminster, UK) and images were analysed by moor LDI software v5.2.

2.12 Mice

2.12.1 MISTRG mice

10-week-old MISTRG mice were used for adoptive transfer experiments. MISTRG mice express human knock-in genes encoding M-CSF, IL-3, GM-CSF, SIRPα and TPO in $RAG2^{-/-}$ $IL\text{-}2Rg^{-/-}$ mice (Rongvaux *et al.,* 2014). Mice were maintained under specific pathogen-free conditions and handled under protocols approved by the Yale Institutional Animal Care and Use Committee.

These experiments were performed by Dr. Simon Yona, UCL in collaboration with Prof. Richard Flavell and Dr. Anthony Rongvaux at Yale University.

2.12.2 Adoptive Transfer

Human blood was collected from healthy volunteers and classical monocytes were isolated by FACS (Section 2.2.3). 1 x10^6 human classical monocytes were adoptively transferred intravenously into MISTRG mice. Peripheral murine blood was collected by cardiac puncture under terminal anaesthesia at 10 minutes, 24, 72 and 96 hours post adoptive transfer and erythrocytes were lysed. Cells were stained with mouse CD45, human CD45, HLA-DR, CD33, CD3, CD19, CD20, CD56, CD66b, CD14 and CD16 and analysed by flow cytometry at each time point.

2.13 Statistical analysis

Prism v8 (GraphPad) software was used to perform statistical analysis. Statistical tests used are reported in the figure legends.

Chapter 3

Monocyte and Dendritic Cell Characterisation

3.1 Introduction and Aims

3.1.1 Introduction

Monocytes and dendritic cells (DC) make-up the circulating mononuclear phagocyte pool in humans. Based on an approved classification of mononuclear phagocytes (Ziegler-Heitbrock *et al.,* 2010), human monocytes are defined as either classical, intermediate or non-classical subsets depending on their expression of CD14 and CD16 (Passlick *et al.,* 1989). However, various strategies have been implemented within the literature to identify monocytes by flow cytometry.

Blood DC can be divided into two conventional (cDC) subsets and plasmacytoid (pDC) subsets. However, since this classification, two independent groups have recently identified several DC populations by single-cell RNA sequencing (See *et al.,* 2017; Villani *et al.,* 2017), which will be discussed in this chapter.

3.1.2 Aims

Identify and characterise monocytes and newly described DC subsets by flow cytometry under steady physiological conditions, laying the foundations for the remainder of this thesis.

3.2 Identification of blood monocyte subsets

3.2.1 Classification of circulating human monocyte subsets

In 1989, Passlick *et al.,* demonstrated monocytes express both CD14 and CD16 antigens (Passlick *et al.,* 1989), leading to the recognition of human monocyte subsets. To date, CD14 and CD16 remain as the two conventional markers to identify human monocytes. Nevertheless, these two markers alone are not enough to identify monocytes from whole blood, as they are also expressed on other leukocyte populations such as T cells (CD3), B cells (CD19 and CD20) NK cells (CD56) and neutrophils (CD66b) (**Figure 3.1**).

A rigorous gating strategy was implemented where T cells, B cells, NK cells and neutrophils were excluded and within the lineage $(Lin)^-$ population, HLA-DR^+ cells were gated to identify monocytes (**Figure 3.2**). Monocytes form a continuum due to the nature of their CD14 and CD16 expression and can be divided into three recognised subsets. Classical monocytes are classified as $CD14^+$ $CD16^-$ cells, intermediate monocytes as $CD14^+$ $CD16^+$ and non-classical monocytes as $CD14^{lo/-}$ $CD16^+$ cells. Due to the nature of this continuum, box gating strategy was utilised to allow for strict identification of monocyte subsets rather than using quadrant gating where imprecision may occur. Of note, the $CD14^-$ $CD16^-$ subset contains circulating DC subsets which are discussed further in Section 3.3.

Classical monocytes are often defined as $CD16^-$ within the literature, however as can be observed from **Figure 3.2**, it would be more accurate to define this dense population as $CD16^{-/lo}$.

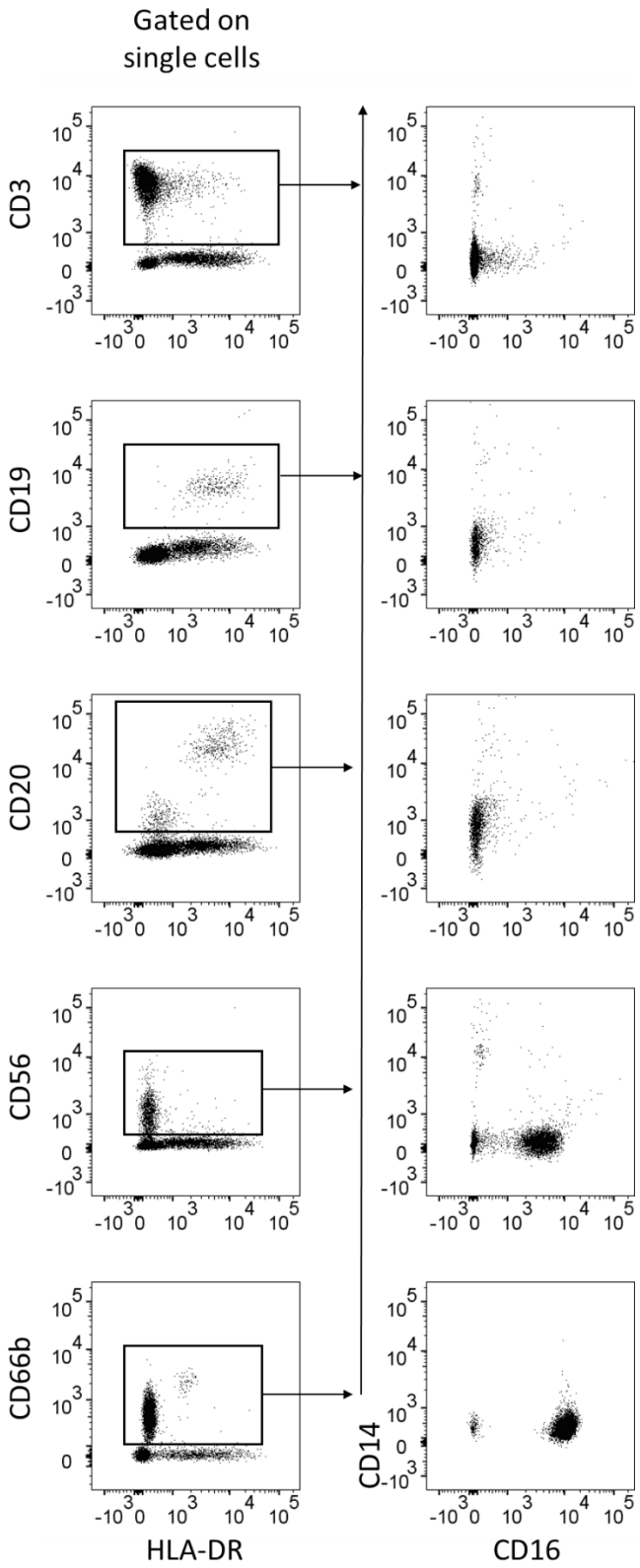

Figure 3.1 **CD14 and CD16 expression on leukocyte subsets**

ACK lysed blood was stained with CD3, CD19, CD20, CD56 or CD66b and HLA-DR. Cells expressing these lineage markers were analysed for CD14 and CD16 expression. Representative of n=3 individual experiments.

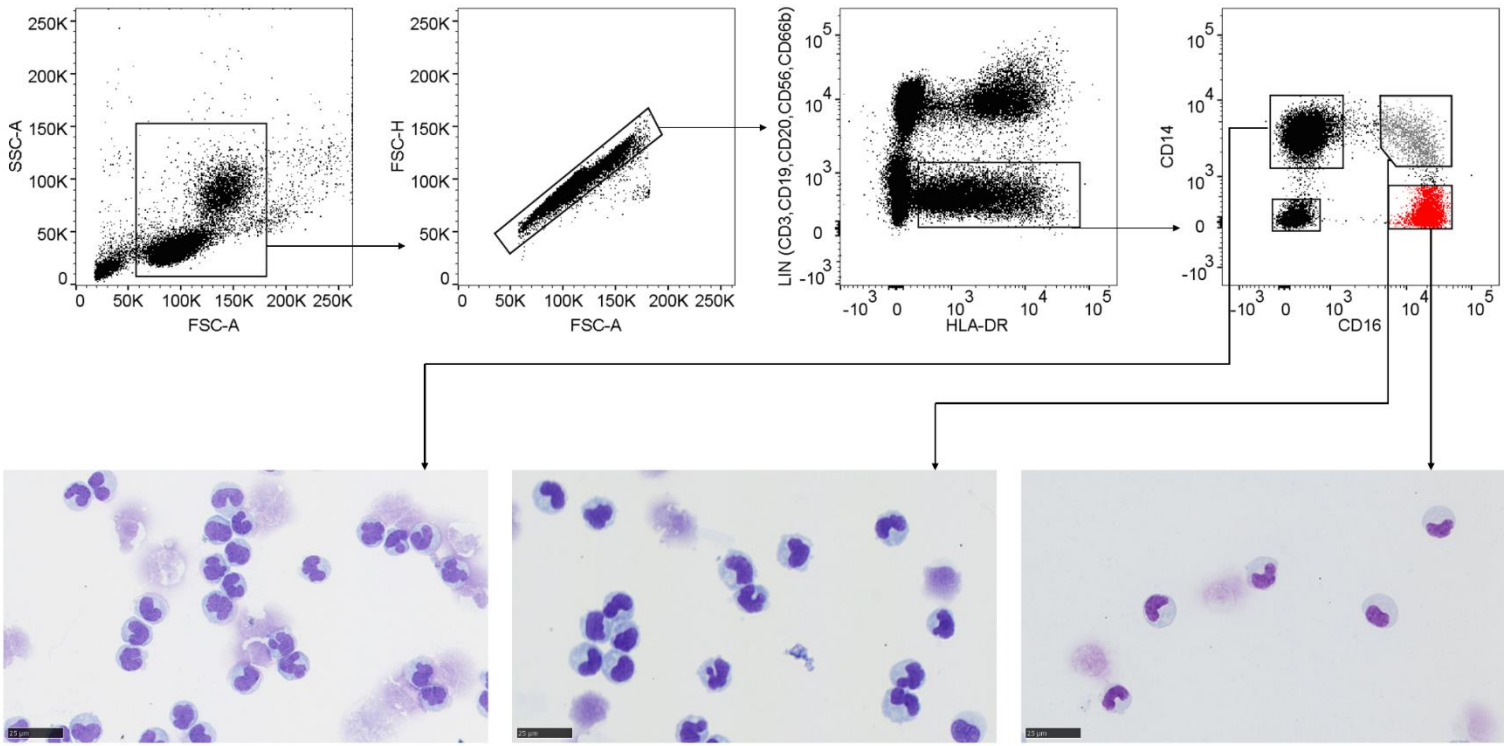

Figure 3.2 **Identification of human blood monocyte subsets**

PBMC were isolated and stained for flow cytometry analysis. Monocytes are found within the Lin (CD3, CD19, CD20, CD56, CD66b)$^-$ HLA-DR$^+$ fraction of PBMC. Classical monocytes are identified as CD14$^+$ CD16$^{-/lo}$ cells (black), intermediate monocytes as CD14$^+$ CD16$^+$ cells (grey) and non-classical monocytes as CD14$^{lo/-}$ CD16$^+$ (red). CD14$^-$ CD16$^-$ cells harbour dendritic cell subsets. Haematoxylin and eosin stains for monocyte subsets are shown below (scale bar, 25µm). Representative of n=15 healthy volunteers.

Haematoxylin and eosin cytospin stains confirmed the mononuclear morphology of these cells with the typical kidney bean-shaped nucleus as historically ascribed to monocytes (**Figure 3.2**).

3.2.2 Circulating monocyte count

Within the literature, monocyte subsets have been identified using quadrant gating or box gating. The latter is a stricter strategy which allows for the exclusion of monocytes that prove difficult to classify. Previous studies in mice have demonstrated a developmental between monocyte subsets (Gamrekelashvili *et al.,* 2016; Mildner *et al.,* 2017; Sunderkötter *et al.,* 2004; Varol *et al.,* 2007; Yona *et al.,* 2013). It was hypothesised that human monocytes are also developmentally related, a question this thesis will aim to address. As a result, box gating will be adopted throughout this thesis (unless stated otherwise) to ensure bona fide classical, intermediate and non-classical monocytes are analysed and not the potentially 'transitioning' monocytes which lie in between (**Figure 3.3a**). Significant differences were found in neither the percentage nor absolute count of monocyte subsets between the two strategies (**Figure 3.3b**), suggesting either method can be used for enumeration of monocyte subsets under steady-state.

Monocytes make up approximately 5% of $CD45^+$ circulating leukocytes (**Figure 3.3b**). Of total monocytes, classical monocytes make up 86.0 (± 5.2) %, intermediate monocytes 5.5 (± 2.7) % and non-classical monocytes 8.4 (± 3.25) % (**Figure 3.3b**). Counting beads were used to enumerate the absolute count of monocyte subsets in blood. Classical monocytes are found at a concentration of approximately 195,000 (± 51,000) cells/ml blood. Whilst intermediate and non-classical monocytes are found at similar concentrations of 12,800 (± 7,500) cells/ml and 20,700 (± 13,300) cells/ml blood, respectively. The total monocyte count falls within the clinical reference range of 0.2 – 1.0 $x10^6$/ml blood (The Doctor's Laboratory).

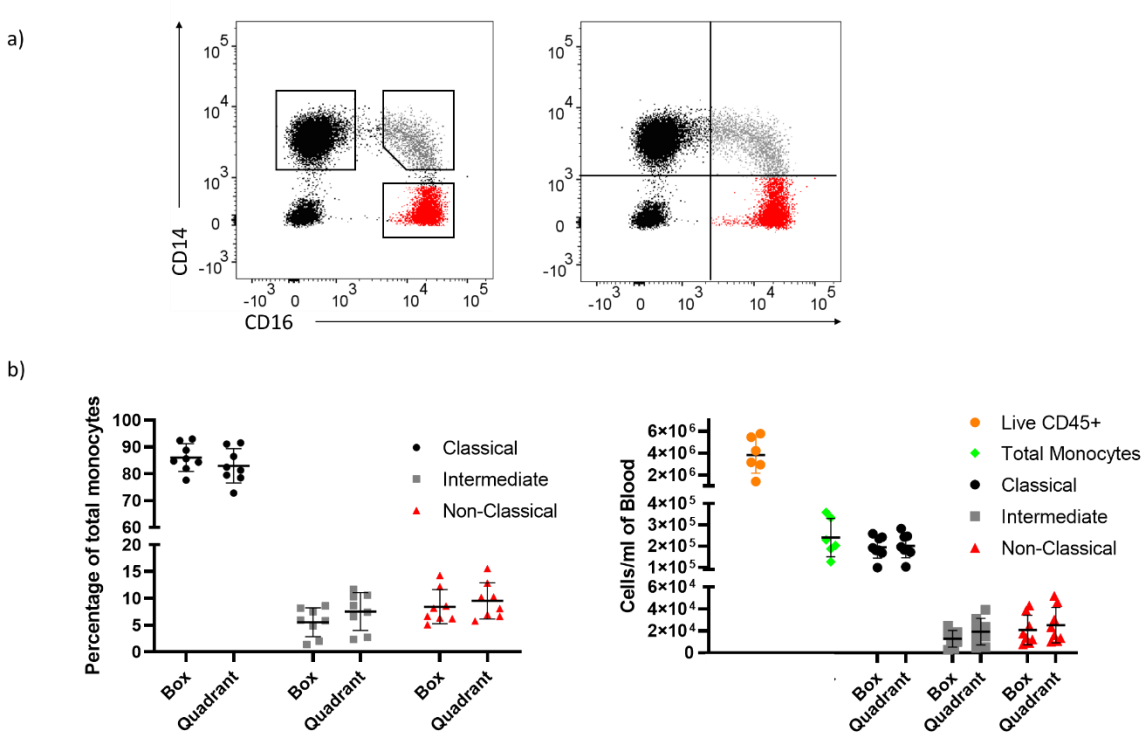

	Classical monocytes (ml/blood)	Intermediate monocytes (ml/blood)	Non-classical monocytes (ml/blood)
Box Gating	195,000 ± 51,000	12,800 ± 7,500	20,700 ± 13,300
Quadrant Gating	201,000 ± 55,400	19,200 ± 12,000	25,200 ± 16,200

Figure 3.3 **Proportion and count of monocyte subsets**

To investigate differences in strategies used to define monocyte subsets, **a)** monocytes were gated using box gating (left) or quadrant gating (right). **b)** Classical (black), intermediate (grey) and non-classical (red) monocytes were expressed as a percentage of total monocytes (left) and absolute count (right) enumerated by box and quadrant gating. No significant differences were observed between the type of gating strategy used. Average count/ml of blood and standard deviation (SD) are shown in the table below for each subset and gating strategy. Analysed by two-way ANOVA and Bonferroni multiple comparisons tests. Bars represent mean ± SD. n=8 individual experiments.

3.2.3 Characterisation of human monocyte subsets

3.2.3.1 Cell membrane marker expression

In mice, Ly6C expression is used to define monocyte subsets, whilst in rats and pigs, CD43 and CD163 are used, respectively (Geissmann *et al.,* 2003; Ziegler-Heitbrock, 2014). To examine whether human subsets resemble those in mice, markers known to be differentially expressed between mouse monocyte subsets were measured on human monocyte subsets and shown as histograms (**Figure 3.4**) which were quantified by calculating the gMFI (**Figure 3.5**). In addition to showing the expression on discrete monocyte subsets, viSNE analysis examined marker expression across the monocyte continuum (**Figure 3.6**).

The chemokine receptors, CCR2 and CX_3CR1 are often used in murine studies to further classify monocytes subsets (Geissmann *et al.,* 2003)**.** Like murine monocytes, classical monocytes expressed higher levels of CCR2 yet lower level of CX_3CR1, whilst the converse was true for non-classical monocytes (**Figure 3.4, Figure 3.5, Figure 3.6**). Additional markers measured were also differentially expressed between human monocyte subsets. Some markers (CD141, CD123) were observed to gradually increase from classical to intermediate to non-classical monocytes, whilst others progressively decreased in expression (CD64, CD62L, CD36). However, CD11b, CD1c, CD11c and HLA-DR expression did not follow the gradual trend and the highest expression was found on intermediate monocytes (**Figure 3.5**).

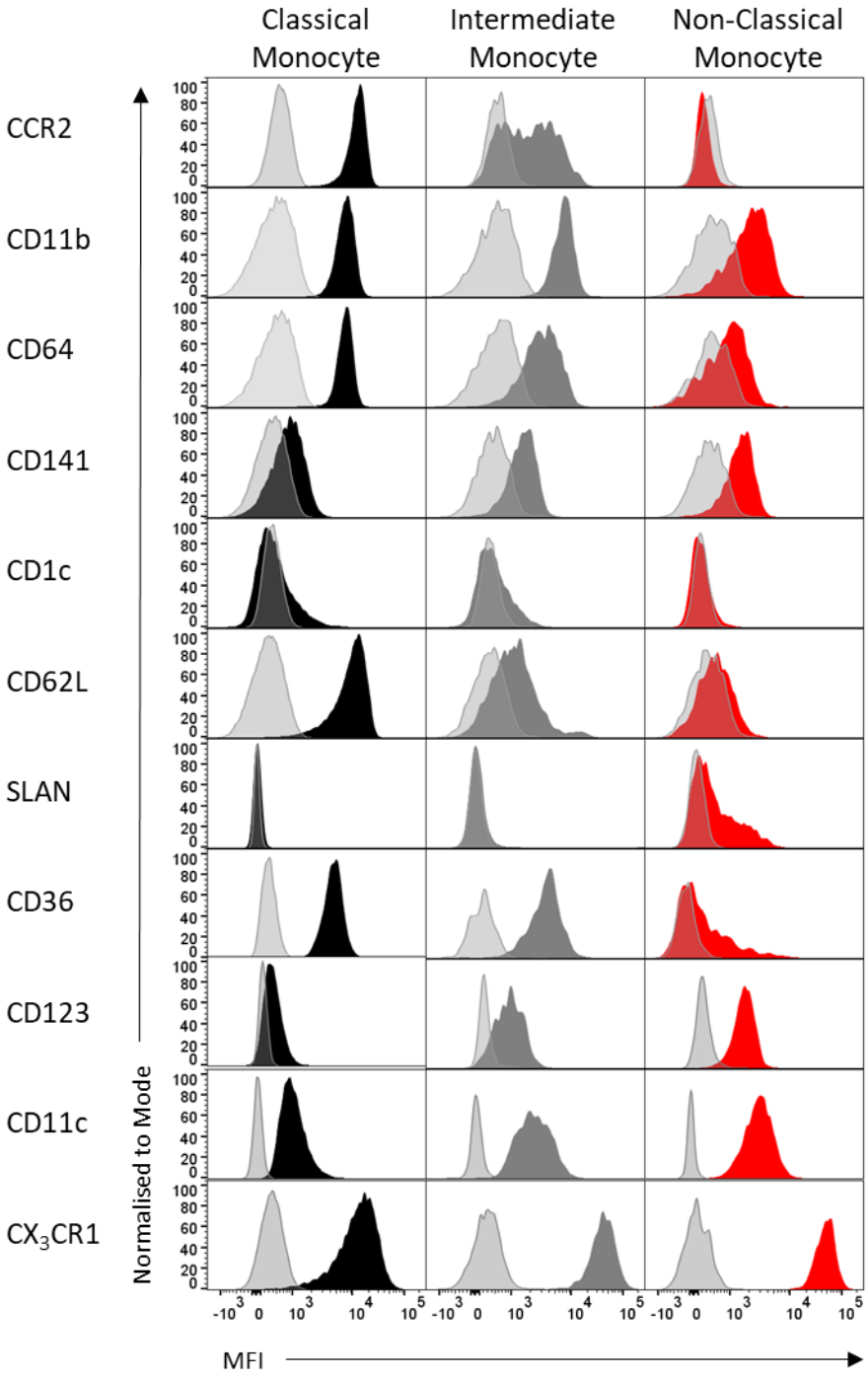

Figure 3.4 **Qualitative surface membrane expression on circulating monocyte subsets**

Monocyte subsets were identified by flow cytometry as in Figure 3.2. CCR2, CD11b, CD64, CD141, CD1c, CD62L, SLAN, CD36, CD123, CD11c, and CX_3CR1 expression was measured on classical (black), intermediate (grey) and non-classical (red) monocytes and shown as histograms. Isotype controls are shown in light grey. Representative of n=6 individuals.

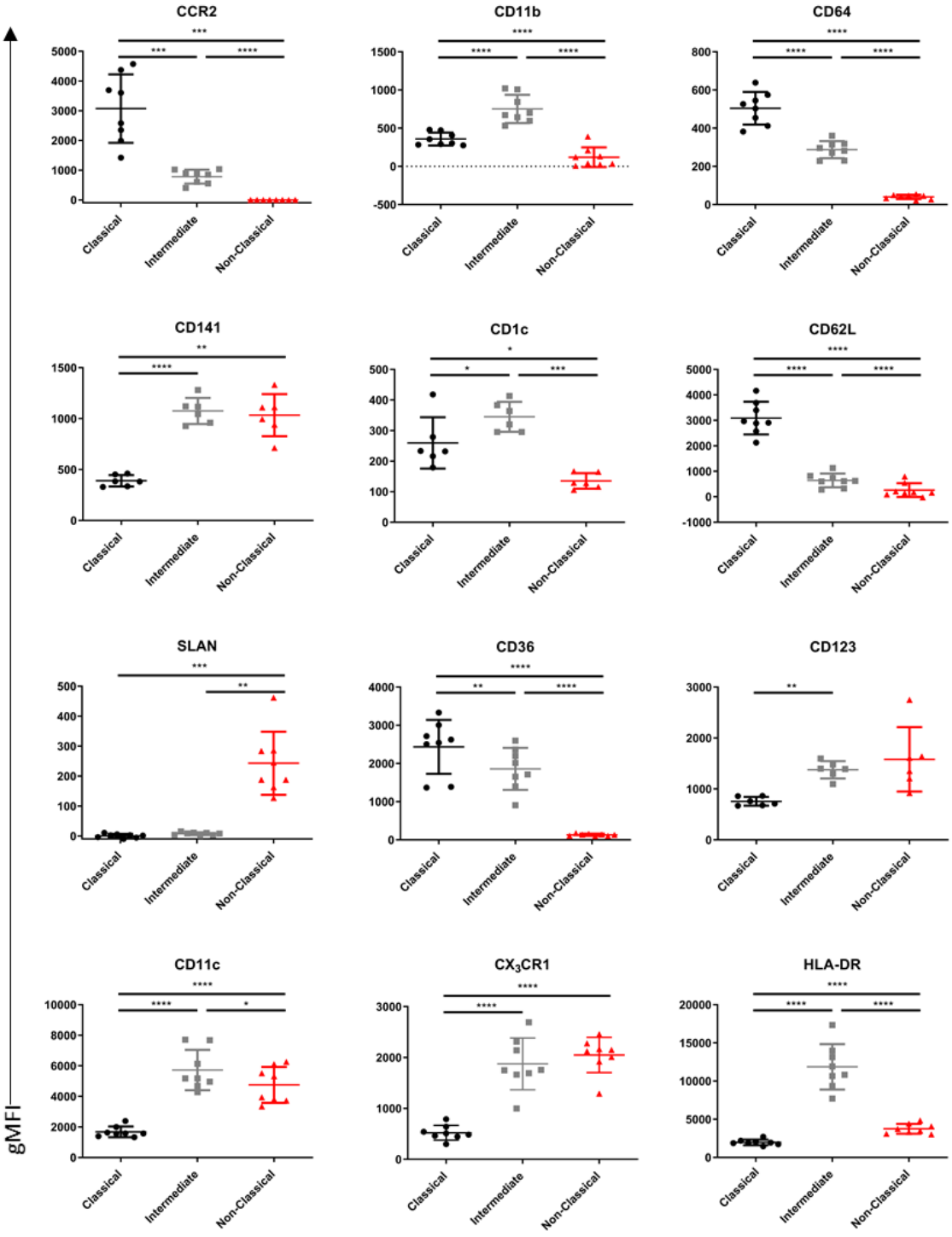

Figure 3.5 **Quantitative surface membrane expression on circulating monocyte subsets**

gMFI values of CCR2, CD11b, CD64, CD141, CD1c, CD62L, SLAN, CD36, CD123, CD11c, CX_3CR1 and HLA-DR expression on classical, intermediate and non-classical monocytes. Analysed by one-way ANOVA , followed by post-hoc Tukey multiple comparisons test. **** $p < 0.0001$, *** $p < 0.001$, ** $p < 0.01$, * $p < 0.05$. Bars represent mean ± SD. n=6-8 individual experiments.

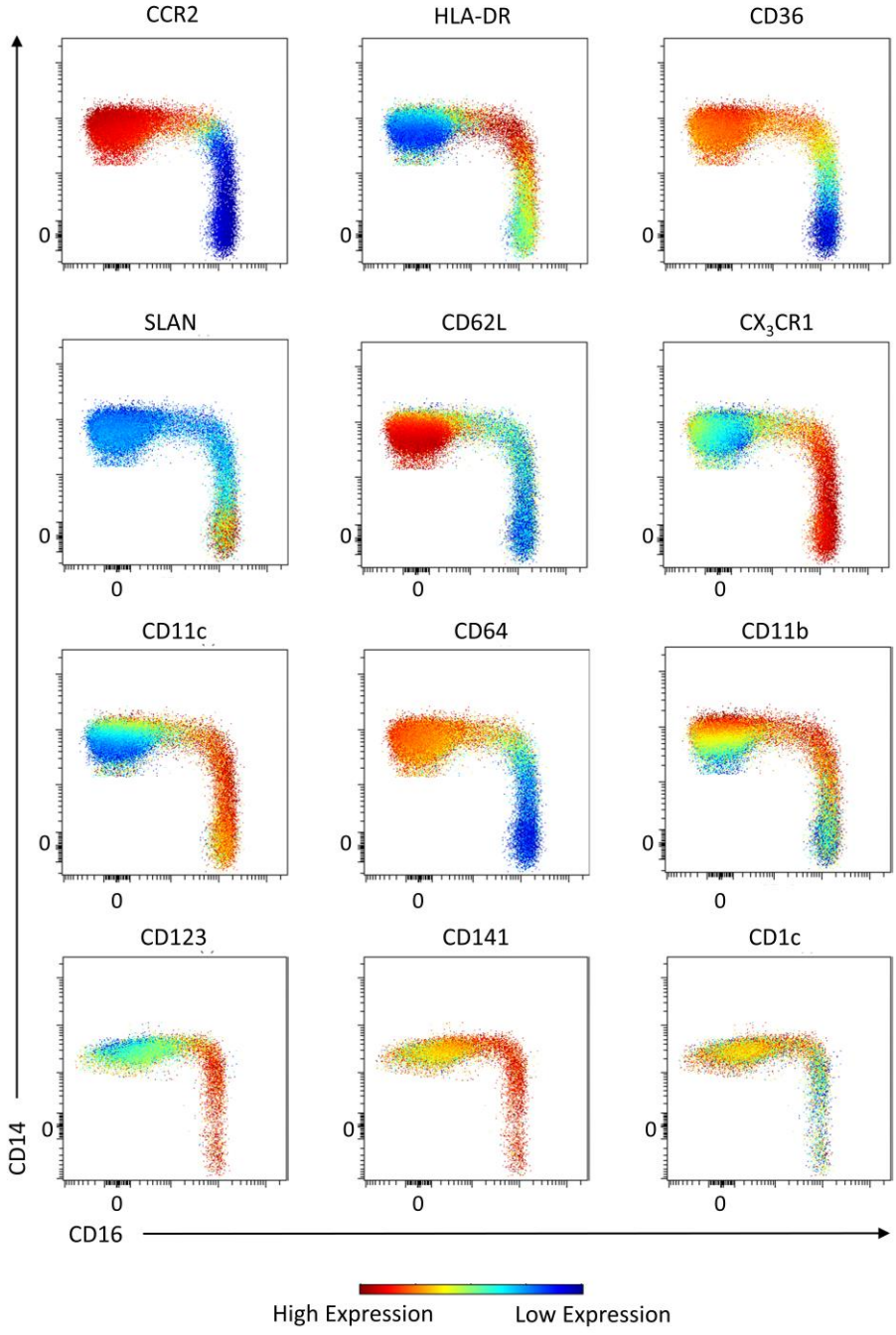

Figure 3.6 **viSNE analysis of membrane expression on monocytes**

Membrane surface marker expression was analysed on monocytes by viSNE analysis. Monocytes were identified as Lin^- $HLA\text{-}DR^+$ cells. Markers were analysed across the monocyte continuum defined by CD14 and CD16 and expression is shown as a heatmap. Representative of n=6 individual experiments.

Interestingly, markers associated with DC identity such as CD11c, CD1c, CD141 and CD123 were also expressed on monocyte subsets. CD141, CD123 and CD11c were highly expressed on intermediate and non-classical monocytes in comparison to classical monocytes. Whereas, CD1c was more highly expressed on classical and intermediate monocytes. However, DC contamination was unlikely as DC are defined by their lack of CD14 and CD16 expression (Haniffa *et al.,* 2012).

viSNE analysis allowed changes to be observed along the monocyte continuum but also demonstrated differences in marker expression within each subset, that would normally be masked by a histogram representation. For example, whilst CD11c and CD11b histograms appear to have uniform peaks on classical monocytes (**Figure 3.4**), viSNE analysis showed gradual changes in expression within this subset (**Figure 3.6**).

3.2.3.2 Non-classical monocyte heterogeneity

Non-classical monocytes were shown to be heterogeneous in terms of SLAN and CD36 expression (**Figure 3.4**). As previously documented (Cros *et al.,* 2010; Schäkel *et al.,* 2002), $SLAN^-$ and $SLAN^+$ non-classical populations could be identified, where the $SLAN^+$ population constitutes approximately 36.7 (± 13.43) % of non-classical monocytes (**Figure 3.7**).

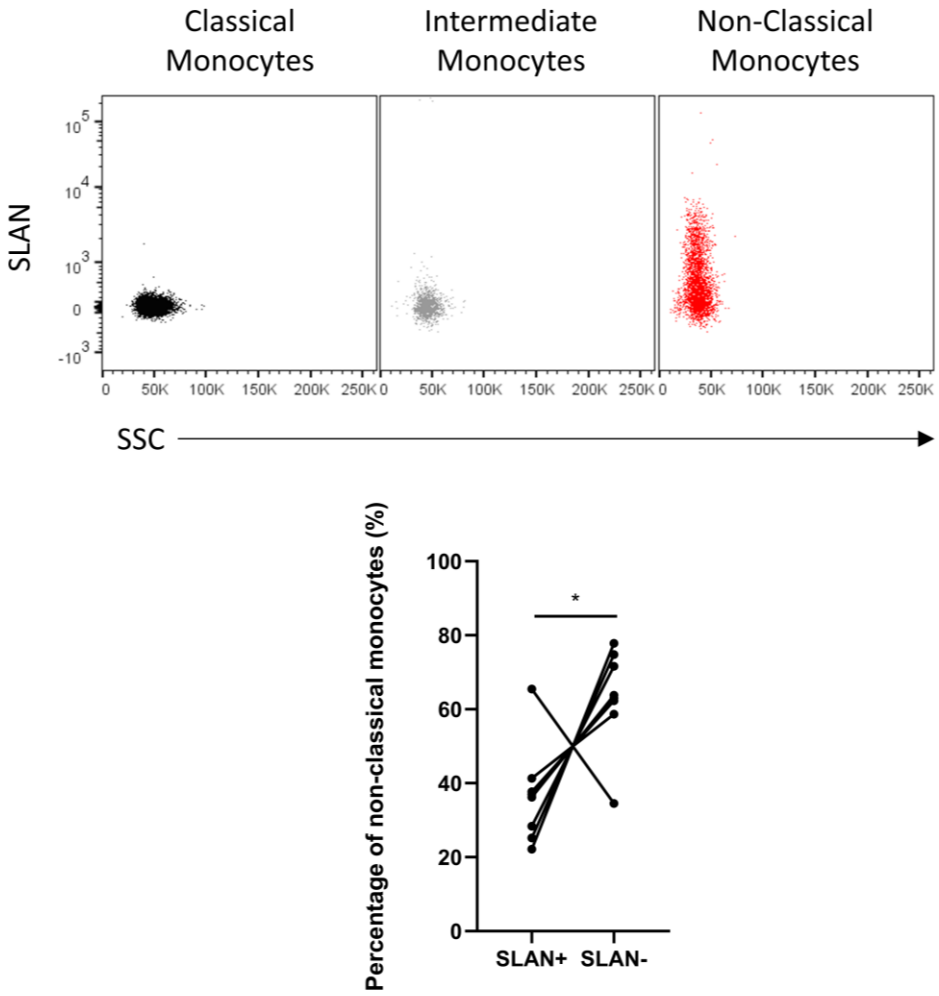

Figure 3.7 **Non-classical monocyte heterogeneity**

SLAN surface marker expression on classical (black), intermediate (grey) and non-classical (red) monocytes. Percentage of $SLAN^+$ and $SLAN^-$ non-classical monocytes. n=8 individual experiments. * $P < 0.05$ (Paired t-test).

Marker expression was analysed between $SLAN^+$ and $SLAN^-$ populations, all markers appeared to have the same level of expression, except CD36. To assess this heterogeneity, non-classical monocytes were divided by SLAN and CD36. Interestingly, all four possible populations could be identified within non-classical monocytes: $SLAN^-$ $CD36^-$, $SLAN^-$ $CD36^+$, $SLAN^+$ $CD36^-$ and $SLAN^+$ $CD36^+$ (**Figure 3.8**).

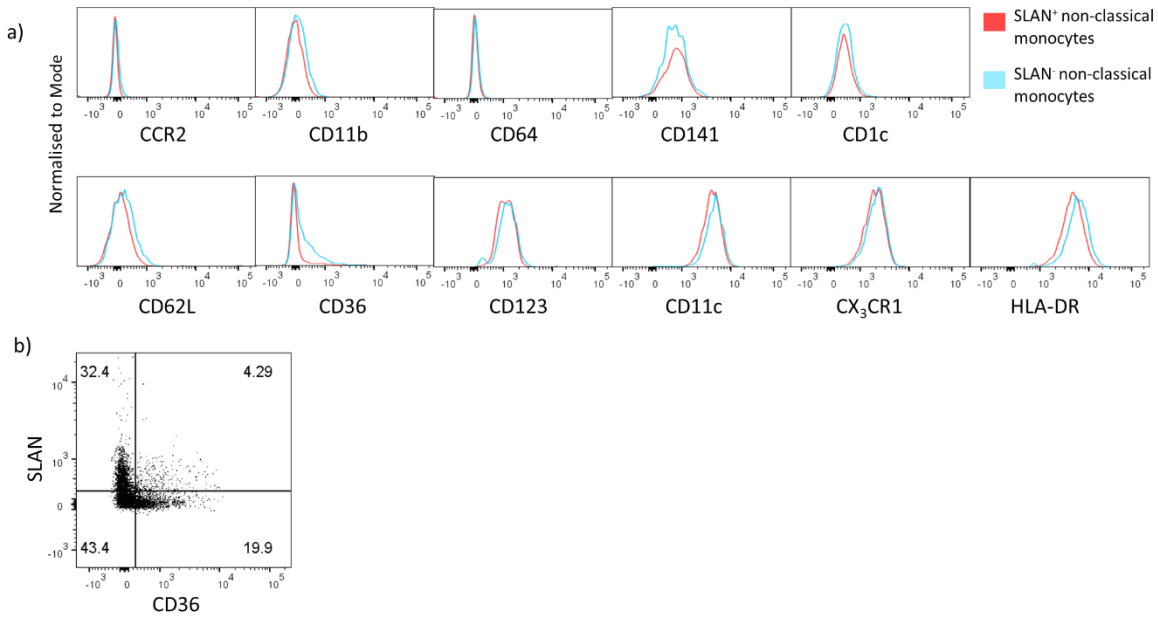

Figure 3.8 **Characterisation of SLAN$^+$ and SLAN$^-$ non-classical monocytes**

Membrane marker expression was analysed on SLAN$^+$ and SLAN$^-$ non-classical monocytes. **a)** CCR2, CD11b, CD64, CD141, CD1c, CD62L, CD36, CD123, CD11c, CX_3CR1, HLA-DR expression was measured on both non-classical monocyte subsets. **b)** Non-classical monocyte heterogeneity defined by SLAN and CD36 expression. Representative of n=5 individual experiments.

3.3 Characterisation of blood dendritic cell subsets

3.3.1 Identification of blood dendritic cell subsets

3.3.1.1 Initial gating strategy

In humans, DC can be found within the circulation unlike in mice. These cells have their own distinct ontogeny from that of monocytes (Lee *et al.,* 2015; Liu *et al.,* 2009; Onai *et al.,* 2007) and can be broadly classified into two groups: Plasmacytoid DC (pDC) and Conventional/Classical DC (cDC) which are further divided into cDC1 and cDC2**.** As mentioned in Section 3.2.1, Lin^- $HLA\text{-}DR^+$ $CD14^-$ $CD16^-$ gate includes bona fide DC. pDC can be identified within this fraction as $CD123^+$ $CD11c^-$ cells, whilst cDC are taken as $CD123^-$ $CD11c^+$ cells which are further split into cDC1 and cDC2 as $CD141^+$ $CD1c^-$ and $CD141^-$ $CD1c^+$ cells, respectively (**Figure 3.9**).

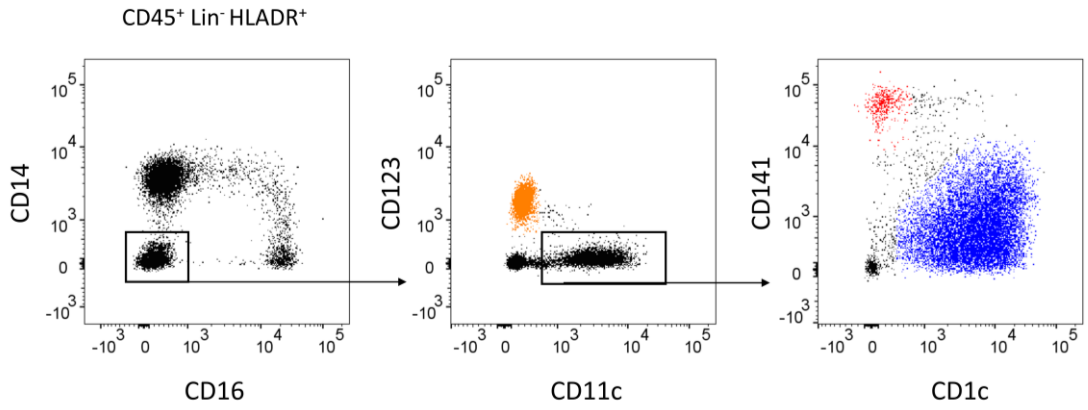

Figure 3.9 **Identification of circulating human dendritic cells**

Isolated PBMC were analysed by flow cytometry to identify DC subsets. Dendritic cells are defined as Lin^- $HLA\text{-}DR^+$ $CD14^-$ $CD16^-$ cells. Plasmacytoid DC (pDC) are identified as $CD123^+$ $CD11c^-$ (orange), conventional DC (cDC) as $CD123^-$ $CD11c^+$ which can be further subdivided into cDC1 and cDC2 as $CD141^+$ $CD1c^-$ cells (red) and $CD141^{lo/-}$ $CD1c^+$ cells (blue), respectively. Representative of n=10.

3.3.1.2 Revised gating strategies

Until recently, human circulating DC have been identified as described in **Figure 3.9**. During the course of this study, it has since been demonstrated by single cell RNA sequencing analysis that further heterogeneity exists within DC subsets (See *et al.,* 2017; Villani *et al.,* 2017), where up to seven DC subsets have been described.

Both strategies will be discussed individually before compared with one another to form a unified DC gating strategy.

Using the same markers and gating strategy defined by Villani *et al.,* the 7 DC populations described within human blood were reproduced (**Figure 3.10a**). cDC1 were still identified using CD141, cDC2 by CD1c but could now be divided into a $CD1c^{hi}$ and $CD1c^{lo}$ subset and pDC were recognised by CD123 expression. Two novel DC subsets were identified: an AXL^+ $Siglec6^+$ (AS^+ DC) population and $CD100^+$ $CD34^{int}$ DC progenitors. The AS^+ DC were further divided into a $CD123^+$ $CD11c^-$ subset and a $CD123^-$ $CD11c^+$ subset. The 7th DC subset was described as $CD1c^-$ $CD141^-$ $CD11c^-$ yet $CD16^+$, however, it has since been demonstrated that this DC subset overlaps with non-classical monocytes (Calzetti *et al.,* 2018; Günther *et al.,* 2019) and is no longer considered a DC.

See and colleagues, also identified heterogeneity within the $CD123^+$ DC fraction, namely a $CD123^+$ CX_3CR1^+ $CD2^+$ population termed 'pre-DC' and a $CD123^+$ CX_3CR1^- $CD2^{+/lo}$ pDC population (**Figure 3.10b**).

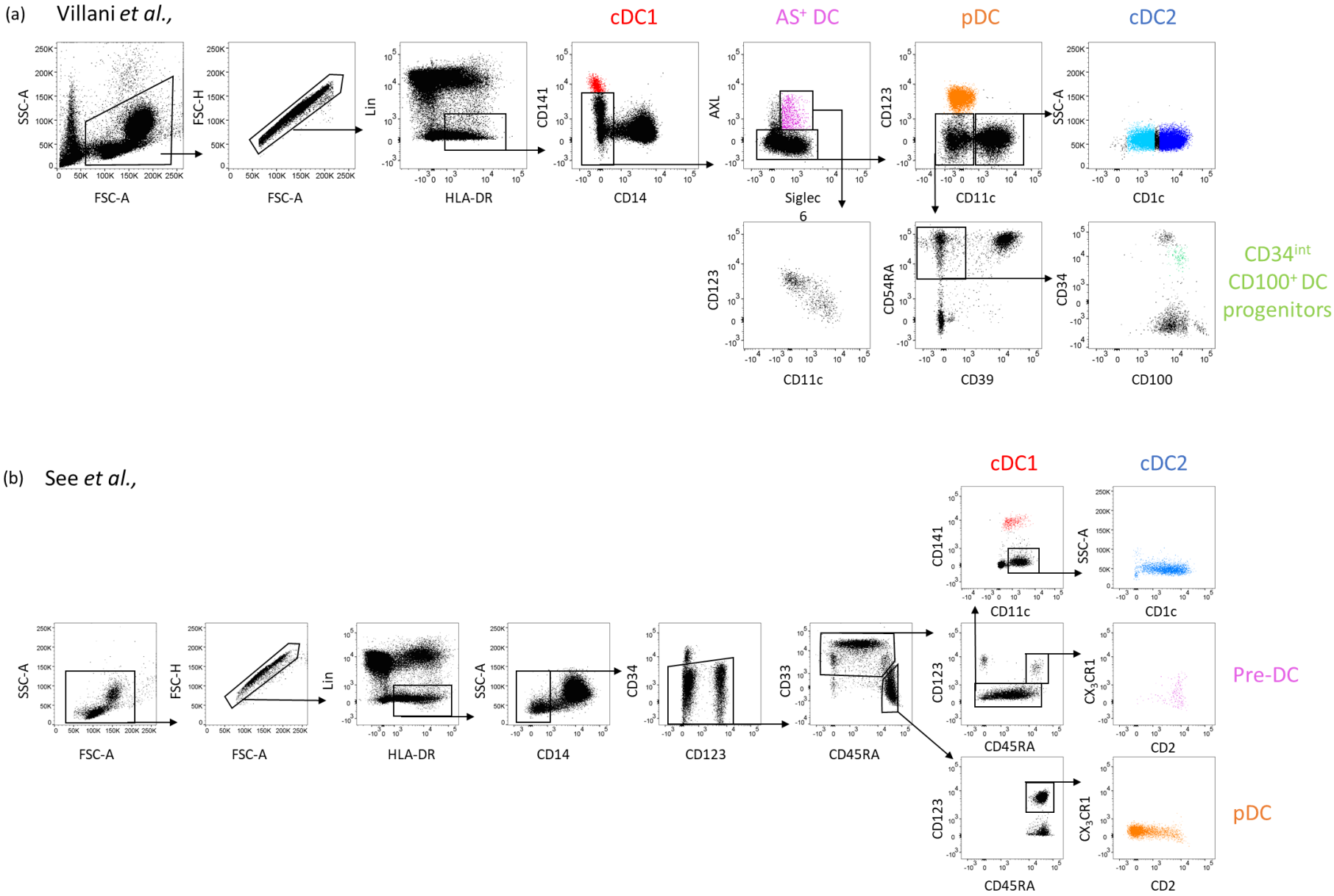
(a) Villani et al.,
cDC1
AS+ DC
pDC
cDC2
SSC-A
FSC-A
FSC-H
FSC-A
Lin
HLA-DR
CD141
CD14
AXL
Siglec 6
CD123
CD11c
SSC-A
CD1c
CD123
CD11c
CD54RA
CD39
CD34
CD100
CD34int CD100+ DC progenitors
(b) See et al.,
cDC1
cDC2
SSC-A
FSC-A
FSC-H
FSC-A
Lin
HLA-DR
SSC-A
CD14
CD34
CD123
CD33
CD45RA
CD141
CD11c
SSC-A
CD1c
CD123
CD45RA
CX3CR1
CD2
Pre-DC
CD123
CD45RA
CX3CR1
CD2
pDC

Figure 3.10 **Villani *et al.,* and See *et al.,* proposed DC strategy**

The DC strategies described by Villani *et al.,* and See *et al.,* were replicated. DC were identified as Lin (CD3, CD19, CD20, CD56, CD66b, CD16)$^{-}$ CD14^{-} HLA-DR^{+} cells. **a)** Villani *et al.,* gating strategy identified cDC1 (red), Siglec6^{+} AXL^{+} DC (purple), pDC (orange), CD1c^{hi} cDC2 (dark blue), CD1c^{lo} cDC2 (light blue) and CD100^{+}CD34^{int} DC progenitors (green). **b)** See *et al.,* gating method identified cDC1 (red), cDC2 (blue), pre-DC (purple) and pDC (orange). Representative n=5 individual experiments.

3.3.2 Comparison of revised gating strategies

With the aim to design a unified DC gating strategy for further studies, both strategies were compared for similarities and differences. The two strategies identified cDC1, cDC2 and pDC, although different markers and gating strategies were applied. In addition, similarities may exist in the newly described populations as the CD123^{+} CX$_3$CR1^{+} CD2^{+} pre-DC subset also expresses Siglec6 and AXL (See *et al.,* 2017), which are markers used by Villani and colleagues to identify AS^{+} DC. A unified panel comprising of markers from both strategies was developed and marker expression was analysed for discrepancies between the subsets described (**Figure 3.11**).

3.3.2.1 pDC comparison

The original CD123^{+} pDC population described in **Figure 3.9**, has now been demonstrated to harbour multiple populations; pDC, pre-DC, and CD123^{+} AS^{+} DC. When comparing the revised bona fide pDC population defined by both strategies, a HLA-DR^{lo} CD45RA^{-} CD33^{+} contaminant was observed in the Villani *et al.,* method (**Figure 3.11**). This population was not described by either group, however, based on the markers expressed, these cells are likely to be basophils as confirmed by the expression of CD203c.

3.3.2.2 cDC2 comparison

Comparison of the cDC2 subset revealed an AXL^{+} subset using the See *et al.,* strategy. This can be explained by the fact that Villani *et al.,* gate out AXL^{+} cells prior to gating cDC2, where the AXL^{+} cDC2 cells can be found. See and colleagues regard the AXL^{+} cDC2 population as committed pre-cDC2 (See *et al.,* 2017).

3.3.2.3 cDC1 comparison

cDC1 were shown to harbour a $CD123^+$ $CD45RA^+$ $CD2^+$ AXL^+ population according to Villani *et al.,* (**Figure 3.11**). As these cells are gated prior to AS^+ DC (**Figure 3.10a**), this explains the expression of AXL within this population. Interestingly this population expresses markers that would be considered a pre-DC by See *et al.,*. Furthermore, the lack of CLEC9a expression on these cells, confirms these cells are not cDC1.

3.3.2.4 AXL^+ $Siglec6^+$ DC comparison

Finally, both studies described a new subset that expressed AXL and Siglec6. Villani *et al.,* take all AXL^+ $Siglec6^+$ cells and divide them further into a $CD123^+$ $CD11c^-$ and a $CD123^-$ $CD11c^+$ population (**Figure 3.10a**). The $CD123^+$ AS^+ DC subset mirror the See *et al.,* $CD123^+$ pre-DC population (**Figure 3.11**). The remaining $CD11c^+$ AS^+ cells are found in See *et al.,* cDC2 fraction as mentioned above (Section 3.3.2.2).

Figure 3.11 **Comparison of See *et al.*, and Villani *et al.*, DC subsets**

pDC, cDC2, cDC1, pre-DC and AS$^+$ DC from See *et al.,* (blue) and Villani *et al.,* (red) were compared for differences in expression of HLA-DR, CD141, CD11c, CD123, CD33, CD45RA, CX_3CR1, CD2, AXL and CD1c. CD203c expression was measured on pDC population to identify the CD45RA$^-$ population and CLEC9a expression on cDC1 to identify the CD123$^+$ population. Representative of n=4 individual experiments.

3.3.3 Refined DC gating strategy

3.3.3.1 Redefining pre-DC

Pre-DC have been documented to express CX_3CR1 (See *et al.,* 2017). However, $CX_3CR1^{lo/-}$ cells were observed within the pre-DC gate (**Figure 3.10b**). These cells are reminiscent of pDC which may have contaminated the pre-DC population as CD33 does not discriminate well between these two populations. Therefore, further characterisation was necessary of the $CD33^{int}$ $CD2^+$ CX_3CR1^- population to correctly identify these cells.

Pre-DC also express AXL (See *et al.,* 2017), therefore $CD33^{int}$ $CD123^+$ $CD45RA^+$ cells were gated by AXL or CX_3CR1 against CD2 (**Figure 3.12**). 41.5% of the $CD33^{int}$ $CD123^+$ $CD45RA^+$ $CD2^+$ population were CX_3CR1^+ and 74.0% were AXL^+. All CX_3CR1^+ cells were also AXL^+ (98.8%), however not all AXL^+ were CX_3CR1^+ (48.6%). While CX_3CR1 and AXL expression are reported to define pre-DC (See *et al.,* 2017), these data demonstrate otherwise.

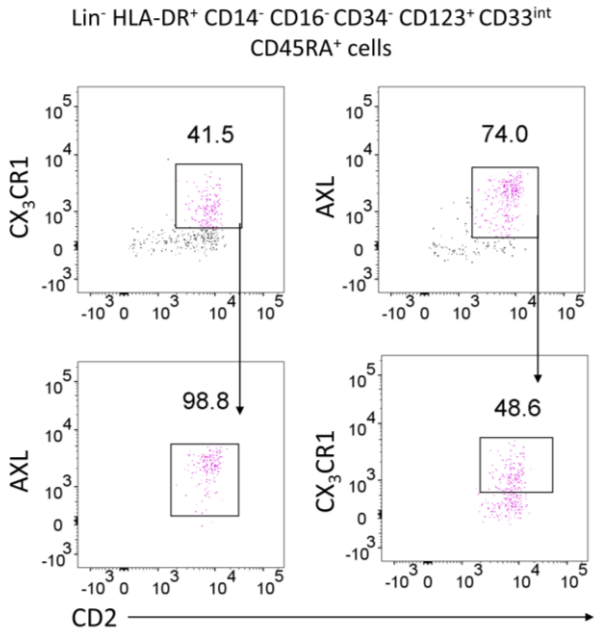

Figure 3.12 **AXL and CX_3CR1 expression on pre-DC**

To assess whether AXL and CX_3CR1 can both identify pre-DC, $CD33^{int}$ $CD123^+$ $CD45RA^+$ cells were gated on CD2 and CX_3CR1 (top left) or AXL (top right) expression. $CD2^+$ CX_3CR1^+ cells were analysed for AXL expression (bottom left) and $CD2^+$ AXL^+ cells were analysed for CX_3CR1 expression (bottom right). Representative of n=3 individual experiments.

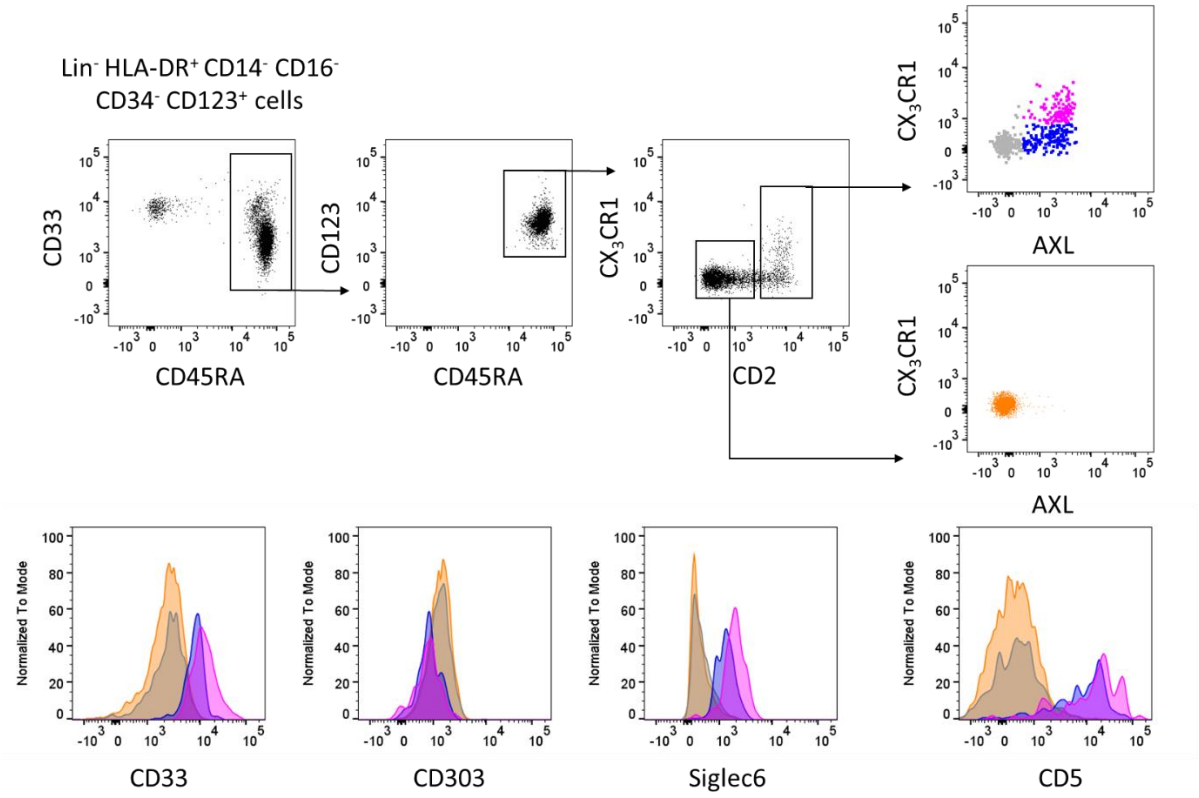

Figure 3.13 **Pre-DC optimisation**

It was investigated whether $CD2^+$ CX_3CR1^{lo} cells are pre-DC or pDC. Within the Lin^- $HLA\text{-}DR^+$ $CD14^-$ $CD16^-$ $CD34^-$ $CD123^+$ fraction of PBMC, $CD45RA^+$ $CD123^+$ cells were divided into $CD2^-$ CX_3CR1^- AXL^- (orange), $CD2^+$ CX_3CR1^- AXL^- (grey), $CD2^+$ CX_3CR1^- AXL^+ (blue) and $CD2^+$ CX_3CR1^+ AXL^+ (purple) populations. CD33, CD303, Siglec6 and CD5 expression was measured on each population. Representative of n=3 individual experiments.

As CD33 poorly discriminates between pre-DC and pDC, all $CD45RA^+$ $CD123^+$ cells were analysed regardless of CD33 expression (**Figure 3.13**). Cell were divided into $CD2^+$ and $CD2^-$ fraction. $CD2^+$ cells were further divided using CX_3CR1 and AXL into $CD2^+$ CX_3CR1^+ AXL^+ (which can be regarded as bona fide pre-DC), $CD2^+$ CX_3CR1^- AXL^- (pDC) and $CD2^+$ CX_3CR1^- AXL^+ cells. Of note, $CD2^-$ CX_3CR1^- AXL^- population are the remaining pDC.

CD33, CD303, Siglec6 and CD5 are differentially expressed between pre-DC and pDC (See *et al.,* 2017) and were measured on these four populations to help define them. The $CD2^+$ CX_3CR1^- AXL^+ (blue) displayed similar marker expression profiles to bona fide pre-DC (purple). As expected, the $CD2^+$ CX_3CR1^- AXL^- (grey) pDC mirrored their $CD2^-$ counterparts (orange).

In summary, the $CX_3CR1^{lo/-}$ cells can be regarded as pre-DC and AXL expression serves as a better discriminator of pre-DC than CX_3CR1.

3.3.3.2 $CD34^+$ progenitors

See *et al.,* exclude $CD34^+$ cells (**Figure 3.10b**) which harbour the $CD100^+$ $CD34^{int}$ progenitors identified by Villani *et al.,*. $CD34^+$ progenitors are regarded as multipotent stem cells that may have the ability to differentiate into several types of leukocytes. While Villani *et al.,* demonstrate the $CD100^+CD34^{int}$ cells have the potential to give rise to cDC1 and cDC2, it was not shown whether these cells have the potential to give rise to other lineages. Furthermore, common DC markers, FLT3 and granulocyte-macrophage colony-stimulating factor are expressed on all DC subsets, including pre-DC, except $CD100^+CD34^{int}$ progenitors (See *et al.,* 2017; Villani *et al.,* 2017), suggesting these cells have a more primitive phenotype. As a result, these cells require further characterisation to be correctly defined as restricted DC progenitors and are not analysed further in this thesis.

The $CD34^+$ cells gated by See *et al.,* do not express DC markers (CD123, CD11c, CD141, CD1c and AXL) (**Figure 3.14**). As a result, it was unnecessary to stain for CD34 as these cells would not fall into DC gates.

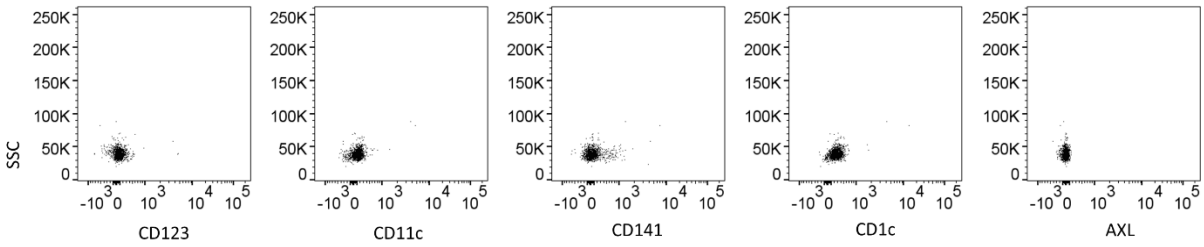

Figure 3.14 **Surface membrane protein expression on $CD34^+$ cells**

Lin^- $HLA\text{-}DR^+$ $CD14^-$ $CD16^-$ $CD34^+$ cells were analysed for expression of DC markers. CD123, CD11c, CD141, CD1c and AXL expression was assessed on this population. Representative of n=3 individual experiments.

3.3.3.3 Proposed DC gating strategy

A new gating strategy for defining DC was designed taking into consideration the two proposed strategies (**Figure 3.15**). Given the heterogeneity observed in pDC and cDC1 gated by Villani *et al.,* (**Figure 3.11**), these subsets were gated using the See *et al.,* strategy. cDC2 were also initially gated as in See *et al.,* however, this subset was divided into an AXL^+ and AXL^- cDC2 subset, the AXL^- subset was further divided into a $CD1c^{hi}$ and $CD1c^{lo}$ subset. Finally, as AXL resulted in better discrimination of pre-DC than CX_3CR1, this marker was used alongside CD2 to identify pre-DC from pDC. **Figure 3.13** also demonstrates CD33 as a redundant marker for distinguishing pre-DC from pDC and was omitted from the final strategy (**Figure 3.15**).

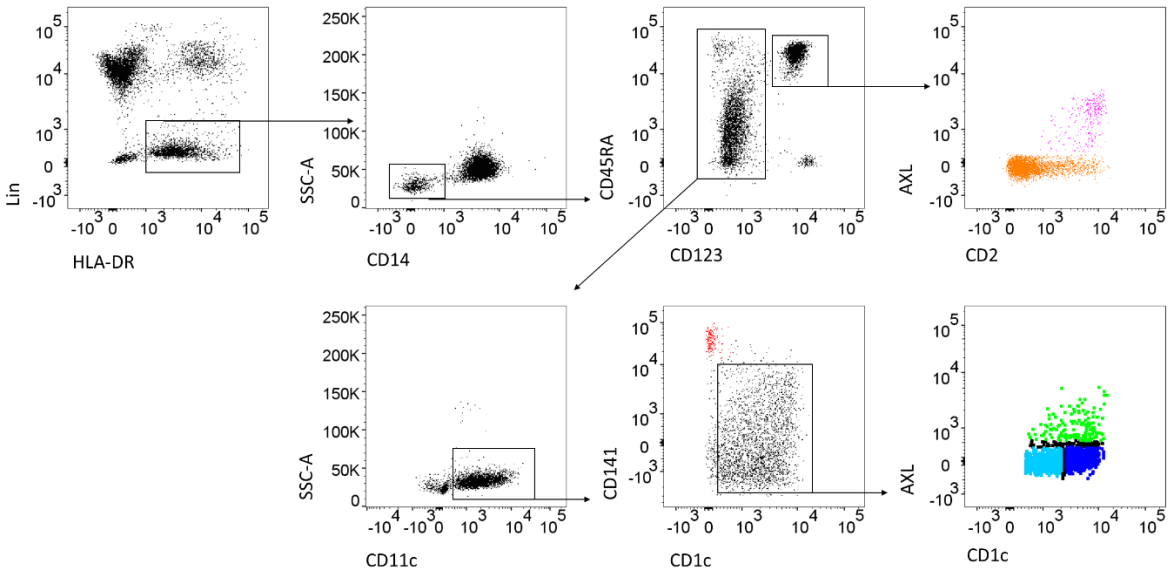

Figure 3.15 **Unified DC gating strategy**

DC were identified within PBMC as Lin (CD3, CD19, CD20, CD56, CD66b, CD16)$^-$ $CD14^-$ $HLA\text{-}DR^+$. pDC (orange) and pre-DC (purple) were identified using AXL and CD2 within the $CD123^+$ $CD45RA^+$ population. $CD123^-$ $CD11c^+$ cDC population were further subdivided in $CD141^+$ $CD1c^-$ cDC1 (red), $CD141^-$ $CD1c^+$ AXL^+ cDC2 (green), $CD141^-$ $CD1c^{lo}$ AXL^- cDC2 (light blue) and $CD141^-$ $CD1c^{hi}$ AXL^- cDC2 (dark blue). Representative of n=5 individual experiments.

Haematoxylin and eosin staining showed that all subsets had indented nuclei like that of monocytes, except pDC which exhibited a more rounded nucleus. After dividing $CD123^+$ cells into pre-DC and pDC, the distinct morphology of pre-DC could be appreciated (**Figure 3.16**), which would have otherwise been masked by the abundant pDC population.

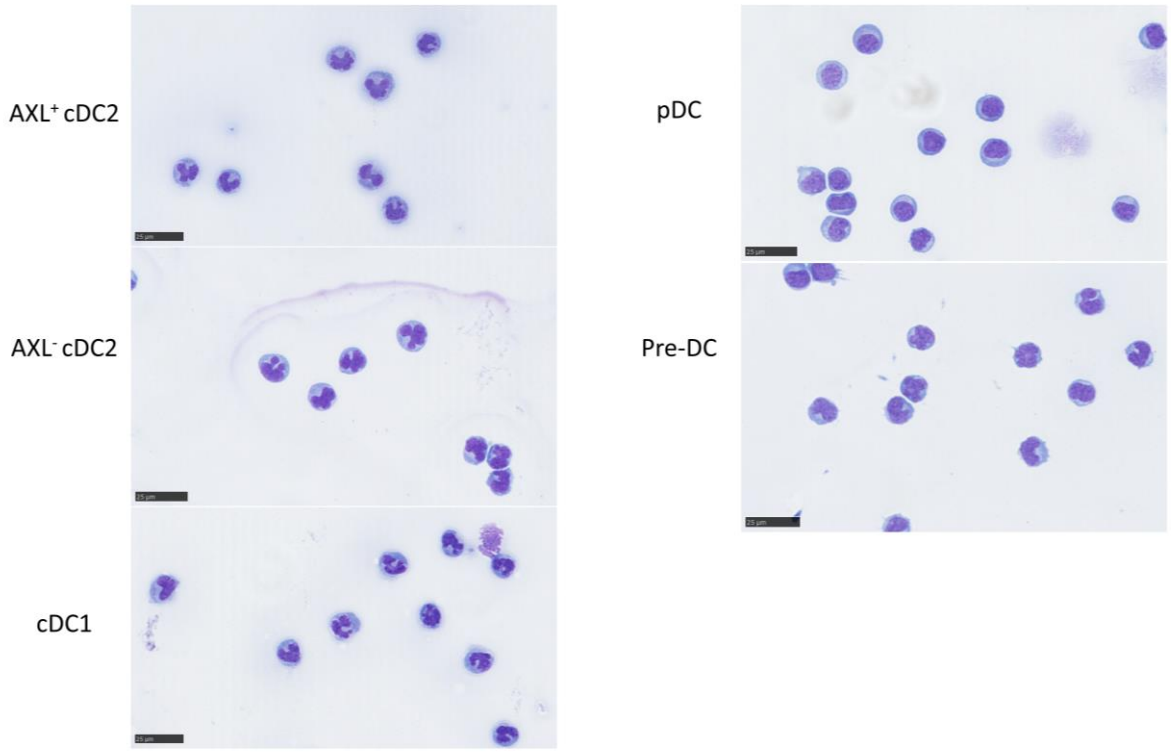

Figure 3.16 **DC morphology**

H&E staining of human DC subsets. AXL^+ cDC2, AXL^- cDC2, cDC1, pDC and pre-DC were sorted by FACS from PBMC and stained with H&E. (Scale bar, 25µm). Representative n=3 individual experiments.

3.3.4 Circulating DC Count

After establishing a finalised strategy to identify DC subsets, the abundance of these cells were enumerated in blood. In relation to monocytes, total DC are found at lower concentrations in blood, at approximately 1.7 $x10^4$/ml of blood (**Figure 3.17**). pDC and AXL^- cDC2 subsets are the most abundant, followed by cDC1, AXL^+ cDC2 and finally pre-DC which were found at approximately 300 cells/ml of blood.

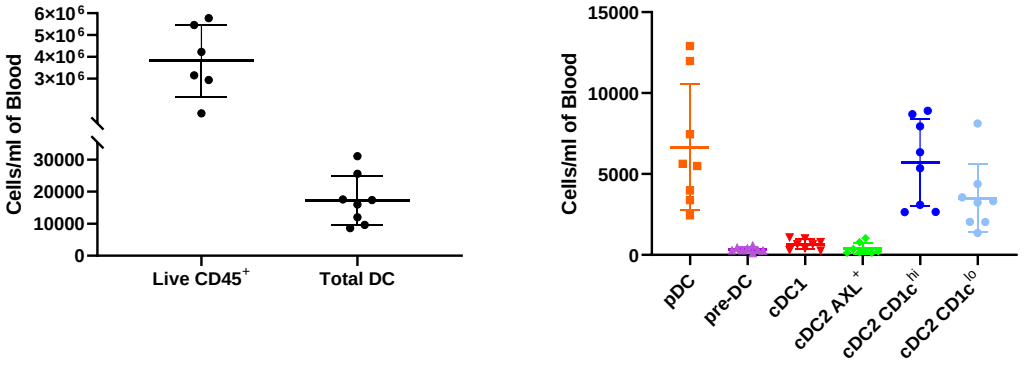

	pDC	pre-DC	cDC1	AXL⁺ cDC2	CD1c^{hi} cDC2	CD1c^{lo} cDC2
Mean count (ml/blood)	6659	332	648	380	5708	3504
SD	3892	145	309	337	2687	2104

Figure 3.17 **Circulating DC count**

Circulating human DC subsets and live CD45⁺ cells were enumerated in healthy individuals by flow cytometry. pDC (orange), pre-DC (purple), cDC1 (red), AXL⁺ cDC2 (green), AXL⁻ CD1c^{hi} cDC2 (dark blue) and AXL⁻ CD1c^{lo} cDC2 (light blue) counts were numerated per ml blood. Table shows the mean count and SD for each DC subset. Bars represent mean ± SD. n=8 individual experiments.

3.3.5 Protein marker expression on human dendritic cell subsets

Next, these newly defined DC subsets were characterised in terms of marker expression (**Figure 3.18**). Typical DC markers were examined on the six DC subsets. CD80 was absent on all subsets, whereas CD86 was expressed on all DC subsets except pre-DC. Although CD34⁺ cells were excluded, pre-DC expressed the highest level of CD34, in line with their role as precursors to cDC1 and cDC2. IRF8 was highly expressed in cDC1, pre-DC and pDC whereas IRF4 was solely expressed in cDC2, pre-DC and pDC. CD303 was solely expressed on pDC, similarly, CLEC9a was only found on cDC1.

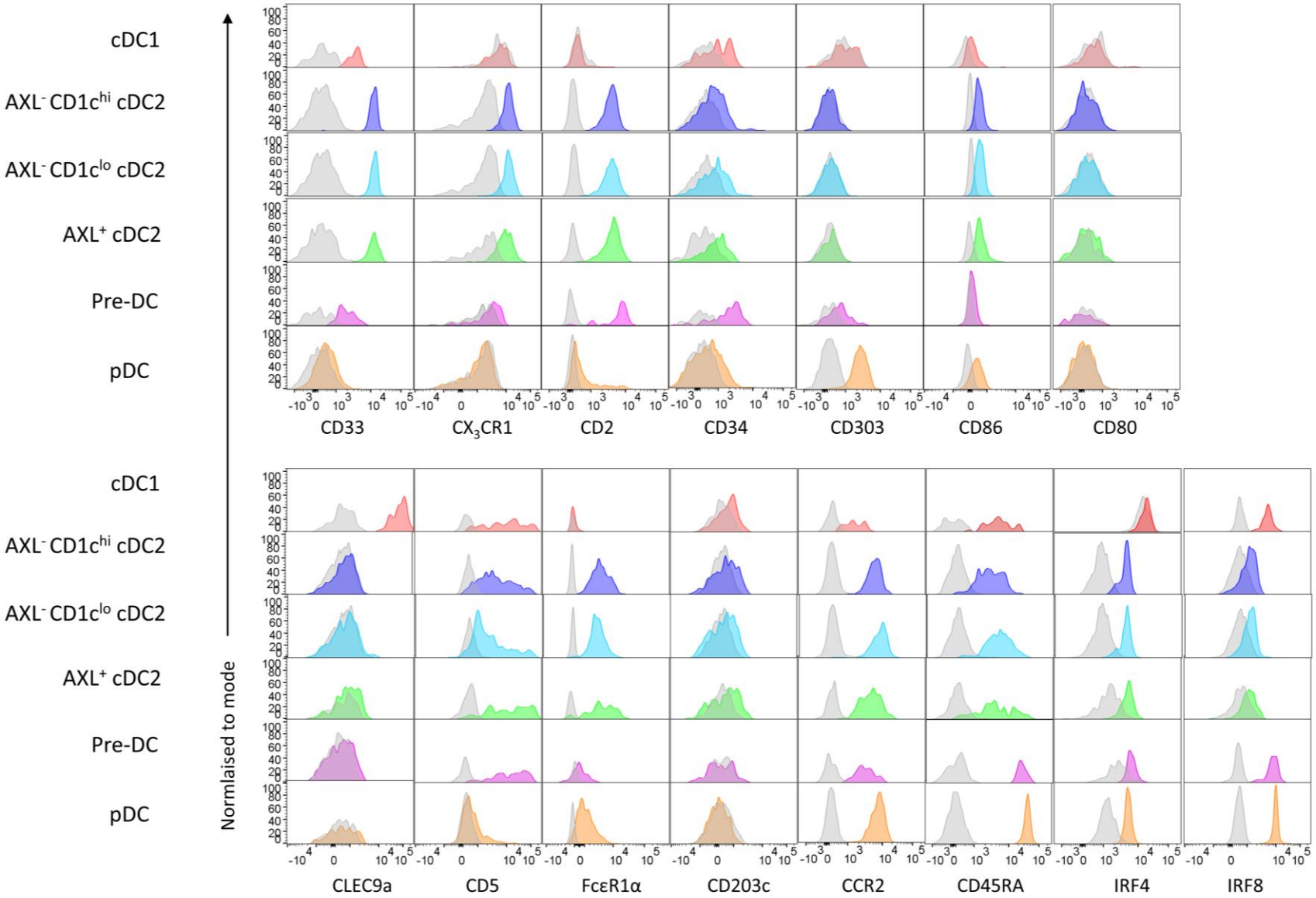
cDC1
AXL⁻ CD1c^hi cDC2
AXL⁻ CD1c^lo cDC2
AXL⁺ cDC2
Pre-DC
pDC
Normlaised to mode
CD33
CX3CR1
CD2
CD34
CD303
CD86
CD80
CLEC9a
CD5
FcεR1α
CD203c
CCR2
CD45RA
IRF4
IRF8

Figure 3.18 **Human DC protein expression**

DC subsets were defined by flow cytometry (Figure 3.15). Surface membrane and intracellular protein expression was measured on cDC1 (red), AXL^- $CD1c^{hi}$ cDC2 (dark blue), AXL^- $CD1c^{lo}$ cDC2 (light blue), AXL^+ cDC2 (green), pre-DC (purple) and pDC (orange). Isotype controls are shown in grey. Representative of n=6 individual experiments.

CD33 was highly expressed on all DC subsets except pDC (**Figure 3.18**). As this marker has been identified as a myeloid marker (Andrews *et al.,* 1983), CD33 expression was also analysed on lymphocytes (T cell, B cells and NK cells) and monocyte subsets (**Figure 3.19**). Whilst CD33 was highly expressed on monocyte subsets, cDC1, cDC2 and pre-DC, almost no expression was observed on pDC and lymphocytes.

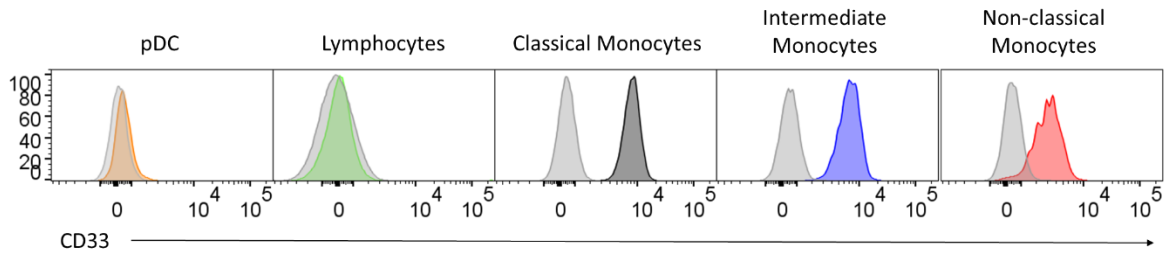

Figure 3.19 **CD33 expression**

CD33 expression was analysed on pDC (orange), lymphocytes (gated as Lin^+) (green) and monocyte subsets (black, blue and red). Isotype controls are shown in grey. Representative of n=3 individual experiments.

3.4 Discussion

3.4.1 Monocyte subset gating strategy

In 2010, the Nomenclature Committee of the International Union of Immunological Societies approved the classification of three monocyte and three DC subsets (Ziegler-Heitbrock *et al.,* 2010). Within the literature, monocytes have been identified by flow cytometry in various ways, either by FSC and SSC alone, or in conjunction with CD14 and CD16, or after the exclusion of other major cell types. Though CD14 is thought to exclusively define monocytes, here it was shown that CD14 and CD16 were expressed on other major leukocyte subsets. As a result, it was important to exclude these cells which could contaminate monocyte populations. In addition to excluding these cell lineages, further exclusion of non-mononuclear phagocytes was achieved by gating on HLA-DR$^+$ cells. Additional gating strategies for identification of human monocyte subsets have since been proposed (Abeles *et al.,* 2012; Ong *et al.,* 2019; Thomas *et al.,* 2017), and closely resemble that in **Figure 3.2**.

Monocyte subsets are not distinct populations, rather they consist of a group of cells with varying CD14 and CD16 expression. Within the literature classical monocytes are defined as CD16$^-$, however, these data demonstrate classical monocytes express minimal amounts CD16 in relation to the DC gate, which can be regarded as CD16$^-$.

In mice, classical monocytes give rise to non-classical monocytes (Sunderkötter *et al.,* 2004; Varol *et al.,* 2007; Yona *et al.,* 2013). With the hypothesis in mind that the human monocyte continuum represents a developmental transition, the use of box gating allows for analysis of 'mature' monocyte subsets and excludes transitioning monocytes of mixed phenotypes.

At the time of performing these experiments, the cells that lie between classical monocytes and DC (CD14^{int} CD16$^-$) have not previously been studied and were not defined as classical monocytes or DC. However, recently it has been suggested these cells may represent a novel CD14$^+$ cDC2 population (Dutertre *et al.,* 2019), which are further examined in Chapter 5.

As shown by other studies (Passlick *et al.,* 1989; Wong *et al.,* 2011), classical monocytes are the most abundant circulating mononuclear phagocyte, making up approximately 86% of total monocytes, with the remainder made up by intermediate and non-classical monocytes. Reasons for the differences in monocyte composition are unclear but may reflect the function/fate of these cells. In mice, Ly6C^{hi} classical monocytes repopulate tissue mononuclear phagocyte compartments under steady-state where embryonic macrophages do not persist (Bain *et al.,* 2014; Mossadegh-Keller *et al.,* 2017; Tamoutounour *et al.,* 2013; Zigmond *et al.,* 2012). In humans, it is also possible a large demand for classical monocytes is required to repopulate tissue mononuclear phagocytes, as has been documented for the dermis (McGovern *et al.,* 2014).

In addition to varying CD14 and CD16 expression, additional surface markers are differentially expressed amongst monocyte subsets. Concordant with previous studies (Ingersoll *et al.,* 2010; Wong *et al.,* 2011), CD62L, CD11c, CD36 and CD64 expression on human monocytes were comparable to profiles seen in mouse monocyte subsets. CCR2 and CX_3CR1 expression on human monocyte subsets also mirrored observations in mice (Geissmann *et al.,* 2003; Ingersoll *et al.,* 2010). CCR2 was highly expressed on classical monocytes and in mice is necessary for bone marrow egression. It is likely similar mechanisms exist in humans, as CCR2 antagonism resulted in a decrease in peripheral monocyte counts in patients with rheumatoid arthritis (Vergunst *et al.,* 2008). Although unpublished, the authors also mention similar observations were previously seen in healthy volunteers. Meanwhile, CX_3CR1 has been implicated in non-classical monocyte retention to the endothelium (Auffray *et al.,* 2007; Carlin *et al.,* 2013; Collison *et al.,* 2015) and survival of monocytes, as supplementation of CX_3CL1 was enough to rescue induced cell death (Landsman *et al.,* 2009). In humans, both classical and non-classical monocytes exhibit endothelium crawling in vitro, however, antagonism of CX_3CR1 only reduced this behaviour in non-classical monocytes (Collison *et al.,* 2015).

SLAN expression on non-classical monocytes was in agreement with previous work (Cros *et al.,* 2010; Hofer *et al.,* 2015). Functional differences have been reported between $SLAN^+$ and $SLAN^-$ subsets, such as the differences in their ability to efferocytose (removal of dying/dead cells) (Hamers *et al.,* 2019), pro-inflammatory cytokine production in both human immunodeficiency virus (HIV) infected patients (Dutertre *et al.,* 2012) and psoriasis patients (Hänsel *et al.,* 2011). The frequency of $SLAN^+$ monocytes also correlates with coronary artery disease severity, where it was suggested these cells are induced to play an atheroprotective role to restore vascular homeostasis (Hamers *et al.,* 2019). These studies imply the distinct role of these subpopulations can be appreciated during inflammation. Here, CD36 was also variably expressed within non-classical monocytes which at the time of performing these experiments had not been previously documented. Alongside SLAN expression, it was shown that non-classical monocytes can be further subdivided into four further subsets (**Figure 3.8**). Recently, Hamers *et al.,* has demonstrated that 3 non-classical monocytes could be identified by mass cytometry; $SLAN^-$, $CD36^+$ $SLAN^+$, $CD36^-$ $SLAN^+$ monocytes (Hamers *et al.,* 2019), however, heterogeneity was not observed within the $SLAN^-$ population. Whilst Hamers and colleagues implicated a role of $SLAN^+$ monocytes in coronary artery disease, CD36 has also been demonstrated as a requirement for non-classical monocyte patrolling in early atherogenesis in mice (Marcovecchio *et al.,* 2017). Therefore, it is possible that the $SLAN^+$ $CD36^+$ non-classical subset is specifically implicated in this setting. Whilst various non-classical monocytes phenotypes are apparent, it is unclear whether this represents the plastic nature of non-classical monocytes or whether these subsets are autonomous populations and are developmentally related.

Hamers and colleagues also demonstrated that 4 subsets of classical monocytes could be identified as $CD93^{hi}$, $CD93^{lo}$, $CD9^+$ and IgE^+ classical monocytes (Hamers *et al.,* 2019). With the markers analysed here, heterogeneity was not observed within classical monocytes from the histogram data. Although from the viSNE plots, marker expression was observed to change at

different positions along the monocyte continuum. Therefore, depending on where the CD14 and CD16 gates are drawn to divide the subsets, markers might change expression at different stages. It could be questioned from these data whether CD14 and CD16 are the best markers to define monocyte subsets.

Whilst mass cytometry has identified multiple monocyte subsets (Hamers *et al.,* 2019), single-cell RNA sequencing has revealed heterogeneity only within intermediate monocytes (Villani *et al.,* 2017). One subset was described by genes related to cell cycle, differentiation and trafficking, whereas the other expressed a cytotoxic gene signature. Additional studies have now demonstrated that the latter subset are $CD56^{dim}$ NK cells and consequently, only three monocyte subsets were identified in these studies (Dutertre *et al.,* 2019; Günther *et al.,* 2019).

Though further heterogeneity has been recently described within the three major monocyte subsets, further studies are needed to form a unified consensus on monocyte subsets and explore the importance of this heterogeneity. These studies are beyond the scope of this thesis and monocytes were studied as classical, intermediate and non-classical subsets in this thesis.

3.4.2 Dendritic cell gating strategy

Three human DC populations have been recognised within the literature (Haniffa *et al.,* 2012; McGovern *et al.,* 2014; Ziegler-Heitbrock *et al.,* 2010); $CD123^{+}$ pDC, $CD141^{+}$ cDC1 and $CD1c^{+}$ cDC2. With advances in technology, single cell RNA sequencing has resulted in further diversification of DC, with at least seven DC described (See *et al.,* 2017; Villani *et al.,* 2017). However, overlap occurs between the two strategies and there is evidence to suggest that some populations described might not be bona fide DC (Calzetti *et al.,* 2018). Here, it was proposed only six DC subsets are apparent. In summary, cDC1 classification remains unchanged, whereas heterogeneity exists with the pDC and cDC2 (**Figure 3.20**).

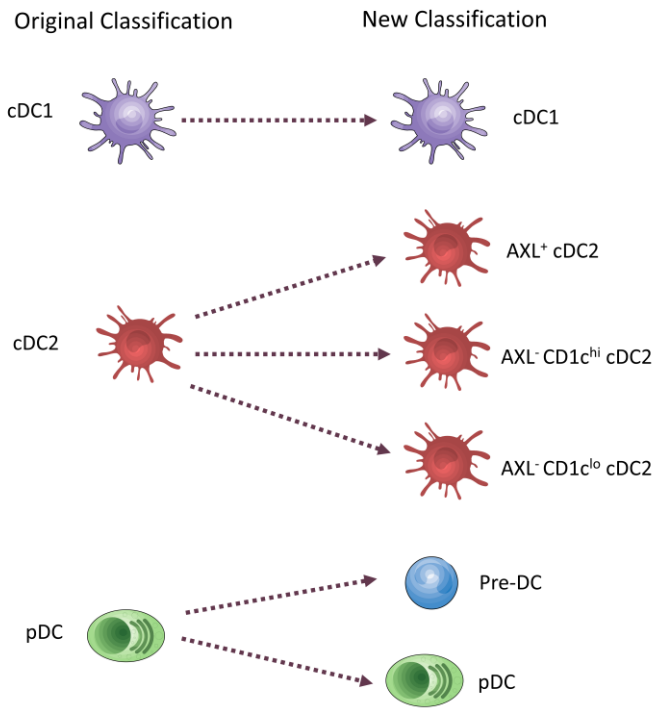

Figure 3.20 **DC Subset summary**

The relationship of novel DC subsets in comparison to the original classification. cDC2 harbour three populations (AXL$^+$, AXL$^-$ CD1c^{hi}, AXL$^-$ CD1c^{lo}) and original pDC contain pre-DC and bona fide pDC.

Prior to single-cell sequencing data, pDC were regarded as CD123$^+$, however it is now clear this population harbours bona fide CD123$^+$ CD2$^{-/lo}$ AXL$^-$ pDC and CD123$^+$ CD2$^+$ AXL$^+$ pre-DC (**Figure 3.20**). It should be mentioned, heterogeneity has previously been described within in pDC, where CD2^{hi} CD5$^+$ pDC have been described to stimulate T cell proliferation unlike their CD2^{hi} CD5$^-$ counterparts (Matsui *et al.,* 2009; Zhang *et al.,* 2017), it is likely the CD2^{hi} CD5$^+$ cells resemble AXL$^+$ pre-DC described here. Circulating human pre-cDC have previously been described (Breton *et al.,* 2015). See *et al.,* demonstrate the pre-cDC described by Breton and colleagues only make up a fraction of the pre-DC described here, due differences in the gating strategy implemented (See *et al.,* 2017).

It was also demonstrated here, that CX$_3$CR1 does not provide as a useful marker to identify pre-DC, as CX$_3$CR1$^{lo/-}$ pre-DC exist. However, AXL expression was demonstrated to successfully

identify pre-DC amongst the $CD123^+$ fraction. Although the $CX_3CR1^{lo/-}$ pre-DC had a similar expression profile to CX_3CR1^+ pre-DC, it remains to be investigated whether the difference in CX_3CR1 expression is of functional importance between the two subsets.

$CD123^+$ $Siglec6^+$ AXL^+ pre-DC can mature into both cDC1 and cDC2 (See *et al.,* 2017), although others have demonstrated pre-DC give rise solely to cDC2 (Cytlak *et al.,* 2019; Villani *et al.,* 2017), reasons for these discrepancies are not clear but nevertheless pre-DC are described as upstream progenitors to cDC.

cDC2 are composed of an AXL^+, AXL^- $CD1c^{hi}$ and AXL^- $CD1c^{lo}$ subset (**Figure 3.20**). In terms of the markers analysed here, the AXL^+ cDC2 subset resembles other cDC2 subsets and are less related to pre-DC, despite AXL expression. It proposed that this subset is a 'late' pre-DC which is restricted to cDC2 development (See *et al.,* 2017; Villani *et al.,* 2017), therefore termed pre-cDC2. The $CD1c^{hi}$ and $CD1c^{lo}$ populations are described as non-inflammatory and inflammatory cDC2, respectively (Villani *et al.,* 2017). The inflammatory $CD1c^{lo}$ cDC2 subset expressed higher CD14 in comparison to its non-inflammatory counterpart, suggestive of a monocyte phenotype. More recent studies have confirmed these cells should be classed as $CD14^+$ $CD1c^+$ cDC2 and not monocytes (Dutertre *et al.,* 2019). These cells are examined further in Chapter 5.

CD33 expression is recognised as a marker of myeloid lineage (Andrews *et al.,* 1983). As expected, expression was observed on monocytes, pre-DC and cDC subsets but was absent on lymphocytes. However, CD33 was also absent on pDC. In addition, the morphology of pDC resembled plasma B cells. These observations are in line with recent studies that have demonstrated pDC are lymphoid derived (Dress *et al.,* 2019; Onai *et al.,* 2013; Rodrigues *et al.,* 2018), nevertheless these cells are currently viewed as a DC.

Having established a method to identify human monocyte and DC subsets, these strategies were implemented in the studies mentioned in this thesis (unless stated otherwise).

Chapter 4

Steady-state Circulating Kinetics of Mononuclear Phagocytes

4.1 Introduction and Aims

4.1.1 Introduction

Examining the function of mononuclear phagocytes is key to understanding their role in homeostasis and pathophysiology. It is equally as imperative to understand the homeostatic maintenance of these cells throughout life and how this may go awry in disease. In patients with chronic inflammation such as sepsis, rheumatoid arthritis and systemic lupus erythematosus (SLE), changes in the frequency and absolute number of monocyte and DC subsets have been reported (Cooper *et al.,* 2012; Grimaldi *et al.,* 2011; Guisset *et al.,* 2007; Mukherjee *et al.,* 2015; Poehlmann *et al.,* 2009; Riccardi *et al.,* 2011). This in turn questions the circulating kinetics of these cells under inflammatory conditions. However, it is first necessary to examine the turnover of mononuclear phagocyte subsets under steady physiological conditions.

Studies in mice have shown the appearance of classical monocytes in the circulation prior to non-classical monocytes as they are precursors to these cells (Liu *et al.,* 2019; Mildner *et al.,* 2017; Varol *et al.,* 2007; Yona *et al.,* 2013). The half-life of murine classical and non-classical monocytes has been approximated at 20 hours and 2.2 days, respectively (Yona *et al.,* 2013). Early studies in humans have reported a circulating monocyte half-life of approximately 2 days (Mohri *et al.,* 2001), or similarly a lifespan of 4.25 days (Whitelaw, 1972). Although, turnover rates for each individual monocyte subset have not yet been examined.

Murine homologues of human blood cDC and pDC subsets have been described (Donnenberg *et al.,* 2001; O'Keeffe *et al.,* 2003), yet are often overlooked due to their low abundance. Consequently, the circulating kinetics of these subsets have not been described. Nevertheless, adoptive transfer experiments in mice have demonstrated circulating DC were cleared within one hour (Liu *et al.,* 2007), suggestive of a high turnover rate. A thorough search of the literature yielded a single study which has examined circulating DC kinetics, performed in macaques

(Sugimoto *et al.,* 2015). The kinetics of circulating human DC populations under steady-state have not been explored.

4.1.2 Aims

Examine the kinetic profiles of circulating mononuclear phagocytes using stable isotope labelling under steady physiological conditions and propose a likely biological scenario.

4.2 Human Monocyte Subset Kinetics

4.2.1 Kinetic profiles of monocyte subsets

Non-toxic *in vivo* labelling in humans has been achieved by the use of deuterated water or glucose (Macallan *et al.,* 2009, 1998). Consequently, this has been applied in humans to study the turnover of T cells (Macallan *et al.,* 2003), B cells (Macallan *et al.,* 2005), NK cells (Zhang *et al.,* 2007) and neutrophils (Lahoz-Beneytez *et al.,* 2016). In collaboration with Prof. Derek Macallan and Dr. Yan Zhang, at St. George's Hospital in London, deuterium glucose labelling was implemented to examine the circulating kinetic profiles of human classical, intermediate and non-classical monocytes.

Volunteers orally consumed deuterated glucose over a 3-hour period, as described in Section 2.8, plasma enrichment was measured before, during and after this period (**Figure 4.1**). Deuterated glucose rapidly appeared in the plasma, plateaued until the end of dosing and sharply declined thereafter, returning to baseline approximately 6 hours following the initial dose. After this time point, negligible amounts of deuterated glucose were detected in the circulation.

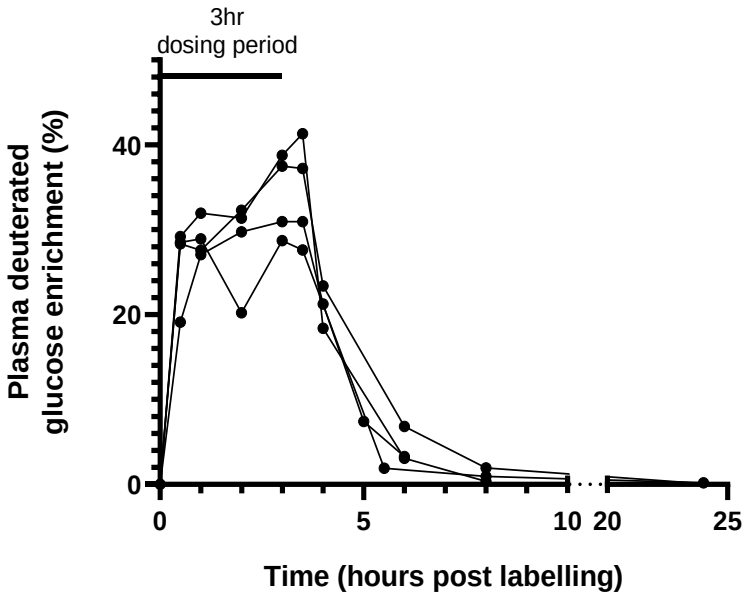

Figure 4.1 **Plasma enrichment of deuterated glucose**

Deuterated glucose was measured in blood samples before, during and after an oral intake of 20g of deuterated glucose over 3 hours. n=4 individual experiments.

Following the oral intake of deuterated glucose, blood samples were taken at specific time points over a period of 30 days. Classical, intermediate and non-classical monocyte subsets were isolated by FACS at these time points. Purities of each subset were examined after cell sorting for each population at each time point (**Figure 4.2**).

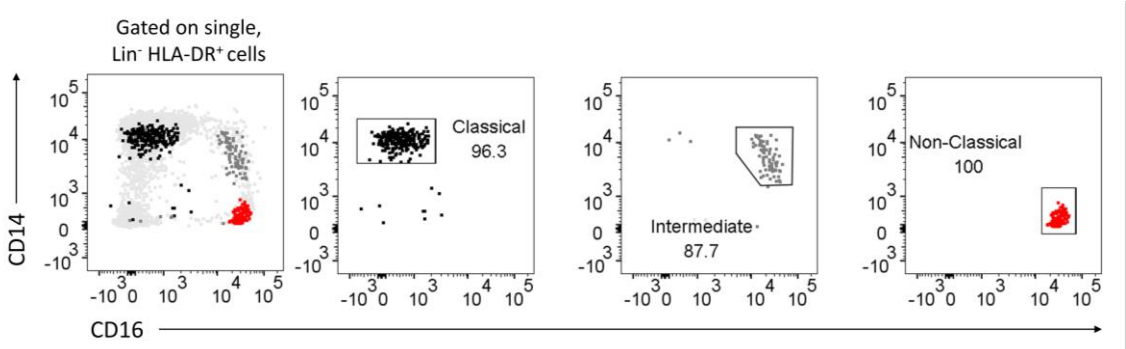

Figure 4.2 **FACS sorted monocyte purity**

Monocyte subsets were identified as Lin⁻ HLA-DR⁺ cells within PBMC and FACS sorted into classical (black), intermediate (grey) and non-classical (red) monocytes. Purities for each subset are expressed as a percentage of total sorted cells. Representative of n=4 individual experiments at all time points.

DNA was isolated from monocyte subsets and analysed for deuterium enrichment by gas chromatography mass spectroscopy (GC/MS) in collaboration with Dr. Yan Zhang. The kinetic profiles of classical, intermediate and non-classical monocytes are shown in **Figure 4.3**. At Day 1 post-labelling, deuterium was not detected in the three subsets. Classical monocytes presented with label first on day 2 and peaked at day 3, intermediate monocytes peaked after at day 7 followed by non-classical monocytes which peaked at day 10 (**Figure 4.3**). The label appeared in a sequential fashion, where the decline in label in classical monocytes coincided with an increase in labelling in intermediate monocytes and similarly between intermediate and non-classical monocytes.

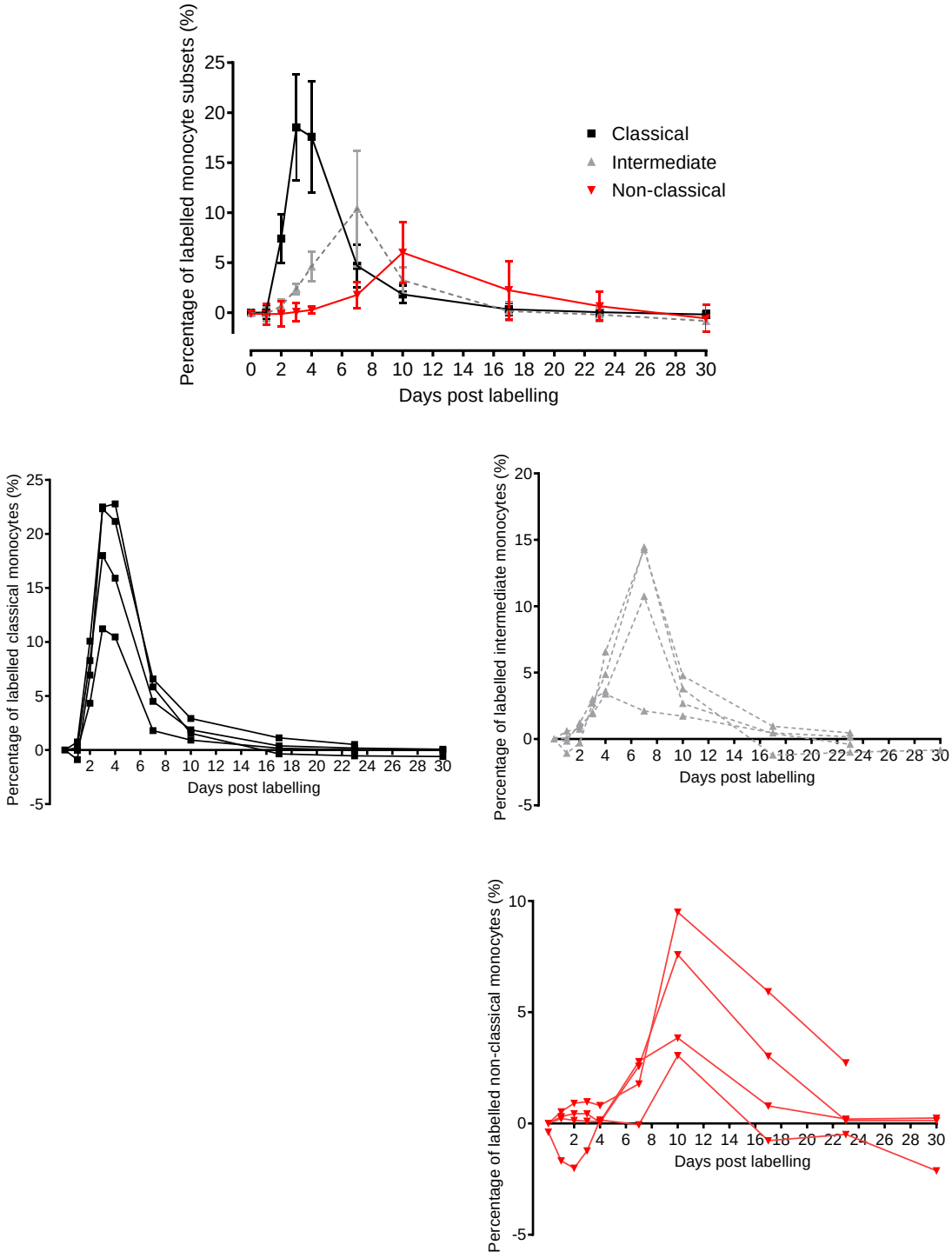

Figure 4.3 **Circulating kinetic profiles of human monocyte subsets**

Following oral administration of deuterated glucose, deuterium enrichment was measured in the DNA of classical, intermediate and non-classical monocytes over a period of 30 days by GC/MS. All subsets are shown overlaid (top graph) and individually with each subject's curves (bottom three graphs). Bars represent mean ± SD. n=4 individual experiments.

4.2.2 Cell cycle profile of circulating monocytes

The observation that deuterium enrichment was absent at day 1 post labelling (**Figure 4.3**), suggests that circulating monocytes do not proliferate. If monocytes did exhibit proliferative potential in the blood, they would be expected to incorporate plasma deuterium during the labelling phase into their DNA and therefore present with label at day 1.

To confirm the non-proliferative behaviour of human monocytes, Ki67 and DAPI expression was assessed in each monocyte subsets (**Figure 4.4**). All subsets were $Ki67^{-}$ $DAPI^{lo}$, indicating circulating monocytes are in G_0 of the cell cycle, whereas $Lineage^{+}$ cells, were found in G_1 ($Ki67^{+}$ $DAPI^{lo}$), S, G_2 and M phase ($Ki67^{+}$ $DAPI^{hi}$) (**Figure 4.4a**).

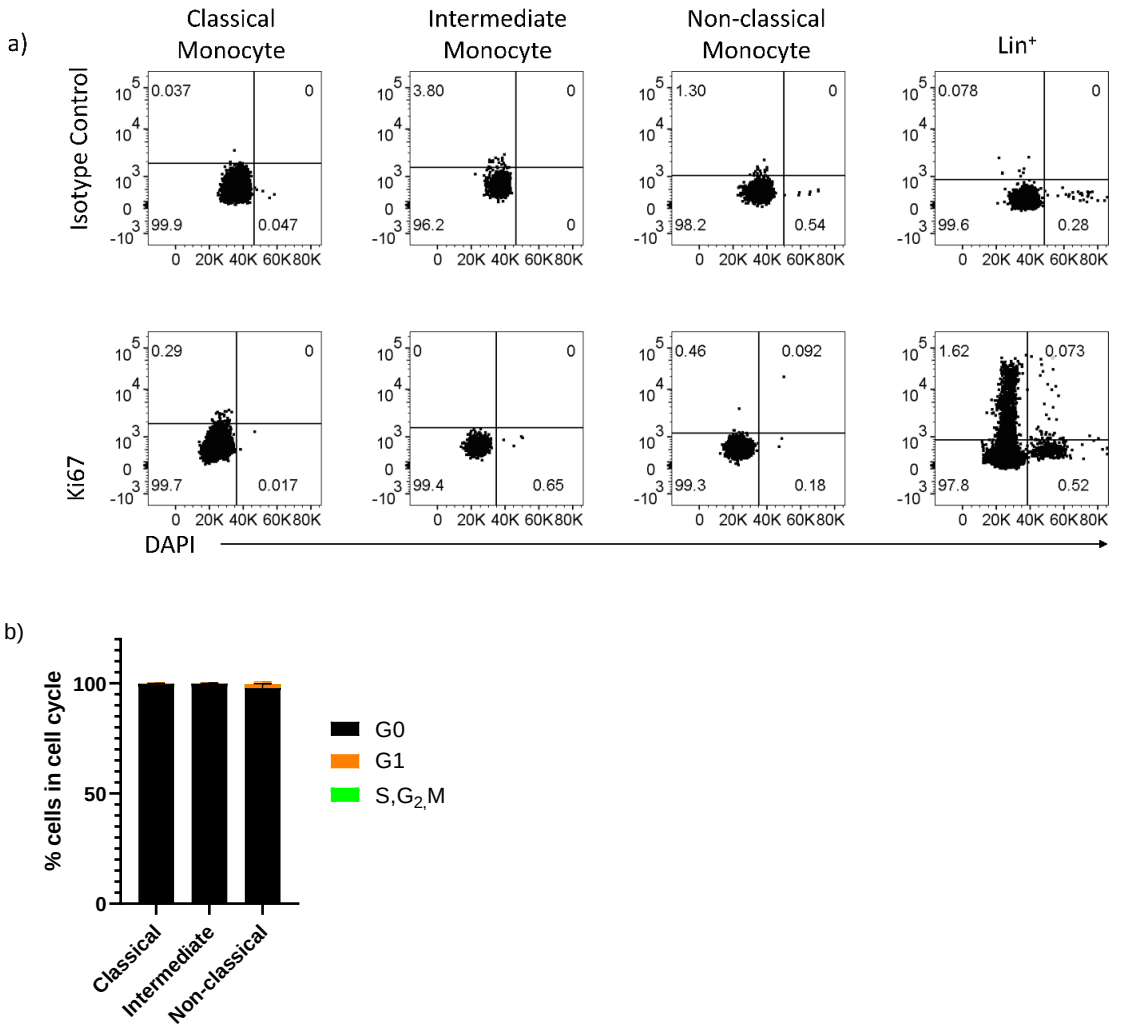

Figure 4.4 **Cell cycle status of circulating monocyte subsets**

Cell cycle status of classical, intermediate and non-classical monocytes was analysed by flow cytometry. **a)** Monocyte subsets and Lin^+ cells were identified by flow cytometry where Ki67 and DAPI expression was analysed on these cells. $KI67^-$ $DAPI^{low}$ = G_0, $KI67^+$ $DAPI^{low}$ = G_1, $KI67^+$ $DAPI^{int/hi}$ = $S/G_2/M$ phase. **b)** The percentage of each monocyte subset in each gate was quantified. Bar represent mean ± SD. n=4 independent experiments.

4.2.3 Modelling human monocyte kinetics

4.2.3.1 Potential Models

Multiple models can be designed around the sequential kinetic profile of monocyte subsets (**Figure 4.5**). Studies in splenectomised and X-irradiated mice where only part of the bone marrow was shielded did not affect the labelling kinetics of monocytes in mice, suggesting monocytes are of bone marrow origin (van Furth and Cohn, 1968).

It is possible all three subsets are present in the bone marrow however differences lie in the egression kinetics (**Figure 4.5a**) or maturation stages/periods (**Figure 4.5b**), hence a lag was observed between the subsets in the circulation. Alternatively, a developmental relationship may exist where circulating classical monocytes mature into non-classical monocytes similar to mice (**Figure 4.5c**).

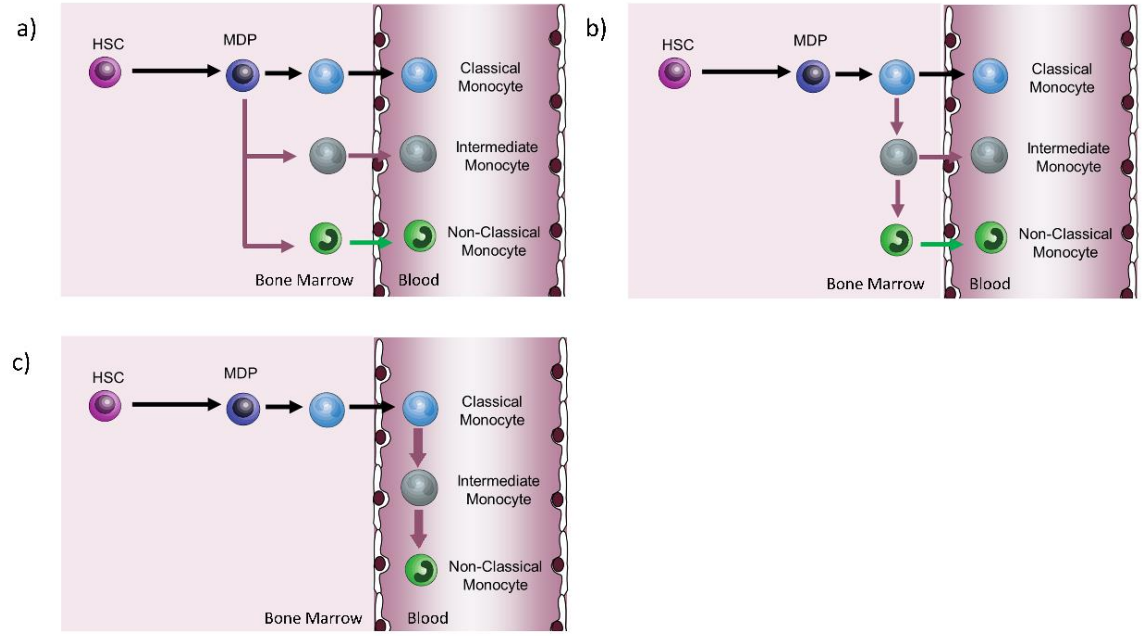

Figure 4.5 **Possible biological scenarios behind human monocyte kinetics**

Based on the kinetic profiles of monocyte subsets, several possible biological scenarios can be drawn. **a)** Differences in egression kinetics or **b)** maturation stages/periods may explain the different time points at which monocyte subsets are seen in the circulation. **c)** Alternatively, a developmental relationship where classical monocytes mature into intermediate then non-classical monocytes may result in the sequential kinetic appearance.

4.2.3.2 Bone Marrow Monocyte Subsets

At least three potential models could explain the kinetic profiles of monocyte subsets. To find the most likely scenario, the composition of monocyte subsets within human bone marrow was examined. In collaboration with Dr. Venetia Bigley at Newcastle University, fresh bone marrow biopsies were analysed by flow cytometry. Monocyte subsets were identified as single, live, Lin^- $HLA\text{-}DR^+$ cells (**Figure 4.6**). As expected all three populations were identified within PBMC (**Figure 4.6b**). Whereas bone marrow biopsies only contained $CD14^+$ $CD16^-$ monocytes resembling classical monocytes (**Figure 4.6a**).

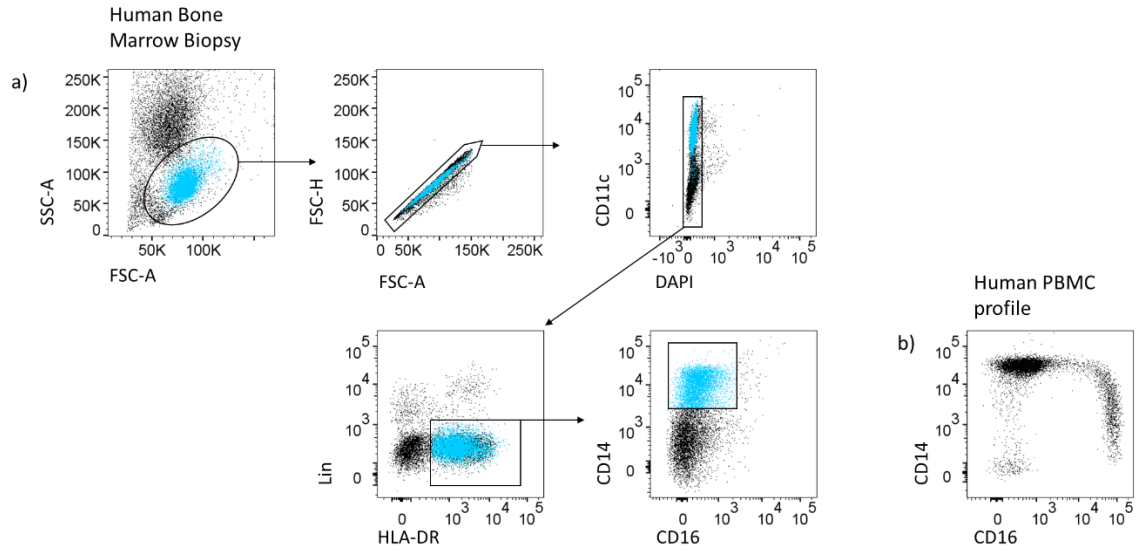

Figure 4.6 **Human bone marrow monocyte composition**

Human bone marrow biopsies and autologous PBMC were analysed by flow cytometry to identify monocyte subsets. **a)** Gating strategy implemented to identify bone marrow monocyte subsets. Classical monocytes are shown in blue. **b)** same gating strategy analysed in autologous PBMC. Representative of n=5 individual experiments.

4.2.3.3 Proposed Model

In light of the bone marrow data (**Figure 4.6**), scenarios where all three subsets were proposed to be present in the bone marrow, were disregarded. Consequently, only one likely model remained where classical monocytes mature into non-classical monocytes via an intermediate phenotype (**Figure 4.5c**). Full details of the model are described in Section 2.9.

The labelling observed within the three monocyte subsets is due to a dynamic system where cells are continuously entering and leaving cellular compartments. Due to this complexity, mathematical modelling was implemented to estimate the lifespan of human monocytes in collaboration with Dr. Becca Asquith and Dr. Lies Boelen at Imperial College London.

In addition to the lifespan of these cells, additional parameters were estimated such as the delay periods and the percentage of monocytes transitioning. The kinetic graphs for each subject were modelled individually and individual estimates were numerated (**Table 4.1**). The model proposes precursors proliferate at an average rate of 42% per day but after the last proliferation, classical monocytes are retained within the bone marrow for approximately 1.6 days which then enter the blood and circulate for 1.01 days (**Figure 4.7 and Table 4.1**). 1.4% of classical monocytes then mature into intermediate monocytes which have a longer circulating lifespan of 4.3 days which then develop to non-classical monocytes which circulate for a further 7.41 days. The remaining 99% of classical monocytes are proposed to enter tissues and/or a marginating pool and/or die.

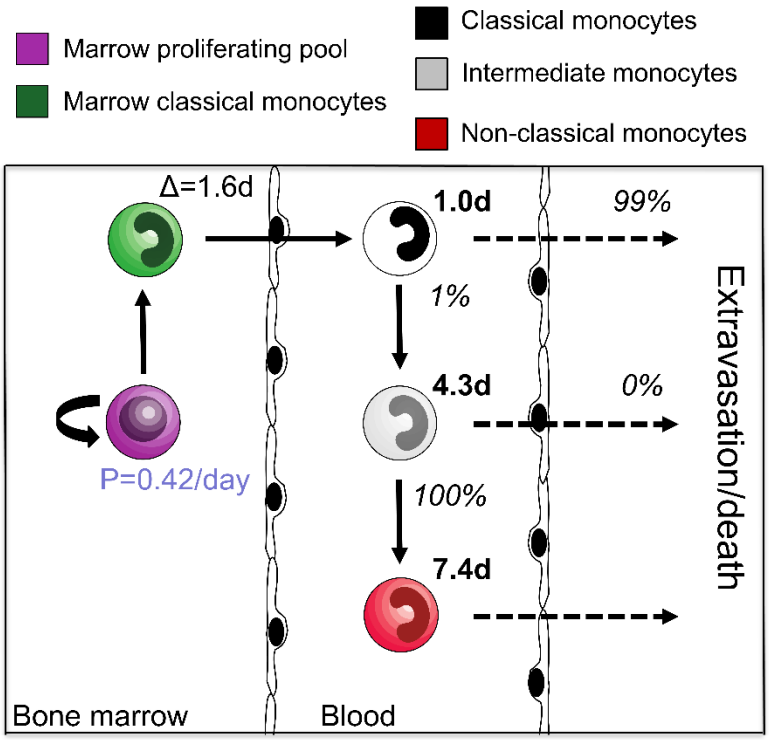

Figure 4.7 **Circulating lifespan of human monocyte subsets**

A likely biological model proposes classical monocytes egress from the bone marrow after a post-mitotic dwell period of approximately 1.6 days, these cells then circulate for 1 day. 1% of classical monocytes mature into intermediate monocytes that circulate for 4.3 days that then mature into non-classical monocytes circulating for a further 7.4 days.

	Proliferation (per day)	Delay (days)	Lifespans (days)			% of total monocytes			% transitioning	
	Bone marrow	Bone marrow-Blood	Classical monocyte	Intermediate monocyte	Non-classical monocyte	Classical monocyte	Intermediate monocyte	Non-classical monocyte	Classical to intermediate	Intermediate to non-classical
Subject 1	0.48	1.53	1.37	4.29	6.44	80	8	12	3.2	100
Subject 2	0.28	1.70	0.5	5.26	7.52	83	7	10	0.8	100
Subject 3	0.26	1.61	0.62	3.55	8.28	90	3	7	0.6	100
Subject 4	0.64	1.70	1.54	4.11	N/R	96	2	2	0.8	N/R
Average	**0.42**	**1.64**	**1.01**	**4.30**	**7.41**	**87**	**5**	**8**	**1.4**	**100**
SD	**0.18**	**0.08**	**0.52**	**0.71**	**0.92**	**7.18**	**2.94**	**4.35**	**1.24**	**0.00**
Confidence Intervals	**0.29-0.69**	**1.43-1.76**	**0.61-2.03**	**2.29-5.94**	**5.11-15.73**	**75.82-98.68**	**0.31-0.68**	**0.82-14.67**	**0.73-3.65**	**37.7-99.03**

Table 4.1 **Individual parameter estimates for modelling monocyte subset kinetics *in vivo***

Proliferation rates, delays, lifespans and percentage of monocytes transitioning for each subject proposed based on the model. The circulating monocyte subset composition was attained from flow cytometry for each individual. N/R = not resolved due to low labelling rate.

4.2.3.4 Models with and without a delay parameter

At the same time as performing these experiments, an independent group also performed similar experiments and demonstrated comparable kinetic profiles for circulating human monocytes (Tak *et al.,* 2017a). However, when modelling these data, they proposed that intermediate monocytes leave the circulation and re-enter as non-classical monocytes suggesting maturation occurs outside the circulation. Next, it was investigated whether the model proposed by Tak and colleagues provided a better fit.

The first model proposed that there was no delay ($\Delta_3 = 0$), i.e. intermediate monocytes convert to non-classical monocytes in the circulation. To investigate whether a delay parameter may allow for a better fit, Δ_3 was allowed to be a free parameter (Section 2.9.1). In subject 1, Δ_3 was estimated at 2.3 days, whereas this value tended to zero for subjects 2 and 3 (**Table 4.3**).

To compare the two models, the Akaike information criterion (AIC) was used as means for model selection. In three out of the four subjects, the AIC suggested that the model without the delay parameter outcompeted the model with the delay (**Table 4.2**). One model outperforms another if the AIC corrected for small sample sizes is 3 units more negative than the other. Although the model proposed by Tak *et al.,* fits their kinetic profiles, this was not true for the kinetic profiles shown in this thesis. Nevertheless, the model with the delay parameter resulted in similar lifespan values compared to the model without a delay for the three subsets (**Table 4.3**).

		$\Delta_3 = 0$	Δ_3 = free
Subject 1	ssr	0.11	0.09
	AICc	-137	-137.4
Subject 2	ssr	0.185	0.185
	AICc	-140.2	-137
Subject 3	ssr	0.19	0.19
	AICc	-139.3	-136.2
Subject 4	ssr	0.18	0.18
	AICc	-140.9	-137.7

Table 4.2 **Model comparison with and without Δ_3**

Models were compared with and without a delay parameter between intermediate and non-classical monocytes (Δ_3). The sum of squared residuals (ssr) and Akaike Information Criterion corrected for small sample size (AICc) are shown for each subject and model.

	Proliferation (per day)	Delay (days)	Lifespans (days)			% of total monocytes			Δ_3 (days)
	Bone Marrow	Bone Marrow-Blood	Classical monocyte	Intermediate monocyte	(days)	Classical monocyte	Intermediate monocyte	Non-classical monocyte	
Subject 1	0.50	1.53	1.44	3.55	5.33	80	8	12	2.1
Subject 2	0.28	1.70	0.35	5.25	7.51	83	7	10	<0.001
Subject 3	0.26	1.61	0.62	3.55	8.29	90	3	7	<0.001
Subject 4	0.64	1.70	1.54	4.11	N/R	96	2	2	N/R
A verage	**0.42**	**1.64**	**0.99**	**4.11**	**7.04**	**87**	**5**	**8**	**-**
SD	**0.18**	**0.08**	**0.59**	**0.80**	**1.53**	**7.18**	**2.94**	**4.35**	**-**
Confidence Intervals	**0.29-0.75**	**1.43-1.74**	**0.62-2.08**	**2.18-5.72**	**5.11-15.73**	**75.82-98.68**	**0.31-0.68**	**0.82-14.67**	**-**

Table 4.3 **Individual parameter estimates allowing Δ_3 to be a free parameter**

Values for each parameter for each subject were estimated as in Table 4.1, where the variable Δ_3 was allowed to be a free parameter. N/R = not resolved due to unreliable estimates for Δ_3 because there was little enrichment in the non-classical monocyte compartment.

4.2.4 *In vivo* monocyte maturation

These lifespan estimates of human monocyte subsets were generated based on a likely biological scenario. It remains to be shown whether a developmental relationship truly exists between human monocyte subsets. To test the hypothesis that classical monocytes mature into non-classical monocytes, adoptive transfer experiments were implemented. In collaboration with Prof. Richard A. Flavell and Dr. Anthony Rongvaux at Yale University, human classical monocyte subsets were isolated by FACS and adoptively transferred into humanised MISTRG mice (**Figure 4.8**). Using human CD45, these adoptively transferred cells could be distinguished from murine cells and allowed the fate of classical monocytes to be examined at selected time points.

At 10 minutes post-adoptive transfer, human $CD45^+$ cells were $CD14^+$ $CD16^{-/lo}$ (**Figure 4.8c**). By 24 hours, these cells became $CD14^+$ $CD16^+$ which phenotypically resembled intermediate monocytes, and by 96 hours they were uniformly $CD14^{-/lo}$ $CD16^+$ cells mirroring non-classical monocytes. This linear developmental further supports the model and demonstrates for the first time that human classical monocytes have the potential to mature into non-classical monocytes.

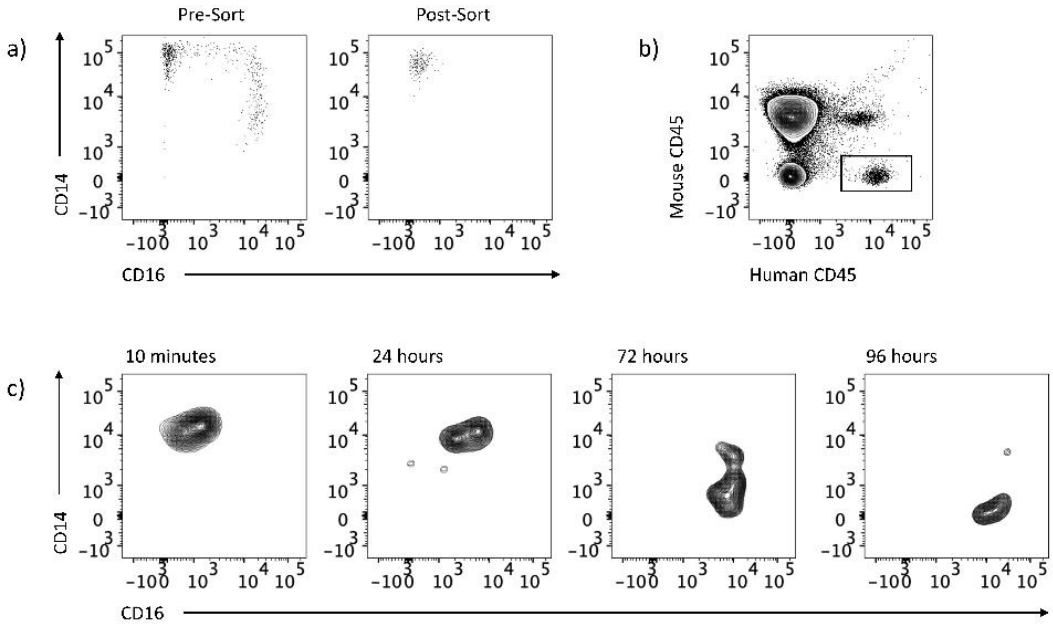

Figure 4.8 **Fate of human classical monocytes**

In vivo fate of classical monocytes was assessed in using humanised MISTRG mice. **a)** 1 x 10^6 human classical monocytes were sorted by FACS and adoptively transferred to MISTRG mice. **b)** adoptively transferred classical monocytes were identified by human CD45 and the fate of these cells was analysed for CD14 and CD16 expression 10 minutes, 24, 72 and 96 hours post-adoptive transfer. Representative of n=3 mice per time point.

4.2.5 *In vitro* monocyte differentiation

MISTRG mice supported the development of human classical monocytes into non-classical monocytes *in vivo*. While performing these experiments, Gamrekelashvili *et al.,* demonstrated that Notch2 signalling via DLL-1 governs Ly6C^{hi} classical monocytes maturation into Ly6C^{lo} non-classical monocytes in mice (Gamrekelashvili *et al.,* 2016). Next, it was examined whether this signalling pathway also plays a role in human monocytes.

1 x10^5 CD14$^+$ CD16$^{lo/-}$ classical monocytes were cultured in the presence or absence of DLL-1. CD14 and CD16 expression were assessed at 0, 24, 48 and 72 hours post culture (**Figure 4.9**). At 24, 48 and 72 hours, both CD14$^+$ CD16$^{lo/-}$ and CD14$^+$ CD16$^+$ monocytes were observed. The percentage of CD14$^+$ CD16$^{lo/-}$ and CD14$^+$ CD16$^+$ monocytes were quantified at each time point (**Figure 4.9**). CD14$^{lo/-}$ CD16$^+$ monocytes were not observed in either condition at the time points measured.

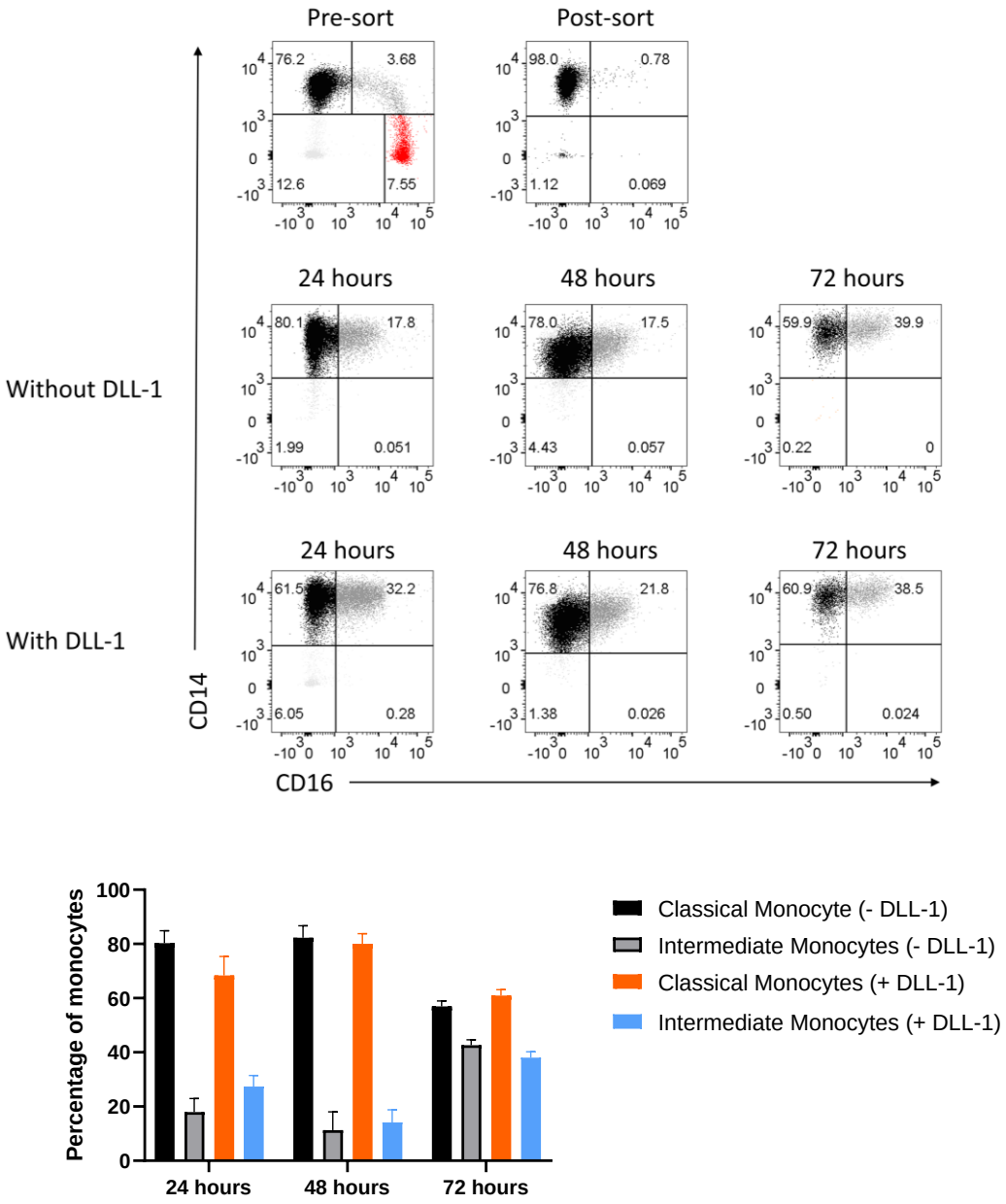

Figure 4.9 ***In vitro*** **culture of classical monocytes**

Classical monocytes subsets were isolated from PBMC by FACS and cultured for 24, 48 or 72 hours, either in the presence or absence of DLL-1. CD14 and CD16 profiles were analysed on pre-sorted PBMC, post sorted classical monocytes and 24, 48 and 72 hours post cultured classical monocytes. Representative flow cytometry plots are shown. Percentages were taken from the $CD14^{+}$ $CD16^{lo/-}$ and $CD14^{+}$ $CD16^{+}$ quadrant and numerated (bar graph). Bars represent mean ± SD. n=3 individual experiments.

In Chapter 3.2.3.1, additional markers were shown to be differentially expressed between the three monocyte subsets. CCR2, CD11c and CD64 were assessed on *in vitro* monocyte subsets in comparison to their blood counterparts at baseline (**Figure 4.10**). Where these markers were

differentially expressed between blood classical and intermediate monocytes at 0 hours, marker expression were comparatively similar between *in vitro* classical and intermediate monocytes. Furthermore, the expression between *in vitro* and *in vivo* counterparts were also visibly different. CCR2 is a well characterised highly expressed chemokine receptor on classical monocytes, however, *in vitro* classical monocytes had a markedly reduced expression of this receptor. Conversely, CD11c increased on *in vitro* classical monocytes compared to blood classical monocytes. Culturing in the presence of DLL-1 did not significantly alter the expression patterns of these measured markers, with the exception of CD64 at 72 hours.

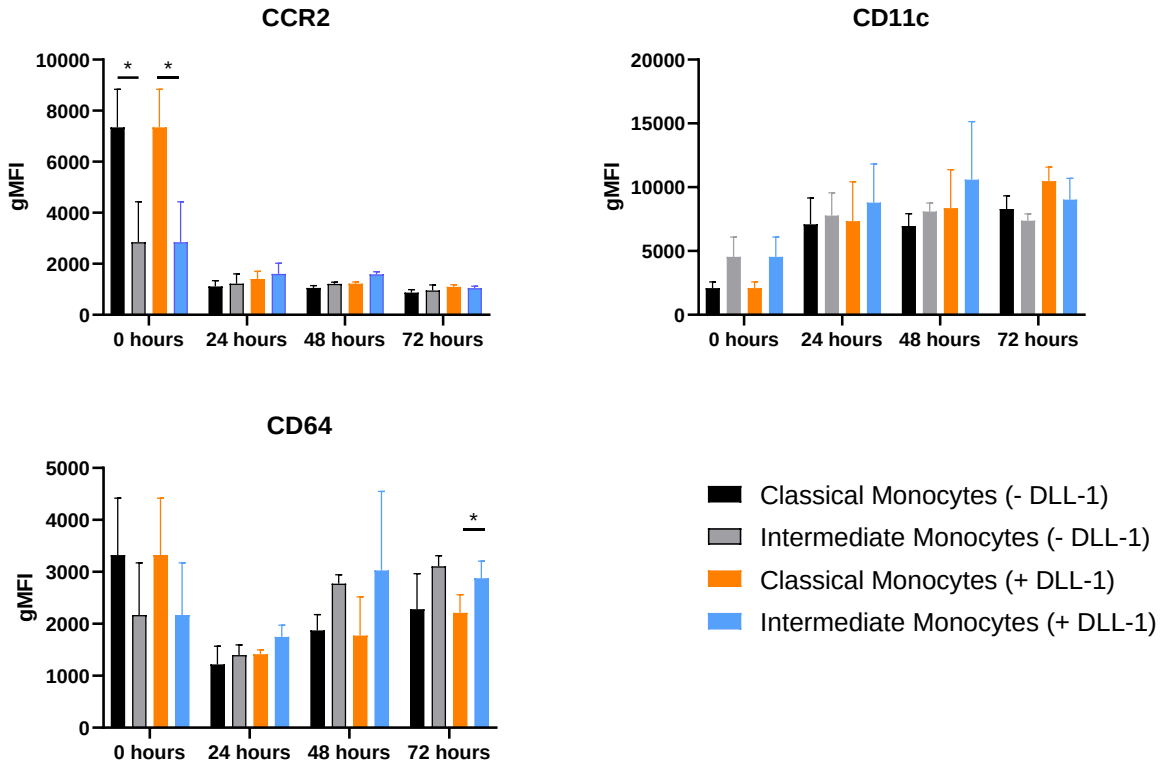

Figure 4.10 ***In vitro* phenotype of monocyte subsets**

Classical monocytes subsets were isolated from PBMC by FACS and cultured for 24, 48 or 96 hours, either in the presence or absence of DLL-1. CCR2, CD11c and CD64 expression were assessed at baseline and each of these time points on *in vitro* and *in vivo* $CD14^{+}$ $CD16^{-/lo}$ classical monocytes and $CD14^{+}$ $CD16^{+}$ intermediate monocytes. Analysed by two-way ANOVA and Tukey multiple comparisons test. * $p < 0.05$, bars represent mean ± SD. n=3 individual experiments.

4.3 Dendritic Cell Kinetics

4.3.1 Preliminary Dendritic Cell Kinetics

While monocytes make up the majority of circulating human mononuclear phagocytes, DC make up the remainder. Given the close developmental relationship of these two cell types, it was examined how similar the kinetics of DC are to monocytes. Fewer studies exist regarding DC kinetics. A study in macaques, demonstrated labelling of cDC2 appeared before monocytes, however pDC peaked around the same time as intermediate monocytes (Sugimoto *et al.,* 2015). With this being the only study to date, it was hypothesised that human DC exhibit a similar kinetic profile.

The labelling protocol for monocytes was also followed for DC subsets (Section 2.8). DC were initially sorted according to the gating strategy shown in **Figure 3.9**. These preliminary data showed that both cDC1 and cDC2 were labelled at very early time points (day 1 post labelling) whereas pDC labelling occurred at a slower rate and peaked around day 10 (**Figure 4.11**). Both cDC1 and cDC2 exhibited a very similar kinetic profile and the label was absent after 7.

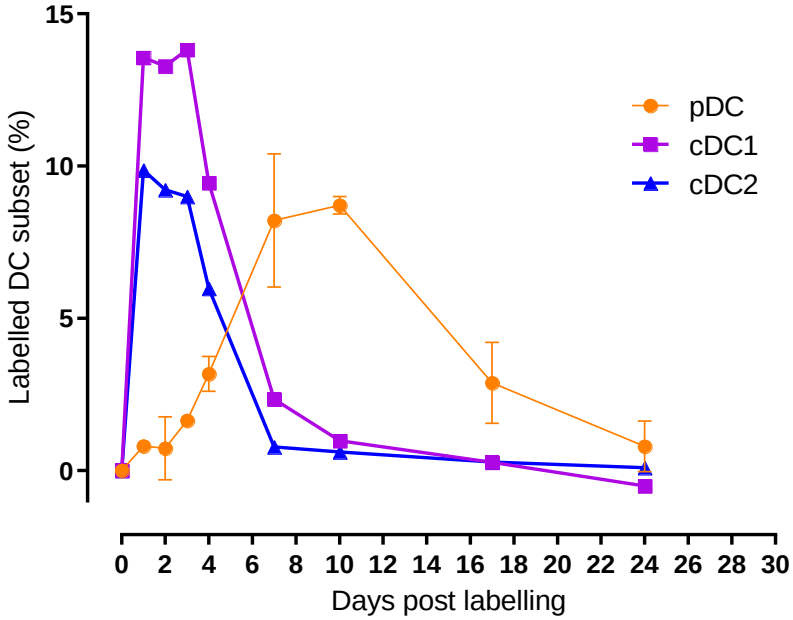

Figure 4.11 **Preliminary human DC subset kinetics**

Circulating cDC1, cDC2 and pDC were sorted by FACS according to the gating strategy shown in Figure 3.9. DC subsets were sorted at specific time points following the administration of deuterated glucose and were analysed for the presence of deuterium in the DNA by GC/MS. Bars represent mean ± SD, n=1 individual for cDC1 and cDC2, n=2 individuals for pDC.

4.3.2 DC Kinetics based on a novel unified gating strategy

4.3.2.1 *In vivo* DC kinetic profiles

While performing the experiments in **Figure 4.11**, See *et al.,* and Villani *et al.,* published that further heterogeneity exists within DC subsets as discussed in Section 3.3.

Following the establishment of a unified DC gating strategy, up to six DC subsets could be identified (**Figure 3.15**). With this advancement in human DC biology, multiple questions arise regarding the relationship of these cells to each other. However, it was not possible to examine the kinetics of all DC populations due to limitations of sorting and the minimum requirement of 10,000 cells for downstream GC/MS analysis. Both See *et al.,* and Villani *et al.,* described cDC development from the $CD123^{+}$ $Siglec6^{+}$ AXL^{+} pre-DC. As the newly discovered pre-DC has gained a considerable amount of attention, it was questioned how the kinetics of these cells compared to the major cDC1, cDC2 and pDC subsets.

Labelling was observed as early as day 1 post labelling in cDC from preliminary data (**Figure 4.12**). Therefore, when examining the kinetics of the DC subsets using the revised gating strategy (**Figure 3.15**), a 6 hour time point was included. Of note, cDC2 were collectively analysed as AXL^- cDC2. In comparison to **Figure 4.11**, similar kinetic profiles were observed for cDC1, AXL^- cDC2 and pDC (**Figure 4.12**). From the original gating strategy, pre-DC would have been masked by the abundant pDC population hence no early signal was detected in the original pDC labelling (**Figure 4.11**). However, with the new gating strategy, pre-DC can now be appreciated as a distinct cell type from pDC with a striking difference in their kinetic curves (**Figure 4.12**).

It was hypothesised that pre-DC are precursors to cDC, and therefore would be labelled earlier. As early as 6 hours post deuterium pulse, a small but prominent label was detected in pre-DC but no labelling was detected in cDC or pDC. Aside from this observation, pre-DC exhibited a similar kinetic profile parallel to blood cDC1 and cDC2.

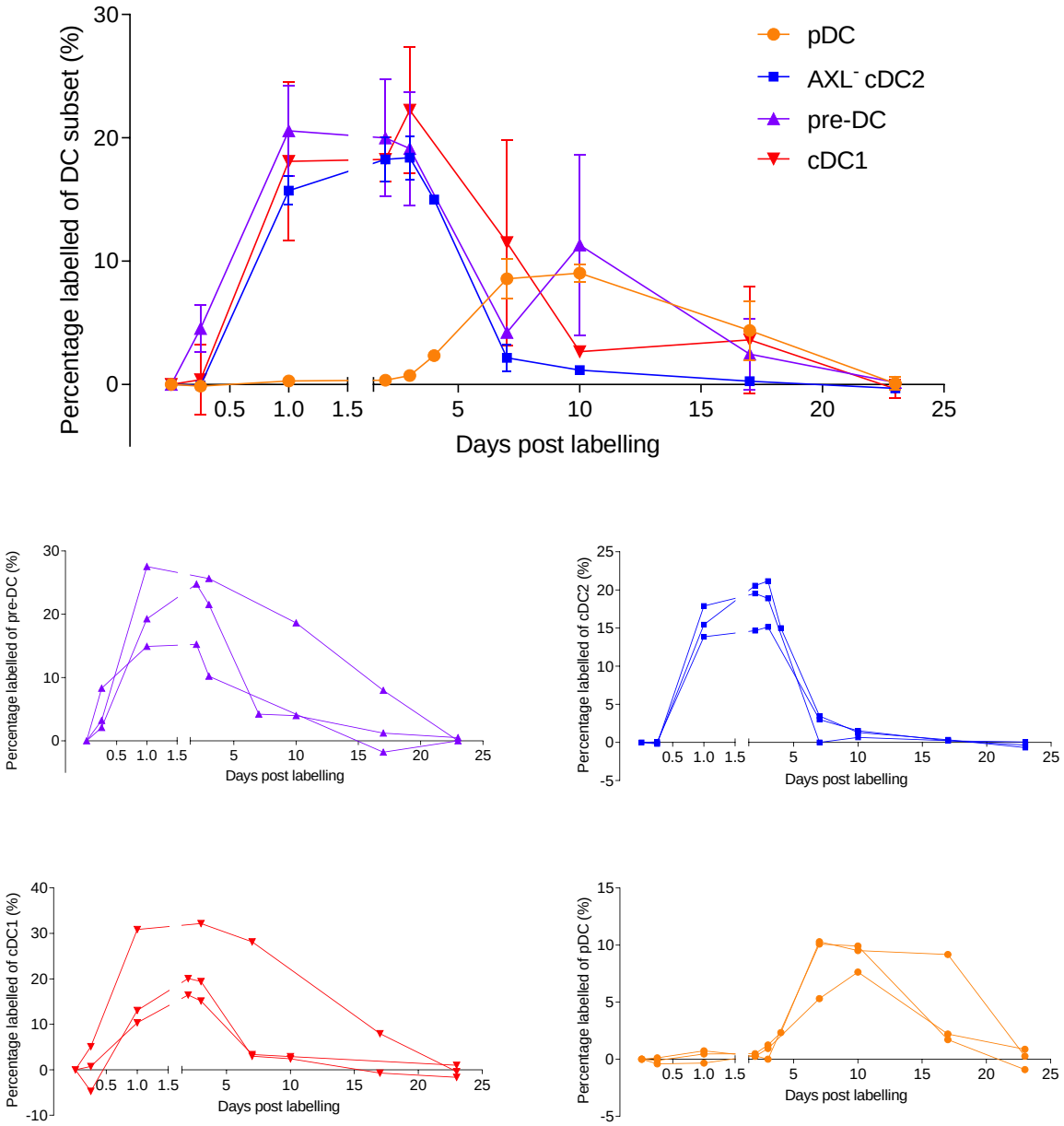

Figure 4.12 **Human DC subset kinetics based on a novel DC gating strategy**

The kinetic profiles of pre-DC, cDC1, AXL- cDC2 and pDC were assessed. DC subsets were FACS sorted using the gating strategy shown in Figure 3.15. Cells were sorted at specific time points following deuterated glucose pulse and measured by GC/MS to measure the presence of deuterium in the DNA. Kinetics profiles for each subset are shown overlaid (top) and individual curves (bottom four graphs). Bars represent mean ± SD. n=3 individual experiments.

4.3.2.2 Cell cycle profile of circulating DC

Although early labelling was observed in pre-DC at 6 hours, it remained unclear whether circulating pre-DC exhibit proliferative potential and therefore incorporate plasma deuterium into their DNA or whether this early labelling represents rapid egression from the bone marrow.

Using DAPI and Ki67, the cell cycle status of blood DC populations was analysed (**Figure 4.13**). Interestingly, all DC subsets were predominantly found in the G_1 stage of the cell cycle although 38% of pDC were found in G_0. However, cells were not observed in further stages of the cell cycle (S phase, G_2 or mitosis). As active DNA replication was not observed, it was concluded circulating DC do not divide in the circulation. The early labelling observed in pre-DC (**Figure 4.12**) was most likely due to the rapid release from the bone marrow.

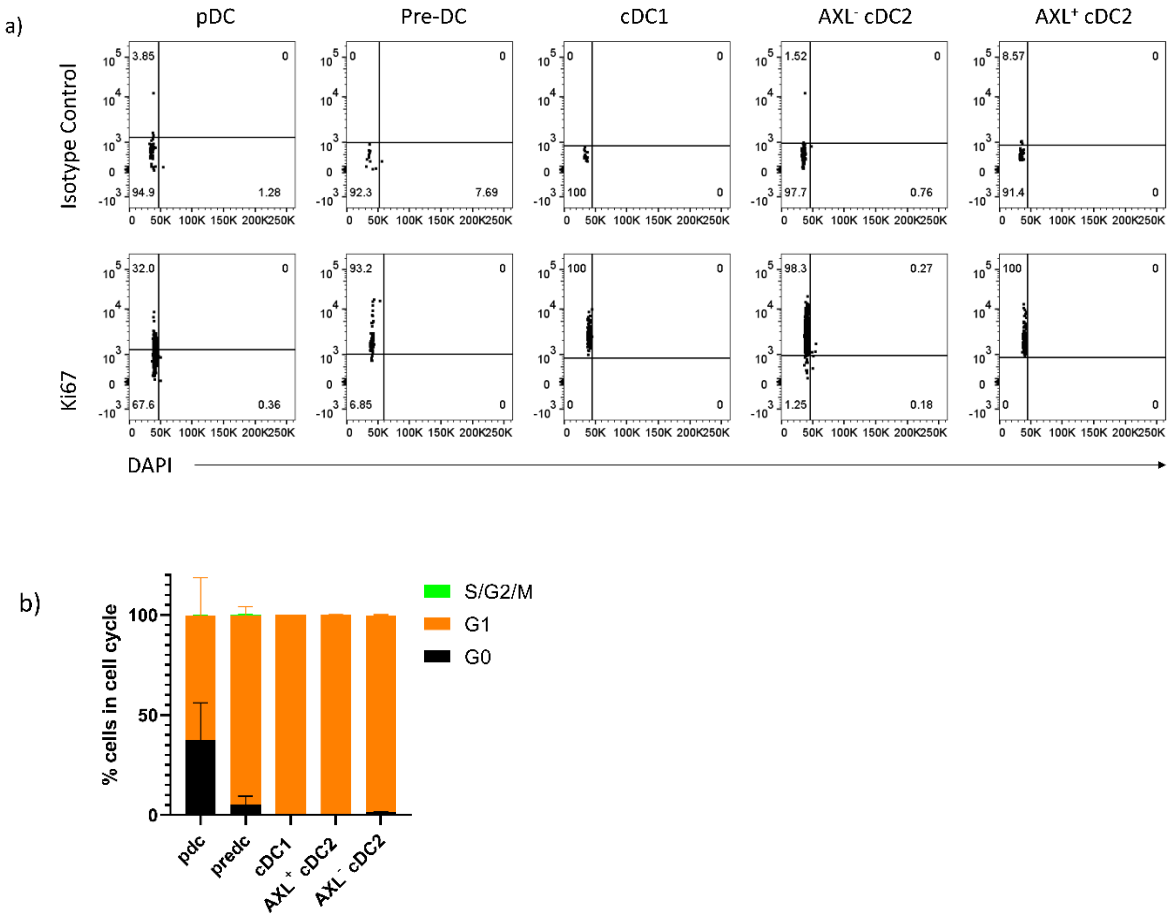

Figure 4.13 **Cell cycle status of circulating DC subsets**

Cell cycle status of circulating DC was analysed. DC subsets were identified by flow cytometry as in Figure 3.15. **a)** Ki67 and DAPI expression were analysed on DC subsets. $KI67^-$ $DAPI^{low}$ = G_0, $KI67^+$ $DAPI^{low}$ = G_1, $KI67^+$ $DAPI^{int/hi}$ = $S/G_2/M$ phase. **b)** The percentage of cells subset in each stage of the cell cycle was quantified. Representative of n=4 independent experiments.

4.3.2.3 Proposed DC models

These data demonstrate that pre-DC may egress from the bone marrow earlier than cDC1 and cDC2 in line with their precursor potential. The literature suggests these cells then mature into cDC1 and cDC2 (See *et al.,* 2017; Villani *et al.,* 2017). The kinetic data presented here showed labelled cDC1 and cDC2 appear 18 hours after labelled pre-DC in the circulation. As pre-DC do not divide (**Figure 4.13**) and are found at a concentration of approximately 330 cells/ml blood, it seems unlikely that the significant labelling in cDC1 and AXL^- cDC2 found at 648 cells/ml blood and 9083 cells/ml blood, respectively (**Figure 3.17**), arise solely from a minute number of non-dividing pre-DC. This may suggest that blood labelling in cDC1 and cDC2 may develop from

another source. Pre-DC and cDC subsets have been identified in the bone marrow (Cytlak *et al.,* 2019), therefore, it is possible that some of the initial labelling in circulating cDC1 and cDC2 arise from the bone marrow egression of these cells. This does not rule out the possibility that pre-DC differentiate into cDC1 and cDC2 in the circulation. To understand the extent pre-DC contribute to the circulating pool, mathematical modelling is necessary. At the time of writing, these data are awaiting to be modelled in collaboration with Dr. Becca Asquith and Mr. Jonas Mackerodt. **Figure 4.14** illustrates the proposed models, where pre-DC maturation is questioned. The first model suggests that pre-DC convert exclusively in the blood as suggested (See *et al.,* 2017) (**Figure 4.14a**). Although, as pre-DC and cDC subsets are present in the bone marrow (Cytlak *et al.,* 2019), maturation may also take place here (**Figure 4.14b**), or alternatively in both compartments (**Figure 4.14c**). Finally, others have suggested that pre-DC map exclusively to the cDC2 route (Cytlak *et al.,* 2019; Villani *et al.,* 2017) (**Figure 4.14c**). It is hoped with the aid of mathematical modelling, a likely model can be proposed.

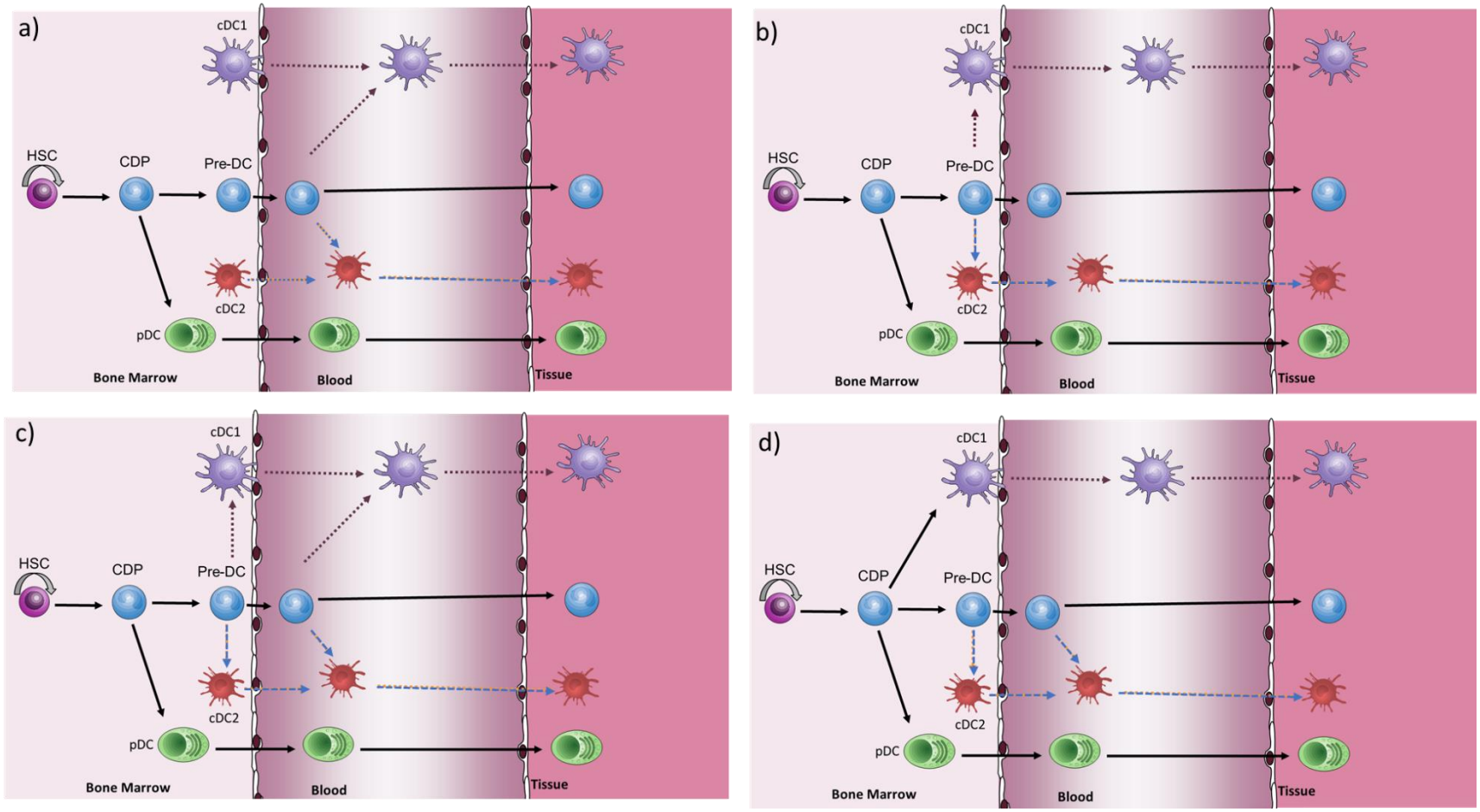

Figure 4.14 **Proposed DC models**

Based on the deuterium labelling data and the published literature, four DC models were proposed. **a)** blood cDC have been described to originate from blood pre-DC, but given the kinetic profiles in the blood, **b)** this differentiation may also occur in the bone marrow. Alternatively, **c)** both processes may occur. **d)** Finally, pre-DC have also been suggested to map exclusively to a cDC2 route.

4.4 Discussion

4.4.1 Steady-state human monocyte kinetics

It has recently been established that the majority of macrophages are maintained independently of monocytes under steady physiological conditions (Ginhoux *et al.,* 2010; Hashimoto *et al.,* 2013; Liu *et al.,* 2019; Schulz *et al.,* 2012; Yona *et al.,* 2013), therefore questioning the true role of monocytes and whether these cells should be regarded as effector cells within their own right. In addition to investigating the role of monocytes during pathology, it is equally important to acknowledge the homeostatic kinetics underlying their steady-state generation, maturation and disappearance that may go awry in inflammation.

Nearly fifty years ago, studies investigated the kinetics of monocytes in humans, using tritiated thymidine (Whitelaw, 1972) and more recently with deuterated glucose (Mohri *et al.,* 2001). However, studies have not investigated the kinetics of the three individual subsets themselves. Interestingly, it has been indirectly shown in patients undergoing HSCT, $CD14^{+}$ monocytes appeared in the circulation prior to $CD16^{+}$ monocytes (McGovern *et al.,* 2014). This is consistent with the kinetic profiles of classical and non-classical monocytes examined in mice (Liu *et al.,* 2019; Yona *et al.,* 2013), rats (Yrlid *et al.,* 2006) and rhesus macaques (Burdo *et al.,* 2010; Sugimoto *et al.,* 2015). In all three species, it was demonstrated classical monocytes present with label initially, while labelled non-classical monocytes appear later. Here, a similar labelling profile was observed in humans, where a sequential appearance of the label was first evident in classical monocytes, followed by intermediate and finally non-classical monocytes.

Analysis of human bone marrow revealed the presence of classical monocytes. Therefore, as intermediate and non-classical monocytes were not detected, it was proposed a linear developmental relationship most likely occurs in the circulation. This compared to observations in mice, where the adoptive transfer of $Ly6C^{hi}$ classical monocytes were shown to mature into $Ly6C^{lo}$ non-classical monocytes (Mildner *et al.,* 2017; Varol *et al.,* 2007; Yona *et al.,* 2013).

Of note, previous studies have reported classical and intermediate monocytes can be detected in the bone marrow (Mandl *et al.,* 2014). However, Mandl and colleagues used cryopreserved bone marrow mononuclear cells that were cultured overnight prior to analysis, whereas bone marrow biopsies were analysed immediately following sample collection in **Figure 4.6**. Overnight culture of blood $CD14^{+}$ $CD16^{-}$ classical monocytes results in the upregulation of CD16, as demonstrated in **Figure 4.9**. It is possible that the intermediate monocytes were an artefact detected by Mandl *et al.,* due to cell preparation.

Together with the kinetic graphs and bone marrow data, it was possible to suggest a likely model for human monocyte development. After modelling these kinetic data to the proposed model, estimates were obtained for the lifespan of these cells, delays and percentage of monocytes transitioning.

The kinetic data demonstrated that labelling in monocytes was not observed until day 2 and mathematical modelling estimated this post-mitotic dwell period to be approximately 1.6 days (**Figure 4.7 and Table 4.1**). Similarly, historical studies have demonstrated that monocytes egress from the bone marrow 13-26 hours following labelling with tritiated thymidine (Whitelaw, 1972) and approximately 2 days following labelling with deuterated glucose (Mohri *et al.,* 2001). It remains unclear why monocytes reside within the bone marrow for this period. Chong and colleagues have demonstrated that bone marrow human classical monocytes are composed of a $CXCR4^{hi}$ and $CXCR4^{lo}$ population (Chong *et al.,* 2016). As $CXCR4^{hi}$ classical monocytes can proliferate, it is possible these cells can take up deuterium, which then mature into non-proliferating $CXCR4^{lo}$ classical monocytes which eventually enter the circulation. Consequently, if $CXCR4^{hi}$ classical monocytes represent the last proliferative step in monocyte development, it can be suggested that time taken for $CXCR4^{hi}$ classical monocytes to mature into $CXCR4^{lo}$ monocytes and enter the circulation is approximately 1.6 days. The transition to $CXCR4^{lo}$ could be rapid and the resulting $CXCR4^{lo}$ classical monocytes act as an emergency squad waiting for the appropriate cue to be recruited to an infection or injury, as observed in mice (Serbina *et*

al., 2009; Serbina and Pamer, 2006). Alternatively, 1.6 days could represent the time taken for the CXCR4^{hi} monocytes to become CXCR4^{lo} monocytes. Bone marrow labelling data would be needed to confirm whether this period represents a maturation period or a mature pool of classical monocytes waiting to be released.

The absence of label at day 1 post labelling signifies that circulating monocytes do not proliferate as confirmed by Ki67 and DAPI expression which also showed monocytes are in G_0 of the cell cycle. This is consistent with previous findings, where peripheral blood monocytes were not observed in S, G_2 or mitosis phases, whereas pre-monocytes and cMoP were (Kawamura *et al.,* 2017).

The model suggests the lifespan of classical monocytes is approximately 1 day, 4.3 days for intermediate monocytes and 7.4 days for non-classical monocytes. In mice, the half-life of classical and non-classical monocytes have been estimated at 20 hours and 2.2 days, respectively (Yona *et al.,* 2013). While in macaques, although the half-life or lifespan was not calculated, non-classical monocytes were present in the circulation for a longer period of time in comparison to classical monocytes. Taken together, these data suggest non-classical monocytes reside within the circulation for a longer period of time and is conserved across species. This may be because non-classical monocytes represent a terminally differentiated monocyte and may consequently represent a 'blood macrophage' (Yona *et al.,* 2013), where their steady-state function resides within the blood where they are constantly monitoring the endothelium (Auffray *et al.,* 2007; Carlin *et al.,* 2013). On the other hand, classical monocytes are continuously recruited to repopulate tissue mononuclear phagocyte compartments (Bain *et al.,* 2014; Epelman *et al.,* 2014; Jakubzick *et al.,* 2006; Kim *et al.,* 2016; Liu *et al.,* 2019; McGovern *et al.,* 2014; Mossadegh-Keller *et al.,* 2017), therefore exhibit a higher turnover.

The first studies in humans approximated the average monocyte lifespan to be 102 hours (4.25 days) (Whitelaw, 1972). Several reasons exist for the discrepancies between these data such as

subject demographics, methods to identify monocytes and the choice of label. Mohri and colleagues also used deuterated glucose and examined total $CD14^+$ monocyte (Mohri *et al.,* 2001). They proposed a half-life of approximately 2.2 days which equates to an average lifespan of approximately 3.2 days, based on first-order decay kinetics. This value represents the lifespan of combined classical and intermediate monocytes, however as classical monocytes are far more abundant than intermediate monocytes, the kinetic profile of $CD14^+$ monocytes is likely to be skewed towards classical monocytes. Therefore, the approximated lifespan of 3.2 days by Mohri and colleagues, is likely to be an under-representation, as the model here proposes classical and intermediate monocytes have a combined lifespan on 5.3 days.

Other independent groups have recently examined human monocyte kinetics (Tak *et al.,* 2017a) and also proposed a model where classical monocytes mature into intermediate then non-classical monocytes. However, it was proposed intermediate monocytes leave the circulation where 82% are estimated to mature into non-classical monocytes which re-enter the circulation after 1.6 days in the tissue and circulate for a further 2.3 days. When modelling the kinetic data in **Figure 4.3** with the model proposed by Tak and colleagues, AICc values suggested that maturation of monocyte subsets occurs within the circulation and that a delay parameter (Δ_3) was unnecessary. Although there is evidence to suggest that classical monocytes enter tissues under steady physiological conditions (Bain *et al.,* 2014; Epelman *et al.,* 2014; Jakubzick *et al.,* 2013; Kim *et al.,* 2016; Liu *et al.,* 2019; McGovern *et al.,* 2014; Mossadegh-Keller *et al.,* 2017), similar observations have not been reported in terms of intermediate monocytes leaving the circulation. Furthermore, once classical monocytes enter the tissue, re-entry into the circulation was not detected (Claudia Jakubzick, oral communication), therefore a similar hypothesis could be extended to intermediate monocytes if they were observed to extravasate.

The model proposed that the majority (99%) of classical monocytes leave the circulation to enter tissues or die and only a small percentage (1%) transition to intermediate monocytes. Although these appear to be extreme values, classical monocytes constitute 86% of all circulating

monocytes while intermediate monocytes make up approximately 5% remainder. It is therefore understandable that not all classical monocytes develop into intermediate monocytes. In addition, as intermediate monocytes have a longer lifespan than classical monocytes, they don't need to be replenished as often. Finally, the infiltration of classical monocytes into tissues is plausible, based on studies demonstrating that under steady-state murine classical monocytes replenish tissue monocyte-derived cells in the lamina propria (Bain *et al.,* 2014), dermis (McGovern *et al.,* 2014), heart (Epelman *et al.,* 2014) peritoneum (Kim *et al.,* 2016), testis (Mossadegh-Keller *et al.,* 2017). Taken together these data support the notion that most classical monocytes do not convert into intermediate monocytes and may leave the circulation to fulfil other functions/fates.

Humanised MISTRG mice (Rongvaux *et al.,* 2014) were used to support the model and confirm the fate of classical monocytes. Adoptively transferred human classical monocytes have the potential to mature into intermediate then non-classical monocytes. This is consistent with murine studies where Ly6C^{hi} classical monocyte mature into Ly6C^{lo} non-classical monocytes (Gamrekelashvili *et al.,* 2016; Mildner *et al.,* 2017; Varol *et al.,* 2007; Yona *et al.,* 2013). RNA-sequencing analysis demonstrated that transferred Ly6C^{hi} monocytes, gradually changed their expression profile which closely resembled bona fide non-classical monocytes (Mildner *et al.,* 2017). Of note, it is possible that additional sources of intermediate and non-classical monocytes exist, as observed under inflammatory conditions (Satoh *et al.,* 2017).

A key question that remains to be answered is the decision behind making some classical monocytes mature into intermediate monocytes and some leave the circulation. It may be possible that classical monocytes are a heterogenous population, as has already been demonstrated in mice (Menezes *et al.,* 2016) and humans (Dutertre *et al.,* 2019; Hamers *et al.,* 2019). Marker analysis of human classical monocytes by viSNE analysis (**Figure 3.6**) demonstrated membrane surface expression was variable within this subset. Therefore, it is possible that an unidentified sub-population of classical monocytes are primed towards

maturation into intermediate and non-classical monocytes. Although single cell RNA sequencing analysis suggested classical monocytes are a homogenous population (Villani *et al.,* 2017), only a small number of cells were analysed, it may be difficult to pick up the unique 1% of classical monocytes that are primed to becoming intermediate monocytes. Hamers and colleagues, demonstrated using mass cytometry that four sub-populations of human classical monocytes could be identified (Hamers *et al.,* 2019). Furthermore, it has been reported that human classical monocytes harbour a $CD14^+$ $CD1c^+$ DC (Dutertre *et al.,* 2019). Although this study focused on the functional role of the $CD14^+$ DC, further heterogeneity was observed within the classical monocyte population, although this was not discussed further. Given this rapidly changing view of monocyte subsets, studies are necessary to clarify this heterogeneity and identify whether populations of classical monocytes exist which are primed to becoming non-classical monocytes.

Concerning the mechanism of classical to non-classical monocyte maturation, several transcription factors have been identified in mice and humans. C/EBPβ, Nr4a1 and Klf2 regulate the development of non-classical monocytes in mice, and have also been shown to be expressed in human monocytes (Hanna *et al.,* 2012, 2011; Mildner *et al.,* 2017; Thomas *et al.,* 2016). Interestingly, human subjects lacking $CD16^+$ monocytes have been described where these individuals only harbour classical monocytes (Frankenberger *et al.,* 2013). NR4A1 was examined as a potential candidate, though a normal sequence was found in these individuals, suggesting additional overriding mechanisms are involved. The genetic defect behind this observation remains unknown.

Upstream of these transcription factors, Notch2 signalling is thought to facilitate the maturation of monocyte subsets (Gamrekelashvili *et al.,* 2016). Specifically, the ligation of delta-like ligand 1 (DLL-1) with Notch2, is necessary to induce a representative $Ly6C^{lo}$ monocyte phenotype from $Ly6C^{hi}$ monocytes. It was examined whether this could be recapitulated in human monocytes. Upon culturing classical monocytes with or without DLL-1, an increase in CD16 expression was observed at 24 hours. These initial results were indicative of maturation into intermediate

monocytes, however, upon further marker analysis, it was revealed these cells were not bona fide intermediate monocytes. *Ex vivo* monocytes are easily polarised to taken on a different phenotype and function. Given the adherent nature of monocytes, the upregulation of CD16 may be an artefact due to adherence to tissue culture plastic. Others have also demonstrated that monocytes cultured as early as 4 hours increase CD16 expression in addition to adhesion markers such as CD11b and CD11c (Golden *et al.,* 2015). Therefore, difficulties remain in studying cultured *ex vivo* monocytes as bona fide 'monocytes' and they should be regarded as monocyte-derived cells. From these data, it cannot be concluded whether DLL-1 plays a role and it may represent the need for a better culture system where monocytes can be studied as 'monocytes'.

4.4.2 Steady-state human DC kinetics

To date, the circulating kinetics of human DC remains largely unknown. Although mice have been described to harbour circulating DC subsets equivalent to humans (Donnenberg *et al.,* 2001; O'Keeffe *et al.,* 2003), the kinetics of these cells have not been described. Nevertheless, following the adoptive transfer of blood DC, 93% of these cells were cleared from the circulation within one hour (Liu *et al.,* 2007). In addition, it was also estimated that blood DC enter tissues at a rate of 4,300 cells per hour which then reside for approximately 10-14 days (Ginhoux *et al.,* 2009; Liu *et al.,* 2007). The circulating kinetics of DC have only been described in macaques, where a rapid appearance of BrdU was observed in cDC2 prior to labelling in monocytes and pDC demonstrated a slower turnover in comparison (Sugimoto *et al.,* 2015).

Following the identification of novel human DC subsets, the kinetic profiles of these subsets were examined for the first time *in vivo*. Circulating pre-DC have been described as a precursor population to cDC (See *et al.,* 2017; Villani *et al.,* 2017), it was anticipated these cells would appear in the circulation prior to cDC. At 6 hours, pre-DC were indeed labelled whereas cDC labelling was not observed. Using monocytes as a reference, it was proposed if one subset matures into another, this would be mirrored as sequential kinetic profiles. However, this was

not observed between pre-DC and cDC subsets. It appears that pre-DC remain the circulation for a longer period than predicted and their kinetic profile is akin to cDC subsets. However, it is important to bear in mind that the cells labelled at day 1 are not necessarily the same cells labelled at day 2. In mice, the half-life of adoptively transferred splenic DCs in the murine circulation is in the order of 2–4 hours (Roberto Bonasio *et al.,* unpublished data, referenced in Bonasio and von Andrian, 2006), there this translates to a significant daily flux of cells from the blood to tissues. Similarly, following the adoptive transfer of blood leukocytes, 93% of murine circulating DC were cleared within 1 hour (Liu *et al.,* 2007). Although it seems pre-DC are in the circulation for a comparable amount of time, the rapid turnover of these cells could be masked by labelled pre-DC which are egressing from the bone marrow.

It is also possible the early cDC labelling arises directly from another source such as the bone marrow and pre-DC may contribute to the circulating cDC pool after residing in the blood for a period of time. In support of this view, human bone marrow analysis has revealed the presence of pDC, cDC1, cDC2 and pre-DC (Cytlak *et al.,* 2019). Therefore, it is likely the egression of bone marrow cDC subsets contributes to the early labelling seen in the circulating cDC pool. It remains unclear regarding the relationship of DC subsets in the bone marrow i.e. whether bone marrow pre-DC give rise to bone marrow cDC subsets or whether cDC arise directly from the CDP. Future experiments could look at deuterium labelling within the bone marrow compartment. This together with the circulating kinetics will help form a better model.

As a result, several models can be proposed from these data and mathematical modelling may help in suggesting a likely biological scenario. Nevertheless, this may not represent the true biology scenario and further experimental data would be necessary to support such a model. Unfortunately, it was not feasible to demonstrate the fate of pre-DC *in vivo* using MISTRG mice as there are insufficient pre-DC to adoptively transfer from a single human donor.

pDC labelling curves were distinct from that of cDC and pre-DC, labelling was observed much later in comparison. In mice, BrdU labelling demonstrated that 25% of bone marrow pDC were labelled by day 7, in contrast to B cells where 75% were labelled (Pelayo *et al.,* 2005), indicating pDC are slowly replenished. In addition, splenic pDC have a lower turnover rate in comparison cDC. 10% of pDC were labelled by day 3, whereas, 70-80% of cDC were labelled at the same time point (O'Keeffe *et al.,* 2002). Therefore, human tissue pDC may also represent long-lived cells and don't require frequent replenishment, consequently, pDC are not released into the circulation rapidly due to smaller demand. Recently, pDC in mice have been described to originate from a lymphoid origin and closely relate to B cells (Dress *et al.,* 2019; Rodrigues *et al.,* 2018). Therefore, it is reasonable to question whether human B cells and pDC share a similar kinetic profile in humans. Studies performed by Macallan and colleagues have demonstrated that following deuterated glucose administration, labelled $CD27^-$ naïve B cells were observed around day 4 post labelling (Macallan *et al.,* 2005), around the same time as pDC labelling was observed. However, as naïve B cells can also divide in the periphery, it is difficult to differentiate the labelling of cells attributed solely to bone marrow egression.

Circulating DC were shown to be in G_1 phase of the cell cycle, although it was deemed unlikely these cells divide in the circulation as no diploid cells were detected. It is probable that these cells advance in G_1 but reach a restriction point which limits their proliferation, at least in the circulation. Others have reported Ki67 expression in peripheral cDC subsets (van Leeuwen-Kerkhoff *et al.,* 2018) and some have even reported that 10-15% of cDC1 and cDC2 are $Ki67^+$ $DAPI^{hi}$ (S phase, G_2 or M phase) (Segura *et al.,* 2012). Discrepancies may be due to the differences in sample preparation and flow cytometry identification of cell populations. In contrast to monocytes which are in G_0, DC subsets appear to have entered the cell cycle are largely in G_1 of the cell cycle (**Figure 4.4 and Figure 4.13**). In addition, DC may resume cell cycling as they have been observed to proliferate in murine tissue (Kabashima *et al.,* 2005; Liu *et al.,* 2007). Similar

observations have been made in humans, where skin DC are found in the S, G_2 and mitosis phase of the cell cycle (Venetia Bigley, by communication).

Estimates for the lifespan of DC subsets are currently being modelled. Together these data demonstrate the kinetic profiles of the circulating mononuclear phagocyte subsets in humans under steady physiological conditions.

Chapter 5

Mononuclear Phagocyte Kinetics in Inflammation

5.1 Introduction and Aims

5.1.1 Introduction

Chapter 4 establishes the kinetic profile of circulating monocyte and dendritic cells subsets under steady physiological conditions. The question arises how the kinetic profiles of human monocyte and dendritic cell subsets are altered under inflammatory conditions.

Studies in mice have demonstrated that systemic inflammation perturbs the monocyte and DC equilibrium resulting in an initial decline in monocyte and DC numbers followed by the repopulation of these cells. (Chong *et al.,* 2016; Ding *et al.,* 2004; Efron *et al.,* 2004; Scumpia *et al.,* 2005; Shi *et al.,* 2011). In the clinical setting, changes in the distribution of circulating monocyte and dendritic cell subsets have been reported in sepsis, SLE and rheumatoid arthritis (Cooper *et al.,* 2012; Grimaldi *et al.,* 2011; Guisset *et al.,* 2007; Mukherjee *et al.,* 2015; Poehlmann *et al.,* 2009; Riccardi *et al.,* 2011). However, as patient samples are often sampled days after the onset of inflammation, the kinetic profiles of monocyte and dendritic cells subsets have not been examined from the initiation through to the resolution of inflammation in humans.

Similarly, the infiltrating kinetics of mononuclear phagocytes have been widely examined in mice in response to local inflammation, where Ly6C^{hi} classical monocytes are recruited to sites of inflammation (Dal-Secco *et al.,* 2015; Hilgendorf *et al.,* 2014; Nahrendorf *et al.,* 2007; Zigmond *et al.,* 2012). Similarly, in previous human models of inflammation, the infiltration of CD14^{+} monocytes has been described (Eguíluz-Gracia *et al.,* 2016; Jenner *et al.,* 2014), however, the infiltration of individual monocyte subsets and the newly described DC subsets has not yet been examined in local inflammation.

5.1.2 Aims

To demonstrate the kinetics of monocyte and dendritic cell subsets during experimental systemic and local inflammation in humans.

5.2 Human Endotoxin Model

5.2.1 Circulating mononuclear phagocyte count

To study the kinetics of mononuclear phagocytes from the initiation of inflammation, human models are needed. One of the most common models of systemic inflammation is intravenous (I.V.) endotoxin administration. In collaboration with Prof. Derek Gilroy and Dr. James Fullerton, male volunteers were challenged with 2ng/kg of National Institutes for Health Clinical Center Reference Endotoxin (CCRE, Escherichia coli O:113:H10:K negative).

Blood samples were taken at 0, 2, 4, 8, 24, 48, 72 hours and 7 days post-endotoxin challenge where absolute monocyte counts were enumerated by The Doctor's Laboratory (**Figure 5.1**). Although counts are reported as 'monocytes', it is understood this count also includes dendritic cells owed to the similarities in morphology.

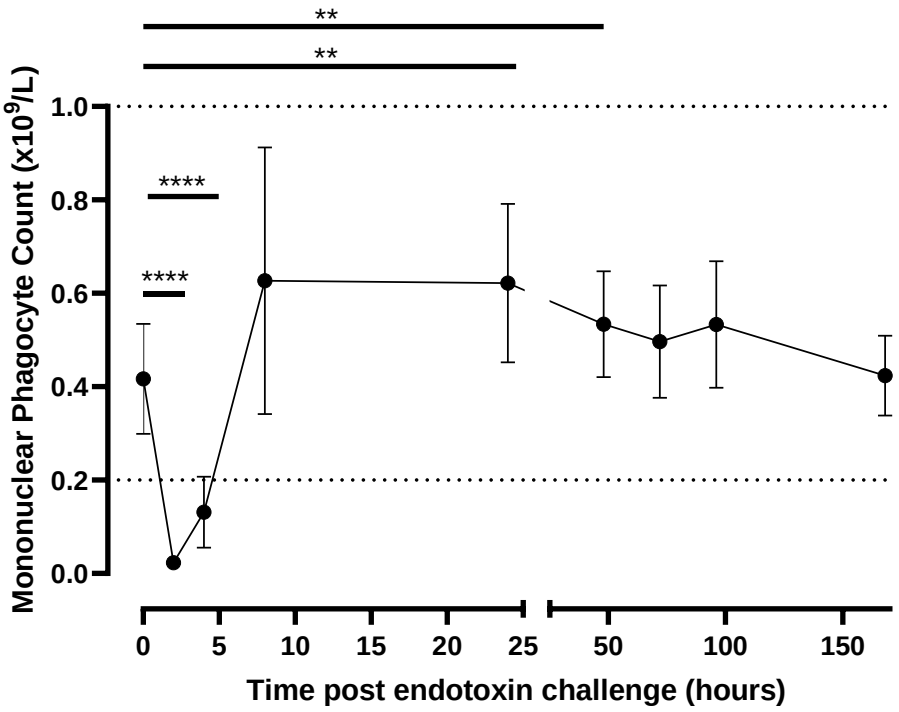

Figure 5.1 **Mononuclear phagocyte count during human endotoxin challenge**

Blood samples were collected at 0, 2, 4, 8, 24, 48, 72 hours and 7 days post endotoxin challenge. Mononuclear phagocyte count was enumerated by The Doctor's Laboratory. Dotted lines show the clinical reference range for a healthy count. Bars represent mean ± SD. Analysed by one-way ANOVA and Bonferroni multiple comparisons tests. n=10 individual volunteers.

At baseline, the total monocyte and DC count was at 0.42 (± 0.12) x10^9/L (**Figure 5.1**). However, 2 hours post endotoxin challenge, the circulating count temporarily fell to 0.02 (±0.01) x10^9/L, below the healthy clinical reference range of 0.2-1 x10^9/L. After 8 hours, the count returned within the reference range but remained significantly different from the baseline count until day 2 and by day 7 returned to the baseline count.

5.2.2 Monocyte and Dendritic Cell composition

Next, it was examined how monocyte and dendritic cells subsets vary during the course of inflammation. Using flow cytometry, monocytes and dendritic cell subsets were identified at each time point (**Figure 5.2**). At the time of performing these experiments, the newly described DC subsets were not known. pDC, cDC1 and cDC2 were identified using the original gating strategy.

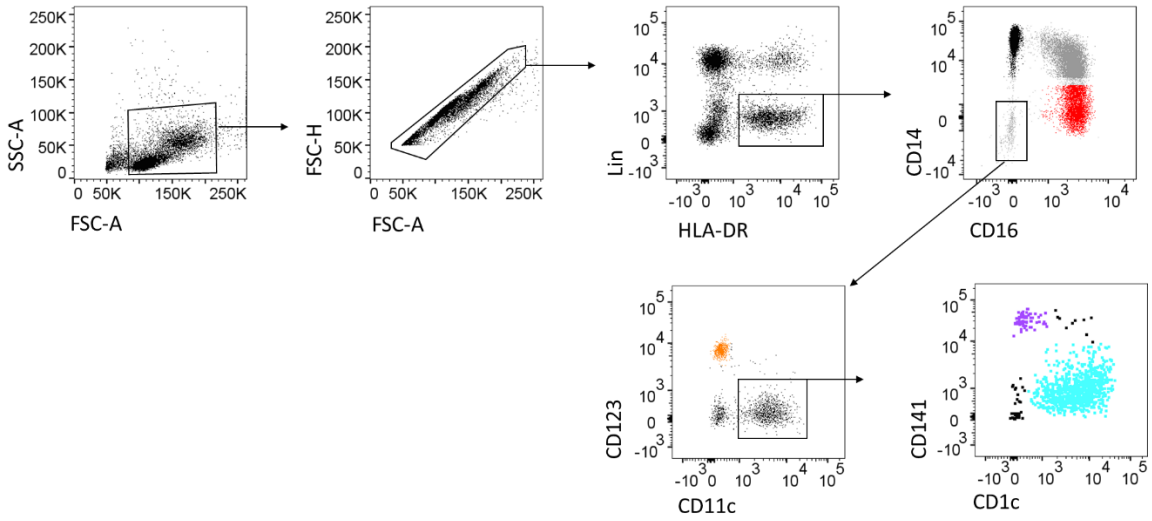

Figure 5.2 **Monocyte and dendritic cell gating strategy during endotoxin challenge**

PBMCs were stained for monocyte and dendritic cells and analysed by flow cytometry at each time point during experimental endotoxin challenge. Lin^- $HLA\text{-}DR^+$ population contains monocytes and dendritic cell subsets: classical monocytes (black), intermediate monocytes (grey), non-classical monocytes (red), pDC (orange), cDC1 (purple), cDC2 (blue). Representative of n=5 individual experiments at 24 hours post-endotoxin challenge where all subsets can be identified.

Changes in the composition of monocyte and dendritic cell subsets during endotoxin challenge were observed from the flow cytometry plots (**Figure 5.3**). All monocyte and DC subsets were identified at baseline. At 2 hours, almost a complete loss of the Lin^- $HLA\text{-}DR^+$ compartment was observed, only a scattering of cells was seen. In terms of monocytes, at 4 hours, only classical monocytes were detected (**Figure 5.3a**). By 24 hours, a bolus of intermediate monocytes was observed, this dense population of cells then appears to shift into the non-classical monocyte gate at 48 hours. By day 7, the monocyte profile resembles that seen at baseline both visually and in terms of composition. In the DC compartment, at 4 hours only pDC are seen and scattering of cDC2. By 8 hours all three DC subsets could be visually appreciated again.

a)

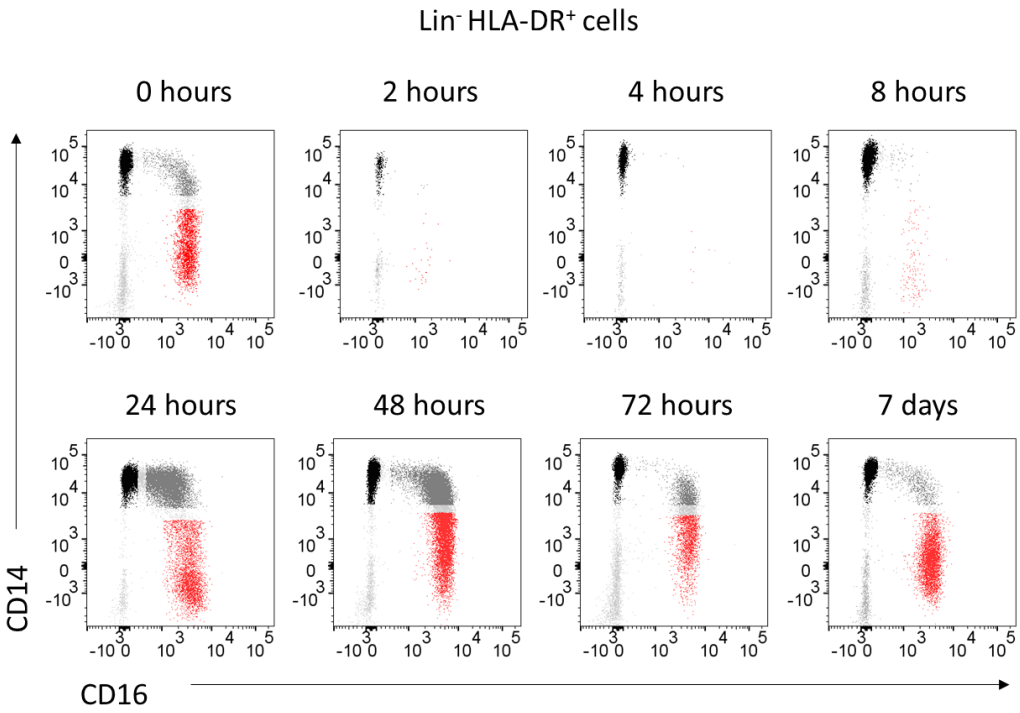
Lin- HLA-DR+ cells
0 hours
2 hours
4 hours
8 hours
24 hours
48 hours
72 hours
7 days
CD14
CD16

b)

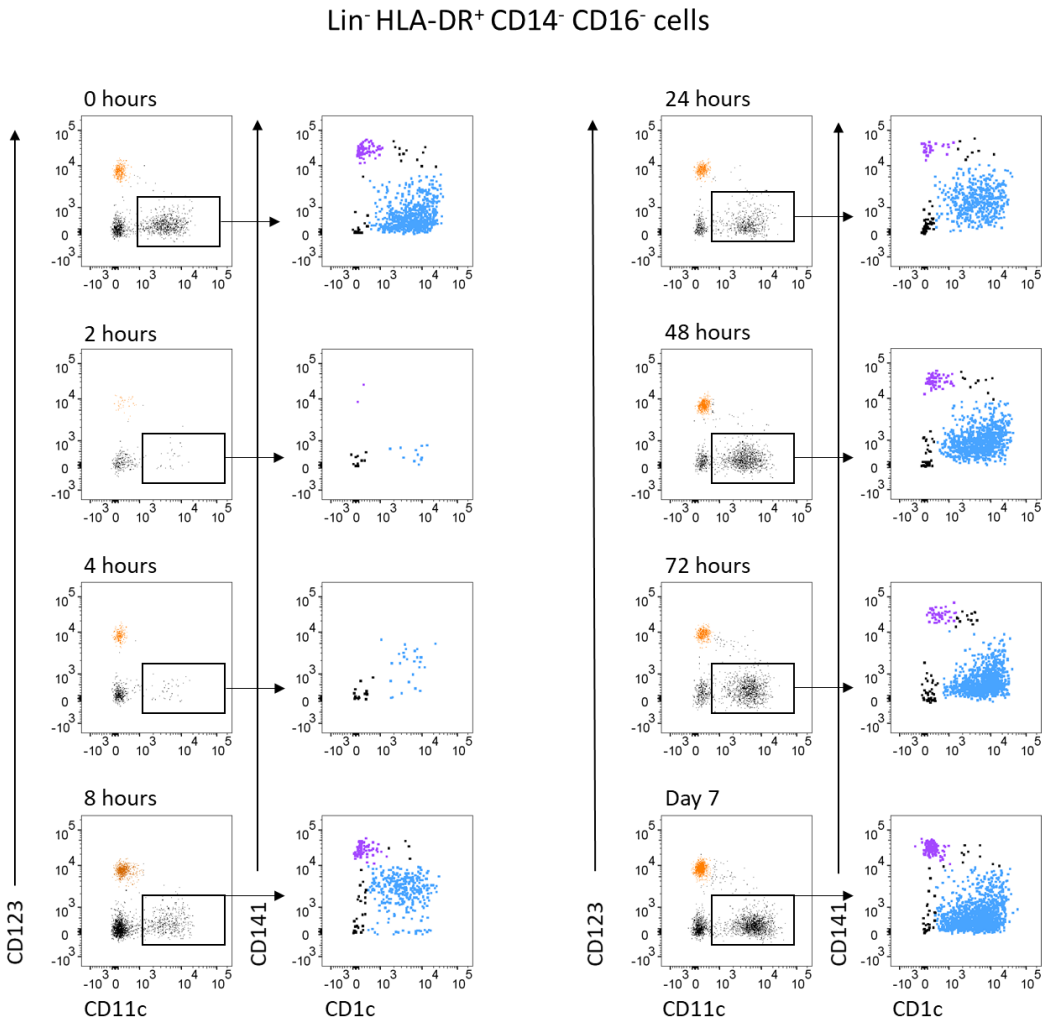
Lin- HLA-DR+ CD14- CD16- cells
0 hours
2 hours
4 hours
8 hours
24 hours
48 hours
72 hours
Day 7
CD123
CD141
CD11c
CD1c

Figure 5.3 **Monocyte and DC subset profile during human endotoxemia**

Blood samples were taken at 0, 2, 4, 8, 24, 48, 72 hours and 7 days post endotoxin challenge. Using flow cytometry, **a)** monocytes (top) and **b)** DC subsets (bottom) were identified within Lin^- $HLA\text{-}DR^+$ cells. Classical (black), intermediate (grey), non-classical (red) monocytes, pDC (orange), cDC1 (purple) and cDC2 (blue) were identified at each time point. Representative of n=5 individual volunteers.

These dynamic changes were enumerated by calculating the percentage of each subset as a total of mononuclear phagocytes (**Figure 5.4**). This total can be regarded as Lin^- $HLA\text{-}DR^+$ population without the $CD14^-$ $CD16^-$ $CD123^-$ $CD11c^-$ population. As expected, classical monocytes were the dominant phagocytes in this compartment at baseline, making up 81.5 (± 5.3) % of mononuclear phagocytes. At 2 hours, of the few cells present, classical monocytes were the predominant mononuclear phagocyte. At 8 hours, classical monocytes constituted almost the whole compartment (97.0 ± 2.1 %) (**Figure 5.4**), despite the reappearance of DC subsets at this point by flow cytometry (**Figure 5.3b**). Interestingly, the percentage of intermediate monocytes expanded from 1.1 (± 1.8) % at 8 hours to 33.6 (± 8.4) % at 24 hours and decreased steadily before returning to a baseline composition of 3.1 (± 2.3) % by day 7. cDC on the other hand were observed to have a slower reconstitution in comparison (**Figure 5.4b**). Non-classical monocytes nor cDC were observed to expand to a percentage higher than baseline at any time.

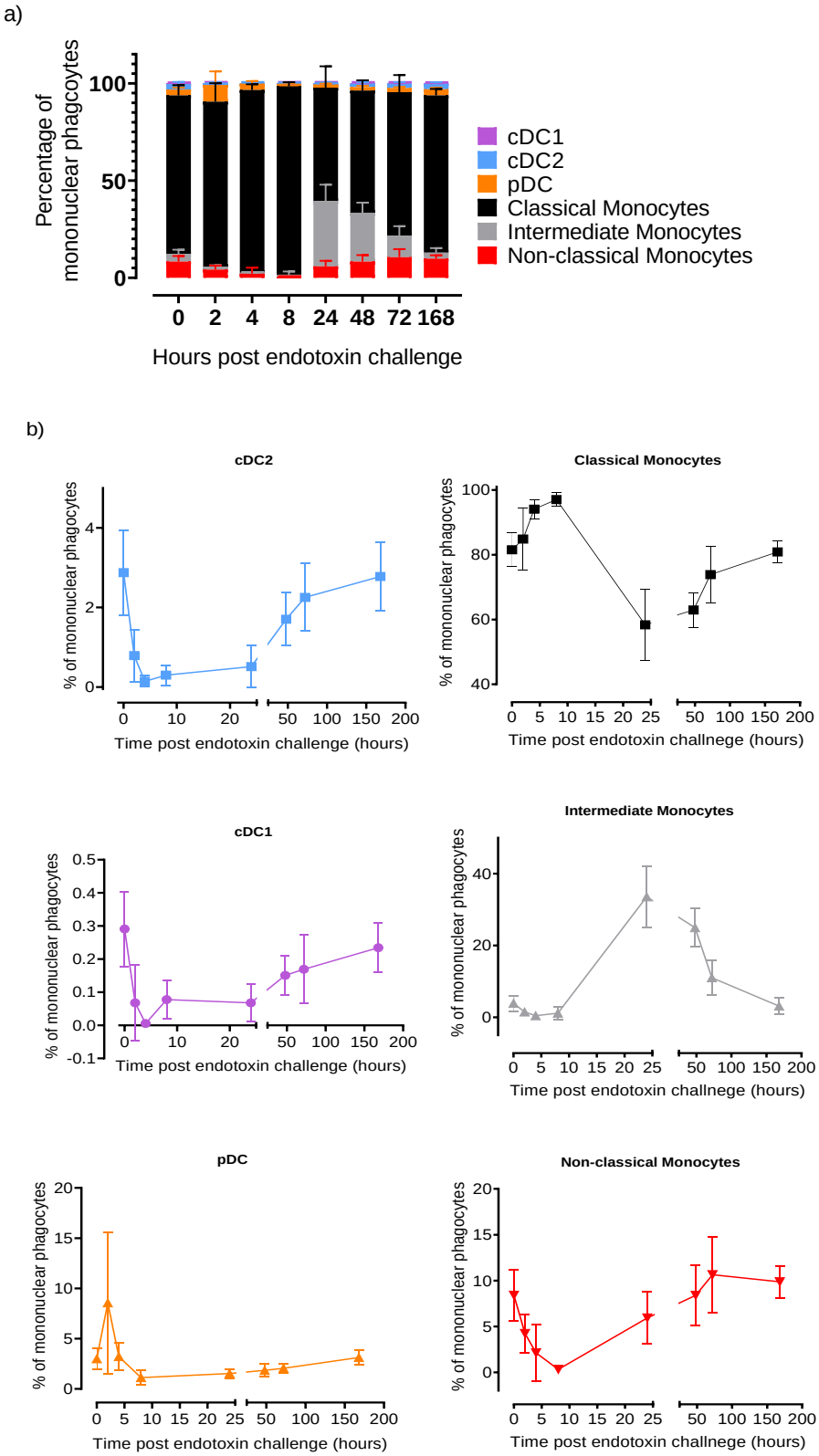

Figure 5.4 **Proportion of monocyte and DC subsets during human endotoxemia**

The percentage of monocyte and DC subsets during human endotoxemia was enumerated at each time point. cDC1: blue, cDC2: purple, pDC: orange, classical monocytes: black, intermediate monocytes: grey, non-classical monocytes: red. Bars represent mean ± SD. n=5 individual experiments.

The percentage composition of mononuclear phagocyte subset can be misleading as the absolute count of the compartment was not constant at each time point, therefore the absolute count for each subset was calculated.

To calculate the absolute count of monocyte and DC subsets, the total mononuclear phagocyte count (**Figure 5.1**) was multiplied by the percentage of each subset in this population (**Figure 5.4**) at each time point.

As expected, 2 hours post-endotoxin challenge a decline was observed in all monocyte and DC subsets (**Figure 5.5**). At 8 hours, a sharp increase was observed in classical monocytes which were followed by a rise in intermediate and non-classical monocytes at 24 hours. Monocytes numbers then steadily return to baseline numbers by day 7. On the other hand, DC subsets had a slow reconstitution and steadily reached homeostatic numbers. cDC2, in particular, did not reach baseline numbers until approximately day 3 post endotoxin.

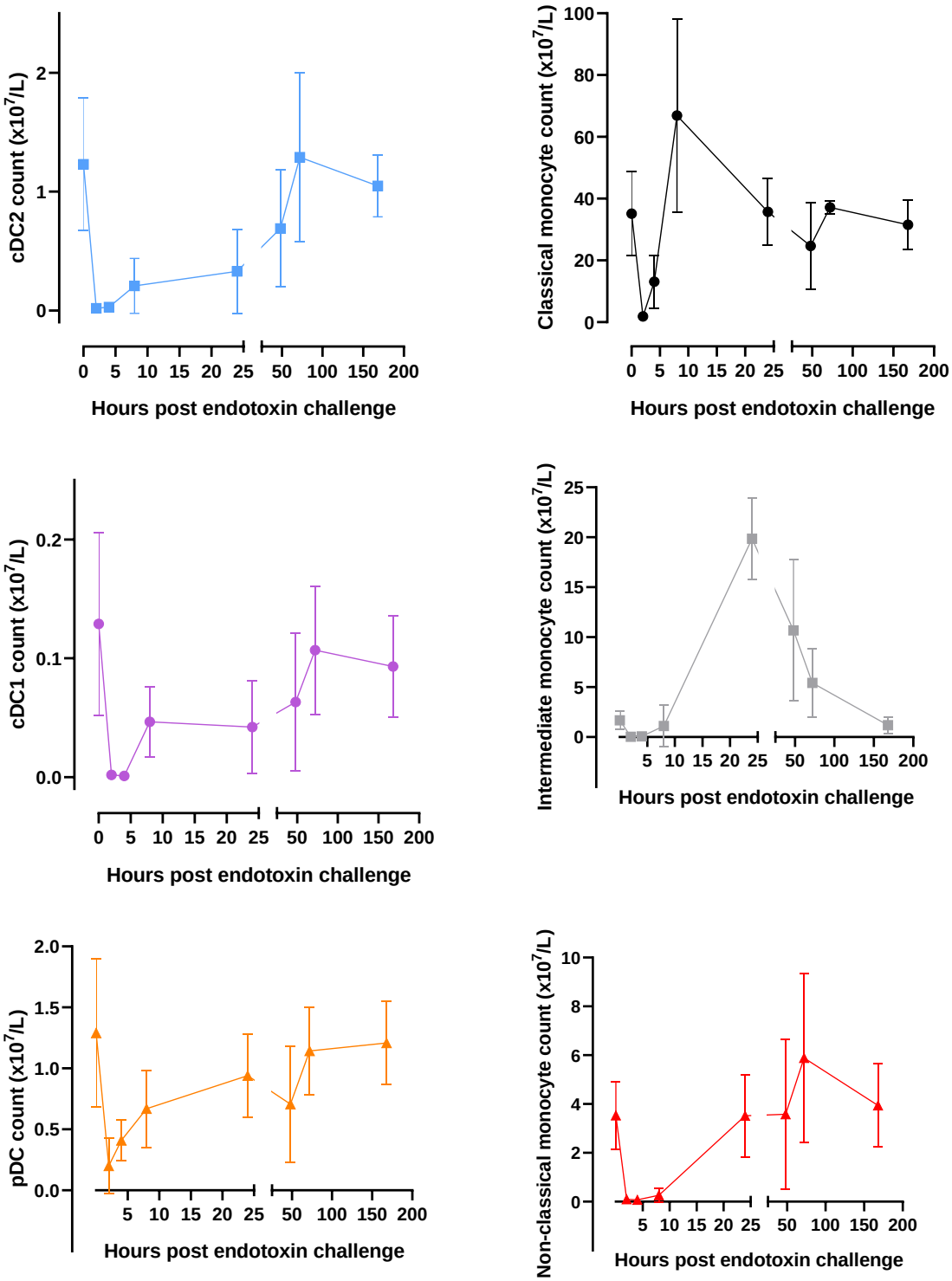

Figure 5.5 **Absolute monocyte subset count during human endotoxemia**

Absolute count of monocyte subsets during human endotoxemia was enumerated by multiplying the percentage of each subset calculated from flow cytometry by the corresponding mononuclear phagocyte count obtained from The Doctor's Laboratory at each time point. Bars represent mean ± SD. n=5 individual experiments.

5.2.3 Origin of monocytes following temporary monocytopenia

From these data, several questions arise. Unfortunately, it was not feasible to examine the fate/destination of the cells at 2 hours in humans. However, from the flow cytometry analysis, monocytes appeared to reconstitute in a sequential fashion, similar to what was observed under steady physiological conditions (**Figure 4.3**). It was questioned whether the monocytes that return after temporary monocytopenia (**Figure 5.5**) are returning from a marginating pool or are the result of released cells from the bone marrow. To investigate this, deuterated glucose was administered 20 hours prior to endotoxin challenge. The reason being, during steady-state, no labelling was detected in circulating monocyte subsets 28 hours post labelling (**Figure 4.3**). It is expected that labelled classical monocytes reside within the bone marrow at this time point. Therefore, if deuterium was given 20 hours prior to endotoxin challenge, if the classical monocytes observed at 8 hours post-challenge (28 hours post labelling) were labelled, this would suggest bone marrow egression contributes to the repopulation of monocytes following systemic inflammation.

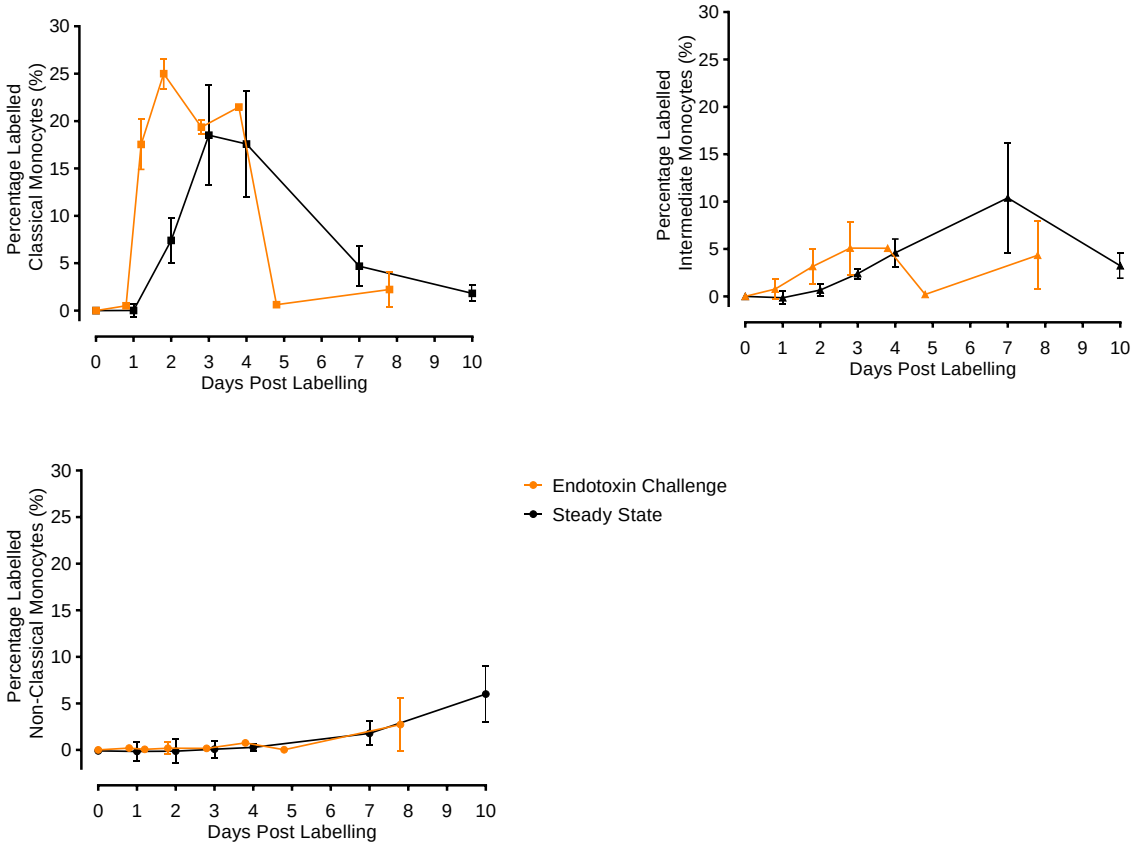

Figure 5.6 **Deuterium labelled monocytes during human endotoxemia**

Volunteers were administered 20g of deuterated glucose prior to 2ng/kg I.V. endotoxin challenge. Monocyte subsets were isolated by FACS at 8, 24, 48, 72, 96 hours and 7 days post endotoxin challenge and analysed for deuterium enrichment by GC/MS. Steady-state data is shown in black and endotoxin challenge is shown in orange. Bars represent mean ± SD. Endotoxin data n=3 individual experiments, steady-state data n=4 individual experiments.

After administering deuterated glucose to volunteers, 20 hours later, 2ng/kg endotoxin was administered. 8 hours post endotoxin classical monocytes makeup 97.0 ± 2.1 % of the mononuclear phagocytes compartment and are found at appreciable numbers for FACS (**Figure 5.3 and Figure 5.5**). At this time point, deuterium was detected in classical monocytes (**Figure 5.6**). At 24 hours post endotoxin, an expansion was observed in intermediate monocytes, however, there was very little difference in labelling in this subset compared to steady-state point (**Figure 5.6**). Non-classical monocytes were also detected 24 hours post endotoxin, however, no labelling was observed at this timepoint. This kinetic profile of this subset mirrored

that seen during steady-state. In addition, the label in classical monocytes was present for 4 days whereas under steady-state it was detected for at least 7 days, which suggests a rapid clearance of these bone marrow released classical monocytes from the circulation following challenge.

5.2.4 Phenotype of reappearing monocytes

In addition to examining the kinetics and potential source of the repopulating monocyte subsets following endotoxin challenge, it was questioned how the phenotype of these cells change in comparison to baseline. CCR2, CX_3CR1, HLA-DR, and CD11b were differentially expressed between monocyte subsets at baseline and were measured at each time point during endotoxin challenge (**Figure 5.7**). Marker expression was measured at all time points despite the reduced number of monocytes at 2 and 4 hours post endotoxin.

Following endotoxin challenge, there was a trend for marker expression change in CCR2 (classical and intermediate monocytes), CX_3CR1 (all subsets), HLA-DR (intermediate and non-classical) and CD11b (classical and intermediate) (**Figure 5.7**). Initially, decreased expression was observed for CCR2, CX_3CR1 and HLA-DR, however, CD11b expression was increased following endotoxin challenge.

Classical and intermediate monocytes exhibited similar levels of CCR2 expression at 8 hours post endotoxin challenge. Similarly, at 24 hours, intermediate and non-classical monocytes demonstrated similar levels of HLA-DR expression. By day 7, expression of the measured markers returned to that seen at baseline.

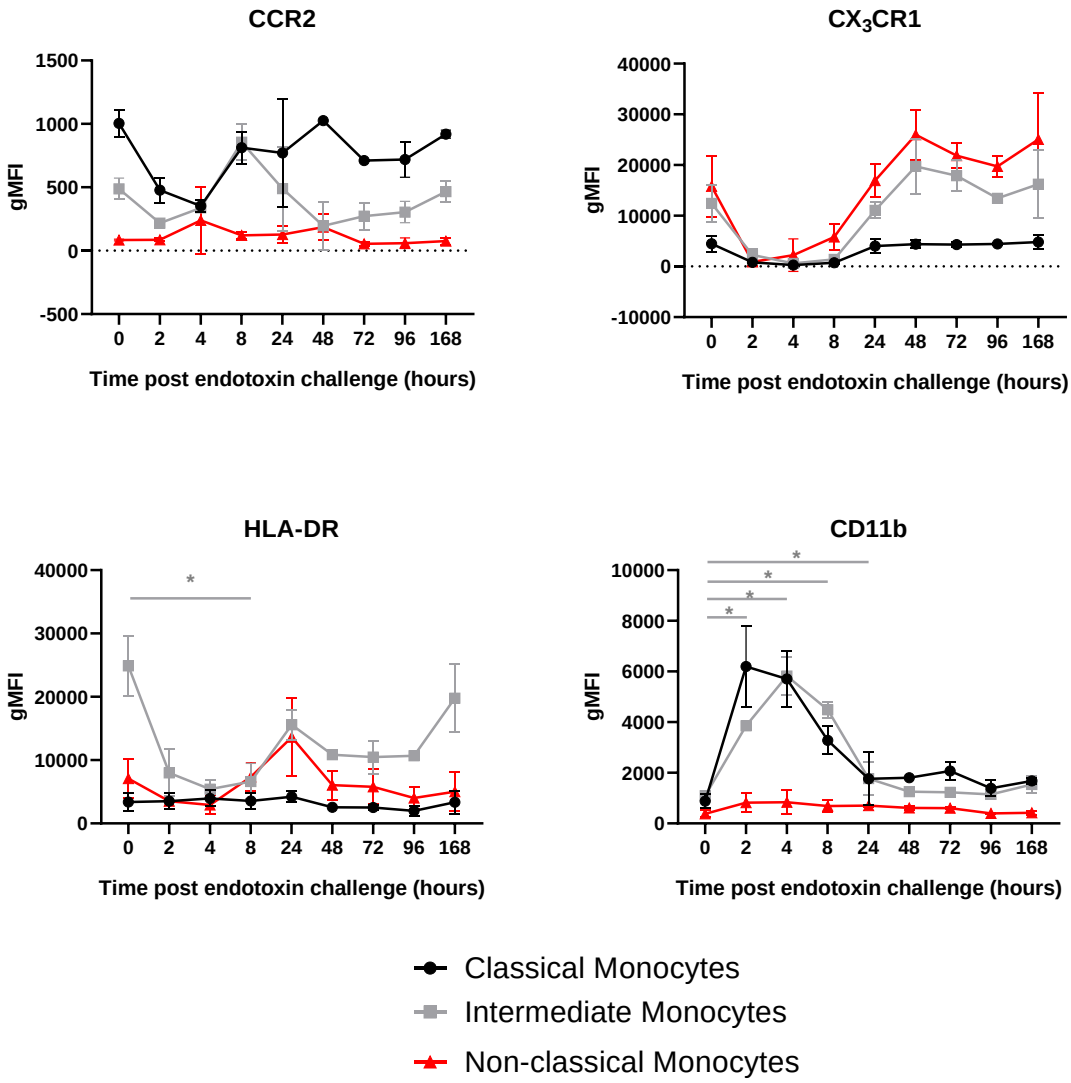

Figure 5.7 **Surface membrane expression on monocytes during endotoxin challenge**

Monocyte subsets were identified at 0, 2, 4, 8, 24, 48, 72 hours and 7 days post endotoxin challenge by flow cytometry. CCR2, CX_3CR1, HLA-DR and CD11b expression was measured on classical (black), intermediate (grey) and non-classical (red) monocytes and reported as gMFI. * $p < 0.05$, bars represent mean ± SD. n=4 individual experiments.

5.3 Acute Local Inflammation Model

Section 5.2 described the effects of systemic inflammation on the circulating kinetics of monocyte and DC subsets. In addition to systemic manifestations, inflammation can also be present at local sites. The kinetic recruitment profile of mononuclear phagocytes was examined following local tissue inflammation using a UV-killed *E. coli* blister model, which has been demonstrated to model the pro-inflammatory and resolution phases of inflammation (Motwani *et al.,* 2016).

5.3.1 Doppler Imaging

Male volunteers were intradermally injected into the forearm with 1.5 x 10^7 UV-killed *E. coli.* Prior to raising suction blisters to analyse the cellular infiltrate, doppler imaging was implemented to measure blood flow at baseline, 4, 6, 24, 48 and 96 hours at the challenged site (**Figure 5.8**). An increase in blood was observed as early as 4 hours. At 6 hours, blood flow was the highest at the site of injection and was also observed in the surrounding tissue. By 48 hours, blood flow appeared to subside and returned to baseline by 96 hours.

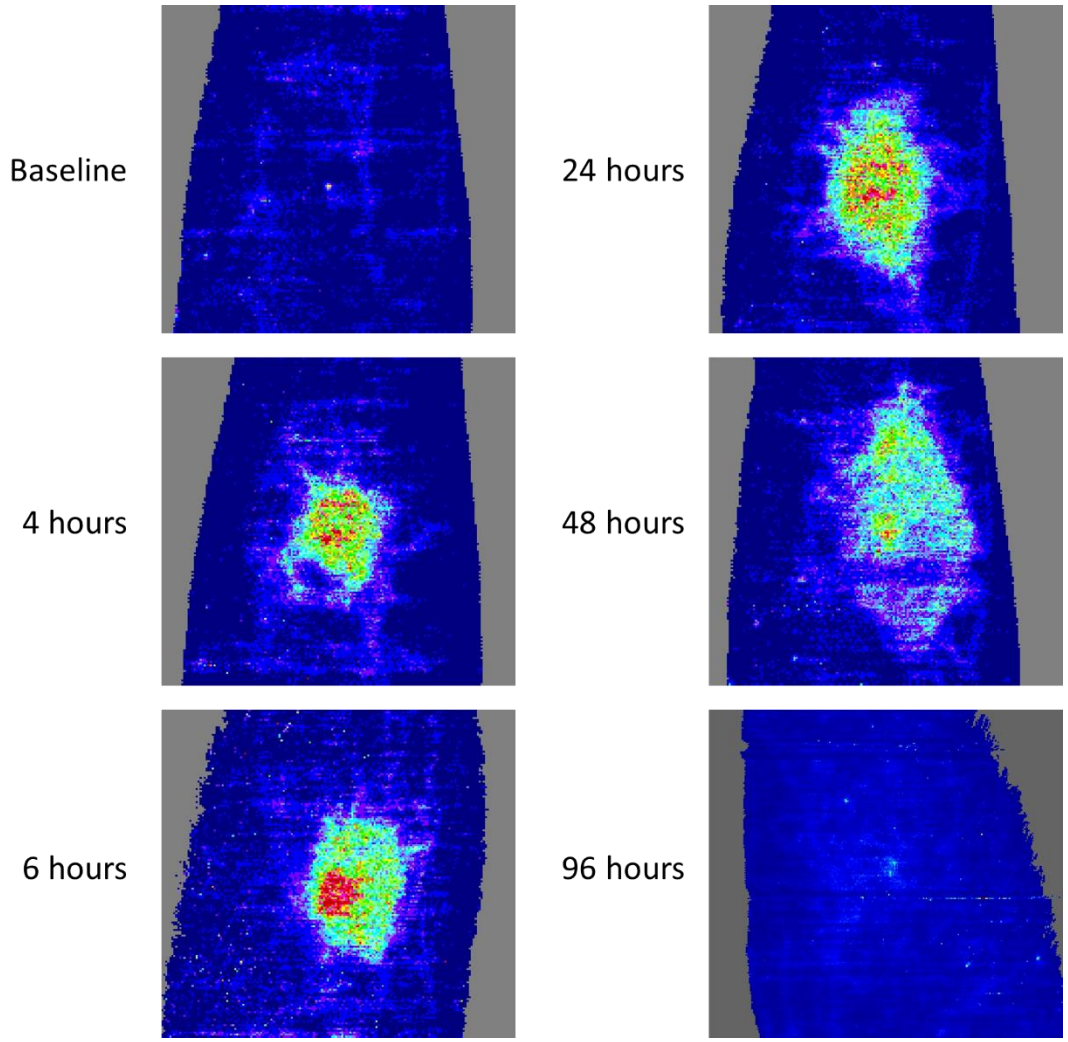

Figure 5.8 **Vascular response following intradermal challenge with UV-killed *E. coli***

Laser doppler imaging was used to visualise the vascular response at baseline, 4, 6, 24, 48 and 96 hours post intradermal challenge with UV-killed *E. coli*. Representative of n=4 at each time point.

5.3.2 Monocyte kinetics and phenotype

5.3.2.1 Monocyte kinetics in local inflammation

Suction blisters were raised at 6, 24, 48 or 96 hours post-challenge. Monocytes were identified as Lin^- $HLA\text{-}DR^+$ cells at each time point in both blood and blister (**Figure 5.9**). The percentage make-up of classical, intermediate and non-classical monocyte subsets at each time point was obtained by flow cytometry (**Figure 5.9**). At 4 hours, classical monocytes were the dominant subset, whereas between 24 and 48 hours, intermediate monocytes made up the majority of blister monocytes. A small scattering of $CD14^{lo/-}$ $CD16^+$ monocytes were sometimes observed

which did not form a discrete population and were disconnected from the 'monocyte waterfall'. Nevertheless, as these cells were Lin$^-$ HLA-DR$^+$ CD14$^{lo/-}$ CD16$^+$, they were analysed as non-classical monocytes.

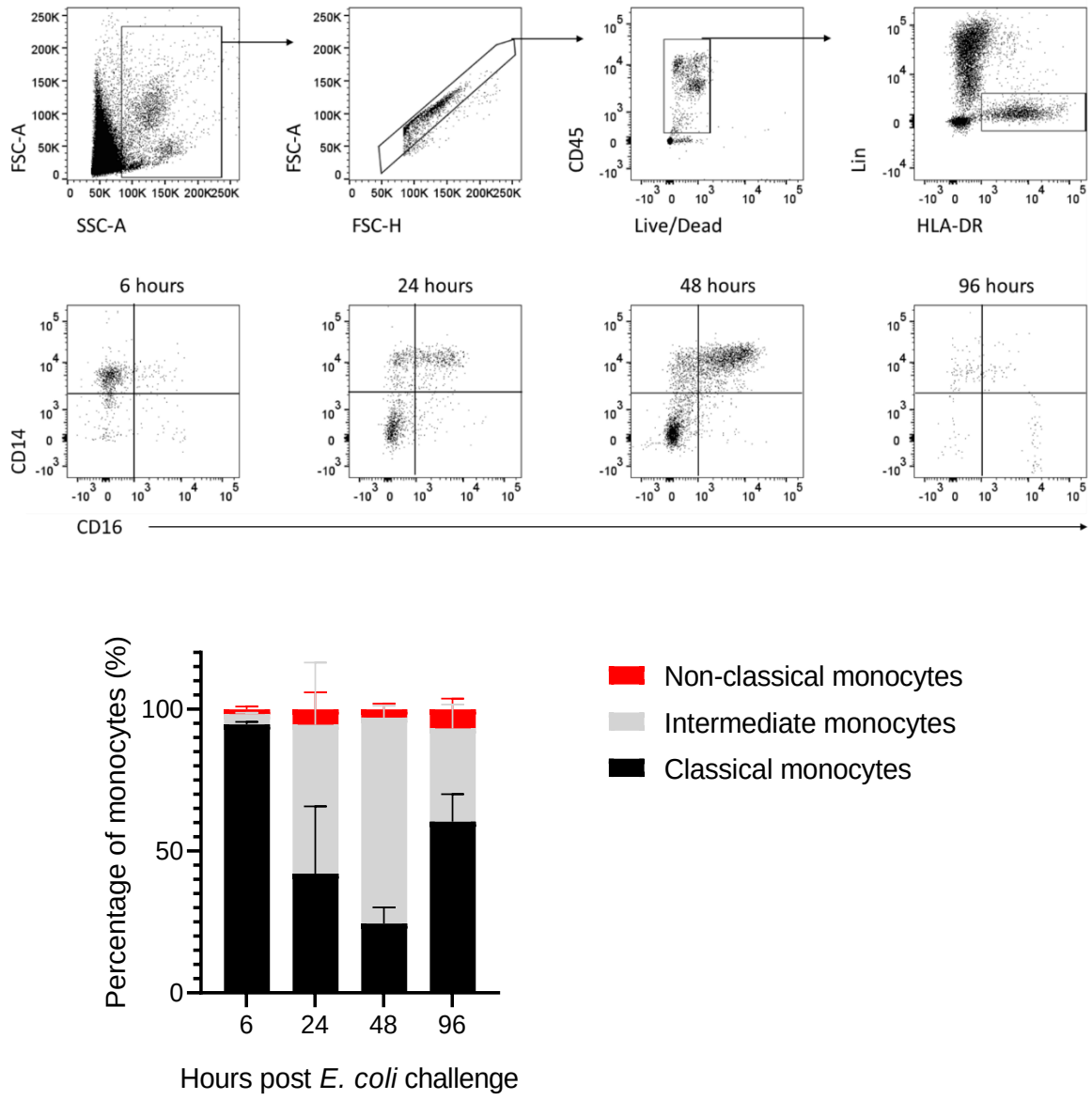

Figure 5.9 **Monocyte Profile during intradermal challenge with UV-killed *E. coli***

Blister cells were analysed by flow cytometry at 6, 24 and 48 hours post challenge. Monocytes were identified as single, Lin$^-$ HLA-DR$^+$ cells. Representative CD14 and CD16 profiles are shown at each time point. The percentage of monocyte subsets of the total monocyte pool was calculated at each time. n=4 individual experiments at each time point.

At the site of inflammation, the absolute count of monocytes was enumerated. Counting beads were not used at the time of performing these experiments, however, as the total sample was run through flow cytometry the total events recorded were regarded as an approximate value for the total cell count. It was later examined when studying DC in the blister (Section 5.3.3), that when running a known number of counting beads, on average 75% of the beads are recorded (Appendix, Section 5.4). Although crude, the monocyte counts here can be regarded as approximately 75% of their true cell count.

Monocytes counts were reported as count/blister (**Figure 5.10a**), however as not all blisters are formed uniformly, counts were adjusted per ml of blister fluid (**Figure 5.10b**). Whilst classical and intermediate monocytes abundantly populated the inflammatory site, very few non-classical monocytes were present at the measured time points. Classical monocytes dominated the early hours of inflammation, but an intermediate monocyte phenotype was observed by 48 hours. By day 4, very few monocytes remained at the site of inflammation.

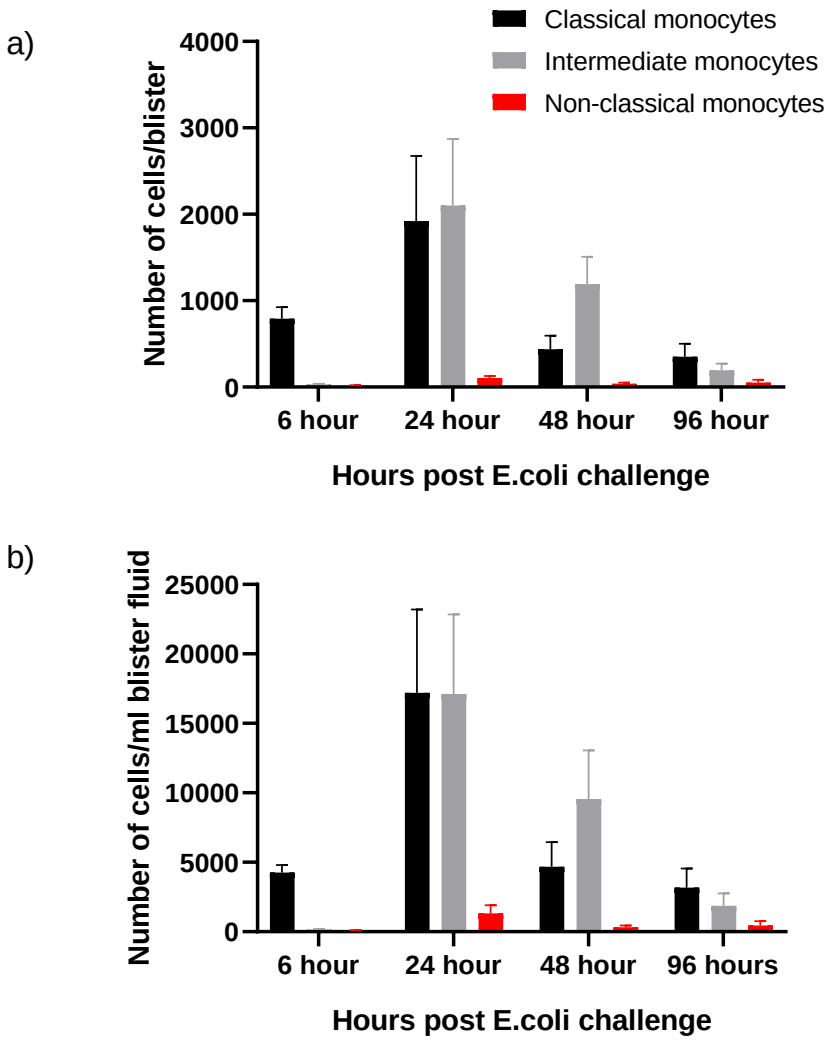

Figure 5.10 **Absolute monocyte count following UV-killed *E. coli* challenge**

Monocyte subsets were enumerated at blister site following intradermal challenge with UV-killed *E. coli*. After running the total sample by flow cytometry, the total event number for each population was taken as the absolute count. The absolute count is shown **a)** per blister and **b)** corrected per ml blister fluid. Bars represent mean ± SD. n=4 individuals at each time point.

In addition to enumerating the number of monocytes at the blister site, blood counts were also obtained at each time point (**Figure 5.11**). At 6 hours, a non-significant increase in the number of blood classical and intermediate monocytes was observed which returned to a baseline by 24 hours, indicative of systemic effects in this model.

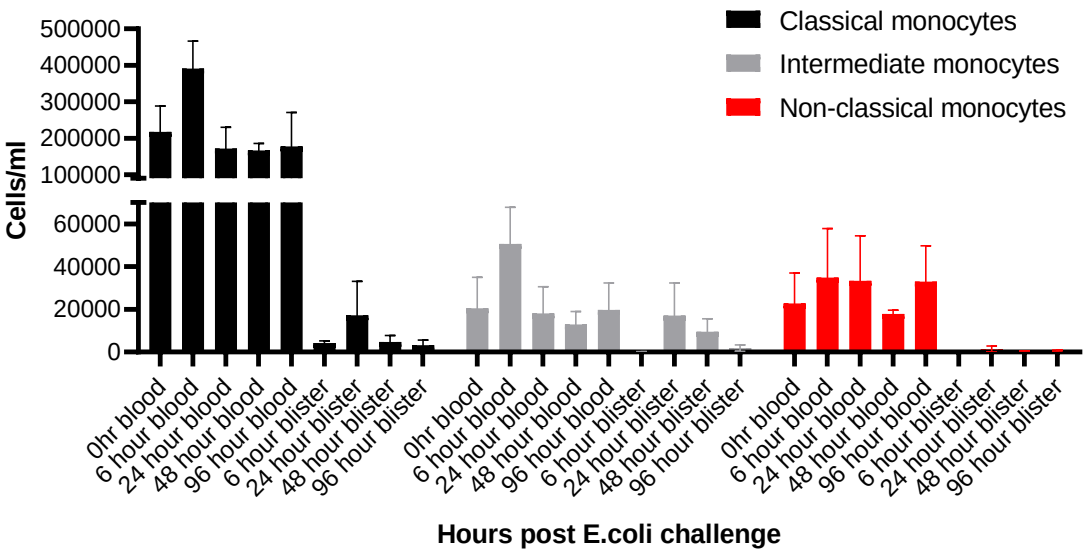

Figure 5.11 **Systemic monocyte count following intradermal challenge**

Monocytes subsets were enumerated by flow cytometry at baseline, 6, 24, 48 and 96 hours following intradermal challenge with UV-killed *E. coli* in the blood (cells/ml blood) and blister (cells/ml blister fluid). Bars represent mean ± SD. n=4 individual experiments.

5.3.2.2 Monocyte phenotype in local inflammation

Classical and intermediate monocytes were observed in the blister at 24 and 48 hours post-challenge (**Figure 5.9**). While these subsets are known to exhibit differences in surface membrane marker expression in blood, it was examined whether these differences are also mirrored in the blister.

CCR2 and CX_3CR1 were measured on classical and intermediate monocytes in both the blood and blister (**Figure 5.12**). As expected, CCR2 expression was significantly higher on blood classical monocytes in comparison to intermediate monocytes, whereas CX_3CR1 expression was higher on intermediate monocytes (**Figure 5.12**). However, the difference in expression profile was not mirrored between these infiltrating subsets in the blister. Rather, classical and intermediate monocyte blister cells had an equivalent expression of CX_3CR1 and CCR2 at the measured time points. At 48 hours, there was a trend for an increase in CCR2 and CX_3CR1 expression in both subsets.

Compared to blood counterparts, blister intermediate monocytes expressed higher levels of CCR2 and lower levels of CX_3CR1 at 24 hours. These data suggest, that blister intermediate monocytes are more alike to blister classical monocytes than blood intermediate monocytes.

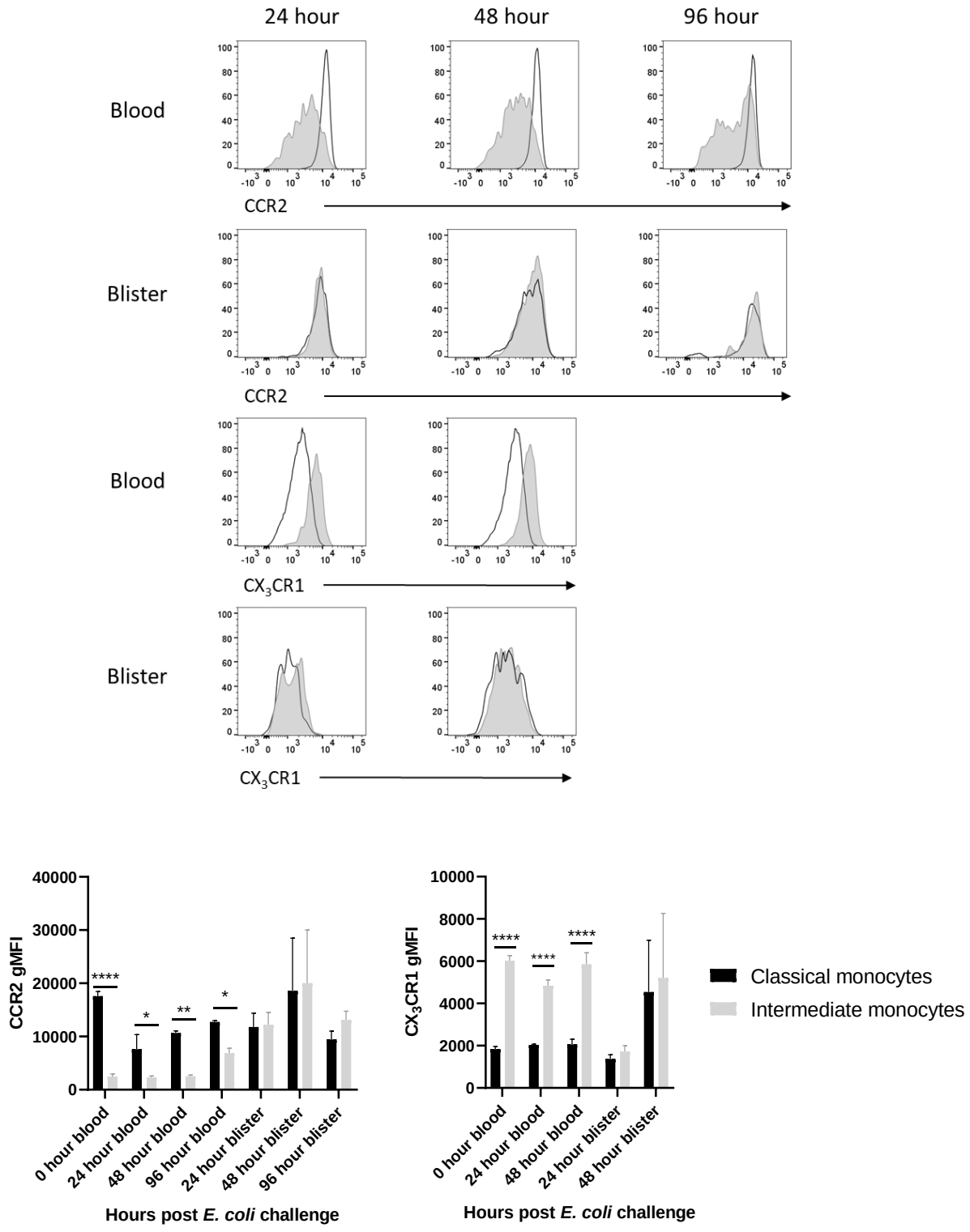

Figure 5.12 **CCR2 and CX_3CR1 blister monocyte expression**

Classical and intermediate monocytes were identified by flow cytometry 24 and 48 hours post intradermal *E. coli* challenge. CCR2 and CX_3CR1 expression were measured on classical (black) and intermediate (grey) subsets in both blood and blister at both time points. Analysed by one-way ANOVA and Bonferroni multiple comparison test. Bars represent mean ± SD. n=4 individual experiments.

5.3.3 Dendritic Cell kinetics in local inflammation

In addition to examining the kinetic profile of monocyte subsets in local inflammation, it was also observed that dendritic cells are recruited as $CD14^-$ $CD16^-$ cells (**Figure 5.9**). Next, it was investigated how local inflammation influences the recruitment of dendritic cell subsets.

Following a similar protocol as described above for examining monocytes subsets, pDC, pre-DC, cDC1, AXL^- and AXL^+ cDC2 were identified at 6, 24, 48 and 96 hours post inflammation by flow cytometry in both blood and blister (**Figure 5.13**).

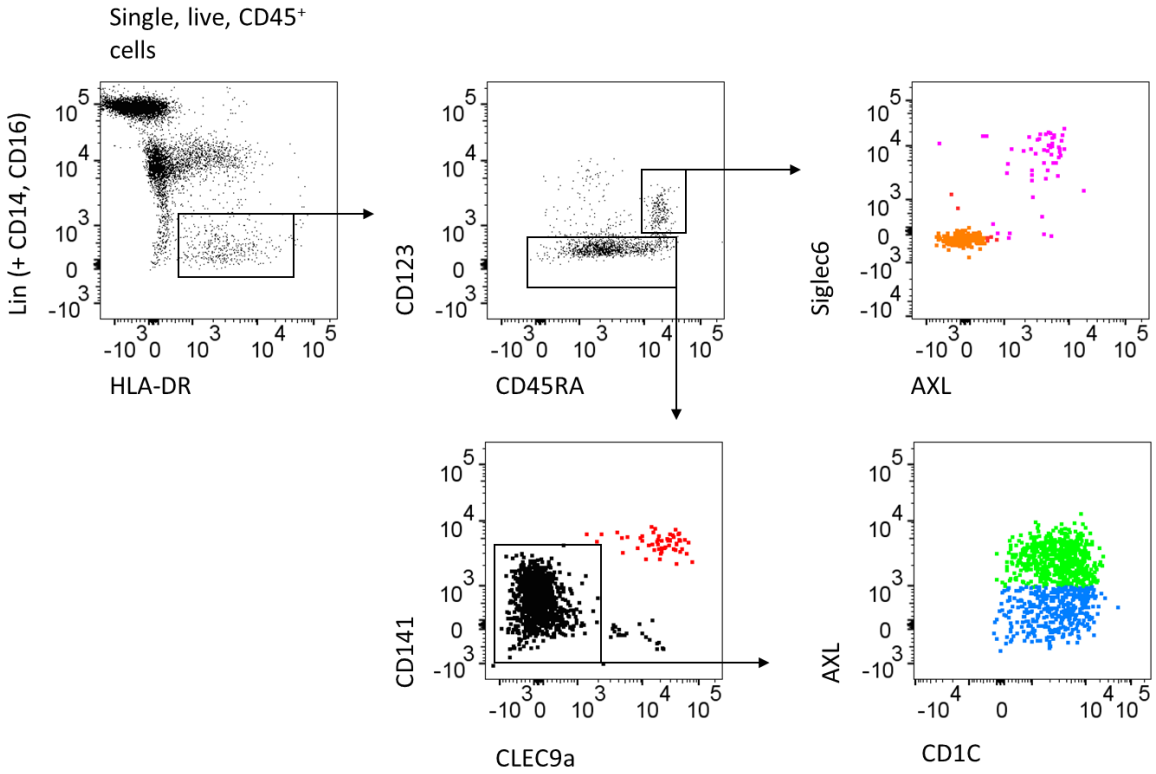

Figure 5.13 **Dendritic cell profile during intradermal challenge with UV-killed *E. coli***

Following intradermal challenge with UV-killed *E. coli*, blister cells were analysed by flow cytometry at 6, 24, 48 and 96 hours post-challenge. Dendritic cells were identified as Lin^-, $CD14^-$, $CD16^-$ cells. pDC (orange), pre-DC (purple), cDC1 (red), AXL^+ cDC2 (green), AXL^- cDC2 (blue) were identified. Representative of n=4 individuals at 24 hours post-challenge.

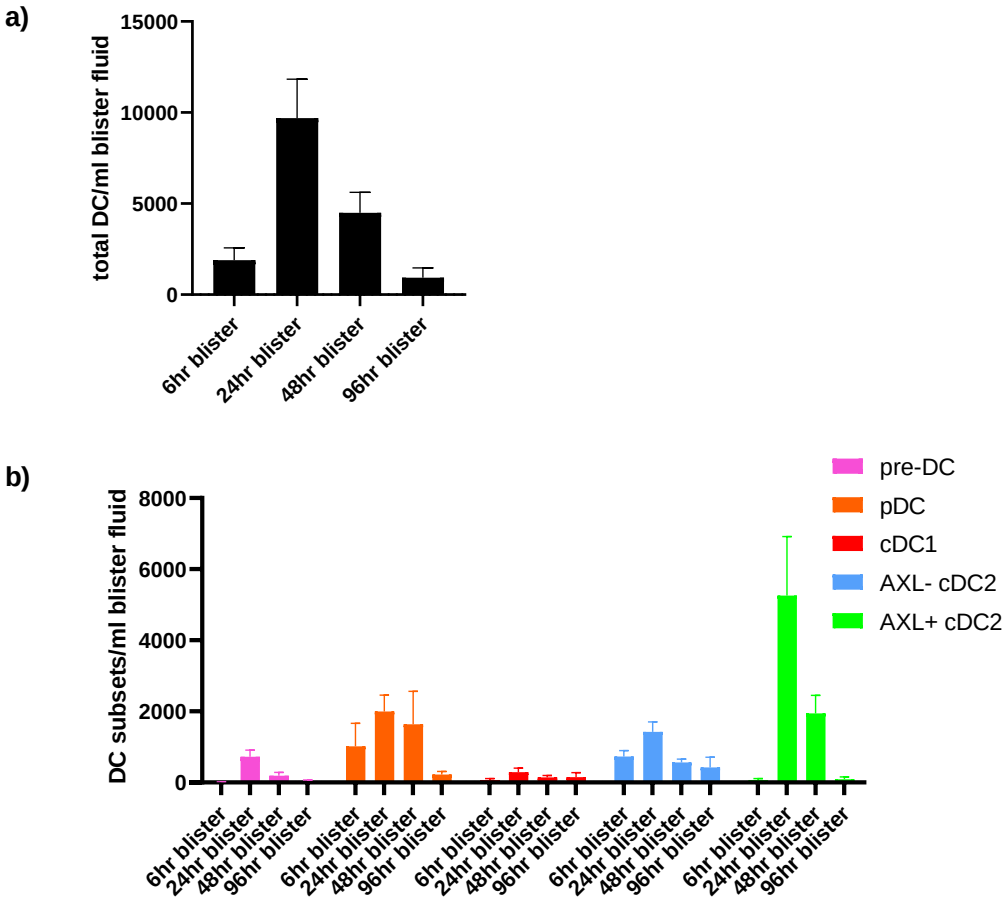

Figure 5.14 **Absolute count of blister DC subsets following intradermal challenge**

Total DC and individual DC subsets were enumerated at 6, 24, 48 and 96 hours post intradermal challenge with UV-killed *E. coli*. **a)** Total DC and **b)** individual subsets were enumerated by flow cytometry at each time point and adjusted per ml of blister fluid. Bars represent mean ± SD. n=4 individuals at each time point.

DC subsets were enumerated in the blister using counting beads. At 6 hours, very few DC were observed (**Figure 5.14a**) which consisted of mainly pDC and AXL^- cDC2 (**Figure 5.14b**). DC were most abundant at 24 hours following insult compared to the other time points examined and declined thereafter. Relative to one another, AXL^+ cDC2 subsets appeared to be the most abundant at 24 hours, followed by pDC, AXL^- cDC2, pre-DC then cDC1 (**Figure 5.14b**).

In addition to blister counts, blood counts were also examined and graphed individually for each subset. In this way, blister DC counts could be observed relative to their blood DC counts on an appropriate scale (**Figure 5.15**). Blood counts for DC subsets remained relatively stable

throughout, although a systemic effect may occur within the pDC subset at 24 hours as reduced numbers were observed compared to baseline.

Whilst **Figure 5.14** suggested an appreciable number of pDC and AXL^- cDC2 in the blister, these cells were found at a lower concentration than they are found in blood at all time points (**Figure 5.15a**). However, pre-DC and AXL^+ cDC2 were found at higher concentrations at 24 and 48 hours relative to the blood compartment. At 24 hours, there was approximately a 2-fold increase in the concentration of pre-DC in the blister, whereas AXL^+ cDC2 were found at almost a 10-fold increase (**Figure 5.15b**).

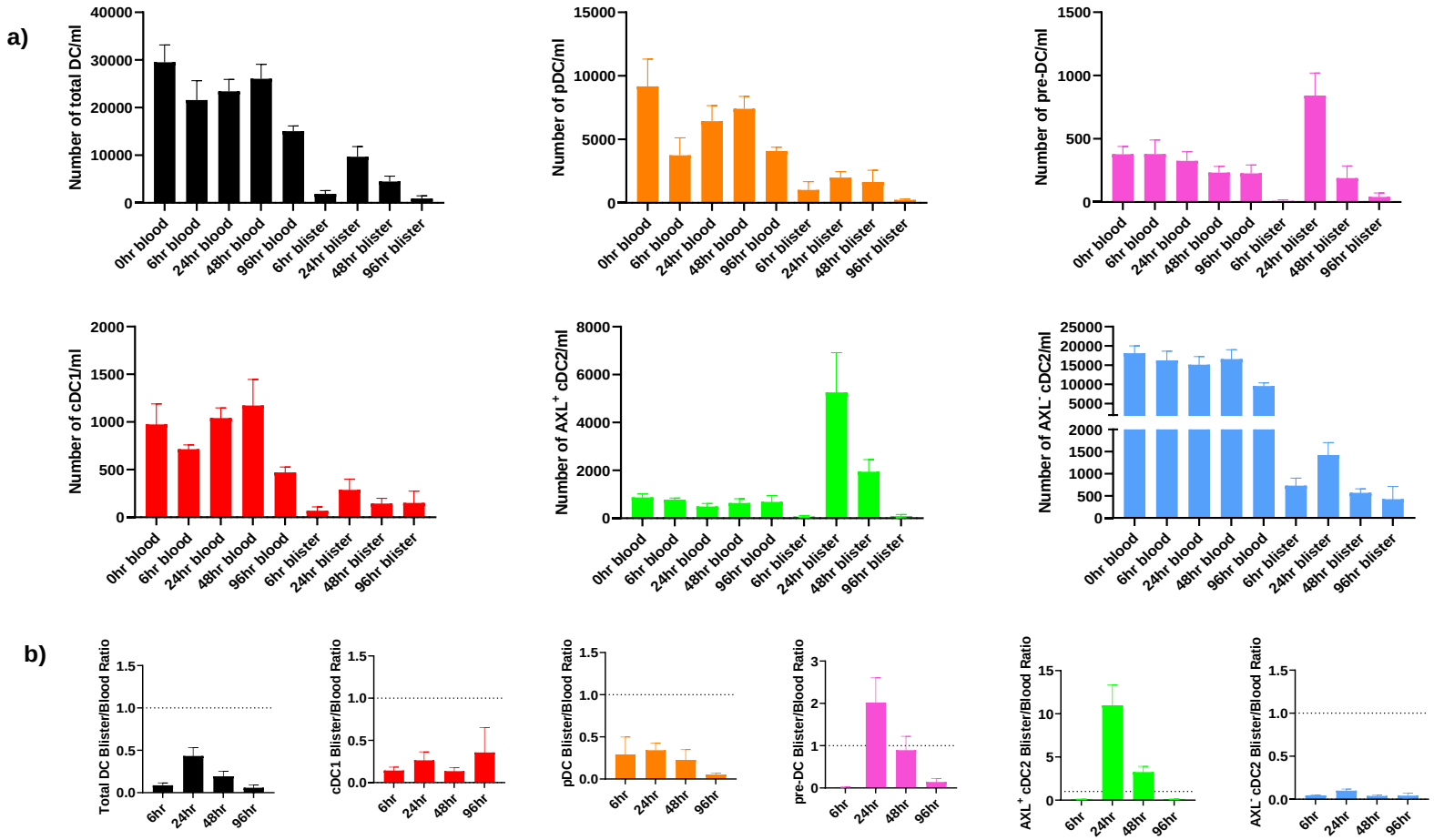

Figure 5.15 **Relative change of blister and blood DC following intradermal challenge**

Concentration of blister and blood DC subset at baseline, 6, 24, 48 and 96 hours post-challenge. **a)** the concentration of DC subsets per ml of blood or per ml blister fluid and the **b)** relative fold change between the concentration in two compartments was calculated. Bars represent mean ± SD. n=4 individuals at each time point.

The high concentration of pre-DC and AXL$^+$ cDC2 may have resulted from selective recruitment of these subsets from the blood or proliferation at the site following initial recruitment. In addition to surface staining, intracellular staining for Ki67 expression was performed at 24 hours. In the blister, Ki67 was observed to be highly expressed in blister pre-DC and AXL$^+$ and AXL$^-$ cDC2 subsets compared to pDC and cDC1 (**Figure 5.16**). In addition, while pDC, cDC1, pre-DC expressed similar levels to their blood counterparts, only cDC2 appeared to upregulate Ki67 after entering the tissue. These data might suggest pre-DC and cDC2 subsets undergo proliferation once at the site of inflammation leading to an increase in their abundance.

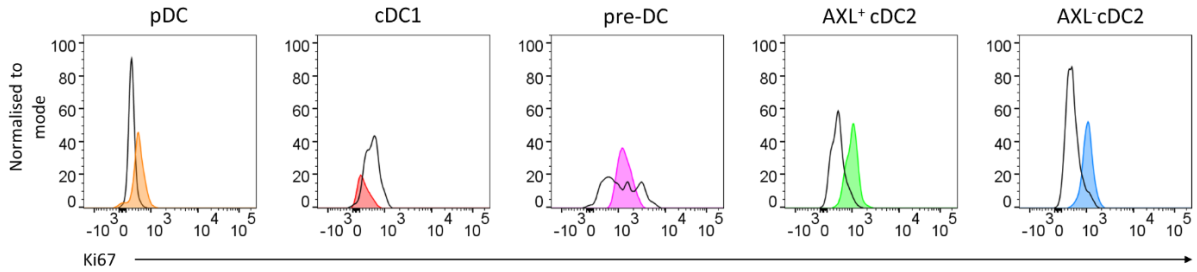

Figure 5.16 **Ki67 expression in DC subsets following intradermal challenge**

Ki67 expression was examined within each DC subset 24 hours following intradermal challenge with UV-killed *E. coli*. Black open histogram represents blood expression and filled histograms represent blister expression. Representative of n=2 individual experiments.

5.3.4 CX_3CR1 expression on pre-DC

In Chapter 3, it was demonstrated pre-DC consist of a CX_3CR1^{hi} and CX_3CR1^{lo} population (**Figure 3.13**), however, the physiological relevance of this is unknown. Here, CX_3CR1 expression was measured on blister pre-DC subsets at 24 hours post-challenge (**Figure 5.17**). In blood, low CX_3CR1 expression was observed on pre-DC in comparison to blister pre-DC. An upregulation of CX_3CR1 was also noted on cDC1, however, no difference was observed in pDC or cDC2 between the two compartments.

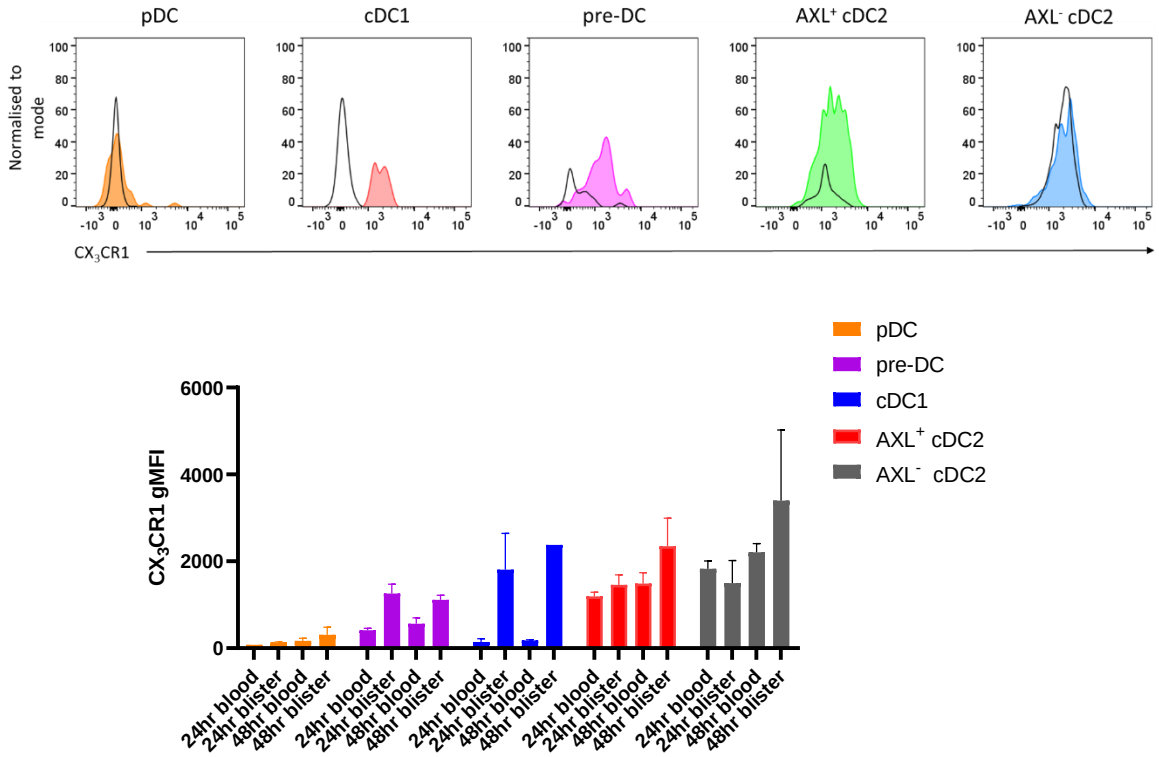

Figure 5.17 **CX_3CR1 expression on DC subsets**

DC subsets were identified by flow cytometry in both blister and blood at 24 hours post-challenge. CX_3CR1 expression was measured on each subset. Black open histograms represent blood, colour histograms represent blister. gMFI were quantified in the graph below for each subset. Bars represent mean ± SD. n=4 individual experiments.

5.3.5 CD1c expression on cDC2

It was also demonstrated in Chapter 3, that cDC2 can be divided into $CD1c^{hi}$ and $CD1c^{lo}$ subsets, which are thought to exhibit non-inflammatory and inflammatory functions, respectively (Villani *et al.,* 2017). It was examined whether CD1c expression changes on cDC2 at the measured time points, which may reflect the functions of these cells. A trend for an increase in CD1c expression was observed between 6 and 24 hours, however these changes were not significantly different at the time points measured (**Figure 5.18**).

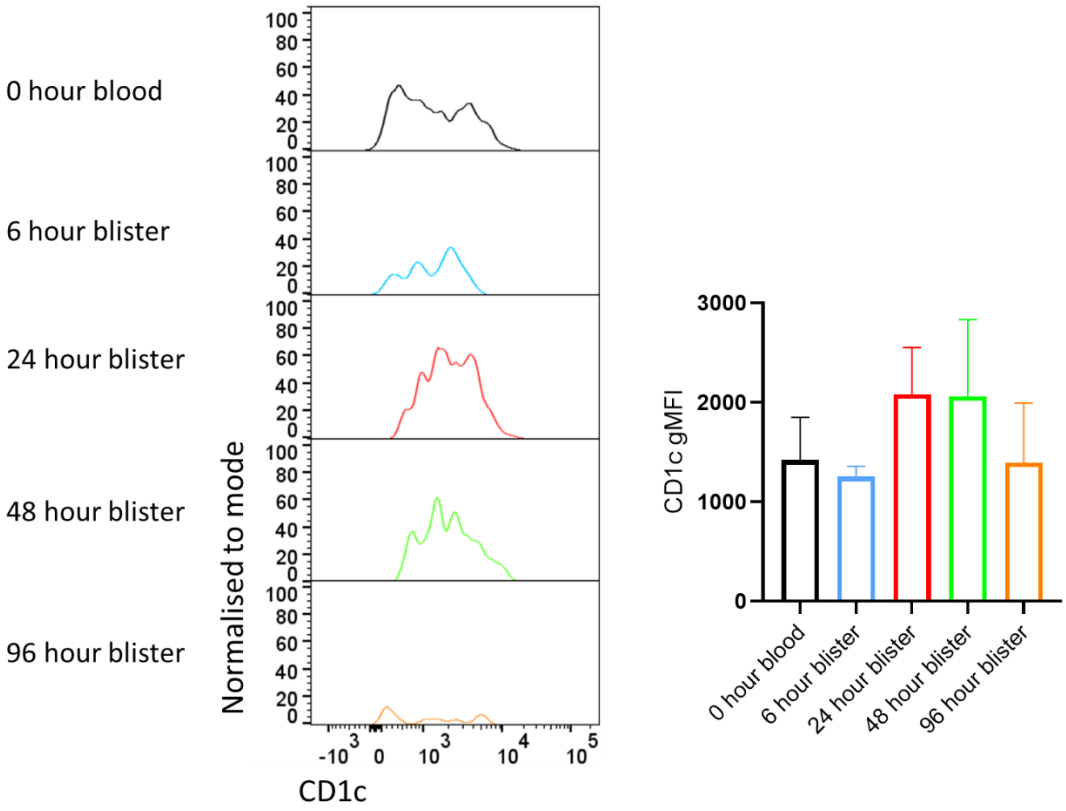

Figure 5.18 **CD1c expression on blister cDC2**

CD1c expression was assessed on blood (0 hours, black) and blister cDC2 at 6 (blue), 24 (red), 48 (green) and 96 (orange) hours post-challenge with UV-killed *E. coli*. Bars represent mean ± SD. n=4 individual experiments.

5.3.6 Re-defining cDC2 subsets

5.3.6.1 Novel gating strategy to identify cDC2 subsets

With the advice of novel gating strategies from Dr. Florent Ginhoux and Dr. Charles-Antoine Dutertre, further heterogeneity was examined within the cDC2 subset and has since been published (Dutertre *et al.,* 2019). It was questioned whether these novel cDC2 subsets could be observed *in vivo* in this model of inflammation.

Interestingly, one of these newly described cDC2 subsets has been described to express CD14 and is normally masked by the classical monocytes population. CD88 and CD89 have been described to be expressed on monocytes and can therefore tease apart bona fide $CD14^{+}$ monocytes from $CD14^{+}$ dendritic cells (Dutertre *et al.,* 2019). Lin^{-}, $HLA\text{-}DR^{+}$ $CD14^{+}$ $CD16^{-/lo}$ cells

(Q1), are composed of CD88$^-$ CD89$^-$, CD88$^-$ CD89$^+$ and CD88$^+$ CD89$^+$ cells (**Figure 5.19**). The CD88$^-$ CD89$^-$ population is thought to resemble the newly described CD14$^+$ DC population. Intermediate (Q2) and non-classical monocytes (Q3) also expressed both CD88 and CD89. As expected, the CD14$^-$ CD16$^-$ population were predominantly CD88$^-$ and CD89$^-$, despite a CD88$^+$ CD123$^+$ CD45RA$^-$ population which resembles contaminating basophils.

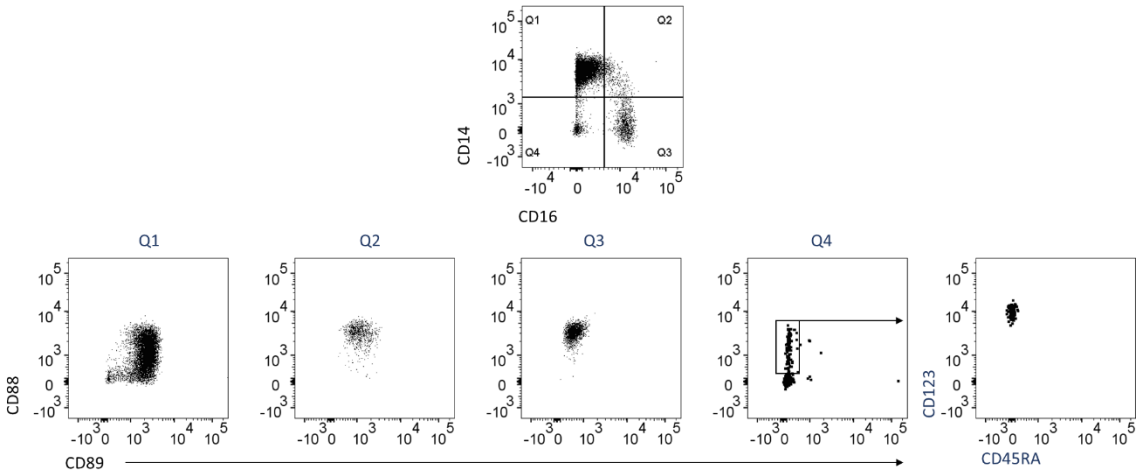

Figure 5.19 **CD88 and CD89 expression on mononuclear phagocytes**

CD88 and CD89 expression were assessed on monocytes and dendritic cells by flow cytometry. Lin$^-$ HLA-DR$^+$ mononuclear phagocytes were divided according to CD14 and CD16 expression into Q1, Q2, Q3 and Q4, where CD88 and CD89 expression was measured on these subsets. The CD88$^+$ population within Q4 was further characterised by CD123 and CD45RA expression. Representative of n=4 individual experiments.

Previously, monocytes were gated out using CD14 and CD16 (**Figure 3.15**), however, to identify the novel cDC2 subsets, monocytes were gated out using CD88 and CD89. As a result, DC were identified as Lin$^-$ HLA-DR$^+$ CD88$^-$ CD89$^-$ CD16$^-$ cells (**Figure 5.20**). pre-DC here were identified by CD5 and their identity was confirmed by Siglec6 expression. cDC1 were identified by high CD141 expression, whereas FcεR1α has been demonstrated as a better marker for cDC2 as CD1c expression is not uniform therefore CD1c^{lo} cDC2 may be lost (Dutertre *et al.,* 2019). Within the FcεR1α$^+$ cDC2 population, the first cDC2 subpopulation can be identified as CD5$^+$ cDC2. CD5$^-$ cDC2 are further divided into a CD14$^-$ CD163$^-$ cDC2, CD163$^+$ CD14$^-$ cDC2 and CD163$^+$ CD14$^+$ cDC2 (**Figure 5.20**).

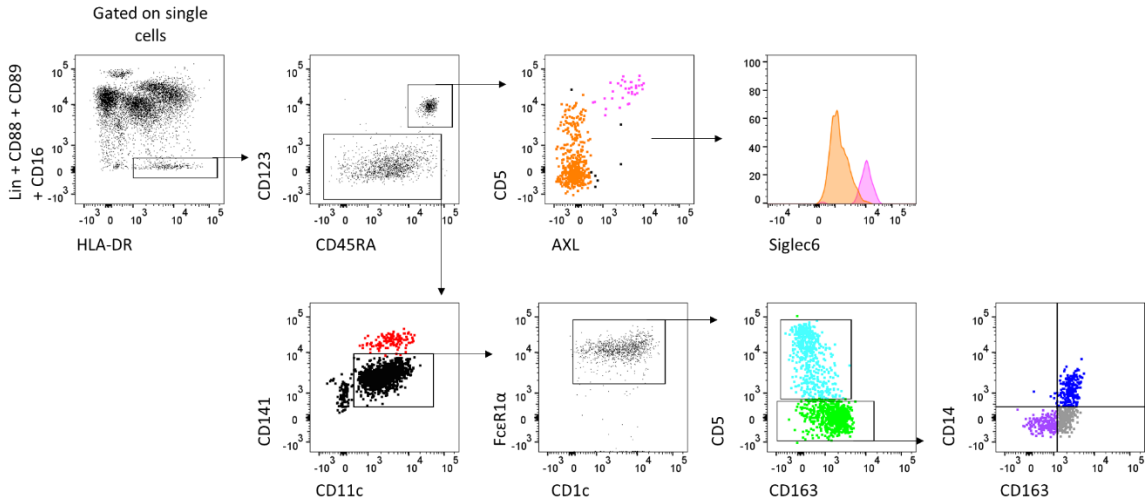

Figure 5.20 **Novel human cDC2 subsets**

Newly described cDC2 subsets (Dutertre *et al.,* 2019) were identified by flow cytometry. DC were identified as Lin$^-$ CD88$^-$ CD89$^-$ CD16$^-$ HLA-DR$^+$ cells. AXL$^-$ pDC (orange), CD5$^+$ Siglec6$^+$ AXL$^+$ pre-DC (pink), cDC1 (red) were identified. cDC2 were identified as FcεR1α$^+$ CD1c$^+$ cells and were subdivided into CD5$^+$ cDC2 (light blue), CD163$^-$ CD14$^-$ cDC2 (purple), CD163$^+$ CD14$^-$ cDC2 (grey) and CD163$^+$ CD14$^+$ cDC2 (dark blue). Representative of n=9 individual experiments.

From the gating strategy established in Chapter 3, cDC2 were divided into AXL$^+$ and AXL$^-$ CD1c^{hi} and AXL$^-$ CD1c^{lo} subsets (**Figure 3.15**). It was examined how these cDC2 subpopulations relate to cDC2 defined in the gating strategy shown in **Figure 5.20**. Under steady physiological conditions, blood AXL$^+$ cDC2 were found to overlap with the CD5$^+$ cDC2 subset (**Figure 5.21**). AXL$^-$ CD1c^{hi} cDC2 consisted of CD5$^+$, CD163$^-$ CD14$^-$ and CD163$^+$ CD14$^-$ cDC2. Finally, AXL$^-$ CD1c^{lo} cDC2 were made up of CD163$^+$ CD14$^+$ and CD163$^+$ CD14$^-$ cDC2.

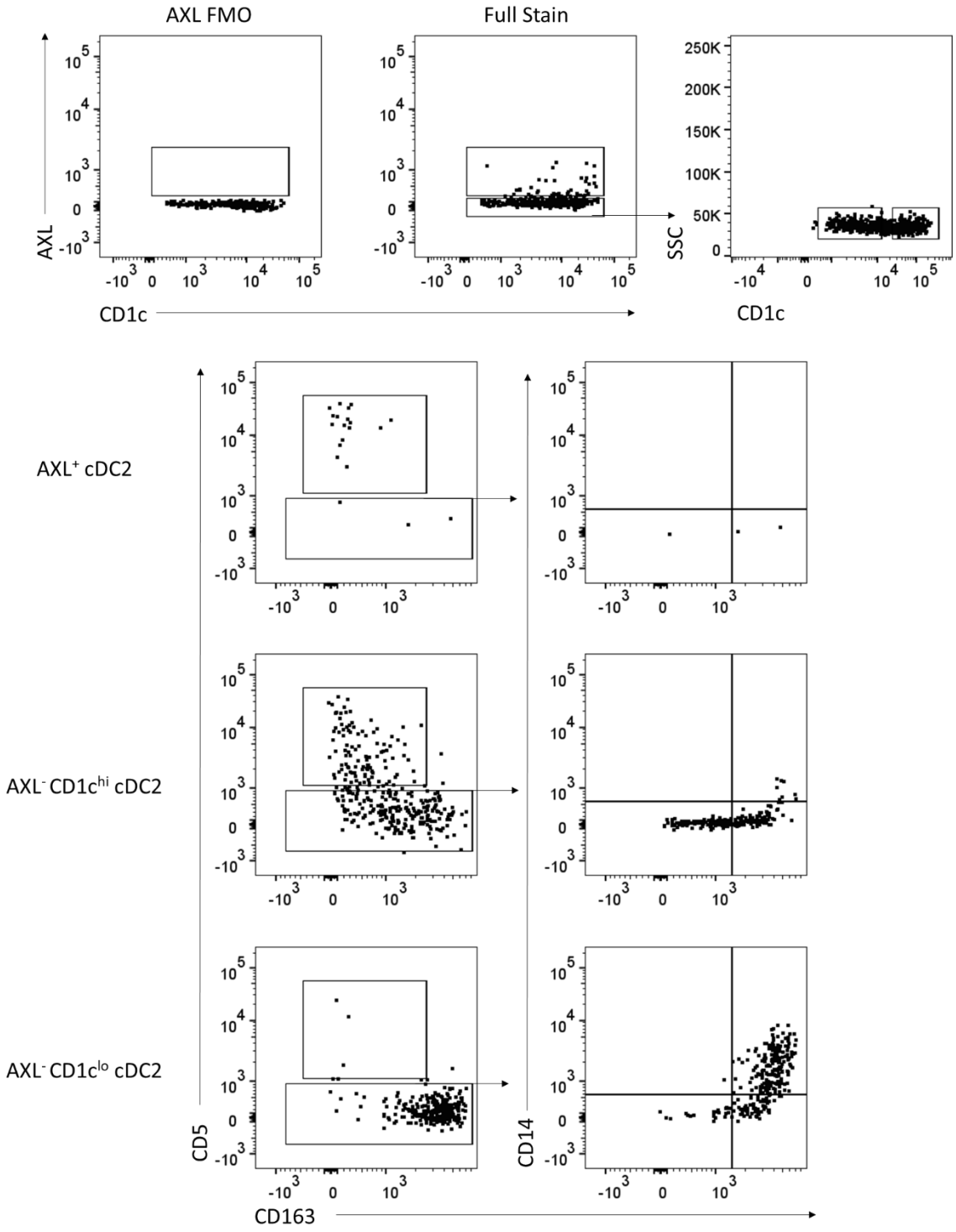

Figure 5.21 **Comparison of AXL$^-$ and AXL$^+$ cDC2 with novel cDC2 subsets**

AXL$^+$, AXL$^-$ CD1c^{hi} and AXL$^-$ CD1c^{lo} cDC2 were identified and characterised using CD5, CD163 and CD14 to understand their relationship to newly described cDC2 subsets. Representative of n=9 individual experiments.

The abundance of these newly described cDC2 were estimated in the blood (**Figure 5.22**). No significant differences were found between the absolute counts of the cDC2 subsets.

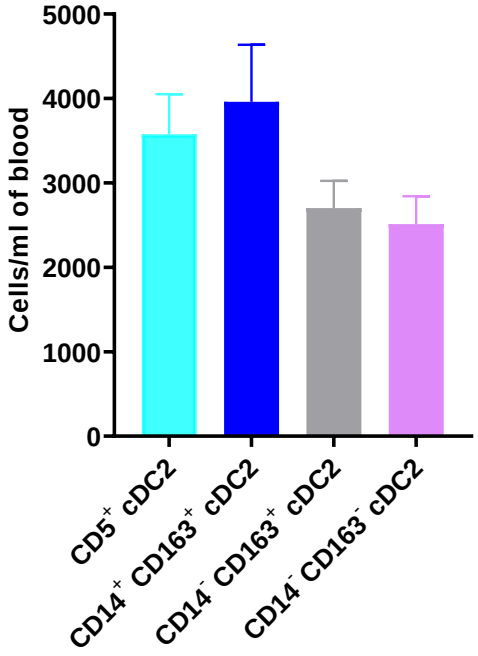

	CD5$^+$ cDC2	CD14$^+$ CD163$^+$ cDC2	CD14$^-$ CD163$^+$ cDC2	CD14$^-$ CD163$^-$ cDC2
Mean count/ ml blood	3576	3960	2701	2512
SD	1425	2025	966	985

Figure 5.22 **Absolute count of circulating novel cDC2 subsets**

The absolute count of circulating cDC2 subsets was enumerated in healthy blood by flow cytometry using counting beads. Bars represent mean ± SD and are shown in the table below. n=9 individual experiments.

5.3.6.2 Novel cDC2 subsets in local inflammation

Following challenge with UV-killed *E. coli*, cDC2 were re-analysed using the new gating strategy at 24 and 48 hours (**Figure 5.23**), where DC were the most abundant in the blister.

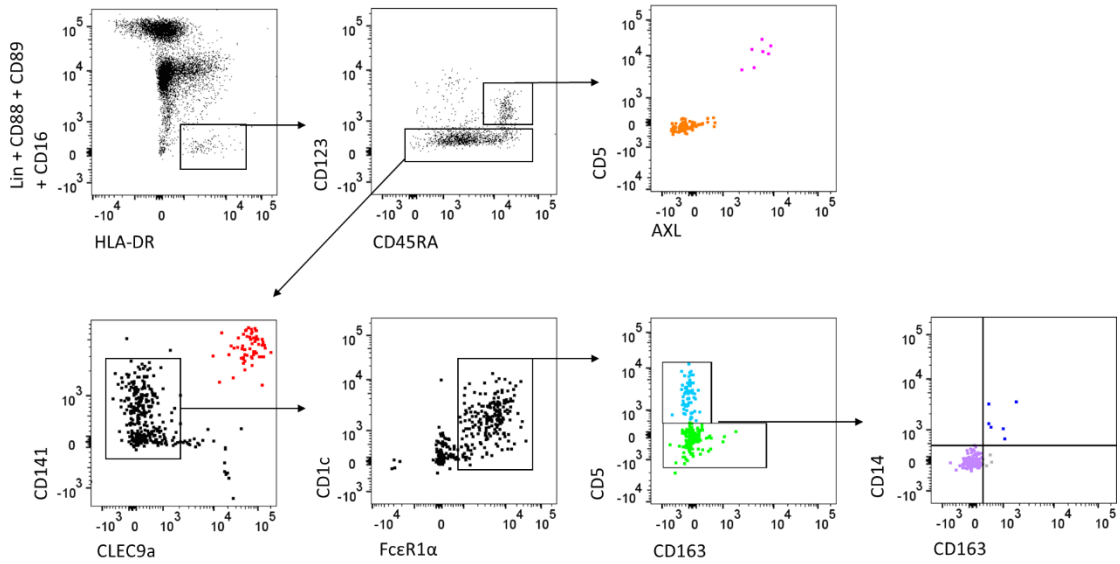

Figure 5.23 **Novel cDC2 subsets following intradermal challenge with UV-killed *E. coli***

Following intradermal challenge with UV-killed *E. coli*, blister cells were analysed by flow cytometry to detect the presence of new cDC2 subsets at 24 and 48 hours. Flow cytometry plots are representative of n=4 individuals at 24 hours.

$CD5^+$ and $CD163^-$ $CD14^-$ cDC2 were the dominant cDC2 subsets present at 24 and 48 hours post-challenge (**Figure 5.23 and Figure 5.24**). Relative to their concentration in blood, all cDC2 subsets were found at lower concentrations in the blister, with the exception of $CD163^-$ $CD14^-$ cDC2 at 24 hours, which was observed at an equivalent concentration to blood.

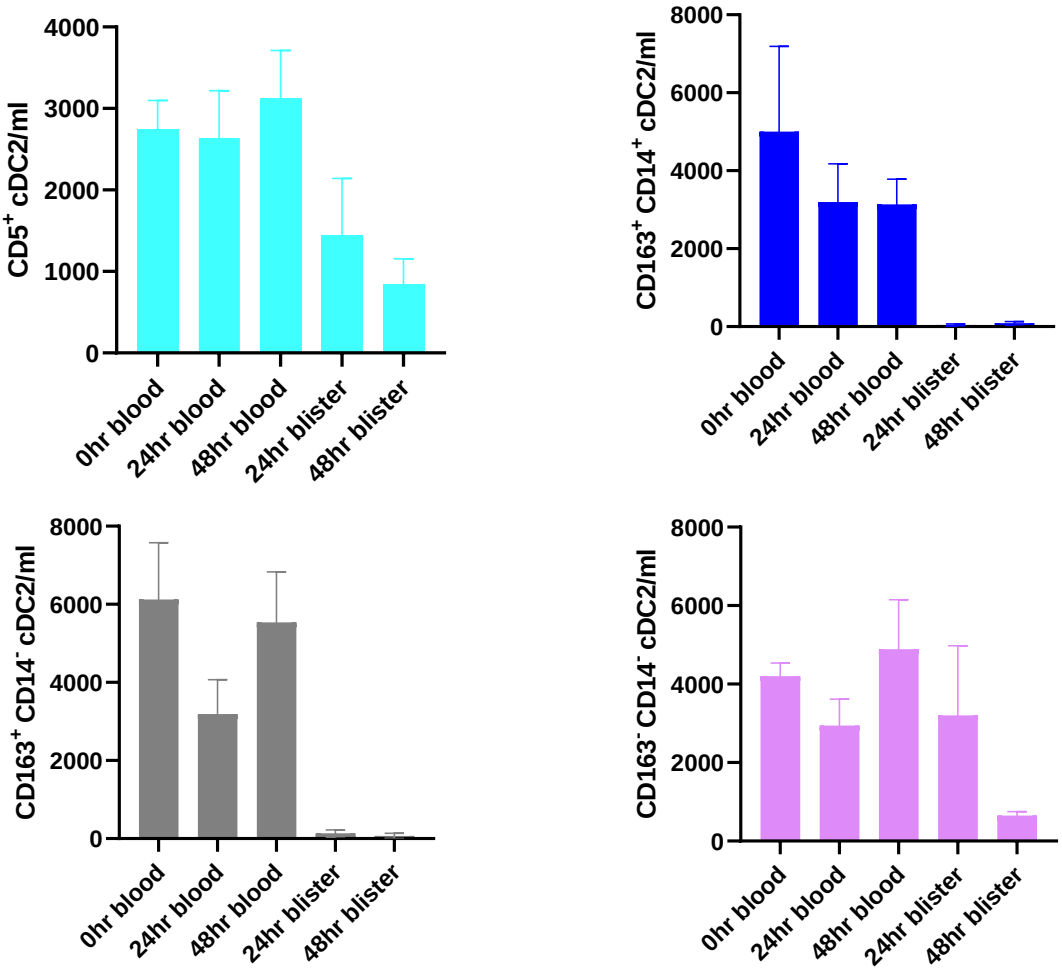

Figure 5.24 **Absolute count of novel cDC2 subsets following intradermal challenge**

Blood and blister cell count of cDC2 subsets were enumerated by flow cytometry using counting beads following intradermal challenge with UV-killed *E. coli*. Counts were adjusted per ml of blood or per ml of blister fluid. Bars represent mean ± SD. n=4 individual experiments.

In the previous gating strategy, cDC2 subsets were defined by AXL expression and a higher proportion of AXL$^+$ cDC2 were observed in the blister compared to blood (**Figure 5.15**). It was therefore questioned how AXL expression was distributed across CD5$^+$ cDC2 and CD163$^-$ CD14$^-$ cDC2. In steady-state, blood AXL$^+$ cDC2 overlap with CD5$^+$ cDC2 (**Figure 5.21**) and make up 10% of total CD5$^+$ cDC2 (**Figure 5.25b**). Consequently, it was hypothesised AXL expression in the blister would be restricted to CD5$^+$ subset. However, following intradermal challenge with UV-killed *E. coli*, AXL was highly expressed on both CD5$^+$ and CD163$^-$ CD14$^-$ cDC2 in the blister and makes up more than 50% of each subset (**Figure 5.25**).

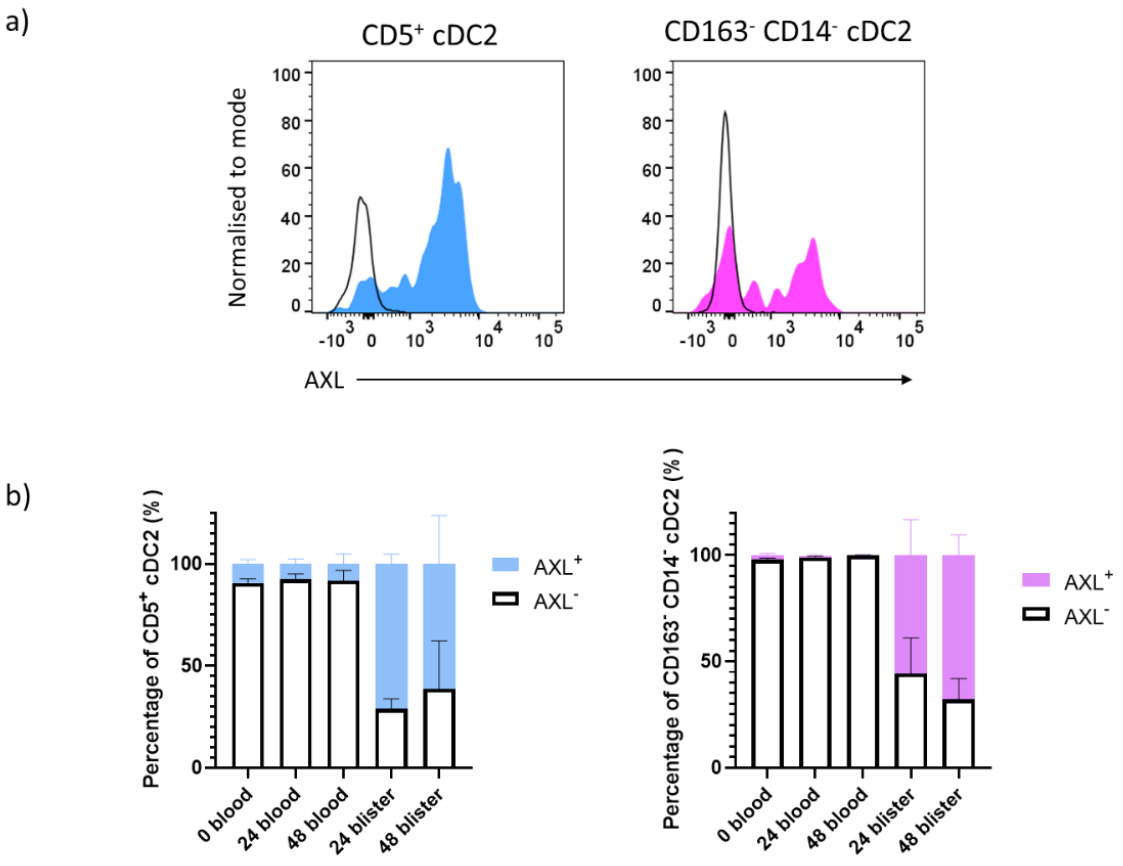

Figure 5.25 **AXL expression on CD5$^+$ cDC2 and CD163$^-$ CD14$^-$ cDC2**

AXL expression was assessed in CD5$^+$ cDC2 and CD163$^-$ CD14$^-$ cDC2 in blood and blister at each time point following intradermal challenge with UV-killed *E. coli*. **a)** AXL expression on CD5$^+$ cDC2 and CD163$^-$ CD14$^-$ cDC2 in the blood (black, unfilled histogram) and blister (filled histogram). Histogram representative of cells at 24 hours post-challenge. **b)** Percentage of AXL$^+$ cells was calculated for each subset in both blood and blister at each time point. Bars represent mean ± SD. n=4 individual experiments.

As AXL may be upregulated under inflammatory conditions, AXL expression was consequently measured on other DC subsets, however, was not found to be expressed on pDC or cDC1 in the blister at either time points (**Figure 5.26**).

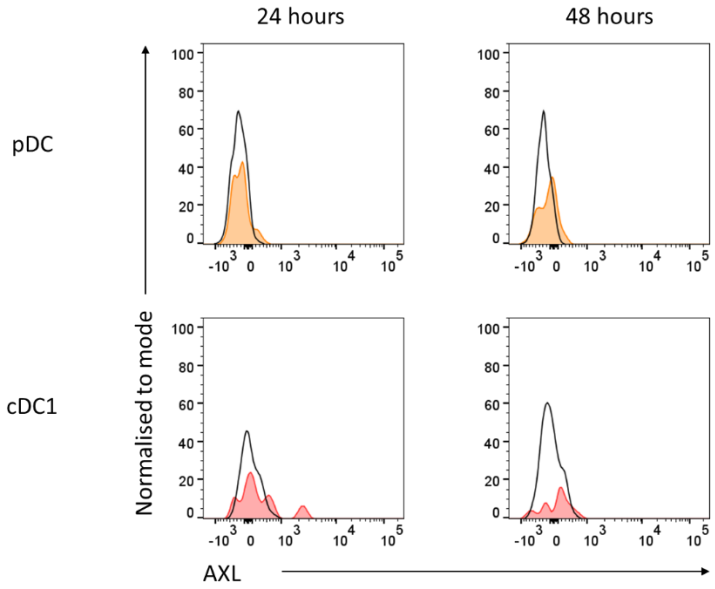

Figure 5.26 **AXL expression on pDC and cDC1 following intradermal challenge**

AXL expression was assessed in blister pDC (orange) and cDC1 (red) and blood counterparts (black, unfilled) at 24 and 48 hours following intradermal challenge with UV-killed *E. coli*. Representative of n=4 individual experiments.

5.3.7 DC phenotype in local inflammation

In addition to measuring AXL expression, co-stimulatory molecules CD80 and CD86 were examined on DC subsets in both blood and blister (**Figure 5.27**). $CD5^+$ and $CD163^-$ $CD14^-$ cDC2 express AXL at high levels only in the blister, therefore CD80 and CD86 expression could not be measured on blood counterparts. CD80 was not expressed on pDC but was found on pre-DC, cDC1, $CD5^+$ cDC2 and $CD163^-$ $CD14^-$ cDC2 at higher levels in the blister compared to blood. CD80 was highly expressed at 24 hours. On the other hand, CD86 expression on blister DC was not distinctly different relative to blood counterparts, although a trend for increased expression in the blister may be present.

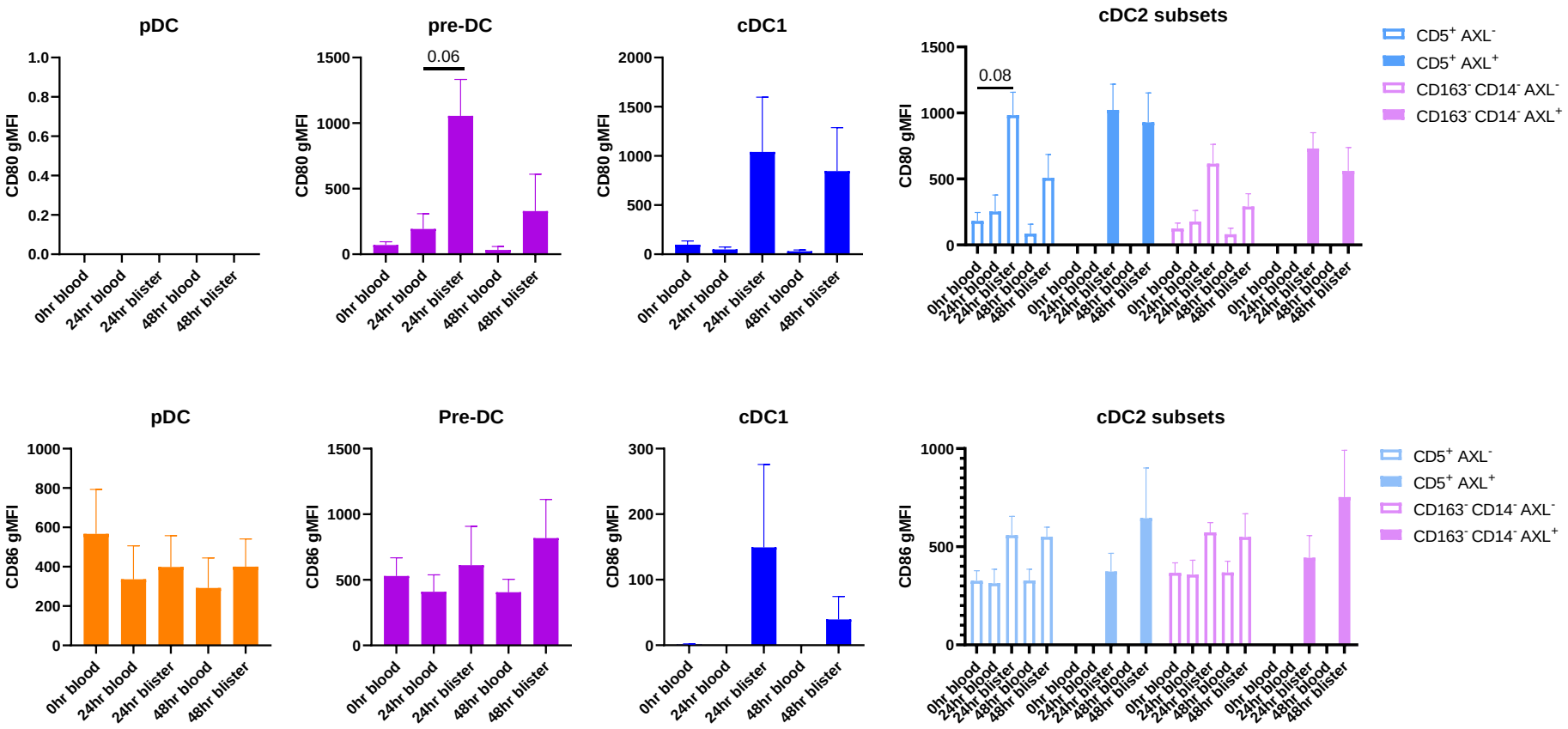

Figure 5.27 **CD80 and CD86 expression in DC subsets following intradermal challenge**

DC subsets were identified by flow cytometry following intradermal challenge with UV-killed *E. coli,* where CD80 and CD86 expression was assessed in blood and blister at each time point. As very few or no AXL$^+$ cDC2 were present in the blood, marker expression was not analysed. Bars represent mean ± SD. n=4 individual experiments at each time point.

Collectively these data demonstrate for the first time, the recruitment of DC subsets into the dermis following acute inflammation, where pre-DC were found at higher concentration in contrast to blood. CD80 and CD86 expression provided initial insights into the function of DC subsets, however as DC are found at very low numbers in the blister, it was not feasible to perform further functional assays. Nevertheless, DC subsets were single-cell sorted by FACS for single-cell RNA sequencing analysis and are currently being analysed in collaboration with Dr. Florent Ginhoux and Dr. Charles-Antoine Dutertre to gain further insight into the possible function of these cells during inflammation.

5.4 Appendix: approximation of blister counts

Unfortunately, not all blister cell counts were enumerated accurately using counting beads. In this instance, cell counts were taken as the total cell event number from flow cytometry. Though the whole sample was recorded, it is understood not all events are recorded. Therefore, by using samples where a known number of counting beads were added, the average bead recovery can consequently be used as a proxy to estimate what fraction of recorded cells were of the total cell count.

The number of beads recovered after recording the whole sample was expressed as a percentage of the total numbers of beads added (**Figure 5.28**). On average, 73.52 (± 7.9)% of beads were recorded. Consequently, the cell counts reported in samples where beads were not added are approximately 75% of the true cell count.

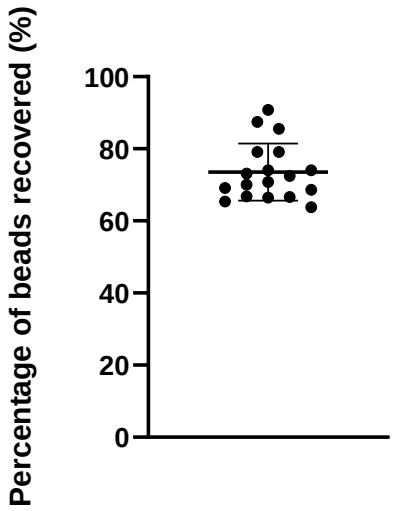

Figure 5.28 **Average counting bead recovery**

A known quantity of counting beads (27'000 beads) was added to blister samples. After recording the total sample, the number of beads recovered was expressed as a percentage. Bars represent mean ± SD. n=18 individual experiments.

5.5 Discussion

In this chapter, it was investigated how systemic inflammation impacts on the kinetic profile of the circulating mononuclear phagocytes and furthermore the kinetic profile of recruited mononuclear phagocytes in response to local inflammation.

5.5.1 Human Endotoxin Model

To study acute systemic inflammation, the endotoxin model was employed in humans as it provides a platform to reproduce immunological and haematological effects to those seen in systemic inflammatory response syndrome (Fullerton *et al.,* 2016). Although referred to as an 'endotoxin' model, LPS rather endotoxin was administered, unfortunately, the two terms are used interchangeably throughout the literature. Although not documented here, it has previously been demonstrated that the human endotoxin model results in a neutrophilia, lymphocytopenia and pro-inflammatory cytokine production (Fullerton *et al.,* 2016) (James Fullerton, UCL, unpublished data from Prof. Derek Gilroy group). In line with the focus of this

thesis on mononuclear phagocytes, the impact on the kinetic profiles of circulating monocyte and dendritic cell subset was examined in this model.

Clinical blood counts demonstrated early monocytopenia. The 'monocyte' count obtained includes both monocyte and dendritic cells and was therefore regarded as the total mononuclear phagocyte count. The loss of circulating monocyte as early as 2 hours has since been observed from additional groups (Tak *et al.,* 2017b; Thaler *et al.,* 2016). These data reflected previous observations in mice, where following the administration of LPS a sharp decline occurs within one hour in the number of Ly6C^{hi} classical and Ly6C^{lo} non-classical monocytes (Chong *et al.,* 2016; Shi *et al.,* 2011). By 8 hours, classical monocytes were observed in humans, interestingly intermediate and non-classical monocytes did not return until 24 hours, suggestive of a sequential re-appearance of monocyte subsets, similar to that observed under steady-state. Unfortunately, no blood samples were taken between 8 and 24 hours post-endotoxin challenge, therefore, it was uncertain whether intermediate monocytes repopulated prior to non-classical monocytes.

In CCR2-deficient mice, the reappearance of circulating Ly6C^{hi} classical monocytes was abolished supporting a likely role of monocyte egression from the bone marrow (Shi *et al.,* 2011). Similarly, augmented CCL2 levels have been documented in humans following endotoxin (Tak *et al.,* 2017b). To investigate whether the bone marrow contributed to the repopulation of circulating monocytes or whether all monocytes were returning from margination, deuterium labelling was implemented. Given that circulating monocytes do not present with label at 24 hours after deuterium dosing under steady-state, if endotoxin administration was timed correctly, labelling of monocytes at this time period would indicate early egression of bone marrow monocytes. Indeed, 28 hours after deuterium dosing (8 hours following endotoxin challenge), classical monocytes were labelled. It should be made clear that deuterated glucose was cleared within 6 hours after labelling, therefore was not available in the circulation at the time endotoxin was administered. Up until 20 hours post labelling, steady-state homeostasis

results in the production of labelled classical monocytes which reside within the marrow. These data demonstrated an 'early emergency release' of classical monocyte from the bone marrow into the circulation. In line with observation, following acute myocardial infarction in humans, a reduction of bone marrow $CD14^+$ monocytes has also been documented (van der Laan *et al.,* 2014). However, it cannot be ruled out that classical monocytes also return from a marginating pool. The lifespan of classical monocytes following endotoxin challenge was not modelled here. However, the label was only present for 4 days, whereas, during steady-state, the label was observed for a much longer period of time of up to 6-9 days. This suggests that the time spent in the circulation is much shorter during inflammation, as has been previously shown in mice (van Furth, 1989; Van Furth *et al.,* 1973).

Given the sequential appearance of monocyte subsets, it is reasonable to think these classical monocytes mature into the intermediate monocytes that are elevated 24 hours post-challenge. Although some labelling was observed in intermediate monocytes at this time point, the majority of these cells were unlabelled. Similarly, non-classical monocytes also appeared at this time point, however were all unlabelled and seemed to follow their kinetic profile under steady-state. It is therefore unlikely, that the labelled classical monocytes mature into non-classical monocytes under these conditions and therefore represent an additional and/or alternative source of intermediate and non-classical monocytes. The spleen has been described as a reservoir of monocytes that are released in response to myocardial infarction (Swirski *et al.,* 2009; van der Laan *et al.,* 2014), however, it has not been documented whether this also holds true for non-sterile systemic inflammation. This was outside the scope of the question addressed with this experiment and further follow-up studies would be necessary to address this observation.

Another outstanding question arises regarding the fate and disappearance of the monocytes present prior to endotoxin challenge. Although it was not feasible to investigate this in humans, in mice, monocytes accumulated in the intravascular compartment of the lung following LPS

challenge (Chong *et al.,* 2016). Given that human lung capillaries have a diameter of approximately 7.48μM (Doerschuk *et al.,* 1993), this already present a problem for monocytes under steady-state as they have a much larger diameter. It is believed cells can deform to allow them to transit through narrow capillaries under steady-state. However, following LPS treatment, an increase in monocyte stiffness has been observed possibly due to an increase in actin assembly (Doherty *et al.,* 1994). This increase in stiffness may result in hindrance in their ability to deform and transit through these narrow capillaries thus resulting in accumulation. In addition, CD11b has been implicated in monocyte extravasation (Schenkel *et al.,* 2004), therefore the upregulation of CD11b observed on classical and intermediate monocytes observed here and by others (Tak *et al.,* 2017b; Thaler *et al.,* 2016), might support tissue extravasation of these cells. Furthermore, CD11b and CD18 together form integrin $\alpha_M\beta_2$. LPS treated monocytes with anti-CD18 mAb, displayed decreased adherence compared to those without anti-CD18 (Doherty *et al.,* 1994), therefore it can be speculated that CD11b plays a role in the adhesion to microvasculature contributing to the observed monocytopenia.

In addition to examining the kinetics of monocytes, additional surface markers were examined on the re-appearing monocytes. Classical monocytes were observed as early as 4 hours following endotoxin challenge, though were $CCR2^{lo}$ CX_3CR1^{-} which did not resemble classical monocytes at steady-state. Deuterium labelling suggested an early release of bone marrow classical monocytes. In mice, pre-monocytes are also $CCR2^{lo}$ CX_3CR1^{lo} (Chong *et al.,* 2016). Therefore, these cells may represent immature bone marrow classical monocytes. However, it cannot be ruled out that the change in phenotype is due to the impact of the inflammatory response. This has been widely documented in sepsis patients, where monocytes exhibit reduced expression of HLA-DR (Landelle *et al.,* 2010; Monneret *et al.,* 2006; Poehlmann *et al.,* 2009; Wu *et al.,* 2011). Here it was demonstrated that the downregulation of HLA-DR expression was specific to intermediate monocytes, as has been observed by others (Tak *et al.,* 2017b). Of note, it would be interesting to observe whether the correlation of HLA-DR expression with mortality and

nosocomial infection in these patients (Landelle *et al.,* 2010; Monneret *et al.,* 2006; Wu *et al.,* 2011) is specific to the intermediate monocyte population.

In the clinical setting, an expansion in the percentage and number of monocyte subsets has been documented in sepsis patients and SLE patient (Mukherjee *et al.,* 2015; Poehlmann *et al.,* 2009). Whilst some studies have reported an expansion classical and intermediate monocytes (Poehlmann *et al.,* 2009), others have reported an elevation in intermediate and non-classical monocytes (Mukherjee *et al.,* 2015). Several reasons exist for this discrepancy, however, based on the kinetic profile shown here, it is possible the difference in the expansion of subsets is reflected in the timings at which patient samples are obtained.

Concerning the dendritic cell response, a similar reduction and reappearance was observed for these subsets. Dendritic cells are not often appreciated as key immune cells in the clinical setting, for example, a dendritic cell count is not reported in a clinical blood report. Nevertheless, 'DC-penia' has been observed in sepsis patients who exhibit a reduced number of circulating cDC and pDC (Grimaldi *et al.,* 2011; Guisset *et al.,* 2007; Poehlmann *et al.,* 2009; Riccardi *et al.,* 2011). In mice, it has been demonstrated that systemic inflammation by cecal ligation puncture, resulted in the reduction of DC in spleen and lymph nodes (Ding *et al.,* 2004; Efron *et al.,* 2004), where this loss was accounted for by cell death (Efron *et al.,* 2004). In this model of human endotoxemia, DC appeared to repopulate at a slower rate than classical monocytes. This was interesting given that under steady-state cDC appear in the circulation before classical monocytes and pDC (**Figure 4.3 and Figure 4.12**). The early appearance of monocytes prior to DC during experimental endotoxemia may be due to the fact that a pool of 'emergency' monocytes reside within the bone marrow unlike that for DC subsets. Furthermore, given the inflammatory milieu, it is possible deviations occur from homeostatic haematopoiesis. An elegant study by Pasquevich and colleagues demonstrated monopoiesis is favoured over DC production following bacterial infection in mice (Pasquevich *et al.,* 2015). Following infection, these mice had reduced numbers of CDP but elevated numbers of cMoP compared with wild-

type mice and it was further demonstrated this effect was mediated via TLR4. In addition, early studies from van Furth and colleagues demonstrated that the time taken from the promonocyte to the monocyte stage is dramatically shortened in response to inflammation, alongside an increase in the number of promonocytes, resulting in an overall increased production of monocytes (Van Furth *et al.,* 1973). Consequently, it is possible that human monocyte production is also favoured over cDC production following systemic challenge with LPS, however, to confirm this hypothesis, future experiments would have to sample the bone marrow in together with endotoxin challenge.

Dendritic cells play a key role in establishing homeostasis following systemic inflammation. Patients who survived sepsis had higher levels of circulating DC comparison to those who did not survive (Guisset *et al.,* 2007), and those who did not acquire secondary infections had higher levels of circulating DC than those who did (Grimaldi *et al.,* 2011). Moreover, apoptosis of DC has been demonstrated as a likely mechanism behind DC loss, the prevention of DC apoptosis consequently, resulted in reduced immunosuppression in mice challenged with LPS (Gautier *et al.,* 2008). Similarly, an increased survival was observed in mice with burn wound infections that received FLT3L (Toliver-Kinsky *et al.,* 2005). These studies suggest DC are required to overcome inflammation and highlight DC turnover as a potential therapeutic target.

5.5.2 Acute Local Inflammation Model

The following part of this chapter examined the kinetic response of mononuclear phagocytes in response to local inflammation. Numerous groups at UCL have collectively helped to establish an acute local model of inflammation using UV-killed *E. coli*. In this model, classical cardinal signs of inflammation have been observed in addition to an immunological response at the cellular level (Motwani *et al.,* 2016).

Following intradermal challenge with UV-killed *E. coli*, suction blisters were raised at the site of injection at specific time points to examine the immune cell profile. Similar to the profile

observed during endotoxin challenge, a somewhat sequential profile of monocyte subsets was observed. Only classical monocytes were observed at early inflammatory time points, and later an intermediate monocyte phenotype was observed. Jardine and colleagues have recently demonstrated, in response to LPS inhalation, only classical and intermediate monocytes were significantly elevated in the bronchoalveolar lavage compared to steady-state (Jardine *et al.,* 2019). The authors also noted, non-classical monocytes were not observed to be significantly elevated, similar to observations made here.

It is unclear whether there are two waves of monocyte infiltration, first by classical monocytes then followed by intermediate monocytes or whether the intermediate monocytes are derived *in situ* from the classical monocytes. Ly6C^{hi} classical monocytes have been demonstrated to give rise to the inflammatory macrophages through to wound healing macrophages, in the context of myocardial infarction and colon inflammation (Hilgendorf *et al.,* 2014; Zigmond *et al.,* 2012). An elegant a model of sterile hepatic injury, using intravital microscopy with fluorescent reporter proteins demonstrated Ly6C^{hi} CCR2^{hi} CX$_3$CR1^{lo} classical monocytes infiltrated and matured *in situ* into CCR2^{lo} CX$_3$CR1^{hi} cells without contribution from non-classical monocytes (Dal-Secco *et al.,* 2015). Consequently, it was hypothesised that the classical CCR2^{hi} CX$_3$CR1^{lo} subset upregulates CD16 expression and resembles intermediate monocytes that are CCR2^{lo} CX$_3$CR1^{hi}. However, both subsets exhibited similar levels of expression at each time point. Given the similarities in marker expression, it is likely that blister intermediate monocytes derive from blister classical monocytes than blood intermediate monocytes. However, this was based on two markers and further studies are needed to conclusively rule out that blister intermediate monocytes are blood-derived. On the other hand, it might be incorrect to divide blister monocytes into two separate monocyte populations. Rather, given how their expression of receptors differs to that in blood, these cells possibly represent monocyte-derived cells. Although CD16 expression increases, this could represent the maturation/plasticity of monocyte-derived cells, as was observed when culturing classical monocytes *in vitro* (Section 4.2.5). Further studies are

necessary to examine how the phenotype of these cells change during the course of inflammation and how this relates to their function.

The kinetic response was measured over a 4 day period, it would be interesting to observe whether some recruited monocytes persist within the skin that may become long-lived cells as in mice (Machiels *et al.,* 2017; Misharin *et al.,* 2017; Newson *et al.,* 2014; Yona *et al.,* 2013). To demonstrate this, monocyte recruitment from the blood would have to be excluded which may be challenging. Evidence that monocytes can engraft into the long-term tissue resident pool in humans has been demonstrated in the setting of liver transplantation in collaboration with Prof. Mala Maini and Dr. Laura Pallett. Preliminary data obtained from analysing liver allografts explanted months to years after transplantation into HLA-mismatched recipients allowed for the identification of donor and recipient derived leukocytes. In this setting, a population of Lin^- $HLA\text{-}DR^+$ $CD14^+$ mononuclear phagocytes were still detectable in the donor-derived leukocyte pool up to 11 years post organ transplantation. These data suggest that a population of Kuppfer cell-like cells are "long-lived" and not replaced by infiltrating recipient derived peripheral populations (unpublished data, personal communication by Dr. Laura Pallett). It would be interesting to examine whether these observations hold true for the dermis, though it has been demonstrated under steady-state that dermal monocyte-derived cells have a half-life of less than 6 days (McGovern *et al.,* 2014).

Dendritic cells numbers also peaked at 24 hours along with monocytes. Monocytes, pDC, cDC1 and AXL^- cDC2 were all found at lower concentrations compared to blood, with the exception of pre-DC and AXL^+ cDC2. Following LPS inhalation in healthy humans, an increase in the percentage of AXL^+ $Siglec6^+$ DC has also been reported in the bronchoalveolar lavage compared to steady-state (Jardine *et al.,* 2019). In steady-state, the human skin lacks AXL^+ DC (Alcántara-Hernández *et al.,* 2017), explaining the low number of pre-DC and AXL^+ cDC2 observed at 6 hours post inflammation. From Ki67 expression data, it is possible these initially recruited cells proliferate at the site contributing to increased numbers, however selective recruitment from the blood

cannot be ruled out. Whilst pre-DC have been described as precursor cells to cDC1 and cDC2 (Cytlak *et al.,* 2019; See *et al.,* 2017; Villani *et al.,* 2017), it was reasoned that as pre-DC decline, conversely an increase would be mirrored in the cDC1 and/or cDC2 subsets, however this was not observed. It is possible the rate at which cDC disappear masks the contribution from the few pre-DC that mature into these cells. On the other hand, under inflammatory conditions, pre-DC maturation may not occur. These cells expressed high levels of CD80 in the blister compared to blood, which suggests that they may take on an effector function. In line with this, pre-DC infected with HIV-1 exhibited reduced differentiation into cDC1 and cDC2 (Philippe Benaroch, unpublished). It may be hypothesised that the pre-DC switch from a precursor to an effector cell phenotype during inflammation.

In chapter one, it was demonstrated that pre-DC could be divided into a CX_3CR1^{hi} and CX_3CR1^{lo} population, however, the functional relevance of these two populations have not yet been explored. Here, it was demonstrated that blister pre-DC expressed higher levels of CX_3CR1. It was unclear whether this represents a selective recruitment of CX_3CR1^{hi} pre-DC, or whether pre-DC upregulate this marker in response to inflammation as was observed for cDC1. Similarly, CD1c expression was measured on cDC2 subsets as $CD1c^{hi}$ and $CD1c^{lo}$ cDC2 subsets have been assigned with a non-inflammatory and inflammatory phenotype, respectively (Villani *et al.,* 2017). Although a trend was observed in the level of CD1c expression, significant differences were not observed. As functional assays were limited by the number of blister cells, single-cell RNA sequencing analysis may allow for the exploration of the functional importance of pre-DC and DC subsets in inflammation.

Whilst performing the experiments for this thesis, DC nomenclature has undergone several revisions (Calzetti *et al.,* 2018; Cytlak *et al.,* 2019; Dutertre *et al.,* 2019; Günther *et al.,* 2019; See *et al.,* 2017; Villani *et al.,* 2017). Initially, the kinetic profile was examined for AXL^+ and AXL^- cDC2 subsets based on unified gating strategy (**Figure 3.15**). However, further revisions regarding the cDC2 subset have divided cDC2 by CD163, CD5 and CD14 expression into four major subsets

(Dutertre *et al.,* 2019). The developmental relationship of these cDC2 subsets remains to be explored. In chronic inflammatory diseases, SLE and systemic sclerosis patients exhibit an expansion in the circulating $CD163^+$ $CD14^+$ cDC2 subset and have consequently been termed 'inflammatory cDC2' (Dutertre *et al.,* 2019). When examining the infiltrating kinetics of this newly defined cDC2 in the blister model, 'inflammatory cDC2' were not observed at the blister site nor were changes observed in the circulating count. It is possible these cells play a role in chronic rather than acute inflammation.

In response to inflammation, AXL expression was upregulated on both $CD5^+$ and $CD163^-$ $CD14^-$ cDC2 in the blister, whereas in blood, the expression was restricted to a small percentage of the $CD5^+$ cDC2 subset. AXL, together with Tyro3 and Mer form the TAM receptors which regulate and prevent a hyper-immune response (Gautier *et al.,* 2013). The upregulation of AXL has previously been observed in bone marrow DC stimulated with LPS and upon binding with its inhibitory molecule, Gas6, resulted in reduced cytokine production and proteins associated with TLR activation pathways (Gautier *et al.,* 2013). To further demonstrate the immunosuppressive functions of this receptor, AXL is regulated by microRNA-34a (miR-34a), where miR-34a inhibits the expression of AXL (Kurowska-Stolarska *et al.,* 2017). Consequently, $miR34a^{-/-}$ DC have high levels of AXL and exhibit an inhibitory DC phenotype with reduced DC/T cell interactions and reduced T cell proliferation (Kurowska-Stolarska *et al.,* 2017; Mildner *et al.,* 2013), however upon introduction of *AXL* siRNA, DC activation was restored (Kurowska-Stolarska *et al.,* 2017). Collectively, these studies demonstrate that AXL plays an immunoregulatory role in DC in function. On the other hand, AXL expression on DC is also important for the uptake of apoptotic cells as murine DC lacking AXL resulted in apoptotic cell accumulation and consequently defective antigen-specific $CD8^+$ T cell activation against herpes simplex virus-1 infection in mice (Subramanian *et al.,* 2014). Therefore AXL-dependent DC efferocytosis of apoptotic cells may be required to elicit cytotoxic T cell activity. In line with this observation, CD80 and CD86 upregulation was observed on DC subsets. CD80 was highly upregulated on DC subsets in

comparison to CD86, but this may reflect the difference observed in the binding affinities to CD28 and CTLA4 (Linsley *et al.,* 1994). In addition, the upregulation of these two molecules alone does not dictate T cell activation, as the balance of far more extensive repertoire of receptors and ligands order such response.

These data demonstrate the kinetic profiles of mononuclear phagocytes from the initiation of inflammation through to the resolution. It is hoped this may provide insight into the kinetics of these cells in the clinical setting which are often missed. With further knowledge regarding the function of these cells, this will deliver a fuller picture of mononuclear phagocytes in health and disease.

Chapter 6

Discussion

6.1 Mononuclear phagocytes diversity

What began as the observation of phagocytosis (Metchnikoff, 1893; Vikhanski, 2016) has now evolved into the classification of several subsets which share this ability (Dutertre *et al.,* 2019; Geissmann *et al.,* 2003; Passlick *et al.,* 1989; See *et al.,* 2017; Villani *et al.,* 2017; Ziegler-Heitbrock *et al.,* 2010). Prior to the studies performed in this thesis, three monocyte and three dendritic cell subsets were recognised in humans (Ziegler-Heitbrock *et al.,* 2010), however recently, further heterogeneity was recognised within the mononuclear phagocyte compartment (Dutertre *et al.,* 2019; See *et al.,* 2017; Villani *et al.,* 2017), and some of these novel subsets were examined here.

The finding of heterogeneity is owed to the advances in technology. This can be appreciated from the data presented in chapter one, where only a few markers were analysed due to the limitations of flow cytometry. However, with the development of mass cytometry and single cell RNA sequencing, this increases the number of parameters that can be measured and consequently improves the chances of finding further heterogeneity. Regarding heterogeneity within classical monocytes, viSNE analysis in Chapter 1 demonstrated surface marker expression does not change at the boundaries of CD14 and CD16 expression used to define the subsets. Therefore, this observed heterogeneity may simply represent the maturation of some markers prior to the upregulation of CD16 or these changes could be indicative of varying functions within classical monocytes. It is therefore questionable whether CD14 and CD16 are the optimal markers to define monocyte subsets.

The recognition of novel subsets has subsequently identified subset-specific functions. For example, within non-classical monocytes, $SLAN^{+}$ cells have been implicated to play a role in HIV infection (Dutertre *et al.,* 2012), cardiovascular disease (Hamers *et al.,* 2019) and psoriasis (Hänsel *et al.,* 2011). Similarly, $CD14^{+}$ cDC2 (previously identified as classical monocytes) have

been shown to expand in SLE patients (Dutertre *et al.,* 2019) and pre-DC (previously grouped with pDC) are highly susceptible to HIV infection (Ruffin *et al.,* 2019).

The heterogeneity of mononuclear phagocytes mentioned in this thesis is summarised in **Figure 6.1**. With future advancements in technology, our knowledge of mononuclear phagocytes will continue to expand.

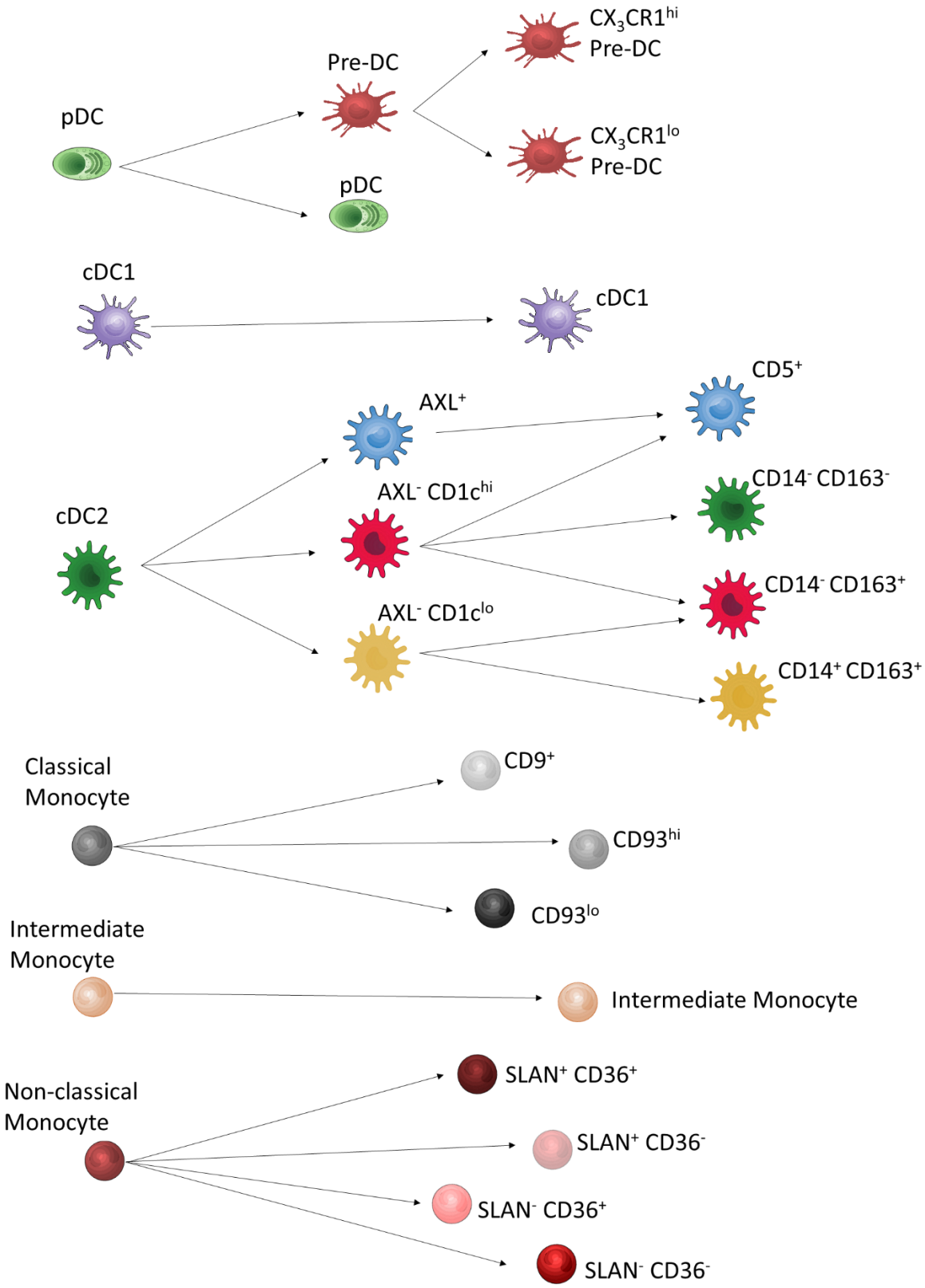

Figure 6.1 **Summary of human mononuclear phagocyte heterogeneity**

Six human monocyte and DC subsets were initially recognised. With the use of single-cell RNA sequencing and mass cytometry, further heterogeneity has been described within these subsets.

6.2 Steady-state kinetics of mononuclear phagocytes

Direct measurements of the circulating lifespan of these mononuclear phagocyte subsets have not yet been made in humans. Examining the generation, maturation and disappearance of these cells underlie their function under steady-state homeostasis and inflammation.

Mice serve as a feasible platform to study the kinetics of cells as demonstrated by adoptive transfer, parabiosis, pulse labelling and fate-mapping. As a result, our knowledge regarding the turnover of the murine immune system is extensive compared to that of the human immune system. A hindrance to studying the kinetic profile of human leukocytes can be attributed to the lack of safe protocols. However, the use of nontoxic deuterated glucose and water has been demonstrated as a safe protocol to efficiently label cells *in vivo* to study human immune cell kinetics. To date, the kinetics of human neutrophils (Lahoz-Beneytez *et al.,* 2016), B cells (Macallan *et al.,* 2005), T cells (Macallan *et al.,* 2003) and NK cells (Zhang *et al.,* 2007) have been established. This thesis focuses on the kinetics of mononuclear phagocytes in humans, specifically monocyte and dendritic cell subsets.

6.2.1 Circulating monocyte kinetics

Studies have previously examined the turnover of monocytes in humans (Mohri *et al.,* 2001; Whitelaw, 1972) but have not yet fully examined the lifespan of individual subsets. McGovern and colleagues have indirectly demonstrated following HSCT in patients, $CD14^+$ monocytes were observed in the circulation prior to $CD16^+$ monocytes (McGovern *et al.,* 2014).

Here, deuterium label was also observed in a sequential manner, first in classical monocytes, followed by intermediate and the non-classical monocytes. It was further demonstrated using humanised mice, that this was most likely due to a developmental relationship between the subsets. Non-classical monocytes have the longest lifespan of monocytes, this may be because their steady-state functions are restricted within the circulation whereas classical monocytes

are recruited to repopulate tissue compartments (Bain *et al.,* 2014; Epelman *et al.,* 2014; Kim *et al.,* 2016; Liu *et al.,* 2019; Mossadegh-Keller *et al.,* 2017; Tamoutounour *et al.,* 2013). As non-classical monocytes represent the end cell following monocyte development, they can in some ways be regarded as a terminally differentiated cell and have even been termed 'blood macrophages' (Yona *et al.,* 2013).

Under steady-state, intermediate monocytes might be regarded as a mere transitioning cell. Yet, these cells expressed higher levels of surface markers such as MHC-II in comparison to classical and non-classical monocytes. The function of intermediate monocytes under steady-state conditions remains to be fully investigated. *In vitro*, these cells are the main producers of inflammatory cytokines in response to LPS stimulation (Cros *et al.,* 2010). Additionally, patients with sepsis, SLE, severe asthma and rheumatoid arthritis exhibit an expansion in this subset (Cooper *et al.,* 2012; Moniuszko *et al.,* 2009; Mukherjee *et al.,* 2015; Poehlmann *et al.,* 2009; Radwan *et al.,* 2016), as was also show here during human endotoxemia which might suggest their function is appreciated during inflammatory challenge.

Although it was demonstrated that classical monocytes can give rise to non-classical monocytes, it is possible unknown sources of intermediate and non-classical monocytes exist. From the model described (**Figure 4.7**), re-entry back into the blood from tissue compartments was deemed unlikely, although, re-entry into the bone marrow from blood has been described in mice (Chong *et al.,* 2016; Varol *et al.,* 2007), therefore presenting a possible limitation to this model in humans.

At the time of performing these studies, monocytes were defined as described in Chapter 3. Since this definition, mononuclear phagocytes have been further re-defined. Within the classical monocyte compartment, $CD14^{+}$ DC have been characterised (Dutertre *et al.,* 2019) and an additional three further subsets have been described (Hamers *et al.,* 2019) (**Figure 6.1**). In addition, non-classical monocytes are made up of populations defined by SLAN (Cros *et al.,* 2010;

Hamers *et al.,* 2019; Schäkel *et al.,* 2002, 1999, 1998). Whilst studies have attempted to analyse the kinetics of SLAN^{+} monocytes following HSCT (Mimiola *et al.,* 2014), the earliest time point sampled was 21 days from HSCT, however, it is likely earlier time points are needed to appreciate whether differences exist between SLAN^{+} and SLAN^{-} monocytes. Future studies could examine the kinetic relationship between these subpopulations of monocyte subsets.

6.2.2. Circulating dendritic cells

The turnover of lymphoid and nonlymphoid tissue DC has been widely examined in mice (Fossum, 1989; Ginhoux *et al.,* 2009; Kamath *et al.,* 2002, 2000; Liu *et al.,* 2007; Steinman *et al.,* 1974), and has been extended to the human setting particularly in the dermis (Haniffa *et al.,* 2009; McGovern *et al.,* 2014). The circulating kinetics have been explored in macaques (Sugimoto *et al.,* 2015) and were consequently used to formulate a hypothesis for the human setting.

In humans, pre-DC, cDC1 and cDC appeared within one day of labelling, before that of monocytes. This adds to the evidence that dendritic cells do not arise from monocytes, as previously once thought. In line with the notion that pre-DC are precursors to cDC, deuterium labelling was observed at 6 hours in pre-DC prior that seen in cDC. It is also likely that bone marrow cDC contribute significantly to the circulating cDC pool. These data are currently being modelled to estimate the circulating lifespan of DC subsets and the relative contribution of blood pre-DC to the circulating cDC subsets.

The distinct kinetics of pDC from that of cDC, may represent a difference in lineage of cells as has been recently described (Dress *et al.,* 2019; Rodrigues *et al.,* 2018). If pDC are a heterogeneous population of myeloid and lymphoid origins, it would be interesting to investigate the turnover of these cells from both lineages once identifiable markers have been found.

The model proposed encompasses pDC, pre-DC, cDC1 and cDC2. Although not examined in this thesis, Villani and colleagues have demonstrated circulating $CD100^{+}$ $CD34^{+}$ progenitors can also give rise to DC populations (Villani *et al.,* 2017), therefore representing another source of DC. In addition, the relationship of the newly described cDC2 subsets described by Dutertre *et al.,* have not yet been explored. If $CD14^{+}$ cDC2 (previously identified as a monocyte) are bona fide DC, it would be expected these cells would exhibit a kinetic profile akin to cDC2 rather than classical monocytes.

In this thesis, the kinetics of monocyte and dendritic cell subsets was assessed in healthy, young males. Blood samples were obtained at the same time of day throughout the study to avoid confounding effects from circadian rhythms (Chong *et al.,* 2016; Nguyen *et al.,* 2013), however, future studies may examine how monocyte turnover varies during the day. Additional factors such as sex may influence turnover. Women have been described to have increased frequency of non-classical monocytes (Jiang *et al.,* 2014), therefore may exhibit differences in monocyte turnover compared to males. Furthermore, the elderly cohort are characterised by an increase in the number of intermediate and non-classical monocytes yet a decrease in DC numbers (Nyugen *et al.,* 2010; Ong *et al.,* 2018; Seidler *et al.,* 2010), which might be suggestive of an a shift towards monopoiesis. Therefore, this might prompt the need for exploring the kinetics of monocyte and dendritic cell precursors in the bone marrow.

These data here, lay the foundations for coming studies to examine changes in the turnover of mononuclear phagocytes in various settings.

6.3 Inflammatory kinetics of mononuclear phagocytes

Laying down the foundations of mononuclear phagocyte kinetics under steady-state in turn allowed for investigations into how the homeostatic turnover was affected under inflammatory conditions.

6.3.1 Human endotoxemia challenge

The endotoxin model initially served as a treatment against tumour malignancies and today serves as a platform to study inflammation in man under controlled experimental conditions. The model allows for the interrogation of the physiological, immunological, haematological and metabolic parameters in response to systemic inflammation (Fullerton *et al.,* 2016).

Following endotoxin challenge, a severe reduction in the number of monocyte and dendritic cells was observed, followed by an expansion in the number of classical and intermediate monocytes. The use of inflammatory models allows for the examination of early changes in cellular kinetics which may be missed in the clinical setting where samples are obtained hours, days or weeks after the initial insult. Therefore, it is possible that when studies report an expansion of circulating intermediate monocytes in patients with sepsis, rheumatoid arthritis or SLE (Cooper *et al.,* 2012; Mukherjee *et al.,* 2015; Poehlmann *et al.,* 2009), this may be due to timing at which samples are taken.

Deuterium labelling alongside the endotoxin model, demonstrated an early emergency release of bone marrow classical monocytes which would normally reside for approximately 1.6 days before being released. This reserve pool of monocytes may act as an emergency squad which are released in response to infection or injury. However, deuterium labelling did not support the *emergency* classical monocytes as a likely progenitor for the reappearing intermediate and non-classical monocytes. It is possible that these cells may return from a marinating source such as the lung or adherence to the endothelium. The spleen may represent a potential source as it has been described as a monocyte reservoir in mice (Swirski *et al.,* 2009) and humans (van der Laan *et al.,* 2014). Furthermore, as steady-state haematopoiesis is likely to be perturbed under these conditions, examination of the bone marrow could also provide insight into the source of intermediate and non-classical monocytes, as novel subsets have been described in mice which appear only under inflammatory conditions (Ikeda *et al.,* 2018; Satoh *et al.,* 2017). The

importance of monocyte kinetics in pathology can appreciated in a simian immunodeficiency virus (SIV) model of acquired immune deficiency syndrome (AIDS) in macaques. It was demonstrated classical monocytes also appeared in the circulation earlier compared to uninfected macaques, where monocyte turnover was shown to be a predictive marker of AIDS progression (Burdo *et al.,* 2010; Hasegawa *et al.,* 2009).

The returning monocytes exhibited a marked alteration in surface marker expression. Reduced HLA-DR expression during sepsis has been associated with an increased risk of nosocomial infections and death (Landelle *et al.,* 2010; Monneret *et al.,* 2006; Wu *et al.,* 2011). Low levels of HLA-DR expression have consequently been used as a marker of unresponsiveness in terms of monocyte function. Here, HLA-DR expression was markedly reduced on intermediate monocytes present at the early time points. As intermediate monocytes exhibit the highest HLA-DR expression, the effects of this reduced expression might be attributed to this subset. Future clinical studies should explore whether the correlation of HLA-DR is specific to intermediate monocytes rather than bulk monocytes.

DC reduction was also observed following endotoxin challenge and has similarly been observed in sepsis patients (Grimaldi *et al.,* 2011; Guisset *et al.,* 2007; Poehlmann *et al.,* 2009; Riccardi *et al.,* 2011). The significance of DC depletion can be appreciated in patients with heterozygous mutations in the *IRF8 allele* (T80A), where these patients have a specific loss of cDC2, and consequently suffer from recurrent bacterial infections (Hambleton *et al.,* 2011). Following systemic inflammation, DC have been observed to undergo apoptosis, the prevention of which improved survival outcome in experimental sepsis in mice (Efron *et al.,* 2004; Scumpia *et al.,* 2005). Similarly, FLT3L administration improved survival outcome in mice with burn wound infections and reversed endotoxin-induced immunosuppression (Toliver-Kinsky *et al.,* 2005; Wysocka *et al.,* 2005)**.** In the human setting, higher DC counts were observed in sepsis patients who survived compared with non-survivors (Guisset *et al.,* 2007), suggesting, restoration of DC is necessary to overcome the immunosuppressive state. Following endotoxin challenge, it has

been shown that neutrophil and lymphocytes numbers are restored by 24-48 hours (Unpublished data from Prof. Derek Gilroy), prior to that of DC. Similar observations have been made in mice (Pasquevich *et al.,* 2015), demonstrating monopoiesis is favoured over DC production following bacterial challenge. Therefore, if DC are the limiting immune cell responsible for the observed immunosuppression, therapeutics could target DC development to increase numbers, possibly with FLT3L administration. In addition to the loss of these cells, the impaired function of DC also likely contributes to pathophysiological basis of sepsis-induced immunosuppression. The inflammatory milieu skews DC function, as reduced cytokine secretion from DC has been observed in a murine cecal ligation punction model (Flohé *et al.,* 2006). In addition, reduced IL-2 secreting T cells were observed when cocultured with DC from these mice compared to control mice, consequently impacting on the adaptive immune system.

In reality, infections manifest at larger sustained doses of living gram-negative bacteria. The results here are in the context of a model of systemic inflammation. Nevertheless, the model serves a platform to study the immune response and identify potential therapeutic approaches which could be extended to the clinical setting.

6.3.2 Local UV-killed *E. coli* challenge

Inflammation can also manifest locally. Using a UV-killed *E. coli* model of acute local inflammation (Motwani *et al.,* 2016), the infiltrating kinetics of mononuclear phagocytes were assessed.

Monocyte and dendritic cells exhibited different circulating kinetic profiles in both steady-state and in response to endotoxin challenge. In response to UV-killed *E. coli*, both cell types were abundant at 24 hours post-challenge and declined thereafter.

Although blister monocytes declined by day 4, a few monocytes were observed. It would be interesting, to observe whether these monocyte-derived cells persisted long term as have previously been described in mice (Blériot *et al.,* 2015; Machiels *et al.,* 2017; Misharin *et al.,*

2017; Newson *et al.,* 2014; Yona *et al.,* 2013). In humans, long term engraftment of $CD14^+$ mononuclear phagocytes have been observed up to 11 years in the setting of liver transplantation in collaboration with Prof. Mala Maini and Dr. Laura Pallett (Unpublished, personal communication). On the other hand, dermal $CD14^+$ monocyte-derived cells have a half-life of fewer than 6 days and are continuously replenished by monocytes under steady-state (McGovern *et al.,* 2014). Although this could be answered with *in vivo* deuterium labelling in humans, the cell numbers required for GC/MS analysis are a current limitation at present

In mice, two major monocytes subsets are widely acknowledged (classical and non-classical), although recently further subsets have been described (Menezes *et al.,* 2016; Mildner *et al.,* 2017). Nevertheless, several murine studies demonstrate classical monocytes are initially recruited to the inflammatory site, which mature into monocyte-derived cells resembling non-classical monocytes (Dal-Secco *et al.,* 2015; Hilgendorf *et al.,* 2014; Zigmond *et al.,* 2012). In the blister model, classical monocytes were also initially seen at the site, which then appeared to take on an intermediate monocyte phenotype. It can be hypothesised that the initially appearing classical phenotype exhibits pro-inflammatory functions, which then mature into $CD16^+$ resolving cells resembling intermediate monocytes which dominate at 48 hours. Recently, in a model of LPS inhalation in humans, gene expression profiles of recruited classical monocytes to the lung demonstrated these cells were primed to modulating the immune response via the upregulation of chemokine and cytokines (Jardine *et al.,* 2019). Unfortunately, the expression profiles of the 'intermediate' phenotype were not assessed.

DC recruitment was also observed, where pre-DC were particularly observed at a higher concentration than in blood. Reasons for this may be owed to the proliferative capacity of pre-DC upon entering an inflamed site, though selective recruitment cannot be ruled out. Given that pre-DC are currently viewed as precursor cells to cDC1 and cDC2, pre-DC upregulated CD80 and CD86 at the inflammatory site. It is possible that under inflammatory conditions pre-DC are effector cells and development into cDC1 and cDC2 is restricted, as observed in HIV infected pre-

DC (Dr. Philippe Benaroch and Dr. Nicolas Ruffin, by communication). Though DC are found at minimal numbers in the blister in comparison to monocytes and other leukocyte populations (Motwani *et al.,* 2016), a single DC can scan up to 500 T cells per hour (Bousso and Robey, 2003), therefore the small number of these cells should not underestimate their potential importance. Due to the low number of DC obtained from a blister, functional assays were not feasible. DC subsets were sorted for single-cell RNA sequencing analysis to gain insight into the possible functions of these cells.

Local inflammation was measured here in response to intradermal challenge with UV-killed *E. coli* in healthy young volunteers. As mentioned above, genetic and lifestyle factors can influence the immune response.

Knowledge of the circulating and infiltrating kinetics may be beneficial in the clinical setting. In rheumatoid arthritis, an increased number of $CCR2^{+}$ cells have been observed in the synovial tissues of these patients. The CCL2-CCR2 axis has been implicated in driving the recruitment of monocytes into this inflammatory environment and consequently, CCR2 antagonists have been tested in rheumatoid arthritis patients (Vergunst *et al.,* 2008). Unfortunately, upon the administration of Plozalizumab, no changes were observed in $CCR2^{+}$ cell count in synovial tissue. The half-life of the drug has not been documented, however, was administered every two weeks. Given classical monocytes which exhibit the highest CCR2 expression exhibit an average lifespan of 1 day, it is possible that frequent doses of the drug are necessary in order to target the newly released classical monocytes to prevent migration into the tissues. However, other explanations are possible to explain these observations.

Collectively, the data shown in this thesis demonstrate the kinetics of human monocytes and dendritic cells under steady physiological conditions and experimental inflammation. Establishing the regulatory mechanisms that control these processes will be the next step in exploring human mononuclear phagocyte biology. These studies lay the foundations for

understanding the fundamental regulation of mononuclear phagocyte generation, differentiation and function will dictate future therapeutic avenues, depleting them when they are detrimental and boosting them when they are beneficial.

References

Abeles, R.D., McPhail, M.J., Sowter, D., Antoniades, C.G., Vergis, N., Vijay, G.K.M., Xystrakis, E., Khamri, W., Shawcross, D.L., Ma, Y., Wendon, J. a., Vergani, D., 2012. CD14, CD16 and HLA-DR reliably identifies human monocytes and their subsets in the context of pathologically reduced HLA-DR expression by CD14hi/CD16neg monocytes: Expansion of CD14hi/CD16pos and contraction of CD14lo/CD16pos monocytes in acute liver fail. Cytom. Part A 81 A, 823–834.

Ajami, B., Bennett, J.L., Krieger, C., McNagny, K.M., Rossi, F.M. V, 2011. Infiltrating monocytes trigger EAE progression, but do not contribute to the resident microglia pool. Nat. Neurosci. 14, 1142–1150.

Akashi, K., Traver, D., Miyamoto, T., Weissman, I.L., 2000. A clonogenic common myeloid progenitor that gives rise to all myeloid lineages. Nature 404, 193–197.

Alcántara-Hernández, M., Leylek, R., Wagar, L.E., Engleman, E.G., Keler, T., Marinkovich, M.P., Davis, M.M., Nolan, G.P., Idoyaga, J., 2017. High-Dimensional Phenotypic Mapping of Human Dendritic Cells Reveals Interindividual Variation and Tissue Specialization. Immunity 47, 1037-1050.e6.

Aliberti, J., Schulz, O., Pennington, D.J., Tsujimura, H., Reis e Sousa, C., Ozato, K., Sher, A., 2003. Essential role for ICSBP in the in vivo development of murine CD8alpha + dendritic cells. Blood 101, 305–310.

Andrews, R.G., Torok-Storb, B., Bernstein, I.D., 1983. Myeloid-Associated Differentiation Antigens on Stem Cells and Their Progeny Identified by Monoclonal Antibodies, Blood.

Ardavin, C., Shortman, K., 1992. Cell surface marker analysis of mouse thymic dendritic cells. Eur. J. Immunol. 22, 859–862.

Arnold, L., Henry, A., Poron, F., Baba-Amer, Y., Van Rooijen, N., Plonquet, A., Gherardi, R.K., Chazaud, B., 2007. Inflammatory monocytes recruited after skeletal muscle injury switch into antiinflammatory macrophages to support myogenesis. J. Exp. Med. 204, 1057–1069.

Arts, R.J.W., Moorlag, S.J.C.F.M., Novakovic, B., Li, Y., Wang, S.Y., Oosting, M., Kumar, V., Xavier, R.J., Wijmenga, C., Joosten, L.A.B., Reusken, C.B.E.M., Benn, C.S., Aaby, P., Koopmans, M.P., Stunnenberg, H.G., van Crevel, R., Netea, M.G., 2018. BCG Vaccination Protects against Experimental Viral Infection in Humans through the Induction of Cytokines Associated with Trained Immunity. Cell Host Microbe 23, 89-100.e5.

Aschoff, L., 1924. Das reticulo-endotheliale System. In: Kraus, F., Meyer, E., Minkowski, O., Müller, F., Sahli, H., Schittenhelm, A., Czerny, A., Heubner, O., Langstein, L. (Eds.), Ergebnisse Der Inneren Medizin Und Kinderheilkunde: Sechsundzwanzigster Band. Springer Berlin Heidelberg, Berlin, Heidelberg, pp. 1–118.

Asselin-Paturel, C., Boonstra, A., Dalod, M., Durand, I., Yessaad, N., Dezutter-Dambuyant, C., Vicari, A., O'Garra, A., Biron, C., Brière, F., Trinchieri, G., 2001. Mouse type I IFN-producing cells are immature APCs with plasmacytoid morphology. Nat. Immunol. 2, 1144–1150.

Auffermann-Gretzinger, S., Eger, L., Bornhäuser, M., Schäkel, K., Oelschlaegel, U., Schaich, M., Illmer, T., Thiede, C., Ehninger, G., 2006. Fast appearance of donor dendritic cells in human skin: Dynamics of skin and blood dendritic cells after allogeneic hematopoietic cell transplantation. Transplantation 81, 866–873.

Auffray, C., Fogg, D., Garfa, M., Elain, G., Join-Lambert, O., Kayal, S., Sarnacki, S., Cumano, A., Lauvau, G., Geissmann, F., 2007. Monitoring of blood vessels and tissues by a population of monocytes with patrolling behavior. Science 317, 666–70.

Bachem, A., Güttler, S., Hartung, E., Ebstein, F., Schaefer, M., Tannert, A., Salama, A., Movassaghi, K., Opitz, C., Mages, H.W., Henn, V., Kloetzel, P.M., Gurka, S., Kroczek, R.A., 2010. Superior antigen cross-presentation and XCR1 expression define human CD11c+CD141+ cells as homologues of mouse CD8+ dendritic cells. J. Exp. Med. 207, 1273–1281.

Bain, C.C., Bravo-Blas, A., Scott, C.L., Gomez Perdiguero, E., Geissmann, F., Henri, S., Malissen, B., Osborne, L.C., Artis, D., Mowat, A.M., 2014. Constant replenishment from circulating monocytes maintains the macrophage pool in the intestine of adult mice. Nat. Immunol. 15, 929–937.

Bajaña, S., Roach, K., Turner, S., Paul, J., Kovats, S., 2012. IRF4 Promotes Cutaneous Dendritic Cell Migration to Lymph Nodes during Homeostasis and Inflammation. J. Immunol. 189, 3368–3377.

Balner, H., 1963. Identification of peritoneal macrophages in mouse radiation chimeras. Transplantation.

Barth, M.W., Hendrzak, J.A., Melnicoff, M.J., Morahan, P.S., 1995. Review of the macrophage disappearance reaction. J. Leukoc. Biol. 57, 361–7.

Bianchini, M., Duchêne, J., Santovito, D., Schloss, M.J., Evrard, M., Winkels, H., Aslani, M., Mohanta, S.K., Horckmans, M., Blanchet, X., Lacy, M., Von Hundelshausen, P., Atzler, D., Habenicht, A., Gerdes, N., Pelisek, J., Ng, L.G., Steffens, S., Weber, C., Megens, R.T.A., 2019. PD-L1 expression on nonclassical monocytes reveals their origin and immunoregulatory function. Sci. Immunol. 4, eaar3054.

Bigley, V., Haniffa, M., Doulatov, S., Wang, X.-N., Dickinson, R., McGovern, N., Jardine, L., Pagan, S., Dimmick, I., Chua, I., Wallis, J., Lordan, J., Morgan, C., Kumararatne, D.S., Doffinger, R., van der Burg, M., van Dongen, J., Cant, A., Dick, J.E., Hambleton, S., Collin, M., 2011. The human syndrome of dendritic cell, monocyte, B and NK lymphoid deficiency. J. Exp. Med. 208, 227–234.

Blériot, C., Dupuis, T., Jouvion, G., Eberl, G., Disson, O., Lecuit, M., 2015. Liver-Resident Macrophage Necroptosis Orchestrates Type 1 Microbicidal Inflammation and Type-2-Mediated Tissue Repair during Bacterial Infection. Immunity 42, 145–158.

Bonasio, R., von Andrian, U.H., 2006. Generation, migration and function of circulating dendritic cells. Curr. Opin. Immunol.

Bousso, P., Robey, E., 2003. Dynamics of CD8+ T cell priming by dendritic cells in intact lymph nodes. Nat. Immunol. 4, 579–585.

Braun, N., Papadopoulos, T., Müller-Hermelink, H.K., 1988. Cell cycle dependent distribution of the proliferation-associated Ki-67 antigen in human embryonic lung cells. Virchows Arch. B. Cell Pathol. Incl. Mol. Pathol. 56, 25–33.

Breton, G., Lee, J., Zhou, Y.J., Schreiber, J.J., Keler, T., Puhr, S., Anandasabapathy, N., Schlesinger, S., Caskey, M., Liu, K., Nussenzweig, M.C., 2015. Circulating precursors of human CD1c+ and CD141+ dendritic cells. J. Exp. Med. 212, 401–13.

Brocker, T., 1999. The role of dendritic cells in T cell selection and survival. J. Leukoc. Biol. 66, 331–335.

Burdo, T.H., Soulas, C., Orzechowski, K., Button, J., Krishnan, A., Sugimoto, C., Alvarez, X., Kuroda, M.J., Williams, K.C., 2010. Increased monocyte turnover from bone marrow correlates with severity of SIV encephalitis and CD163 levels in plasma. PLoS Pathog. 6, e1000842.

Buttgereit, A., Lelios, I., Yu, X., Vrohlings, M., Krakoski, N.R., Gautier, E.L., Nishinakamura, R., Becher, B., Greter, M., 2016. Sall1 is a transcriptional regulator defining microglia identity and function. Nat. Immunol. 17, 1397–1406.

Cabeza-Cabrerizo, M., van Blijswijk, J., Wienert, S., Heim, D., Jenkins, R.P., Chakravarty, P., Rogers, N., Frederico, B., Acton, S., Beerling, E., van Rheenen, J., Clevers, H., Schraml, B.U., Bajénoff, M., Gerner, M., Germain, R.N., Sahai, E., Klauschen, F., Reis e Sousa, C., 2019. Tissue clonality of dendritic cell subsets and emergency DCpoiesis revealed by multicolor fate mapping of DC progenitors. Sci. Immunol. 4, eaaw1941.

Cailhier, J.F., Partolina, M., Vuthoori, S., Wu, S., Ko, K., Watson, S., Savill, J., Hughes, J., Lang, R.A., 2005. Conditional macrophage ablation demonstrates that resident macrophages initiate acute peritoneal inflammation. J. Immunol. 174, 2336–42.

Calzetti, F., Tamassia, N., Micheletti, A., Finotti, G., Bianchetto-Aguilera, F., Cassatella, M.A., 2018. Human dendritic cell subset 4 (DC4) correlates to a subset of CD14 dim/− CD16 ++ monocytes. J. Allergy Clin. Immunol. 141, 2276-2279.e3.

Carlin, L.M., Stamatiades, E.G., Auffray, C., Hanna, R.N., Glover, L., Vizcay-Barrena, G., Hedrick, C.C., Cook, H.T., Diebold, S., Geissmann, F., 2013. Nr4a1-dependent Ly6Clow monocytes monitor endothelial cells and orchestrate their disposal. Cell 153, 362–375.

Carrel, A., Ebeling, A.H., 1926. The fundamental properties of the fibroblast and the macrophage. J. Exp. Med. 44, 285–306.

Chain, B.M., Kay, P.M., Feldmann, M., 1986. The cellular pathway of antigen presentation: biochemical and functional analysis of antigen processing in dendritic cells and macrophages. Immunology 58, 271–6.

Chong, S.Z., Evrard, M., Devi, S., Chen, J., Lim, J.Y., See, P., Zhang, Y., Adrover, J.M., Lee, B., Tan, L., Li, J.L.Y., Liong, K.H., Phua, C., Balachander, A., Boey, A., Liebl, D., Tan, S.M., Chan, J.K.Y., Balabanian, K., Harris, J.E., Bianchini, M., Weber, C., Duchene, J., Lum, J., Poidinger, M., Chen, Q., Rénia, L., Wang, C.-I., Larbi, A., Randolph, G.J., Weninger, W., Looney, M.R., Krummel, M.F., Biswas, S.K., Ginhoux, F., Hidalgo, A., Bachelerie, F., Ng, L.G., 2016. CXCR4 identifies transitional bone marrow premonocytes that replenish the mature monocyte pool for peripheral responses. J. Exp. Med. 213, 2293–2314.

Cisse, B., Caton, M.L., Lehner, M., Maeda, T., Scheu, S., Locksley, R., Holmberg, D., Zweier, C., den Hollander, N.S., Kant, S.G., Holter, W., Rauch, A., Zhuang, Y., Reizis, B., 2008. Transcription Factor E2-2 Is an Essential and Specific Regulator of Plasmacytoid Dendritic Cell Development. Cell 135, 37–48.

Cline, M.J., Moore, M.A., 1972. Embryonic origin of the mouse macrophage. Blood 39, 842–9.

Collison, J.L., Carlin, L.M., Eichmann, M., Geissmann, F., Peakman, M., 2015. Heterogeneity in the Locomotory Behavior of Human Monocyte Subsets over Human Vascular Endothelium In Vitro. J. Immunol. 195, 1162–70.

Coombes, J.L., Siddiqui, K.R.R., Arancibia-Cárcamo, C. V., Hall, J., Sun, C.M., Belkaid, Y., Powrie, F., 2007. A functionally specialized population of mucosal CD103+ DCs induces Foxp3+ regulatory T cells via a TGF-β -and retinoic acid-dependent mechanism. J. Exp. Med. 204, 1757–1764.

Cooper, D.L., Martin, S.G., Robinson, J.I., Mackie, S.L., Charles, C.J., Nam, J., Isaacs, J.D., Emery, P., Morgan, A.W., 2012. FcγRIIIa expression on monocytes in rheumatoid arthritis: Role in immune-complex stimulated TNF production and non-response to methotrexate therapy. PLoS One 7, e28918.

Coquet, J.M., Ribot, J.C., Bąbała, N., Middendorp, S., van der Horst, G., Xiao, Y., Neves, J.F., Fonseca-Pereira, D., Jacobs, H., Pennington, D.J., Silva-Santos, B., Borst, J., 2013. Epithelial and dendritic cells in the thymic medulla promote CD4+Foxp3+ regulatory T cell development via the CD27-CD70 pathway. J. Exp. Med. 210, 715–28.

Cros, J., Cagnard, N., Woollard, K., Patey, N., Zhang, S.-Y., Senechal, B., Puel, A., Biswas, S.K., Moshous, D., Picard, C., Jais, J.-P., D'Cruz, D., Casanova, J.-L., Trouillet, C., Geissmann, F., 2010. Human CD14dim Monocytes Patrol and Sense Nucleic Acids and Viruses via TLR7 and TLR8 Receptors. Immunity 33, 375–386.

Cytlak, U., Resteu, A., Pagan, S., Green, K., Milne, P., Maisuria, S., McDonald, D., Hulme, G., Filby, A., Carpenter, B., Queen, R., Hambleton, S., Hague, R., Allen, H.L., Thaventhiran, J., Doody, G., Collin, M., Bigley, V., 2019. Differential IRF8 Requirement Defines Two Pathways of Dendritic Cell Development in Humans. Immun. (Sneak Peak, under Rev.

Dai, X.-M., Ryan, G.R., Hapel, A.J., Dominguez, M.G., Russell, R.G., Kapp, S., Sylvestre, V., Stanley, E.R., 2002. Targeted disruption of the mouse colony-stimulating factor 1 receptor gene results in osteopetrosis, mononuclear phagocyte deficiency, increased primitive progenitor cell frequencies, and reproductive defects. Blood 99, 111–20.

Dal-Secco, D., Wang, J., Zeng, Z., Kolaczkowska, E., Wong, C.H.Y., Petri, B., Ransohoff, R.M., Charo, I.F., Jenne, C.N., Kubes, P., 2015. A dynamic spectrum of monocytes arising from the in situ reprogramming of CCR2 + monocytes at a site of sterile injury. J. Exp. Med. 212, 447–456.

Damasceno, D., Andrés, M.P., van den Bossche, W.B., Flores-Montero, J., de Bruin, S., Teodosio, C., van Dongen, J.J., Orfao, A., Almeida, J., 2016. Expression profile of novel cell surface molecules on different subsets of human peripheral blood antigen-presenting cells. Clin. Transl. Immunol. 5, e100.

Davey, G.M., Wojtasiak, M., Proietto, A.I., Carbone, F.R., Heath, W.R., Bedoui, S., 2010. Cutting edge: priming of CD8 T cell immunity to herpes simplex virus type 1 requires cognate TLR3 expression in vivo. J. Immunol. 184, 2243–6.

Davies, L.C., Rosas, M., Jenkins, S.J., Liao, C.-T., Scurr, M.J., Brombacher, F., Fraser, D.J., Allen, J.E., Jones, S. a, Taylor, P.R., 2013. Distinct bone marrow-derived and tissue-resident macrophage lineages proliferate at key stages during inflammation. Nat. Commun. 4, 1886.

Davies, L.C., Rosas, M., Smith, P.J., Fraser, D.J., Jones, S.A., Taylor, P.R., 2011. A quantifiable proliferative burst of tissue macrophages restores homeostatic macrophage populations after acute inflammation. Eur. J. Immunol. 41, 2155–2164.

Delamarre, L., Pack, M., Chang, H., Mellman, I., Trombetta, E.S., 2005. Differential lysosomal proteolysis in antigen-presenting cells determines antigen fate. Science 307, 1630–4.

den Haan, J.M., Lehar, S.M., Bevan, M.J., 2000. CD8(+) but not CD8(-) dendritic cells cross-prime cytotoxic T cells in vivo. J. Exp. Med. 192, 1685–96.

Desch, A.N., Randolph, G.J., Murphy, K., Gautier, E.L., Kedl, R.M., Lahoud, M.H., Caminschi, I., Shortman, K., Henson, P.M., Jakubzick, C. V, 2011. CD103 + pulmonary dendritic cells preferentially acquire and present apoptotic cell-associated antigen. J. Exp. Med. 208, 1789–1797.

Ding, Y., Chung, C.-S., Newton, S., Chen, Y., Carlton, S., Albina, J.E., Ayala, A., 2004. Polymicrobial sepsis induces divergent effects on splenic and peritoneal dendritic cell function in mice. Shock 22, 137–44.

Doerschuk, C.M., Beyers, N., Coxson, H.O., Wiggs, B., Hogg, J.C., 1993. Comparison of neutrophil and capillary diameters and their relation to neutrophil sequestration in the lung. J. Appl. Physiol. 74, 3040–5.

Doherty, D.E., Downey, G.P., Schwab, B., Elson, E., Worthen, G.S., 1994. Lipolysaccharide-induced monocyte retention in the lung. Role of monocyte stiffness, actin assembly, and CD18-dependent adherence. J. Immunol. 153, 241–55.

Donnenberg, V.S., O'Connell, P.J., Logar, A.J., Zeevi, A., Thomson, A.W., Donnenberg, A.D., 2001. Rare-event analysis of circulating human dendritic cell subsets and their presumptive mouse counterparts. Transplantation 72, 1946–1951.

Dorner, B.G., Dorner, M.B., Zhou, X., Opitz, C., Mora, A., Güttler, S., Hutloff, A., Mages, H.W., Ranke, K., Schaefer, M., Jack, R.S., Henn, V., Kroczek, R.A., 2009. Selective Expression of the Chemokine Receptor XCR1 on Cross-presenting Dendritic Cells Determines Cooperation with CD8 + T Cells. Immunity 31, 823–833.

Dress, R.J., Dutertre, C.A., Giladi, A., Schlitzer, A., Low, I., Shadan, N.B., Tay, A., Lum, J., Kairi, M.F.B.M., Hwang, Y.Y., Becht, E., Cheng, Y., Chevrier, M., Larbi, A., Newell, E.W., Amit, I., Chen, J., Ginhoux, F., 2019. Plasmacytoid dendritic cells develop from Ly6D+ lymphoid progenitors distinct from the myeloid lineage. Nat. Immunol. 20, 852–864.

Dudziak, D., Kamphorst, A.O., Heidkamp, G.F., Buchholz, V.R., Trumpfheller, C., Yamazaki, S., Cheong, C., Liu, K., Lee, H.W., Chae, G.P., Steinman, R.M., Nussenzweig, M.C., 2007. Differential antigen processing by dendritic cell subsets in vivo. Science (80-.). 315, 107–111.

Dutertre, C.-A., Amraoui, S., DeRosa, A., Jourdain, J.-P., Vimeux, L., Goguet, M., Degrelle, S., Feuillet, V., Liovat, A.-S., Müller-Trutwin, M., Decroix, N., Deveau, C., Meyer, L., Goujard, C., Loulergue, P., Launay, O., Richard, Y., Hosmalin, A., 2012. Pivotal role of M-DC8+ monocytes from viremic HIV-infected patients in TNFα overproduction in response to microbial products. Blood 120, 2259–2268.

Dutertre, C.-A., Becht, E., Irac, S.E., Khalilnezhad, A., Narang, V., Khalilnezhad, S., Ng, P.Y., van den Hoogen, L.L., Leong, J.Y., Lee, B., Chevrier, M., Zhang, X.M., Yong, P.J.A., Koh, G., Lum, J., Howland, S.W., Mok, E., Chen, J., Larbi, A., Tan, H.K.K., Lim, T.K.H., Karagianni, P., Tzioufas, A.G., Malleret, B., Brody, J., Albani, S., van Roon, J., Radstake, T., Newell, E.W., Ginhoux, F., 2019. Single-Cell Analysis of Human Mononuclear Phagocytes Reveals Subset-Defining Markers and Identifies Circulating Inflammatory Dendritic Cells. Immunity 51, 573-589.e8.

Ebert, R.H., Florey, H.W., 1939. The Extravascular Development of the Monocyte Observed In vivo. Br. J. Exp. Pathol. 20, 342.

Efron, P.A., Martins, A., Minnich, D., Tinsley, K., Ungaro, R., Bahjat, F.R., Hotchkiss, R., Clare-Salzler, M., Moldawer, L.L., 2004. Characterization of the systemic loss of dendritic cells in murine lymph nodes during polymicrobial sepsis. J. Immunol. 173, 3035–43.

Eguíluz-Gracia, I., Bosco, A., Dollner, R., Melum, G.R., Lexberg, M.H., Jones, A.C., Dheyauldeen, S.A., Holt, P.G., Bækkevold, E.S., Jahnsen, F.L., 2016. Rapid recruitment of CD14+ monocytes in experimentally induced allergic rhinitis in human subjects. J. Allergy Clin. Immunol. 137, 1872-1881.e12.

Epelman, S., Lavine, K.J., Beaudin, A.E., Sojka, D.K., Carrero, J.A., Calderon, B., Brija, T., Gautier, E.L., Ivanov, S., Satpathy, A.T., Schilling, J.D., Schwendener, R., Sergin, I., Razani, B., Forsberg, E.C., Yokoyama, W.M., Unanue, E.R., Colonna, M., Randolph, G.J., Mann, D.L., 2014. Embryonic and adult-derived resident cardiac macrophages are maintained through distinct mechanisms at steady state and during inflammation. Immunity 40, 91–104.

Feldman, M., Fitzgerald-Bocarsly, P., 1990. Sequential enrichment and immunocytochemical visualization of human interferon-alpha-producing cells. J. Interferon Res. 10, 435–46.

Flohé, S.B., Agrawal, H., Schmitz, D., Gertz, M., Flohé, S., Schade, F.U., 2006. Dendritic cells during polymicrobial sepsis rapidly mature but fail to initiate a protective Th1-type immune response. J. Leukoc. Biol. 79, 473–81.

Foote, J.R., Patel, A.A., Yona, S., Segal, A.W., 2019. Variations in the phagosomal environment of human neutrophils and mononuclear phagocyte subsets. Front. Immunol. 10, 188.

Fossum, S., 1989. The life history of dendritic leukocytes (DL). Curr. Top. Pathol. 79, 101–24.

Frankenberger, M., Ekici, A.B., Angstwurm, M.W., Hoffmann, H., Hofer, T.P.J., Heimbeck, I., Meyer, P., Lohse, P., Wjst, M., Häussinger, K., Reis, A., Ziegler-Heitbrock, L., 2013. A defect of CD16-positive monocytes can occur without disease. Immunobiology 218, 169–174.

Fullerton, J.N., Segre, E., De Maeyer, R.P.H., Maini, A.A.N., Gilroy, D.W., 2016. Intravenous Endotoxin Challenge in Healthy Humans: An Experimental Platform to Investigate and Modulate Systemic Inflammation. J. Vis. Exp. 1–8.

Gamrekelashvili, J., Giagnorio, R., Jussofie, J., Soehnlein, O., Duchene, J., Briseño, C.G., Ramasamy, S.K., Krishnasamy, K., Limbourg, A., Häger, C., Kapanadze, T., Ishifune, C., Hinkel, R., Radtke, F., Strobl, L.J., Zimber-Strobl, U., Napp, L.C., Bauersachs, J., Haller, H., Yasutomo, K., Kupatt, C., Murphy, K.M., Adams, R.H., Weber, C., Limbourg, F.P., 2016. Regulation of monocyte cell fate by blood vessels mediated by Notch signalling. Nat. Commun. 7, 12597.

Gautier, E.L., Huby, T., Saint-Charles, F., Ouzilleau, B., Chapman, M.J., Lesnik, P., 2008. Enhanced Dendritic Cell Survival Attenuates Lipopolysaccharide-Induced Immunosuppression and Increases Resistance to Lethal Endotoxic Shock. J. Immunol. 180, 6941–6946.

Gautier, E.L., Ivanov, S., Lesnik, P., Randolph, G.J., 2013. Local apoptosis mediates clearance of macrophages from resolving inflammation in mice. Blood 122, 2714–2722.

Geissmann, F., Jung, S., Littman, D.R., 2003. Blood monocytes consist of two principal subsets with distinct migratory properties. Immunity 19, 71–82.

Gerdes, J., Lemke, H., Baisch, H., Wacker, H.H., Schwab, U., Stein, H., 1984. Cell cycle analysis of a cell proliferation-associated human nuclear antigen defined by the monoclonal antibody Ki-67. J. Immunol. 133, 1710–5.

Ghosh, H.S., Cisse, B., Bunin, A., Lewis, K.L., Reizis, B., 2010. Continuous Expression of the Transcription Factor E2-2 Maintains the Cell Fate of Mature Plasmacytoid Dendritic Cells. Immunity 33, 905–916.

Ginhoux, F., Greter, M., Leboeuf, M., Nandi, S., See, P., Gokhan, S., Mehler, M.F., Conway, S.J., Ng, L.G., Stanley, E.R., Samokhvalov, I.M., Merad, M., 2010. Fate mapping analysis reveals that adult microglia derive from primitive macrophages. Science 330, 841–5.

Ginhoux, F., Liu, K., Helft, J., Bogunovic, M., Greter, M., Hashimoto, D., Price, J., Yin, N., Bromberg, J., Lira, S.A., Stanley, E.R., Nussenzweig, M., Merad, M., 2009. The origin and development of nonlymphoid tissue CD103 + DCs. J. Exp. Med. 206, 3115–3130.

Golden, J.B., Groft, S.G., Squeri, M. V, Debanne, S.M., Ward, N.L., McCormick, T.S., Cooper, K.D., 2015. Chronic Psoriatic Skin Inflammation Leads to Increased Monocyte Adhesion and Aggregation. J. Immunol. 195, 2006–2018.

Gordon, S., 2008. Elie Metchnikoff: Father of natural immunity. Eur. J. Immunol. 38, 3257–3264.

Grajales-Reyes, G.E., Iwata, A., Albring, J., Wu, X., Tussiwand, R., KC, W., Kretzer, N.M., Briseño, C.G., Durai, V., Bagadia, P., Haldar, M., Schönheit, J., Rosenbauer, F., Murphy, T.L., Murphy, K.M., 2015. Batf3 maintains autoactivation of Irf8 for commitment of a CD8α+ conventional DC clonogenic progenitor. Nat. Immunol. 16, 708–717.

Griffin, J.D., Ritz, J., Nadler, L.M., Schlossman, S.F., 1981. Expression of myeloid differentiation antigens on normal and malignant myeloid cells. J. Clin. Invest. 68, 932–41.

Grimaldi, D., Louis, S., Pène, F., Sirgo, G., Rousseau, C., Claessens, Y.E., Vimeux, L., Cariou, A., Mira, J.P., Hosmalin, A., Chiche, J.D., 2011. Profound and persistent decrease of circulating dendritic cells is associated with ICU-acquired infection in patients with septic shock. Intensive Care Med. 37, 1438–1446.

Guilliams, M., Crozat, K., Henri, S., Tamoutounour, S., Grenot, P., Devilard, E., Bovis, B. de, Alexopoulou, L., Dalod, M., Malissen, B., 2010. Skin-draining lymph nodes contain dermis-derived CD103− dendritic cells that constitutively produce retinoic acid and induce Foxp3+ regulatory T cells. Blood 115, 1958–1968.

Guilliams, M., Dutertre, C.-A., Scott, C.L., McGovern, N., Sichien, D., Chakarov, S., Van Gassen, S., Chen, J., Poidinger, M., De Prijck, S., Tavernier, S.J., Low, I., Irac, S.E., Mattar, C.N., Sumatoh, H.R., Low, G.H.L., Chung, T.J.K., Chan, D.K.H., Tan, K.K., Hon, T.L.K., Fossum, E., Bogen, B., Choolani, M., Chan, J.K.Y., Larbi, A., Luche, H., Henri, S., Saeys, Y., Newell, E.W., Lambrecht, B.N., Malissen, B., Ginhoux, F., 2016. Unsupervised High-Dimensional Analysis Aligns Dendritic Cells across Tissues and Species. Immunity 45, 669–684.

Guilliams, M., Mildner, A., Yona, S., 2018. Developmental and Functional Heterogeneity of Monocytes. Immunity.

Guilliams, M., Scott, C.L., 2017. Does niche competition determine the origin of tissue-resident macrophages? Nat. Rev. Immunol. 17, 451–460.

Guisset, O., Dilhuydy, M.-S., Thiébaut, R., Lefèvre, J., Camou, F., Sarrat, A., Gabinski, C., Moreau, J.-F., Blanco, P., 2007. Decrease in circulating dendritic cells predicts fatal outcome in septic shock. Intensive Care Med. 33, 148–152.

Günther, P., Cirovic, B., Baßler, K., Händler, K., Becker, M., Dutertre, C.A.A., Bigley, V., Newell, E., Collin, M., Ginhoux, F., Schlitzer, A., Schultze, J.L.L., 2019. A rule-based data-informed cellular consensus map of the human mononuclear phagocyte cell space. bioRxiv 658179.

Hacker, C., Kirsch, R.D., Ju, X.-S., Hieronymus, T., Gust, T.C., Kuhl, C., Jorgas, T., Kurz, S.M., Rose-John, S., Yokota, Y., Zenke, M., 2003. Transcriptional profiling identifies Id2 function in dendritic cell development. Nat. Immunol. 4, 380–386.

Hambleton, S., Salem, S., Bustamante, J., Bigley, V., Boisson-Dupuis, S., Azevedo, J., Fortin, A., Haniffa, M., Ceron-Gutierrez, L., Bacon, C.M., Menon, G., Trouillet, C., McDonald, D., Carey, P., Ginhoux, F., Alsina, L., Zumwalt, T.J., Kong, X.-F., Kumararatne, D., Butler, K., Hubeau, M., Feinberg, J., Al-Muhsen, S., Cant, A., Abel, L., Chaussabel, D., Doffinger, R., Talesnik, E., Grumach, A., Duarte, A., Abarca, K., Moraes-Vasconcelos, D., Burk, D., Berghuis, A., Geissmann, F., Collin, M., Casanova, J.-L., Gros, P., 2011. *IRF8* Mutations and Human Dendritic-Cell Immunodeficiency. N. Engl. J. Med. 365, 127–138.

Hamers, A.A.J., Dinh, H.Q., Thomas, G.D., Marcovecchio, P., Blatchley, A., Nakao, C.S., Kim, C., McSkimming, C., Taylor, A.M., Nguyen, A.T., McNamara, C.A., Hedrick, C.C., 2019. Human Monocyte Heterogeneity as Revealed by High-Dimensional Mass Cytometry. Arterioscler. Thromb. Vasc. Biol. 39, 25–36.

Haniffa, M., Ginhoux, F., Wang, X., Bigley, V., Abel, M., Dimmick, I., Bullock, S., Grisotto, M., Booth, T., Taub, P., Hilkens, C., Merad, M., Collin, M., 2009. Differential rates of replacement of human dermal dendritic cells and macrophages during hematopoietic stem cell transplantation. J. Exp. Med. 206, 371–85.

Haniffa, M., Shin, A., Bigley, V., McGovern, N., Teo, P., See, P., Wasan, P.S., Wang, X.-N., Malinarich, F., Malleret, B., Larbi, A., Tan, P., Zhao, H., Poidinger, M., Pagan, S., Cookson, S., Dickinson, R., Dimmick, I., Jarrett, R.F., Renia, L., Tam, J., Song, C., Connolly, J., Chan, J.K.Y.Y., Gehring, A., Bertoletti, A., Collin, M., Ginhoux, F., 2012. Human tissues contain CD141hi cross-presenting dendritic cells with functional homology to mouse CD103+ nonlymphoid dendritic cells. Immunity 37, 60–73.

Hanna, R.N., Carlin, L.M., Hubbeling, H.G., Nackiewicz, D., Green, A.M., Punt, J.A., Geissmann, F., Hedrick, C.C., 2011. The transcription factor NR4A1 (Nur77) controls bone marrow differentiation and the survival of Ly6C− monocytes. Nat. Immunol. 12, 778–785.

Hanna, R.N., Cekic, C., Sag, D., Tacke, R., Thomas, G.D., Nowyhed, H., Herrley, E., Mcardle, S., Wu, R., Peluso, E., 2015. Patrolling monocytes control tumor metastasis to the lung. Science (80-.). 1–9.

Hanna, R.N., Shaked, I., Hubbeling, H.G., Punt, J.A., Wu, R., Herrley, E., Zaugg, C., Pei, H., Geissmann, F., Ley, K., Hedrick, C.C., 2012. NR4A1 (Nur77) deletion polarizes macrophages toward an inflammatory phenotype and increases atherosclerosis. Circ. Res. 110, 416–27.

Hänsel, A., Günther, C., Ingwersen, J., Starke, J., Schmitz, M., Bachmann, M., Meurer, M., Rieber, E.P., Schäkel, K., 2011. Human slan (6-sulfo LacNAc) dendritic cells are inflammatory dermal dendritic cells in psoriasis and drive strong Th17/Th1 T-cell responses. J. Allergy Clin. Immunol. 127, 787-794.e9.

Hasegawa, A., Liu, H., Ling, B., Borda, J.T., Alvarez, X., Sugimoto, C., Vinet-Oliphant, H., Kim, W.-K., Williams, K.C., Ribeiro, R.M., Lackner, A.A., Veazey, R.S., Kuroda, M.J., 2009. The level of monocyte turnover predicts disease progression in the macaque model of AIDS. Blood 114, 2917–25.

Hashimoto, D., Chow, A., Noizat, C., Teo, P., Beasley, M.B., Leboeuf, M., Becker, C.D., See, P., Price, J., Lucas, D., Greter, M., Mortha, A., Boyer, S.W., Forsberg, E.C., Tanaka, M., van Rooijen, N., García-Sastre, A., Stanley, E.R., Ginhoux, F., Frenette, P.S., Merad, M., 2013. Tissue-Resident Macrophages Self-Maintain Locally throughout Adult Life with Minimal Contribution from Circulating Monocytes. Immunity 38, 792–804.

Hassanzadeh Ghassabeh, G., De Baetselier, P., Brys, L., Noël, W., Van Ginderachter, J.A., Meerschaut, S., Beschin, A., Brombacher, F., Raes, G., 2006. Identification of a common gene signature for type II cytokine–associated myeloid cells elicited in vivo in different pathologic conditions. Blood 108, 575–583.

Hawiger, D., Inaba, K., Dorsett, Y., Guo, M., Mahnke, K., Rivera, M., Ravetch, J. V., Steinman, R.M., Nussenzweig, M.C., 2001. Dendritic cells induce peripheral T cell unresponsiveness under steady state conditions in vivo. J. Exp. Med. 194, 769–779.

Helft, J., Anjos-Afonso, F., van der Veen, A.G., Chakravarty, P., Bonnet, D., Reis e Sousa, C., 2017. Dendritic Cell Lineage Potential in Human Early Hematopoietic Progenitors. Cell Rep. 20, 529–537.

Hémont, C., Neel, A., Heslan, M., Braudeau, C., Josien, R., 2013. Human blood mDC subsets exhibit distinct TLR repertoire and responsiveness. J. Leukoc. Biol. 93, 599–609.

Hettinger, J., Richards, D.M., Hansson, J., Barra, M.M., Joschko, A.-C.C., Krijgsveld, J., Feuerer, M., 2013. Origin of monocytes and macrophages in a committed progenitor. Nat. Immunol. 14, 821–30.

Hildner, K., Edelson, B.T., Purtha, W.E., Diamond, M., Matsushita, H., Kohyama, M., Calderon, B., Schraml, B.U., Unanue, E.R., Diamond, M.S., Schreiber, R.D., Murphy, T.L., Murphy, K.M., 2008. Batf3 deficiency reveals a critical role for CD8alpha+ dendritic cells in cytotoxic T cell immunity. Science 322, 1097–100.

Hilgendorf, I., Gerhardt, L.M.S., Tan, T.C., Winter, C., Holderried, T.A.W., Chousterman, B.G., Iwamoto, Y., Liao, R., Zirlik, A., Scherer-Crosbie, M., Hedrick, C.C., Libby, P., Nahrendorf, M., Weissleder, R., Swirski, F.K., 2014. Ly-6Chigh monocytes depend on Nr4a1 to balance both inflammatory and reparative phases in the infarcted myocardium. Circ. Res. 114, 1611–22.

Hoeffel, G., Wang, Y., Greter, M., See, P., Teo, P., Malleret, B., Leboeuf, M., Low, D., Oller, G., Almeida, F., Choy, S.H.Y., Grisotto, M., Renia, L., Conway, S.J., Stanley, E.R., Chan, J.K.Y., Ng, L.G., Samokhvalov, I.M., Merad, M., Ginhoux, F., 2012. Adult Langerhans cells derive predominantly from embryonic fetal liver monocytes with a minor contribution of yolk sac-derived macrophages. J. Exp. Med. 209, 1167–81.

Hofer, T.P., Zawada, A.M., Frankenberger, M., Skokann, K., Satzl, A.A., Gesierich, W., Schuberth, M., Levin, J., Danek, A., Rotter, B., Heine, G.H., Ziegler-Heitbrock, L., 2015. slan-defined subsets of CD16-positive monocytes: impact of granulomatous inflammation and M-CSF receptor mutation. Blood 126, 2601–2610.

Ikeda, N., Asano, K., Kikuchi, K., Uchida, Y., Ikegami, H., Takagi, R., Yotsumoto, S., Shibuya, T., Makino-Okamura, C., Fukuyama, H., Watanabe, T., Ohmuraya, M., Araki, K., Nishitai, G., Tanaka, M., 2018. Emergence of immunoregulatory Ym1 + Ly6C hi monocytes during recovery phase of tissue injury. Sci. Immunol. 3, eaat0207.

Ingersoll, M.A., Spanbroek, R., Lottaz, C., Gautier, E.L., Frankenberger, M., Hoffmann, R., Lang, R., Haniffa, M., Collin, M., Tacke, F., Habenicht, A.J.R., Ziegler-Heitbrock, L., Randolph, G.J., 2010. Comparison of gene expression profiles between human and mouse monocyte subsets. Blood 115, e10-9.

Isaacs, A., Lindenmann, J., 1957. Virus interference. I. The interferon. Proc. R. Soc. London. Ser. B, Biol. Sci. 147, 258–67.

Iwasaki, H., Akashi, K., 2007. Myeloid lineage commitment from the hematopoietic stem cell. Immunity 26, 726–40.

Jackson, J.T., Hu, Y., Liu, R., Masson, F., D'Amico, A., Carotta, S., Xin, A., Camilleri, M.J., Mount, A.M., Kallies, A., Wu, L., Smyth, G.K., Nutt, S.L., Belz, G.T., 2011. Id2 expression delineates differential checkpoints in the genetic program of CD8α+ and CD103+ dendritic cell lineages. EMBO J. 30, 2690–704.

Jakubzick, C., Gautier, E.L., Gibbings, S.L., Sojka, D.K., Schlitzer, A., Johnson, T.E., Ivanov, S., Duan, Q., Bala, S., Condon, T., van Rooijen, N., Grainger, J.R., Belkaid, Y., Ma'ayan, A., Riches, D.W.H., Yokoyama, W.M., Ginhoux, F., Henson, P.M., Randolph, G.J., 2013. Minimal differentiation of classical monocytes as they survey steady-state tissues and transport antigen to lymph nodes. Immunity 39, 599–610.

Jakubzick, C., Tacke, F., Llodra, J., van Rooijen, N., Randolph, G.J., 2006. Modulation of Dendritic Cell Trafficking to and from the Airways. J. Immunol. 176, 3578–3584.

Janssen, W.J., Barthel, L., Muldrow, A., Oberley-Deegan, R.E., Kearns, M.T., Jakubzick, C., Henson, P.M., 2011. Fas determines differential fates of resident and recruited macrophages during resolution of acute lung injury. Am. J. Respir. Crit. Care Med. 184, 547–560.

Jardine, L., Wiscombe, S., Reynolds, G., McDonald, D., Fuller, A., Green, K., Filby, A., Forrest, I., Ruchaud-Sparagano, M.-H., Scott, J., Collin, M., Haniffa, M., Simpson, A.J., 2019. Lipopolysaccharide inhalation recruits monocytes and dendritic cell subsets to the alveolar airspace. Nat. Commun. 10, 1999.

Jenkins, S.J., Ruckerl, D., Cook, P.C., Jones, L.H., Finkelman, F.D., van Rooijen, N., MacDonald, A.S., Allen, J.E., 2011. Local Macrophage Proliferation, Rather than Recruitment from the Blood, Is a Signature of TH2 Inflammation. Science (80-.). 332, 1284–1288.

Jenner, W., Motwani, M., Veighey, K., Newson, J., Audzevich, T., Nicolaou, A., Murphy, S., MacAllister, R., Gilroy, D.W., 2014. Characterisation of leukocytes in a human skin blister model of acute inflammation and resolution. PLoS One 9, e89375.

Jiang, W., Zhang, L., Lang, R., Li, Z., Gilkeson, G., 2014. Sex Differences in Monocyte Activation in Systemic Lupus Erythematosus (SLE). PLoS One 9, e114589.

Jones, A., Bourque, J., Kuehm, L., Opejin, A., Teague, R.M., Gross, C., Hawiger, D., 2016. Immunomodulatory Functions of BTLA and HVEM Govern Induction of Extrathymic Regulatory T Cells and Tolerance by Dendritic Cells. Immunity 45, 1066–1077.

Jung, H., Mithal, D.S., Park, J.E., Miller, R.J., 2015. Localized CCR2 activation in the bone marrow niche mobilizes monocytes by desensitizing CXCR4. PLoS One 10, e0128387.

Jung, S., Unutmaz, D., Wong, P., Sano, G.I., De Los Santos, K., Sparwasser, T., Wu, S., Vuthoori, S., Ko, K., Zavala, F., Pamer, E.G., Littman, D.R., Lang, R.A., 2002. In vivo depletion of CD11c+ dendritic cells abrogates priming of CD8+ T cells by exogenous cell-associated antigens. Immunity 17, 211–220.

Kabashima, K., Banks, T.A., Ansel, K.M., Lu, T.T., Ware, C.F., Cyster, J.G., 2005. Intrinsic lymphotoxin-β receptor requirement for homeostasis of lymphoid tissue dendritic cells. Immunity.

Kamath, A.T., Henri, S., Battye, F., Tough, D.F., Shortman, K., 2002. Developmental kinetics and lifespan of dendritic cells in mouse lymphoid organs. Blood 100, 1734–41.

Kamath, A.T., Pooley, J., O'Keeffe, M.A., Vremec, D., Zhan, Y., Lew, A.M., D'Amico, A., Wu, L., Tough, D.F., Shortman, K., 2000. The Development, Maturation, and Turnover Rate of Mouse Spleen Dendritic Cell Populations. J. Immunol. 165, 6762–6770.

Kanitakis, J., Morelon, E., Petruzzo, P., Badet, L., Dubernard, J.M., 2011. Self-renewal capacity of human epidermal Langerhans cells: Observations made on a composite tissue allograft. Exp. Dermatol.

Kashiwada, M., Pham, N.L.L., Pewe, L.L., Harty, J.T., Rothman, P.B., 2011. NFIL3/E4BP4 is a key transcription factor for CD8α+ dendritic cell development. Blood 117, 6193–6197.

Kawamura, S., Onai, N., Miya, F., Sato, T., Tsunoda, T., Kurabayashi, K., Yotsumoto, S., Kuroda, S., Takenaka, K., Akashi, K., Ohteki, T., 2017. Identification of a Human Clonogenic Progenitor with Strict Monocyte Differentiation Potential: A Counterpart of Mouse cMoPs. Immunity 46, 835-848.e4.

Kim, K.-W., Williams, J.W., Wang, Y.-T., Ivanov, S., Gilfillan, S., Colonna, M., Virgin, H.W., Gautier, E.L., Randolph, G.J., 2016. MHC II + resident peritoneal and pleural macrophages rely on IRF4 for development from circulating monocytes. J. Exp. Med. 213, 1951–1959.

Klechevsky, E., Morita, R., Liu, M., Cao, Y., Coquery, S., Thompson-Snipes, L., Briere, F., Chaussabel, D., Zurawski, G., Palucka, A.K., Reiter, Y., Banchereau, J., Ueno, H., 2008. Functional Specializations of Human Epidermal Langerhans Cells and CD14+ Dermal Dendritic Cells. Immunity 29, 497–510.

Kohyama, M., Ise, W., Edelson, B.T., Wilker, P.R., Hildner, K., Mejia, C., Frazier, W. a, Murphy, T.L., Murphy, K.M., 2009. Role for Spi-C in the development of red pulp macrophages and splenic iron homeostasis. Nature 457, 318–21.

Kondo, M., Weissman, I.L., Akashi, K., 1997. Identification of clonogenic common lymphoid progenitors in mouse bone marrow. Cell 91, 661–672.

Kurihara, T., Warr, G., Loy, J., Bravo, R., 1997. Defects in macrophage recruitment and host defense in mice lacking the CCR2 chemokine receptor. J. Exp. Med. 186, 1757–1762.

Kurowska-Stolarska, M., Alivernini, S., Melchor, E.G., Elmesmari, A., Tolusso, B., Tange, C., Petricca, L., Gilchrist, D.S., Di Sante, G., Keijzer, C., Stewart, L., Di Mario, C., Morrison, V., Brewer, J.M., Porter, D., Milling, S., Baxter, R.D., McCarey, D., Gremese, E., Lemke, G., Ferraccioli, G., McSharry, C., McInnes, I.B., 2017. MicroRNA-34a dependent regulation of AXL controls the activation of dendritic cells in inflammatory arthritis. Nat. Commun. 8, 15877.

Kusunoki, T., Sugai, M., Katakai, T., Omatsu, Y., Iyoda, T., Inaba, K., Nakahata, T., Shimizu, A., Yokota, Y., 2003. TH2 dominance and defective development of a CD8+ dendritic cell subset in Id2-deficient mice. J. Allergy Clin. Immunol. 111, 136–142.

Lahoz-Beneytez, J., Elemans, M., Zhang, Y., Ahmed, R., Salam, A., Block, M., Niederalt, C., Asquith, B., Macallan, D., 2016. Human neutrophil kinetics: Modeling of stable isotope labeling data supports short blood neutrophil half-lives. Blood 127, 3431–3438.

Landelle, C., Lepape, A., Voirin, N., Tognet, E., Venet, F., Bohé, J., Vanhems, P., Monneret, G., 2010. Low monocyte human leukocyte antigen-DR is independently associated with nosocomial infections after septic shock. Intensive Care Med. 36, 1859–66.

Landsman, L., Bar-On, L., Zernecke, A., Kim, K.-W., Krauthgamer, R., Shagdarsuren, E., Lira, S. a, Weissman, I.L., Weber, C., Jung, S., 2009. CX3CR1 is required for monocyte homeostasis and atherogenesis by promoting cell survival. Blood 113, 963–72.

Lauder, S.N., Taylor, P.R., Clark, S.R., Evans, R.L., Hindley, J.P., Smart, K., Leach, H., Kidd, E.J., Broadley, K.J., Jones, S.A., Wise, M.P., Godkin, A.J., O'Donnell, V., Gallimore, A.M., 2011. Paracetamol reduces influenza-induced immunopathology in a mouse model of infection without compromising virus clearance or the generation of protective immunity. Thorax 66, 368–74.

Lavin, Y., Winter, D., Blecher-Gonen, R., David, E., Keren-Shaul, H., Merad, M., Jung, S., Amit, I., 2014. Tissue-resident macrophage enhancer landscapes are shaped by the local microenvironment. Cell 159, 1312–1326.

Lee, J., Breton, G., Oliveira, T.Y.K., Zhou, Y.J., Aljoufi, A., Puhr, S., Cameron, M.J., Sékaly, R.-P., Nussenzweig, M.C., Liu, K., 2015. Restricted dendritic cell and monocyte progenitors in human cord blood and bone marrow. J. Exp. Med. 212, 385–399.

Lewis, K.L., Caton, M.L., Bogunovic, M., Greter, M., Grajkowska, L.T., Ng, D., Klinakis, A., Charo, I.F., Jung, S., Gommerman, J.L., Ivanov, I.I., Liu, K., Merad, M., Reizis, B., 2011. Notch2 receptor signaling controls functional differentiation of dendritic cells in the spleen and intestine. Immunity 35, 780–791.

Linsley, P.S., Greene, J.L., Brady, W., Bajorath, J., Ledbetter, J.A., Peach, R., 1994. Human B7-1 (CD80) and B7-2 (CD86) bind with similar avidities but distinct kinetics to CD28 and CTLA-4 receptors. Immunity 1, 793–801.

Liu, K., Iyoda, T., Saternus, M., Kimura, Y., Inaba, K., Steinman, R.M., 2002. Immune tolerance after delivery of dying cells to dendritic cells in situ. J. Exp. Med. 196, 1091–7.

Liu, K., Victora, G.D., Schwickert, T.A., Guermonprez, P., Meredith, M.M., Yao, K., Chu, F.-F.F.-F., Randolph, G.J., Rudensky, A.Y., Nussenzweig, M., 2009. In Vivo Analysis of Dendritic Cell Development and Homeostasis. Science 324, 392–397.

Liu, K., Waskow, C., Liu, X., Yao, K., Hoh, J., Nussenzweig, M., 2007. Origin of dendritic cells in peripheral lymphoid organs of mice. Nat. Immunol. 8, 578–83.

Liu, Zhaoyuan, Gu, Y., Chakarov, S., Bleriot, C., Kwok, I., Chen, X., Shin, A., Huang, W., Dress, R.J., Dutertre, C.-A., Schlitzer, A., Chen, J., Ng, L.G., Wang, H., Liu, Zhiduo, Su, B., Ginhoux, F., 2019. Fate Mapping via Ms4a3-Expression History Traces Monocyte-Derived Cells. Cell 178, 1509-1525.e19.

Macallan, D.C., Asquith, B., Irvine, A.J., Wallace, D.L., Worth, A., Ghattas, H., Zhang, Y., Griffin, G.E., Tough, D.F., Beverley, P.C., 2003. Measurement and modeling of human T cell kinetics. Eur. J. Immunol. 33, 2316–26.

Macallan, D.C., Asquith, B., Zhang, Y., de Lara, C., Ghattas, H., Defoiche, J., Beverley, P.C.L., 2009. Measurement of proliferation and disappearance of rapid turnover cell populations in human studies using deuterium-labeled glucose. Nat. Protoc. 4, 1313–27.

Macallan, D.C., Fullerton, C.A., Neese, R.A., Haddock, K., Park, S.S., Hellerstein, M.K., 1998. Measurement of cell proliferation by labeling of DNA with stable isotope-labeled glucose: Studies in vitro, in animals, and in humans. Proc. Natl. Acad. Sci. U. S. A. 95, 708–713.

Macallan, D.C., Wallace, D.L., Zhang, Y., Ghattas, H., Asquith, B., de Lara, C., Worth, A., Panayiotakopoulos, G., Griffin, G.E., Tough, D.F., Beverley, P.C.L., 2005. B-cell kinetics in humans: rapid turnover of peripheral blood memory cells. Blood 105, 3633–40.

Machiels, B., Dourcy, M., Xiao, X., Javaux, J., Mesnil, C., Sabatel, C., Desmecht, D., Lallemand, F., Martinive, P., Hammad, H., Guilliams, M., Dewals, B., Vanderplasschen, A., Lambrecht, B.N., Bureau, F., Gillet, L., 2017. A gammaherpesvirus provides protection against allergic asthma by inducing the replacement of resident alveolar macrophages with regulatory monocytes. Nat. Immunol. 18, 1310–1320.

Mandl, M., Schmitz, S., Weber, C., Hristov, M., 2014. Characterization of the CD14++CD16+ monocyte population in human bone marrow. PLoS One 9, e112140.

Mantovani, A., Sica, A., Sozzani, S., Allavena, P., Vecchi, A., Locati, M., 2004. The chemokine system in diverse forms of macrophage activation and polarization. Trends Immunol.

Manz, M.G., Traver, D., Miyamoto, T., Weissman, I.L., Akashi, K., 2001. Dendritic cell potentials of early lymphoid and myeloid progenitors. Blood 97, 3333–41.

Marcovecchio, P.M., Thomas, G.D., Mikulski, Z., Ehinger, E., Mueller, K.A.L., Blatchley, A., Wu, R., Miller, Y.I., Nguyen, A.T., Taylor, A.M., McNamara, C.A., Ley, K., Hedrick, C.C., 2017. Scavenger Receptor CD36 Directs Nonclassical Monocyte Patrolling Along the Endothelium During Early Atherogenesis. Arterioscler. Thromb. Vasc. Biol. 37, 2043–2052.

Martín-Gayo, E., Sierra-Filardi, E., Corbí, A.L., Toribio, M.L., 2010. Plasmacytoid dendritic cells resident in human thymus drive natural Treg cell development. Blood 115, 5366–5375.

Mass, E., Ballesteros, I., Farlik, M., Halbritter, F., Günther, P., Crozet, L., Jacome-Galarza, C.E., Händler, K., Klughammer, J., Kobayashi, Y., Gomez-Perdiguero, E., Schultze, J.L., Beyer, M., Bock, C., Geissmann, F., 2016. Specification of tissue-resident macrophages during organogenesis. Science 353, aaf4238–aaf4238.

Matsui, T., Connolly, J.E., Michnevitz, M., Chaussabel, D., Yu, C.-I., Glaser, C., Tindle, S., Pypaert, M., Freitas, H., Piqueras, B., Banchereau, J., Palucka, A.K., 2009. CD2 Distinguishes Two Subsets of Human Plasmacytoid Dendritic Cells with Distinct Phenotype and Functions. J. Immunol. 182, 6815–6823.

Maximow, Alexander, 1927. Bindegewebe und blutbildende Gewebe. In: Brodersen, J., Maximow, A, Schaffer, J. (Eds.), Die Gewebe Teil Epithel- Und Drüsengewebe ·Bindegewebe Und Blutbildende Gewebe ·Blut. Springer Berlin Heidelberg, Berlin, Heidelberg, pp. 232–583.

McGovern, N., Schlitzer, A., Gunawan, M., Jardine, L., Shin, A., Poyner, E., Green, K., Dickinson, R., Wang, X.-N., Low, D., Best, K., Covins, S., Milne, P., Pagan, S., Aljefri, K., Windebank, M., Miranda-Saavedra, D., Saavedra, D.M., Larbi, A., Wasan, P.S., Duan, K., Poidinger, M., Bigley, V., Ginhoux, F., Collin, M., Haniffa, M., 2014. Human dermal $CD14^{+}$ cells are a transient population of monocyte-derived macrophages. Immunity 41, 465–77.

Menezes, S., Melandri, D., Anselmi, G., Perchet, T., Loschko, J., Dubrot, J., Patel, R., Gautier, E.L., Hugues, S., Longhi, M.P., Henry, J.Y., Quezada, S.A., Lauvau, G., Lennon-Duménil, A.-M., Gutiérrez-Martínez, E., Bessis, A., Gomez-Perdiguero, E., Jacome-Galarza, C.E., Garner, H., Geissmann, F., Golub, R., Nussenzweig, M.C., Guermonprez, P., 2016. The Heterogeneity of Ly6Chi Monocytes Controls Their Differentiation into iNOS+ Macrophages or Monocyte-Derived Dendritic Cells. Immunity 45, 1205–1218.

Metchnikoff, E., 1893. Lectures on the comparative pathology of inflammation : delivered at the Pasteur Institute in 1891. London Kegan Paul.

Metchnikov, E., 1892. Leçons sur la pathologie comparée de l'inflammation. Paris : G. Masson.

Michaud, J.-P., Bellavance, M.-A., Préfontaine, P., Rivest, S., 2013. Real-Time In Vivo Imaging Reveals the Ability of Monocytes to Clear Vascular Amyloid Beta. Cell Rep. 5, 646–653.

Mildner, A., Chapnik, E., Manor, O., Yona, S., Kim, K.-W., Aychek, T., Varol, D., Beck, G., Itzhaki, Z.B., Feldmesser, E., Amit, I., Hornstein, E., Jung, S., 2013. Mononuclear phagocyte miRNome analysis identifies miR-142 as critical regulator of murine dendritic cell homeostasis. Blood 121, 1016–1027.

Mildner, A., Schönheit, J., Giladi, A., David, E., Lara-Astiaso, D., Lorenzo-Vivas, E., Paul, F., Chappell-Maor, L., Priller, J., Leutz, A., Amit, I., Jung, S., 2017. Genomic Characterization of Murine Monocytes Reveals C/EBPβ Transcription Factor Dependence of Ly6C − Cells. Immunity 46, 849-862.e7.

Mills, C.D., 2012. M1 and M2 Macrophages: Oracles of Health and Disease. Crit. Rev. Immunol. 32, 463–88.

Mills, C.D., Kincaid, K., Alt, J.M., Heilman, M.J., Hill, A.M., 2000. M-1/M-2 Macrophages and the Th1/Th2 Paradigm. J. Immunol. 164, 6166–6173.

Mimiola, E., Marini, O., Perbellini, O., Micheletti, A., Vermi, W., Lonardi, S., Costantini, C., Meneghelli, E., Andreini, A., Bonetto, C., Vassanelli, A., Cantini, M., Zoratti, E., Massi, D., Zamo, A., Leso, A., Quaresmini, G., Benedetti, F., Pizzolo, G., Cassatella, M.A., Tecchio, C., 2014. Rapid reconstitution of functionally active 6-sulfoLacNAc + dendritic cells (slanDCs) of donor origin following allogeneic haematopoietic stem cell transplant. Clin. Exp. Immunol. 178, 129–141.

Misharin, A. V., Cuda, C.M., Saber, R., Turner, J.D., Gierut, A.K., Haines, G.K., Berdnikovs, S., Filer, A., Clark, A.R., Buckley, C.D., Mutlu, G.M., Budinger, G.R.S., Perlman, H., 2014. Nonclassical Ly6C− Monocytes Drive the Development of Inflammatory Arthritis in Mice. Cell Rep. 9, 591–604.

Misharin, A. V, Morales-Nebreda, L., Reyfman, P.A., Cuda, C.M., Walter, J.M., McQuattie-Pimentel, A.C., Chen, C.-I., Anekalla, K.R., Joshi, N., Williams, K.J.N., Abdala-Valencia, H., Yacoub, T.J., Chi, M., Chiu, S., Gonzalez-Gonzalez, F.J., Gates, K., Lam, A.P., Nicholson, T.T., Homan, P.J., Soberanes, S., Dominguez, S., Morgan, V.K., Saber, R., Shaffer, A., Hinchcliff, M., Marshall, S.A., Bharat, A., Berdnikovs, S., Bhorade, S.M., Bartom, E.T., Morimoto, R.I., Balch, W.E., Sznajder, J.I., Chandel, N.S., Mutlu, G.M., Jain, M., Gottardi, C.J., Singer, B.D., Ridge, K.M., Bagheri, N., Shilatifard, A., Budinger, G.R.S., Perlman, H., 2017. Monocyte-derived alveolar macrophages drive lung fibrosis and persist in the lung over the life span. J. Exp. Med. 214, 2387–2404.

Mitroulis, I., Ruppova, K., Wang, B., Chen, L.S., Grzybek, M., Grinenko, T., Eugster, A., Troullinaki, M., Palladini, A., Kourtzelis, I., Chatzigeorgiou, A., Schlitzer, A., Beyer, M., Joosten, L.A.B., Isermann, B., Lesche, M., Petzold, A., Simons, K., Henry, I., Dahl, A., Schultze, J.L., Wielockx, B., Zamboni, N., Mirtschink, P., Coskun, Ü., Hajishengallis, G., Netea, M.G., Chavakis, T., 2018. Modulation of Myelopoiesis Progenitors Is an Integral Component of Trained Immunity. Cell 172, 147-161.e12.

Mohri, H., Perelson, a S., Tung, K., Ribeiro, R.M., Ramratnam, B., Markowitz, M., Kost, R., Hurley, A., Weinberger, L., Cesar, D., Hellerstein, M.K., Ho, D.D., 2001. Increased turnover of T lymphocytes in HIV-1 infection and its reduction by antiretroviral therapy. J. Exp. Med. 194, 1277–1287.

Moniuszko, M., Bodzenta-Lukaszyk, A., Kowal, K., Lenczewska, D., Dabrowska, M., 2009. Enhanced frequencies of CD14++CD16+, but not CD14+CD16+, peripheral blood monocytes in severe asthmatic patients. Clin. Immunol. 130, 338–346.

Monneret, G., Lepape, A., Voirin, N., Bohé, J., Venet, F., Debard, A.-L., Thizy, H., Bienvenu, J., Gueyffier, F., Vanhems, P., 2006. Persisting low monocyte human leukocyte antigen-DR expression predicts mortality in septic shock. Intensive Care Med. 32, 1175–83.

Mossadegh-Keller, N., Gentek, R., Gimenez, G., Bigot, S., Mailfert, S., Sieweke, M.H., 2017. Developmental origin and maintenance of distinct testicular macrophage populations. J. Exp. Med. 214, 2829–2841.

Motwani, M.P., Flint, J.D., De Maeyer, R.P., Fullerton, J.N., Smith, A.M., Marks, D.J., Gilroy, D.W., 2016. Novel translational model of resolving inflammation triggered by UV-killed E. coli. J. Pathol. Clin. Res. 2, 154–165.

Mukherjee, R., Kanti Barman, P., Kumar Thatoi, P., Tripathy, R., Kumar Das, B., Ravindran, B., 2015. Non-Classical monocytes display inflammatory features: Validation in Sepsis and Systemic Lupus Erythematous. Sci. Rep. 5, 13886.

Murata, A., Okuyama, K., Sakano, S., Kajiki, M., Hirata, T., Yagita, H., Zúñiga-Pflücker, J.C., Miyake, K., Akashi-Takamura, S., Moriwaki, S., Niida, S., Yoshino, M., Hayashi, S.-I., 2010. A Notch Ligand, Delta-Like 1 Functions As an Adhesion Molecule for Mast Cells. J. Immunol. 185, 3905–3912.

Naegeli, O., 1908. Blutkrankheiten und Blutdiagnostik : Lehrbuch der morpho- logischen Heamatologie. Veit & comp.,: Veit & comp., Leipzig.

Nahrendorf, M., Swirski, F.K., Aikawa, E., Stangenberg, L., Wurdinger, T., Figueiredo, J.-L., Libby, P., Weissleder, R., Pittet, M.J., 2007. The healing myocardium sequentially mobilizes two monocyte subsets with divergent and complementary functions. J. Exp. Med. 204, 3037–47.

Naik, S.H., Metcalf, D., van Nieuwenhuijze, A., Wicks, I., Wu, L., O'Keeffe, M., Shortman, K., 2006. Intrasplenic steady-state dendritic cell precursors that are distinct from monocytes. Nat. Immunol. 7, 663–71.

Naik, S.H., Sathe, P., Park, H.-Y., Metcalf, D., Proietto, A.I., Dakic, A., Carotta, S., O'Keeffe, M., Bahlo, M., Papenfuss, A., Kwak, J.-Y., Wu, L., Shortman, K., 2007. Development of plasmacytoid and conventional dendritic cell subtypes from single precursor cells derived in vitro and in vivo. Nat. Immunol. 8, 1217–26.

Nayak, D.K., Zhou, F., Xu, M., Huang, J., Tsuji, M., Hachem, R., Mohanakumar, T., 2016. Long-Term Persistence of Donor Alveolar Macrophages in Human Lung Transplant Recipients That Influences Donor-Specific Immune Responses. Am. J. Transplant. 16, 2300–2311.

Nelson, D.S., 1963. Reaction to antigens in vivo of the peritoneal macrophages of guinea-pigs with delayed type hypersensitivity. Effects of anticoagulants and other drugs. Lancet 282, 175–176.

Nestle, F.O., Zheng, X.G., Thompson, C.B., Turka, L.A., Nickoloff, B.J., 1993. Characterization of dermal dendritic cells obtained from normal human skin reveals phenotypic and functionally distinctive subsets. J. Immunol. 151, 6535–45.

Newson, J., Stables, M., Karra, E., Arce-Vargas, F., Quezada, S., Motwani, M., Mack, M., Yona, S., Audzevich, T., Gilroy, D.W., 2014. Resolution of acute inflammation bridges the gap between innate and adaptive immunity. Blood 124, 1748–64.

Nguyen, K.D., Fentress, S.J., Qiu, Y., Yun, K., Cox, J.S., Chawla, A., 2013. Circadian Gene Bmal1 Regulates Diurnal Oscillations of Ly6Chi Inflammatory Monocytes. Science (80-.). 341, 1483–1488.

Nussenzweig, M.C., Steinman, R.M., 1980. Contribution of dendritic cells to stimulation of the murine syngeneic mixed leukocyte reaction. J. Exp. Med. 151, 1196–1212.

Nussenzweig, M.C., Steinman, R.M., Gutchinov, B., Cohn, Z.A., 1980. Dendritic cells are accessory cells for the development of anti-trinitrophenyl cytotoxic T lymphocytes. J. Exp. Med. 152, 1070–84.

Nyugen, J., Agrawal, S., Gollapudi, S., Gupta, S., 2010. Impaired Functions of Peripheral Blood Monocyte Subpopulations in Aged Humans. J. Clin. Immunol. 30, 806–813.

O'Keeffe, M., Hochrein, H., Vremec, D., Caminschi, I., Miller, J.L., Anders, E.M., Wu, L., Lahoud, M.H., Henri, S., Scott, B., Hertzog, P., Tatarczuch, L., Shortman, K., 2002. Mouse plasmacytoid cells: long-lived cells, heterogeneous in surface phenotype and function, that differentiate into CD8(+) dendritic cells only after microbial stimulus. J. Exp. Med. 196, 1307–19.

O'Keeffe, M., Hochrein, H., Vremec, D., Scott, B., Hertzog, P., Tatarczuch, L., Shortman, K., 2003. Dendritic cell precursor populations of mouse blood: Identification of the murine homologues of human blood plasmacytoid pre-DC2 and CD11c+ DC1 precursors. Blood 101, 1453–1459.

Ohnmacht, C., Pullner, A., King, S.B.S., Drexler, I., Meier, S., Brocker, T., Voehringer, D., 2009. Constitutive ablation of dendritic cells breaks self-tolerance of CD4 T cells and results in spontaneous fatal autoimmunity. J. Exp. Med. 206, 549–559.

Onai, N., Kurabayashi, K., Hosoi-Amaike, M., Toyama-Sorimachi, N., Matsushima, K., Inaba, K., Ohteki, T., 2013. A Clonogenic Progenitor with Prominent Plasmacytoid Dendritic Cell Developmental Potential. Immunity 38, 943–957.

Onai, N., Obata-Onai, A., Schmid, M. a, Ohteki, T., Jarrossay, D., Manz, M.G., 2007. Identification of clonogenic common Flt3+M-CSFR+ plasmacytoid and conventional dendritic cell progenitors in mouse bone marrow. Nat. Immunol. 8, 1207–16.

Ong, S.-M., Hadadi, E., Dang, T.-M., Yeap, W.-H., Tan, C.T.-Y., Ng, T.-P., Larbi, A., Wong, S.-C., 2018. The pro-inflammatory phenotype of the human non-classical monocyte subset is attributed to senescence. Cell Death Dis. 9, 266.

Ong, S.-M., Teng, K., Newell, E., Chen, H., Chen, J., Loy, T., Yeo, T.-W., Fink, K., Wong, S.-C., 2019. A Novel, Five-Marker Alternative to CD16–CD14 Gating to Identify the Three Human Monocyte Subsets. Front. Immunol. 10, 1761.

Palis, J., Robertson, S., Kennedy, M., Wall, C., Keller, G., 1999. Development of erythroid and myeloid progenitors in the yolk sac and embryo proper of the mouse. Development 126, 5073–5084.

Paolicelli, R.C., Bolasco, G., Pagani, F., Maggi, L., Scianni, M., Panzanelli, P., Giustetto, M., Ferreira, T.A., Guiducci, E., Dumas, L., Ragozzino, D., Gross, C.T., 2011. Synaptic pruning by microglia is necessary for normal brain development. Science 333, 1456–8.

Pappenheim, A., Ferrata, A., 1910. Uber die verschiedenen lymphoiden Zellformen des normalen und pathologischen Blutes. Folia Haematol. (Frankf.) 10, 72–208.

Pasquevich, K.A., Bieber, K., Günter, M., Grauer, M., Pötz, O., Schleicher, U., Biedermann, T., Beer-Hammer, S., Bühring, H.-J.J., Rammensee, H.-G.G., Zender, L., Autenrieth, I.B., Lengerke, C., Autenrieth, S.E., 2015. Innate immune system favors emergency monopoiesis at the expense of DC-differentiation to control systemic bacterial infection in mice. Eur. J. Immunol. 45, 2821–2833.

Passlick, B., Flieger, D., Ziegler-Heitbrock, H.W., 1989. Identification and characterization of a novel monocyte subpopulation in human peripheral blood. Blood 74, 2527–34.

Patel, A.A., Yona, S., 2018. Phagocyte Development. In: ELS. John Wiley & Sons, Ltd, Chichester, UK, pp. 1–13.

Pelayo, R., Hirose, J., Huang, J., Garrett, K.P., Delogu, A., Busslinger, M., Kincade, P.W., 2005. Derivation of 2 categories of plasmacytoid dendritic cells in murine bone marrow. Blood 105, 4407–15.

Perussia, B., Fanning, V., Trinchieri, G., 1985. A leukocyte subset bearing HLA-DR antigens is responsible for in vitro alpha interferon production in response to viruses. Nat. Immun. Cell Growth Regul. 4, 120–37.

Poehlmann, H., Schefold, J.C., Zuckermann-Becker, H., Volk, H.-D., Meisel, C., 2009. Phenotype changes and impaired function of dendritic cell subsets in patients with sepsis: a prospective observational analysis. Crit. Care 13, R119.

Pooley, J.L., Heath, W.R., Shortman, K., 2001. Cutting edge: intravenous soluble antigen is presented to CD4 T cells by CD8- dendritic cells, but cross-presented to CD8 T cells by CD8+ dendritic cells. J. Immunol. 166, 5327–30.

Pozarowski, P., Darzynkiewicz, Z., 2004. Analysis of cell cycle by flow cytometry. Methods Mol. Biol. 281, 301–11.

Proietto, A.I., Dommelen, S. van, Zhou, P., Rizzitelli, A., D'Amico, A., Steptoe, R.J., Naik, S.H., Lahoud, M.H., Liu, Y., Zheng, P., Shortman, K., Wu, L., 2008. Dendritic cells in the thymus contribute to T-regulatory cell induction. Proc. Natl. Acad. Sci. 105, 19869–19874.

Qiu, C.-H., Miyake, Y., Kaise, H., Kitamura, H., Ohara, O., Tanaka, M., 2009. Novel subset of CD8{alpha}+ dendritic cells localized in the marginal zone is responsible for tolerance to cell-associated antigens. J. Immunol. 182, 4127–36.

Quintin, J., Saeed, S., Martens, J.H.A., Giamarellos-Bourboulis, E.J., Ifrim, D.C., Logie, C., Jacobs, L., Jansen, T., Kullberg, B.J., Wijmenga, C., Joosten, L.A.B., Xavier, R.J., Van Der Meer, J.W.M., Stunnenberg, H.G., Netea, M.G., 2012. Candida albicans infection affords protection against reinfection via functional reprogramming of monocytes. Cell Host Microbe 12, 223–232.

Radwan, W.M., Khalifa, K.A., Esaily, H.A., Lashin, N.A., 2016. CD14++CD16+ monocyte subset expansion in rheumatoid arthritis patients: Relation to disease activity and interleukin-17. Egypt. Rheumatol. 38, 161–169.

Réu, P., Khosravi, A., Bernard, S., Mold, J.E., Salehpour, M., Alkass, K., Perl, S., Tisdale, J., Possnert, G., Druid, H., Frisén, J., 2017. The Lifespan and Turnover of Microglia in the Human Brain. Cell Rep. 20, 779–784.

Riccardi, F., Della Porta, M.G., Rovati, B., Casazza, A., Radolovich, D., De Amici, M., Danova, M., Langer, M., 2011. Flow cytometric analysis of peripheral blood dendritic cells in patients with severe sepsis. Cytom. Part B Clin. Cytom. 80B, 14–21.

Roberts, A.W., Lee, B.L., Deguine, J., John, S., Shlomchik, M.J., Barton, G.M., 2017. Tissue-Resident Macrophages Are Locally Programmed for Silent Clearance of Apoptotic Cells. Immunity 47, 913-927.e6.

Rodrigues, P.F., Alberti-Servera, L., Eremin, A., Grajales-Reyes, G.E., Ivanek, R., Tussiwand, R., 2018. Distinct progenitor lineages contribute to the heterogeneity of plasmacytoid dendritic cells. Nat. Immunol. 19, 711–722.

Rongvaux, A., Willinger, T., Martinek, J., Strowig, T., Gearty, S. V, Teichmann, L.L., Saito, Y., Marches, F., Halene, S., Palucka, a K., Manz, M.G., Flavell, R. a, 2014. Development and function of human innate immune cells in a humanized mouse model. Nat. Biotechnol. 32, 364–72.

Ruffin, N., Gea-Mallorquí, E., Brouiller, F., Jouve, M., Silvin, A., See, P., Dutertre, C.-A., Ginhoux, F., Benaroch, P., 2019. Constitutive Siglec-1 expression confers susceptibility to HIV-1 infection of human dendritic cell precursors. Proc. Natl. Acad. Sci. U. S. A. 116, 21685–21693.

Ryan, G.R., Dai, X.M., Dominguez, M.G., Tong, W., Chuan, F., Chisholm, O., Russell, R.G., Pollard, J.W., Stanley, E.R., 2001. Rescue of the colony-stimulating factor 1 (CSF-1)-nullizygous mouse (Csf1(op)/Csf1(op)) phenotype with a CSF-1 transgene and identification of sites of local CSF-1 synthesis. Blood 98, 74–84.

Sancho, D., Joffre, O.P., Keller, A.M., Rogers, N.C., Martínez, D., Hernanz-Falcón, P., Rosewell, I., Sousa, C.R. e, 2009. Identification of a dendritic cell receptor that couples sensing of necrosis to immunity. Nature 458, 899–903.

Satoh, T., Nakagawa, K., Sugihara, F., Kuwahara, R., Ashihara, M., Yamane, F., Minowa, Y., Fukushima, K., Ebina, I., Yoshioka, Y., Kumanogoh, A., Akira, S., 2017. Identification of an atypical monocyte and committed progenitor involved in fibrosis. Nature 541, 96–101.

Satpathy, A.T., Briseño, C.G., Lee, J.S., Ng, D., Manieri, N.A., Kc, W., Wu, X., Thomas, S.R., Lee, W.L., Turkoz, M., McDonald, K.G., Meredith, M.M., Song, C., Guidos, C.J., Newberry, R.D., Ouyang, W., Murphy, T.L., Stappenbeck, T.S., Gommerman, J.L., Nussenzweig, M.C., Colonna, M., Kopan, R., Murphy, K.M., 2013. Notch2-dependent classical dendritic cells orchestrate intestinal immunity to attaching-and-effacing bacterial pathogens. Nat. Immunol. 14, 937–948.

Schäkel, K., Kannagi, R., Kniep, B., Goto, Y., Mitsuoka, C., Zwirner, J., Soruri, A., von Kietzell, M., Rieber, E., 2002. 6-Sulfo LacNAc, a novel carbohydrate modification of PSGL-1, defines an inflammatory type of human dendritic cells. Immunity 17, 289–301.

Schäkel, K., Mayer, E., Federle, C., Schmitz, M., Riethmüller, G., Rieber, E.P., 1998. A novel dendritic cell population in human blood: one-step immunomagnetic isolation by a specific mAb (M-DC8) and in vitro priming of cytotoxic T lymphocytes. Eur. J. Immunol. 28, 4084–93.

Schäkel, K., Poppe, C., Mayer, E., Federle, C., Riethmüller, G., Rieber, E.P., 1999. M-DC8+ leukocytes--a novel human dendritic cell population. Pathobiology 67, 287–90.

Schenkel, A.R., Mamdouh, Z., Muller, W.A., 2004. Locomotion of monocytes on endothelium is a critical step during extravasation. Nat. Immunol. 5, 393–400.

Schlenner, S.M., Madan, V., Busch, K., Tietz, A., Läufle, C., Costa, C., Blum, C., Fehling, H.J., Rodewald, H.R., 2010. Fate Mapping Reveals Separate Origins of T Cells and Myeloid Lineages in the Thymus. Immunity 32, 426–436.

Schlitzer, A., McGovern, N., Teo, P., Zelante, T., Atarashi, K., Low, D., Ho, A.W.S., See, P., Shin, A., Wasan, P.S., Hoeffel, G., Malleret, B., Heiseke, A., Chew, S., Jardine, L., Purvis, H.A., Hilkens, C.M.U., Tam, J., Poidinger, M., Stanley, E.R., Krug, A.B., Renia, L., Sivasankar, B., Ng, L.G., Collin, M., Ricciardi-Castagnoli, P., Honda, K., Haniffa, M., Ginhoux, F., 2013. IRF4 Transcription Factor-Dependent CD11b+ Dendritic Cells in Human and Mouse Control Mucosal IL-17 Cytokine Responses. Immunity 38, 970–983.

Schlitzer, A., Sivakamasundari, V., Chen, J., Sumatoh, H.R. Bin, Schreuder, J., Lum, J., Malleret, B., Zhang, S., Larbi, A., Zolezzi, F., Renia, L., Poidinger, M., Naik, S., Newell, E.W., Robson, P., Ginhoux, F., 2015. Identification of cDC1- and cDC2-committed DC progenitors reveals early lineage priming at the common DC progenitor stage in the bone marrow. Nat Immunol 16, 718–728.

Schraml, B.U., van Blijswijk, J., Zelenay, S., Whitney, P.G., Filby, A., Acton, S.E., Rogers, N.C., Moncaut, N., Carvajal, J.J., Reis e Sousa, C., 2013. Genetic Tracing via DNGR-1 Expression History Defines Dendritic Cells as a Hematopoietic Lineage. Cell 154, 843–858.

Schulz, C., Perdiguero, E.G., Chorro, L., Szabo-Rogers, H., Cagnard, N., Kierdorf, K., Prinz, M., Wu, B., Jacobsen, S.E.W., Pollard, J.W., Frampton, J., Liu, K.J., Geissmann, F., 2012. A Lineage of Myeloid Cells Independent of Myb and Hematopoietic Stem Cells. Science (80-.). 336, 86–90.

Scott, Charlotte L., Soen, B., Martens, L., Skrypek, N., Saelens, W., Taminau, J., Blancke, G., Van Isterdael, G., Huylebroeck, D., Haigh, J., Saeys, Y., Guilliams, M., Lambrecht, B.N., Berx, G., 2016. The transcription factor Zeb2 regulates development of conventional and plasmacytoid DCs by repressing Id2. J. Exp. Med. 213, 897–911.

Scott, Charlotte L, Zheng, F., De Baetselier, P., Martens, L., Saeys, Y., De Prijck, S., Lippens, S., Abels, C., Schoonooghe, S., Raes, G., Devoogdt, N., Lambrecht, B.N., Beschin, A., Guilliams, M., 2016. Bone marrow-derived monocytes give rise to self-renewing and fully differentiated Kupffer cells. Nat. Commun. 7, 10321.

Scumpia, P.O., McAuliffe, P.F., O'Malley, K.A., Ungaro, R., Uchida, T., Matsumoto, T., Remick, D.G., Clare-Salzler, M.J., Moldawer, L.L., Efron, P.A., 2005. CD11c + Dendritic Cells Are Required for Survival in Murine Polymicrobial Sepsis. J. Immunol. 175, 3282–3286.

See, P., Dutertre, C.-A., Chen, J., Günther, P., McGovern, N., Irac, S.E., Gunawan, M., Beyer, M., Händler, K., Duan, K., Sumatoh, H.R. Bin, Ruffin, N., Jouve, M., Gea-Mallorquí, E., Hennekam, R.C.M., Lim, T., Yip, C.C., Wen, M., Malleret, B., Low, I., Shadan, N.B., Fen, C.F.S., Tay, A., Lum, J., Zolezzi, F., Larbi, A., Poidinger, M., Chan, J.K.Y., Chen, Q., Rénia, L., Haniffa, M., Benaroch, P., Schlitzer, A., Schultze, J.L., Newell, E.W., Ginhoux, F., 2017. Mapping the human DC lineage through the integration of high-dimensional techniques. Science 356, eaag3009.

Segura, E., Valladeau-Guilemond, J., Donnadieu, M.-H., Sastre-Garau, X., Soumelis, V., Amigorena, S., 2012. Characterization of resident and migratory dendritic cells in human lymph nodes. J. Exp. Med. 209, 653–60.

Seidler, S., Zimmermann, H.W., Bartneck, M., Trautwein, C., Tacke, F., 2010. Age-dependent alterations of monocyte subsets and monocyte-related chemokine pathways in healthy adults. BMC Immunol. 11, 30.

Serbina, N. V., Hohl, T.M., Cherny, M., Pamer, E.G., 2009. Selective Expansion of the Monocytic Lineage Directed by Bacterial Infection. J. Immunol. 183, 1900–1910.

Serbina, N. V, Pamer, E.G., 2006. Monocyte emigration from bone marrow during bacterial infection requires signals mediated by chemokine receptor CCR2. Nat. Immunol. 7, 311–317.

Serbina, N. V, Salazar-Mather, T.P., Biron, C.A., Kuziel, W.A., Pamer, E.G., 2003. TNF/iNOS-producing dendritic cells mediate innate immune defense against bacterial infection. Immunity 19, 59–70.

Shi, C., Jia, T., Mendez-Ferrer, S., Hohl, T.M., Serbina, N. V., Lipuma, L., Leiner, I., Li, M.O., Frenette, P.S., Pamer, E.G., 2011. Bone Marrow Mesenchymal Stem and Progenitor Cells Induce Monocyte Emigration in Response to Circulating Toll-like Receptor Ligands. Immunity 34, 590–601.

Sichien, D., Scott, C.L., Martens, L., Vanderkerken, M., Van Gassen, S., Plantinga, M., Joeris, T., De Prijck, S., Vanhoutte, L., Vanheerswynghels, M., Van Isterdael, G., Toussaint, W., Madeira, F.B., Vergote, K., Agace, W.W., Clausen, B.E., Hammad, H., Dalod, M., Saeys, Y., Lambrecht, B.N., Guilliams, M., 2016. IRF8 Transcription Factor Controls Survival and Function of Terminally Differentiated Conventional and Plasmacytoid Dendritic Cells, Respectively. Immunity 45, 626–640.

Siegal, F.P., Kadowaki, N., Shodell, M., Fitzgerald-Bocarsly, P.A., Shah, K., Ho, S., Antonenko, S., Liu, Y.J., 1999. The nature of the principal Type 1 interferon-producing cells in human blood. Science (80-.). 284, 1835–1837.

Steinman, R.M., Cohn, Z. a, 1973. Identification of a novel cell type in peripheral lymphoid organs of mice. I. Morphology, quantitation, tissue distribution. J. Exp. Med. 137, 1142–1162.

Steinman, R.M., Gutchinov, B., Witmer, M.D., Nussenzweig, M.C., 1983. Dendritic cells are the principal stimulators of the primary mixed leukocyte reaction in mice. J. Exp. Med. 157, 613–627.

Steinman, R.M., Kaplan, G., Witmer, M.D., Cohn, Z.A., 1979. Identification of a novel cell type in peripheral lymphoid organs of mice. V. Purification of spleen dendritic cells, new surface markers, and maintenance in vitro. J. Exp. Med. 149, 1–16.

Steinman, R.M., Lustig, D.S., Cohn, Z.A., 1974. Identification of a novel cell type in peripheral lymphoid organs of mice. 3. Functional properties in vivo. J. Exp. Med. 139, 1431–45.

Steinman, R.M., Witmer, M.D., 1978. Lymphoid dendritic cells are potent stimulators of the primary mixed leukocyte reaction in mice. Proc. Natl. Acad. Sci. U. S. A. 75, 5132.

Subramanian, M., Hayes, C.D., Thome, J.J., Thorp, E., Matsushima, G.K., Herz, J., Farber, D.L., Liu, K., Lakshmana, M., Tabas, I., 2014. An AXL/LRP-1/RANBP9 complex mediates DC efferocytosis and antigen cross-presentation in vivo. J. Clin. Invest. 124, 1296–1308.

Sugimoto, C., Hasegawa, A., Saito, Y., Fukuyo, Y., Chiu, K.B., Cai, Y., Breed, M.W., Mori, K., Roy, C.J., Lackner, A.A., Kim, W.-K., Didier, E.S., Kuroda, M.J., 2015. Differentiation Kinetics of Blood Monocytes and Dendritic Cells in Macaques: Insights to Understanding Human Myeloid Cell Development. J. Immunol. 195, 1774–1781.

Sunderkötter, C., Nikolic, T., Dillon, M.J., van Rooijen, N., Stehling, M., Drevets, D.A., Leenen, P.J.M., 2004. Subpopulations of Mouse Blood Monocytes Differ in Maturation Stage and Inflammatory Response. J. Immunol. 172, 4410–4417.

Suzuki, S., Honma, K., Matsuyama, T., Suzuki, K., Toriyama, K., Akitoyo, I., Yamamoto, K., Suematsu, T., Nakamura, M., Yui, K., Kumatori, A., 2004. Critical roles of interferon regulatory factor 4 in CD11bhighCD8alpha- dendritic cell development. Proc Natl Acad Sci U S A 101, 8981–6.

Swirski, F.K., Nahrendorf, M., Etzrodt, M., Wildgruber, M., Cortez-Retamozo, V., Panizzi, P., Figueiredo, J.-L., Kohler, R.H., Chudnovskiy, A., Waterman, P., Aikawa, E., Mempel, T.R., Libby, P., Weissleder, R., Pittet, M.J., 2009. Identification of Splenic Reservoir Monocytes and Their Deployment to Inflammatory Sites. Science (80-.). 325, 612–616.

Tak, T., Drylewicz, J., Conemans, L., de Boer, R.J., Koenderman, L., Borghans, J.A.M., Tesselaar, K., 2017a. Circulatory and maturation kinetics of human monocyte subsets in vivo. Blood 130, 1474–1477.

Tak, T., van Groenendael, R., Pickkers, P., Koenderman, L., 2017b. Monocyte Subsets Are Differentially Lost from the Circulation during Acute Inflammation Induced by Human Experimental Endotoxemia. J. Innate Immun. 9, 464–474.

Takahashi, K., 1989. Differentiation , Maturation , and Proliferation Macrophages in the Mouse Yolk Sac : of and Ultrastructural Study. J. Leukoc. Biol. 96, 87–96.

Tamoutounour, S., Guilliams, M., Montanana Sanchis, F., Liu, H., Terhorst, D., Malosse, C., Pollet, E., Ardouin, L., Luche, H., Sanchez, C., Dalod, M., Malissen, B., Henri, S., 2013. Origins and Functional Specialization of Macrophages and of Conventional and Monocyte-Derived Dendritic Cells in Mouse Skin. Immunity 39, 925–938.

Thaler, B., Hohensinner, P.J., Krychtiuk, K.A., Matzneller, P., Koller, L., Brekalo, M., Maurer, G., Huber, K., Zeitlinger, M., Jilma, B., Wojta, J., Speidl, W.S., 2016. Differential in vivo activation of monocyte subsets during low-grade inflammation through experimental endotoxemia in humans. Sci. Rep. 6, 30162.

Thomas, G.D., Hamers, A.A.J., Nakao, C., Marcovecchio, P., Taylor, A.M., McSkimming, C., Nguyen, A.T., McNamara, C.A., Hedrick, C.C., 2017. Human Blood Monocyte Subsets: A New Gating Strategy Defned Using Cell Surface Markers Identifed by Mass Cytometry. Arterioscler. Thromb. Vasc. Biol. 37, 1548–1558.

Thomas, G.D., Hanna, R.N., Vasudevan, N.T., Hamers, A.A., Romanoski, C.E., McArdle, S., Ross, K.D., Blatchley, A., Yoakum, D., Hamilton, B.A., Mikulski, Z., Jain, M.K., Glass, C.K., Hedrick, C.C., 2016. Deleting an Nr4a1 Super-Enhancer Subdomain Ablates Ly6Clow Monocytes while Preserving Macrophage Gene Function. Immunity 45, 975–987.

Toliver-Kinsky, T.E., Cui, W., Murphey, E.D., Lin, C., Sherwood, E.R., 2005. Enhancement of Dendritic Cell Production by Fms-Like Tyrosine Kinase-3 Ligand Increases the Resistance of Mice to a Burn Wound Infection. J. Immunol. 174, 404–410.

Traver, D., Akashi, K., Manz, M., Merad, M., Miyamoto, T., Engleman, E.G., Weissman, I.L., 2000. Development of CD8 -Positive Dendritic Cells from a Common Myeloid Progenitor. Science (80-.). 290, 2152–2154.

Tsou, C.L., Peters, W., Si, Y., Slaymaker, S., Aslanian, A.M., Weisberg, S.P., Mack, M., Charo, I.F., 2007. Critical roles for CCR2 and MCP-3 in monocyte mobilization from bone marrow and recruitment to inflammatory sites. J. Clin. Invest. 117, 902–909.

Tussiwand, R., Everts, B., Grajales-Reyes, G.E., Kretzer, N.M., Iwata, A., Bagaitkar, J., Wu, X., Wong, R., Anderson, D.A., Murphy, T.L., Pearce, E.J., Murphy, K.M., 2015. Klf4 Expression in Conventional Dendritic Cells Is Required for T Helper 2 Cell Responses. Immunity 42, 916–928.

Uderhardt, S., Martins, A.J., Tsang, J.S., Lämmermann, T., Germain, R.N., 2019. Resident Macrophages Cloak Tissue Microlesions to Prevent Neutrophil-Driven Inflammatory Damage. Cell 177, 541-555.e17.

Unanue, E.R., Cerottini, J.C., 1970. The immunogenicity of antigen bound to the plasma membrane of macrophages. J. Exp. Med. 131, 711–725.

van de Laar, L., Saelens, W., De Prijck, S., Martens, L., Scott, C.L., Van Isterdael, G., Hoffmann, E., Beyaert, R., Saeys, Y., Lambrecht, B.N., Guilliams, M., 2016. Yolk Sac Macrophages, Fetal Liver, and Adult Monocytes Can Colonize an Empty Niche and Develop into Functional Tissue-Resident Macrophages. Immunity 44, 755–768.

van der Laan, A.M., ter Horst, E.N., Delewi, R., Begieneman, M.P. V, Krijnen, P.A.J., Hirsch, A., Lavaei, M., Nahrendorf, M., Horrevoets, A.J., Niessen, H.W.M., Piek, J.J., 2014. Monocyte subset accumulation in the human heart following acute myocardial infarction and the role of the spleen as monocyte reservoir. Eur. Heart J. 35, 376–385.

van Furth, R., 1989. Origin and Turnover of Monocytes and Macrophages. In: Iversen, O.H. (Ed.), Cell Kinetics of the Inflammatory Reaction. Springer Berlin Heidelberg, Berlin, Heidelberg, pp. 125–150.

van Furth, R., Cohn, Z.A., 1968. The origin and kinetics of mononuclear phagocytes. J. Exp. Med. 128, 415–35.

van Furth, R., Cohn, Z.A., Hirsch, J.G., Humphrey, J.H., Spector, W.G., Langevoort, H.L., 1972. The mononuclear phagocyte system: a new classification of macrophages, monocytes, and their precursor cells. Bull. World Health Organ. 46, 845–852.

Van Furth, R., Diesselhoff-den Dulk, M.C., Mattie, H., 1973. Quantitative study on the production and kinetics of mononuclear phagocytes during an acute inflammatory reaction. J. Exp. Med. 138, 1314–30.

van Furth, R., Spector, W.G., Humphrey, J.H., Hirsch, J.G., Cohn, Z.A., Langevoort, H.L., 1970. The nomenclature of mononuclear phagocytic cells - proposal for a new classification. In: Mononuclear Phagocytes. Blackwell, pp. 1–6.

van Leeuwen-Kerkhoff, N., Lundberg, K., Westers, T.M., Kordasti, S., Bontkes, H.J., Lindstedt, M., de Gruijl, T.D., van de Loosdrecht, A.A., 2018. Human bone marrow-derived myeloid dendritic cells show an immature transcriptional and functional profile compared to their peripheral blood counterparts and separate from slan+ non-classical monocytes. Front. Immunol. 9, 1619.

Van Voorhis, W.C., Hair, L.S., Steinman, R.M., Kaplan, G., 1982. Human dendritic cells. Enrichment and characterization from peripheral blood. J. Exp. Med. 155, 1172–1187.

Varol, C., Landsman, L., Fogg, D.K., Greenshtein, L., Gildor, B., Margalit, R., Kalchenko, V., Geissmann, F., Jung, S., 2007. Monocytes give rise to mucosal, but not splenic, conventional dendritic cells. J. Exp. Med. 204, 171–80.

Vergunst, C.E., Gerlag, D.M., Lopatinskaya, L., Klareskog, L., Smith, M.D., van den Bosch, F., Dinant, H.J., Lee, Y., Wyant, T., Jacobson, E.W., Baeten, D., Tak, P.P., 2008. Modulation of CCR2 in rheumatoid arthritis: A double-blind, randomized, placebo-controlled clinical trial. Arthritis Rheum. 58, 1931–1939.

Vikhanski, L., 2016. Immunity: How Elie Metchnikoff changed the course of modern medicine. Chicago Review Press (US).

Villani, A.-C., Satija, R., Reynolds, G., Sarkizova, S., Shekhar, K., Fletcher, J., Griesbeck, M., Butler, A., Zheng, S., Lazo, S., Jardine, L., Dixon, D., Stephenson, E., Nilsson, E., Grundberg, I., McDonald, D., Filby, A., Li, W., De Jager, P.L., Rozenblatt-Rosen, O., Lane, A.A., Haniffa, M., Regev, A., Hacohen, N., 2017. Single-cell RNA-seq reveals new types of human blood dendritic cells, monocytes, and progenitors. Science (80-.). 356, eaah4573.

Vremec, D., Zorbas, M., Scollay, R., Saunders, D.J., Ardavin, C.F., Wu, L., Shortman, K., 1992. The surface phenotype of dendritic cells purified from mouse thymus and spleen: investigation of the CD8 expression by a subpopulation of dendritic cells. J. Exp. Med. 176, 47–58.

Waskow, C., Liu, K., Darrasse-Jèze, G., Guermonprez, P., Ginhoux, F., Merad, M., Shengelia, T., Yao, K., Nussenzweig, M., 2008. The receptor tyrosine kinase Flt3 is required for dendritic cell development in peripheral lymphoid tissues. Nat. Immunol. 9, 676–83.

Whitelaw, D.M., 1972. Observations on human monocyte kinetics after pulse labelling. Cell Prolif. 5, 311–317.

Wong, K.L., Tai, J.J.-Y., Wong, W.-C., Han, H., Sem, X., Yeap, W.-H., Kourilsky, P., Wong, S.-C., 2011. Gene expression profiling reveals the defining features of the classical, intermediate, and nonclassical human monocyte subsets. Blood 118, e16-31.

Wu, J.-F., Ma, J., Chen, J., Ou-Yang, B., Chen, M.-Y., Li, L.-F., Liu, Y.-J., Lin, A.-H., Guan, X.-D., 2011. Changes of monocyte human leukocyte antigen-DR expression as a reliable predictor of mortality in severe sepsis. Crit. Care 15, R220.

Wysocka, M., Montaner, L.J., Karp, C.L., 2005. Flt3 Ligand Treatment Reverses Endotoxin Tolerance-Related Immunoparalysis. J. Immunol. 174, 7398–7402.

Yáñez, A., Coetzee, S.G., Olsson, A., Muench, D.E., Berman, B.P., Hazelett, D.J., Salomonis, N., Grimes, H.L., Goodridge, H.S., 2017. Granulocyte-Monocyte Progenitors and Monocyte-Dendritic Cell Progenitors Independently Produce Functionally Distinct Monocytes. Immunity 47, 890-902.e4.

Yona, S., Kim, K.-W., Wolf, Y., Mildner, A., Varol, D., Breker, M., Strauss-Ayali, D., Viukov, S., Guilliams, M., Misharin, A., Hume, D.A., Perlman, H., Malissen, B., Zelzer, E., Jung, S., 2013. Fate mapping reveals origins and dynamics of monocytes and tissue macrophages under homeostasis. Immunity 38, 79–91.

Yrlid, U., Jenkins, C.D., MacPherson, G.G., 2006. Relationships between distinct blood monocyte subsets and migrating intestinal lymph dendritic cells in vivo under steady-state conditions. J. Immunol. 176, 4155–62.

Yu, C.I., Becker, C., Wang, Y., Marches, F., Helft, J., Leboeuf, M., Anguiano, E., Pourpe, S., Goller, K., Pascual, V., Banchereau, J., Merad, M., Palucka, K., 2013. Human CD1c+ Dendritic Cells Drive the Differentiation of CD103+ CD8+ Mucosal Effector T Cells via the Cytokine TGF-β. Immunity 38, 818–830.

Zhang, H., Gregorio, J.D., Iwahori, T., Zhang, X., Choi, O., Tolentino, L.L., Prestwood, T., Carmi, Y., Engleman, E.G., 2017. A distinct subset of plasmacytoid dendritic cells induces activation and differentiation of B and T lymphocytes. Proc. Natl. Acad. Sci. U. S. A. 114, 1988–1993.

Zhang, N., Czepielewski, R.S., Jarjour, N.N., Erlich, E.C., Esaulova, E., Saunders, B.T., Grover, S.P., Cleuren, A.C., Broze, G.J., Edelson, B.T., Mackman, N., Zinselmeyer, B.H., Randolph, G.J., 2019. Expression of factor V by resident macrophages boosts host defense in the peritoneal cavity. J. Exp. Med. 216, 1291–1300.

Zhang, Y., Wallace, D.L., De Lara, C.M., Ghattas, H., Asquith, B., Worth, A., Griffin, G.E., Taylor, G.P., Tough, D.F., Beverley, P.C.L., Macallan, D.C., 2007. In vivo kinetics of human natural killer cells: The effects of ageing and acute and chronic viral infection. Immunology 121, 258–265.

Ziegler-Heitbrock, L., 2014. Monocyte subsets in man and other species. Cell. Immunol. 289, 135–139.

Ziegler-Heitbrock, L., Ancuta, P., Crowe, S., Dalod, M., Grau, V., Hart, D.N., Leenen, P.J.M., Liu, Y., MacPherson, G., Randolph, G.J., Scherberich, J., Schmitz, J., Shortman, K., Sozzani, S., Strobl, H., Zembala, M., Austyn, J.M., Lutz, M.B., 2010. Nomenclature of monocytes and dendritic cells in blood. Blood 116, e74-80.

Zigmond, E., Varol, C., Farache, J., Elmaliah, E., Satpathy, A.T., Friedlander, G., Mack, M., Shpigel, N., Boneca, I.G., Murphy, K.M., Shakhar, G., Halpern, Z., Jung, S., 2012. Ly6Chi Monocytes in the Inflamed Colon Give Rise to Proinflammatory Effector Cells and Migratory Antigen-Presenting Cells. Immunity 37, 1076–1090.